

***Crystalline architectures of copper(II)
complexes derived from halogen substituted
carbonyl compounds: Interplay of covalent
and non-covalent forces***

Thesis submitted to

Cochin University of Science and Technology

in partial fulfillment of the requirements

for the award of the degree of

Doctor of Philosophy

in

Chemistry

In the Faculty of Science

by

Aiswarya N.

(Reg. No: 4340)



**Department of Applied Chemistry
Cochin University of Science and Technology
Kochi - 22, Kerala, India**

October 2016

“Crystalline architectures of copper(II) complexes derived from halogen substituted carbonyl compounds: Interplay of covalent and non-covalent forces”

Ph.D. Thesis in the Faculty of Science

By

Aiswarya N.

Research Fellow

Department of Applied Chemistry

Cochin University of Science and Technology

Kochi, India 682 022

Email: ashiyer2007@gmail.com, iyerchem@cusat.ac.in

Research Advisor

Dr. M.R. Prathapachandra Kurup

Professor & Head

Department of Applied Chemistry

Cochin University of Science and Technology

Kochi 682 022

India

Email: mrp@cusat.ac.in

Department of Applied Chemistry

Cochin University of Science and Technology

Kochi 682 022

India

October 2016

Front cover: 3D glossy image of molecule

Back cover: Stair-like polymeric structure of one of the complexes



The Gayatri Mantra

ॐ भूर्भुवः स्वः
तत्सवितुर्वरेण्यं
भर्गो देवस्य धीमहि
धियो योनः प्रचोदयात् ।

*Om Bhoor Bhuvah Svah
Tat Savitur Varenyam
Bhargo Devasya Dheemahi
Dhiyo Yonah Prachodayaat.*

**Oh Creator of the Universe!
We meditate upon thy supreme
splendor.**

**May thy radiant power
illuminate our intellects,
destroy our sins, and guide us
in the right direction!**



*'Fear... Uncertainty... & Discomfort...
Is What Will Move You
Towards Your Growth...'*

*“Parents are like a bow,
And children like arrows.
The more the bow bends and stretches, the farther the arrow flies.
I fly, not because I am special, but because they stretched for me”*

[Khalil Gibran]

Dedicated to my amma & appa.....



Phone Off. 0484-2862423
Phone Res. 0484-2562904
Telex: 885-5019 CUIIN
Fax: 0484-2577595
Email: mrp@cusat.ac.in
mrp_k@yahoo.com

DEPARTMENT OF APPLIED CHEMISTRY
COCHIN UNIVERSITY OF SCIENCE AND TECHNOLOGY
KOCHI – 682 022, INDIA

Dr. M.R. Prathapachandra Kurup
Professor & Head

Date: 04-10-2016

Certificate

This is to certify that the thesis entitled “**Crystalline architectures of copper(II) complexes derived from halogen substituted carbonyl compounds: Interplay of covalent and non-covalent forces**” submitted by **Ms. Aiswarya N.**, in partial fulfillment of the requirements for the degree of Doctor of Philosophy, to the Cochin University of Science and Technology, Kochi-22, is an authentic record of the original research work carried out by her under my guidance and supervision. The results embodied in this thesis, in full or in part, have not been submitted for the award of any other degree. All the relevant corrections and modifications suggested by the audience and recommended by the doctoral committee of the candidate during the presynopsis seminar have been incorporated in the thesis.

M.R. Prathapachandra Kurup
(Supervising Guide)

Declaration

I hereby declare that the work presented in this thesis entitled “**Crystalline architectures of copper(II) complexes derived from halogen substituted carbonyl compounds: Interplay of covalent and non-covalent forces**” is entirely original and was carried out independently under the supervision of **Prof. M.R. Prathapachandra Kurup**, Department of Applied Chemistry, Cochin University of Science and Technology and has not been included in any other thesis submitted previously for the award of any other degree.

Kochi-22
04/10/2016

Aiswarya N.

Acknowledgement

After an intensive period of five years, today is the day – to wind up the thesis work with a note of thanks to all those who have supported me directly or otherwise. Past five years, definitely not a short span of life has been a period of learning not only in scientific arena but also at personal level. Unlike all other pages of the thesis which flowed from brain, I find it more difficult to complete these pages as it involves my heart also.

Right from finding an appropriate research problem to the final process of thesis writing, my advisor Prof. M.R. Prathapachandra Kurup sir has offered unreserved help and guidance, while providing me the space to work with all freedom. Apart from academic guidance, I have learned these qualities from him – to be simple, serene and to be always smiling.

I extend my sincere thanks to my doctoral committee member, Dr. P.A. Unnikrishnan sir for the timely suggestions. My studies on catecholase activity of the complexes would not have become fruitful without the helping hand of Dr. S. Sugunan sir. I also thank all other faculty members of the department including the former heads, Dr. N. Manoj sir and Dr. K. Sreekumar sir for allowing me to use the facilities of this department. Non-teaching staff of the department deserve special mention without whom the thesis submission would not have been speeded up. I thank the librarians, Siju sir and Abhilash sir who supported me by lending books. I bow my head in front of all gurus who instilled in me the behavioural sense and moral values. I also extend my gratitude to UGC for providing me the financial assistance for carrying out the research work.

Research work is always a concerted effort. I would like to thank Dr. Sarita G. Bhat, Dept. of Biotechnology and Dr. M. Kailasanath, International School of Photonics, CUSAT for providing me the facilities to carry out the application studies of our samples without any delay. Dr. Harisree chechi of Biotechnology wing and Ms. Ajina of Photonics section requires special mention in this regard. I owe my thanks to Dr. Anantharaman sir, Dept. of Physics for helping me to carry out fluorescence studies. Dr. Shibu sir, Adarsh sir, Shyam chettan and Nanitha of

SATF, STIC, Cusat offered timely help and suggestions for the completion of the thesis.

When we look back, what we have is a handful of memories to cherish. Shakespeare once said – ‘Life is a stage where each has a role to enact’. I take this opportunity to mention all my friends who shared my stage of life at CUSAT and made it a beautiful play.

My heartfelt thanks to seniors – Dr. M. Sithambaraesan, Dr. Jayakumar sir, Dr. Roji J. Kunnath, Dr. Jessy miss, Dr. Annie miss, Jinsa chechi, Bibitha chechi, Nisha chechi and Sajitha chechi. Eesan sir, you are like a wizard – your magical words have always astonished me and have influenced both my personal and academic life. Life of a Ph.D. student witnesses more setbacks and there are moments when we feel like quitting. I should openly admit that his words have inspired me to move forward from such difficult situations. Jayakumar sir and Roji sir – you are still a good source of inspiration for me.

Adapting to a new environment is quite a painful and difficult task. But I should say that my peers – Ambili, Mridula, Vineetha and Sreejithettan made it most comfortable with their company. Thanks for all those wonderful moments during the first two years of research life. Moments with you also helped me to evolve as an individual.

Support from blood relations is not a surprise. A person who is not your blood relation, but who cares you, teases you, supports you and fights with you – Sreejithetta, you are more like a brother for me. Our discussions on research topics, friendly fights and debates – when I think that these are coming to an end, it fills in me a deep sense of grief. The picture is incomplete without you, dear Nithya. I had many ups and downs particularly during the last phase of research life and whenever I needed a shoulder to bank upon, unsolicitedly you both were there. You both are simply awesome. I am sure my work would not have taken its final form without the team effort of Sreejithettan, Nithya and no doubt, Lincy. Tom, as I used to call you.....you always took time to fill our starving stomachs in between the hectic work hours of lab and I always admire your cool attitude to everything and anything. It will be ungrateful if I didn't mention Kala, Vineetha and

Aswathy of organic lab - the academic discussions with you were all fruitful, Thank you so much.

I remember (Late) Vishnu who always took pains to supply us with the required chemicals on time. He was one among us.

My juniors – Fousia (moosa), Daly, Asha, Manjari – You all are really a catalyst working in the right direction for a peaceful and intriguing environment in the lab. Thank you all for creating a cordial atmosphere. Your company reduced my stress level during the tiresome thesis writing.

There are two important persons in my life – Friends who squeezed time in between their busy schedule just to comfort me; friends who always wanted and wished the best for me; who have confidence in me; who rendered their hand whenever needed, whom I can call at any time; with whom I need not be conscious while conversing – my besties, dearest Sowmya chechi and Seleena. ... your presence made the hostel hours worth remembering. You are my left and right, who balanced me throughout to reach my goal.

My roomies, Lisha and Rani – thanks for enduring all my mood swings throughout these years. Thanks to my buddies – Bincy, Srinath, Prashanth, and Sheeja who supported me right from my degree days till now. My M.Sc. friends – Anjumol, Geethus and Siby whose sound itself comforted me.

I thank Binoop chettan of Indu photos, who provided all the technical support and helped me to bring out the thesis in its final form.

The thesis is actually an outcome of the struggles endured by Amma and Appa. I am just an instrument who worked with the support and prayers of my dearest parents. You never stood against my dreams, rather gave me all the mental strength to move on even when the circumstances were odd. A word of acknowledgement will be a mere formality which I don't wish. I pray almighty to give me all the strength to act in such a way that make my parents proud of me. And I specially thank my brother, Arun (arunna...) for understanding the awe and agony that underpins the doctoral life span. Thanks a lot for teaching me the important lessons of life.

This is also the time to remember my grand parents who took great pains to bring me up.

I kneel down before the divine source.....Its that power which is with me throughout, which gives me the mental and physical strength to move on.....While penning down these pages, I strongly feel that tears have replaced the ink of my pen.

With all due respect to my seniors and with all sincere wishes and prayers for my juniors, I take leave...

Aiswarya

||| Preface |||

The current scenario of coordination chemistry is witnessing the exploitation of coordination bonds and noncovalent interactions to generate self-assemblies of various dimensions having not only aesthetic values but also countless applications and that paved way for supramolecular chemistry/crystal engineering. Most of such fascinating work employs Schiff bases obtained by the condensation of an amine and a carbonyl compound. The use of diamines in the synthesis of high-nuclearity complexes utilizes the bridging capacity of phenoxo atoms. Whereas in the case of N_2O donor tridentate Schiff bases (*N*-substituted diamines with salicylaldehyde or its derivatives), coligands are employed to generate structures of variable composition apart from satisfying the coordination number. Among the various coligands known, pseudohalides (azido, cyanato, thiocyanato, dicyanamido) deserve special attention on account of its versatile modes of binding. In addition to the structural variety, such Schiff base complexes have its signature in the field of catalysis, luminescence, gas adsorption and magnetic materials which make the arena conspicuous. The recognition of plasticity of copper(II) metal with respect to its coordination number and its ubiquitous nature as active sites in many metallo-enzymes fuelled us to work with this metal. The results of our efforts to explore the role of various interaction forces constitute the subject matter of the thesis entitled ***“Crystalline architectures of copper(II) complexes derived from halogen substituted carbonyl compounds: Interplay of covalent and non-covalent forces”***. The work embodied in this thesis was carried out by the author in the Department of Applied Chemistry, CUSAT, Kochi, during the period 2011-2016 and is divided into eight chapters.

An introduction to N_2O tridentate Schiff base systems as blocking ligands and the pseudohalides as the bridging ligands is given in first chapter. It also includes an excerpt highlighting the various studies like DNA binding/cleavage, NLO and catecholase like activity. The chapter details the objectives of the work and various analytical methods used for the characterization of the synthesized systems. Chapters 2-6 throw light upon the interaction forces responsible for the variety of crystalline architectures obtained from Schiff base systems. Any work becomes significant when we identify it with some applications and our work is also buttressed by such application level studies. Chapter 7 gives an idea about the pharmacological relevance, non-linear optical applications and catecholase like biomimetic activity of our complexes. The final session consolidates all our research findings and brings into focus the various possibilities and challenges of the pursuing area. This is infact a baton for further research in this evergreen area.

Contents

Chapter 1

A vignette on metal complexes of Schiff bases

and its applications..... 01-27

| | |
|--|----|
| 1.1 Introduction | 01 |
| 1.2 Outline of the systems employed in our study | 02 |
| 1.3 Application of metal complexes of Schiff bases | 05 |
| 1.3.1 Transition metal Schiff base complexes as pharmacological agents | 05 |
| 1.3.2 Third order non-linear optical studies of metal complexes of Schiff bases | 07 |
| 1.3.3 Biomimetic activity of Schiff base complexes | 08 |
| 1.4 Theory behind the effect of solvents on the coordination geometry of the complexes | 09 |
| 1.4.1 Effect of solvents on square planar structure | 10 |
| 1.4.2 Effect of solvents on square pyramidal structure | 11 |
| 1.5 Scope and objectives of the present study | 12 |
| 1.6 Physical Measurements | 13 |
| 1.6.1 Spectral methods | 13 |
| 1.6.1.1 Infrared Spectroscopy | 13 |
| 1.6.1.2 Electronic Spectroscopy | 13 |
| 1.6.1.3 EPR spectroscopy | 14 |
| 1.6.1.4 Fluorescence spectroscopy | 17 |
| 1.6.2 Elemental analysis | 19 |
| 1.6.3 Thermal analysis..... | 20 |
| 1.6.4 Single crystal X-ray diffraction studies | 21 |
| References | 22 |

Chapter 2

Polymeric polymorphs and monomers of pseudohalide incorporated Cu(II) complexes of *N,N*-dimethylethylenediamine and 3,5-dichlorosalicylaldehyde.....

29-81

| | |
|---|----|
| <i>Conspectus</i> | 29 |
| 2.1 Introduction | 30 |
| 2.2 Experimental..... | 30 |
| 2.2.1 Materials..... | 30 |
| 2.2.2 Synthesis of Cu(II) complexes | 30 |
| 2.2.2.1 Synthesis of $[\text{Cu}(\text{L}^1)(\text{N}_3)]_n$ (1a)..... | 30 |

| | | |
|-----------|--|----|
| 2.2.2.2 | Synthesis of $[\text{Cu}(\text{L}^1)(\text{N}_3)]_n$ (1b) | 31 |
| 2.2.2.3 | Synthesis of $[\text{Cu}(\text{L}^1)(\text{NCO})]$ (2) and $[\text{Cu}(\text{L}^1)(\text{NCS})]$ (3) | 31 |
| 2.3 | Results and discussion | 32 |
| 2.3.1 | Spectral Characterization | 33 |
| 2.3.1.1 | IR and electronic spectra | 33 |
| 2.3.1.2 | Solvatochromic studies | 35 |
| 2.3.2 | X-ray crystallography and structural description | 40 |
| 2.3.2.1 | $[\text{Cu}(\text{L}^1)(\text{N}_3)]_n$ (1a) | 43 |
| 2.3.2.2 | $[\text{Cu}(\text{L}^1)(\text{N}_3)]_n$ (1b) | 47 |
| 2.3.2.2.1 | Comparison of polymorphic structures | 51 |
| 2.3.2.3 | $[\text{Cu}(\text{L}^1)(\text{NCO})]$ (2) | 52 |
| 2.3.2.4 | $[\text{Cu}(\text{L}^1)(\text{NCS})]$ (3) | 54 |
| 2.3.2.5 | Supramolecular features as structural adhesives | 55 |
| 2.3.3 | Photoluminescence studies | 70 |
| 2.3.4 | Thermal studies | 72 |
| 2.3.5 | EPR spectral studies | 73 |
| | References | 79 |

Chapter 3

Coordination polymers derived from *N,N*-dimethyl-1,3-propanediamine and 3,5-dichlorosalicylaldehyde..... 83-106

| | | |
|------------------|---|-----|
| <i>Conspetus</i> | | 83 |
| 3.1 | Introduction | 84 |
| 3.2 | Experimental | 84 |
| 3.2.1 | Materials | 84 |
| 3.2.2 | Synthesis of Cu(II) complexes | 84 |
| 3.2.2.1 | Synthesis of complexes, $[\text{Cu}(\text{L}^2)(\text{X})]_n$, ($\text{X} = \text{N}_3^-$, $\text{N}(\text{CN})_2^-$) (4 and 5) | 84 |
| 3.3 | Results and discussion | 85 |
| 3.3.1 | Spectroscopic features | 86 |
| 3.3.1.1 | IR and electronic spectra | 86 |
| 3.3.1.2 | Solvatochromic studies | 88 |
| 3.3.2 | X-ray crystallography and structural description | 91 |
| 3.3.2.1 | $[\text{Cu}(\text{L}^2)(\text{N}_3)]_n$ (4) | 92 |
| 3.3.2.2 | $[\text{Cu}(\text{L}^2)(\text{N}(\text{CN})_2)]_n$ (5) | 97 |
| 3.3.3 | Optical emissive response | 101 |
| 3.3.4 | Thermal studies | 102 |
| 3.3.5 | EPR spectral studies | 103 |
| | References | 106 |

Chapter 4

Monomers, polymers and a dimer based on *N,N*-dimethylethylenediamine / *N*-methyl 1,3-propanediamine and 3,5-dichloro-2-hydroxyacetophenone107-154

| | |
|--|-----|
| <i>Conspectus</i> | 107 |
| 4.1 Introduction | 108 |
| 4.2 Experimental..... | 108 |
| 4.2.1 Materials..... | 108 |
| 4.2.2 Synthetic strategy | 108 |
| 4.2.2.1 Synthesis of [Cu(L ³)(N ₃) _n] (6)..... | 108 |
| 4.2.2.2 Synthesis of [Cu(L ³)(NCS)] (7)..... | 109 |
| 4.2.2.3 Synthesis of [Cu(L ³)(NCO)] (8)..... | 109 |
| 4.2.2.4 Synthesis of [Cu(L ³)[N(CN) ₂] _n] (9)..... | 110 |
| 4.2.2.5 Synthesis of [Cu(L ⁴)(N ₃) ₂] (10)..... | 110 |
| 4.3 Results and discussion..... | 110 |
| 4.3.1 Spectroscopic signature..... | 112 |
| 4.3.3.1 IR and electronic spectra | 112 |
| 4.3.3.2 Solvatochromic studies | 114 |
| 4.3.2 X-ray crystallography and crystal structure description..... | 119 |
| 4.3.2.1 [Cu(L ³)(N ₃) _n] (6) | 119 |
| 4.3.2.2 [Cu(L ³)(NCS)] (7)..... | 125 |
| 4.3.2.3 [Cu(L ³)(NCO)] (8)..... | 128 |
| 4.3.2.4 [Cu(L ³)[N(CN) ₂] _n] (9)..... | 132 |
| 4.3.2.5 [Cu(L ⁴)(N ₃) ₂] (10)..... | 138 |
| 4.3.3 Optical emissive response | 141 |
| 4.3.4 Thermal studies | 142 |
| 4.3.5 EPR spectral studies..... | 144 |
| References | 152 |

Chapter 5

Complexes derived from *N,N*-dimethylethylenediamine and mono halosubstituted carbonyl compounds.....155-232

| | |
|-------------------------|-----|
| <i>Conspectus</i> | 155 |
| 5.1 Introduction | 156 |
| Section A | |
| 5.2 Experimental..... | 156 |
| 5.2.1 Materials..... | 156 |

| | | |
|---------|--|-----|
| 5.2.2 | Synthetic protocol..... | 156 |
| 5.2.2.1 | Synthesis of [Cu(L ⁵)(NCO)] (11) / [Cu(L ⁵)(NCS)] (12) | 156 |
| 5.2.2.2 | Synthesis of [Cu(L ⁶)(N ₃) _n] (13) | 157 |
| 5.3 | Results and discussion..... | 158 |
| 5.3.1 | Spectroscopic features..... | 159 |
| 5.3.1.1 | IR and electronic spectroscopy..... | 159 |
| 5.3.1.2 | Solvatochromic studies | 161 |
| 5.3.2 | X-ray crystallography and crystal structure description..... | 164 |
| 5.3.2.1 | [Cu(L ⁵)(NCO)] (11) | 165 |
| 5.3.2.2 | [Cu(L ⁵)(NCS)] (12)..... | 170 |
| 5.3.2.3 | [Cu(L ⁶)(N ₃) _n] (13) | 174 |
| 5.3.3 | Photoluminescence studies | 180 |
| 5.3.4 | Thermal studies | 181 |
| 5.3.5 | EPR spectral studies | 182 |

Section B

| | | |
|---------|--|-----|
| 5.4 | Experimental..... | 186 |
| 5.4.1 | Synthesis of [Cu(L ⁷)(NCS)] (14)..... | 186 |
| 5.5 | Results and discussion..... | 186 |
| 5.5.1 | Spectral features | 187 |
| 5.5.2 | Description of the crystal structures..... | 190 |
| 5.5.2.1 | Structural adhesives..... | 193 |
| 5.5.3 | Photoluminescence study | 195 |
| 5.5.4 | Thermal study | 196 |
| 5.5.5 | EPR spectral study..... | 196 |

Section C

| | | |
|------------|--|-----|
| 5.6 | Experimental..... | 199 |
| 5.6.1 | Synthesis of [Cu(L ⁸)(N ₃) _n] (15) / [Cu(L ⁸)(NCS)] _n (16)..... | 199 |
| 5.6.2 | Synthesis of [Cu(L ⁹)(N ₃) _n] (17) | 199 |
| 5.7 | Results and discussion..... | 200 |
| 5.7.1 | Spectral features | 201 |
| 5.7.1.1 | IR and linear electronic response..... | 201 |
| 5.7.1.2 | Solvatochromic studies | 202 |
| 5.7.2 | Description of crystal structures..... | 206 |
| 5.7.2.1 | [Cu(L ⁸)(N ₃) _n] (15)..... | 206 |
| 5.7.2.2 | [Cu(L ⁸)(NCS)] _n (16) | 211 |
| 5.7.2.3 | [Cu(L ⁹)(N ₃) _n] (17) | 216 |
| 5.7.2.3.1 | Supramolecular features..... | 220 |
| 5.7.3 | Photoluminescence studies | 225 |
| 5.7.4 | Thermal studies | 225 |
| 5.7.5 | EPR spectral studies..... | 226 |
| References | | 231 |

Chapter 6

Complexes derived from 1-aminopyrrolidin-2-one and 5-chloro/5-bromosalicylaldehyde233-261

| | |
|---|-----|
| <i>Conspectus</i> | 233 |
| 6.1 Introduction | 233 |
| 6.2 Experimental..... | 234 |
| 6.2.1 Materials..... | 234 |
| 6.2.2 Synthetic protocol..... | 234 |
| 6.2.2.1 Synthesis of proligands | 234 |
| 6.2.2.1.1 Preparation of HL ¹⁰ | 234 |
| 6.2.2.1.2 Preparation of HL ¹¹ | 235 |
| 6.2.2.2 Synthesis of copper complexes..... | 235 |
| 6.2.2.2.1 Synthesis of [Cu(L ¹⁰)Cl] (18)/[Cu(L ¹¹)Cl] (19)..... | 235 |
| 6.3 Results and discussion..... | 237 |
| 6.3.1 Spectroscopic features..... | 237 |
| 6.3.1.1 IR and electronic spectroscopy..... | 237 |
| 6.3.2 X-ray crystallography and crystal structure description..... | 239 |
| 6.3.2.1 (<i>E</i>)-1-(5-bromo-2-hydroxybenzylideneamino)pyrrolidin-2-one (HL ¹⁰)..... | 240 |
| 6.3.2.2 (<i>E</i>)-1-(5-chloro-2-hydroxybenzylideneamino)pyrrolidin-2-one (HL ¹¹) | 244 |
| 6.3.2.3 [Cu(L ¹⁰)Cl] (18)..... | 248 |
| 6.3.2.4 [Cu(L ¹¹)Cl] (19)..... | 253 |
| 6.3.2.5 Comparison of ligand and its complex..... | 256 |
| a. HL ¹⁰ and [Cu(L ¹⁰)Cl] (18)..... | 256 |
| b. HL ¹¹ and [Cu(L ¹¹)Cl] (19)..... | 256 |
| 6.3.3 Photoluminescence studies | 256 |
| 6.3.4 Thermal studies | 257 |
| 6.3.5 EPR spectral studies..... | 258 |
| References | 261 |

Chapter 7

Pharmacological, non-linear optical and catecholase activity studies.....263-298

| | |
|-------------------------------------|-----|
| <i>Conspectus</i> | 263 |
| 7.1 Introduction | 263 |
| 7.2 Pharmacological studies | 264 |
| 7.2.1 DNA interaction studies | 264 |
| 7.2.1.1 DNA binding..... | 264 |
| a. Intercalative binding..... | 265 |

| | |
|--|-----|
| b. Groove binding | 266 |
| 7.2.1.1.1 Experimental..... | 268 |
| 7.2.1.1.2 Results and discussion | 269 |
| 7.2.1.2 DNA cleavage | 271 |
| 7.2.1.2.1 Experimental..... | 272 |
| 7.2.1.2.2 Results and discussion | 274 |
| 7.3 Non-linear optical studies | 276 |
| 7.3.1 Fundamentals of non-linear optics..... | 277 |
| 7.3.1.1 Symmetry requirement for NLO materials | 278 |
| 7.3.1.2 Non-linear optical effects | 278 |
| 7.3.1.2.1 Non-linear absorption | 278 |
| 7.3.1.2.2 Non-linear refraction | 279 |
| 7.3.1.3 Methods for determining third order NLO property..... | 280 |
| 7.3.2 Experimental..... | 280 |
| 7.3.3 Results and discussion..... | 281 |
| 7.4 Catecholase activity of copper complex | 286 |
| 7.4.1 Bioinorganic catalysis | 286 |
| 7.4.1.1 Structure of catechol oxidase | 286 |
| 7.4.1.2 General mechanism of catechol oxidation..... | 287 |
| 7.4.1.3 Factors affecting catecholase activity | 289 |
| 7.4.1.4 Reaction mimicking the bioinorganic enzyme catalysis | 290 |
| 7.4.1.5 Why 3,5-DTBC as substrate ?..... | 290 |
| 7.4.2 Experimental..... | 290 |
| 7.4.3 Results and discussion..... | 291 |
| References | 294 |

Chapter 8

Summary, conclusions and outlook.....299-312

| | |
|--|-----|
| 8.1 Summary of the work done..... | 299 |
| 8.2 Concluding remarks based on structure-spectroscopic correlation studies..... | 302 |
| 8.2.1 Structure-spectroscopic correlation studies of Chapters 2 and 3 | 302 |
| 8.2.2 Structure-spectroscopic correlation studies of Chapters 2 and 4 | 303 |
| 8.2.2.1 Structural correlation of [Cu(L ³)(NCS)] (7) and [Cu(L ³)(NCO)] (8) with the electronic response..... | 303 |
| 8.2.2.2 Comparison of the complexes of Chapters 2 and 4 | 304 |
| 8.2.3 Structure-spectroscopic correlation studies of chapters 2 and 5..... | 305 |
| 8.2.3.1 Comparison of the complexes [Cu(L ¹)(NCS)] (3) and [Cu(L ⁵)(NCS)] (12)..... | 305 |
| 8.2.3.2 Structural correlation of [Cu(L ⁸)(N ₃) _n] (15) and [Cu(L ⁸)(NCS)] (16) with the electronic response | 306 |

| | |
|---------------------------------|---------|
| 8.3 Outlook | 307 |
| 8.3.1 Challenges before us..... | 307 |
| 8.3.2 Possibilities..... | 308 |
| References | 308 |
| Abbreviations..... | 309-310 |
| Publications | 311-312 |

.....

A vignette on metal complexes of Schiff bases and its applications

- 1.1. *Introduction*
- 1.2. *Outline of the systems employed in our study*
- 1.3. *Application of metal complexes of Schiff bases*
- 1.4. *Theory behind the effect of solvents on the coordination geometry of the complexes*
- 1.5. *Scope and objectives of the present study*
- 1.6. *Physical measurements*

1.1. Introduction

Schiff bases or imines, have long been known to be useful metal ligands [1] with key roles in biology as intermediates of many enzymatic reactions [2], and applications in chemistry, such as in asymmetric catalysis [3]. Due to relatively simple yet robust synthetic procedure, Schiff base formation and complexation has always become the subject matter of research. Unlike a synthetic organic chemist, who enjoys the luxury of a large number of reliable reactions at their disposal for preparing small molecules, coordination chemists with only a relatively few number of high-yielding reactions are always at a challenge. Therefore, strategies with an aim to harness the directional bonding afforded by metal centers and the weak metal-ligand interactions in coordination complexes were developed [4] and the spate of publications in supramolecular chemistry in the last few decades corroborates the fact. Slowly, the traditional distinct boundaries of sciences started to fade away ultimately making the field interdisciplinary.

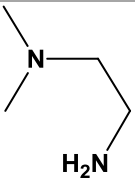
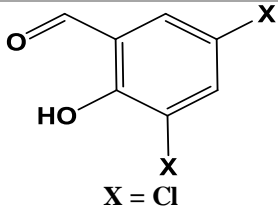
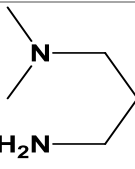
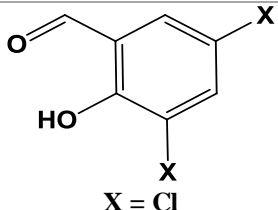
1.2. Outline of the systems employed in our study

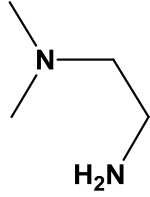
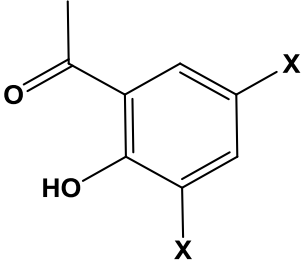
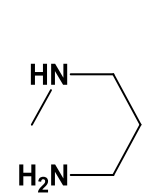
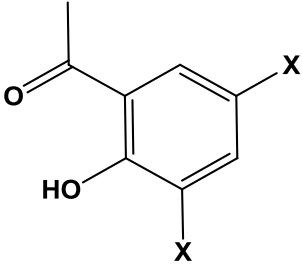
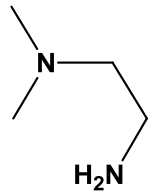
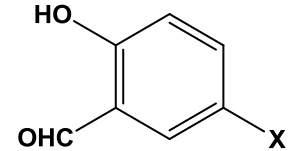
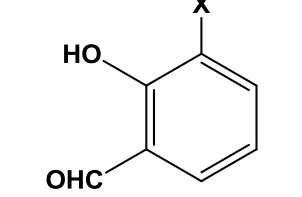
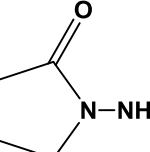
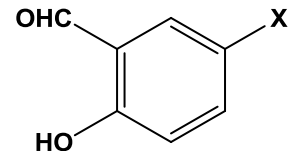
Schiff bases derived from carbonyl compounds are a kind of versatile ligands in coordination chemistry, on account of their structure-activity relationships. Among the plethora of Schiff base systems available, N₂O tridentate systems are popular particularly if the intension is to build a polymeric system by employing coligands.

We have designed our work in such a fashion that major part is centered around disubstituted amines. Hydrogen bonding, lone pair $\cdots\pi$, C–H $\cdots\pi$, cation $\cdots\pi$ and anion $\cdots\pi$ interactions are the most common and widely accepted supramolecular forces [5-7], and hydrogen bond interactions are the protagonist among the many. It was therefore a judicious choice from our group to select bisubstituted amines so as to deliberately suppress the hydrogen bonding capability of the resulting tridentate Schiff base thereby highlighting the role of other weak interactions in the construction of supramolecular architectures [8]. In addition to this, we have a NO₂ tridentate system derived from 1-aminopyrrolidine-2-one · hydrochloride also.

The various systems that we have employed for our study are given in Table 1.1.

Table 1.1. Nutshell description of the Schiff base systems and the nuclearity of the complexes obtained from them

| Amines | Carbonyl portion | Polymers | Monomers | Dimers |
|---|---|----------|----------|--------|
|  |  | 2 | 2 | NIL |
|  |  | 2 | NIL | NIL |

| | | | | |
|---|---|-------------|-------------|-----|
|  |  X = Cl | 2 | 2 | NIL |
|  |  X = Cl | NIL | NIL | 1 |
|  |  X = Cl, Br | 1 X = Cl | 2 | NIL |
| | | NIL | 1 X = Br | NIL |
| |  X = F | 2 | NIL | NIL |
|  |  X = Cl, Br | NIL | 2 | NIL |

Apart from the known non-covalent forces of interaction, the supramolecular toolbox has been reinforced by a new force: halogen bonding (XB) interaction [9]. As a counterpart of hydrogen bonding (HB) interaction, halogen bonding interaction encompasses any type of non-covalent interactions involving a halogen atom as an acceptor of electronic density. Since not much of experimental work highlighting the halogen interaction is known, our group employed halogen substituted salicylaldehydes/ketones to explore more on halogen interactions [10], a new tool for crystal engineers and to discuss the role of various other weak interactions in stabilizing a specific crystal system.

As already discussed, in the case of N_2O donor tridentate Schiff bases (*N*-substituted diamines with salicylaldehyde or its derivatives), coligands can be employed to generate structures of variable composition apart from satisfying the coordination number [11,12]. Design and construction of polymeric structures of the complexes with Schiff bases are of peculiar interest in structural chemistry. Halides and pseudohalides are charming groups that can link two or more metals, yielding various polynuclear complexes [13–15]. These potential polydentate ligands are capable of mediating magnetic exchange interactions and the nature of interaction is modulated by the mode of bonding as well as the metrical parameters like the metal–N–metal bridge angle, metal–N–N–metal torsion angle, metal–N–N angle and metal–N distance [16-19].

Of the various transition metals, the chemistry of polynuclear/dinuclear copper(II) complexes is getting more importance now-a-days because of its relevance to various metallo-proteins and metallo-enzymes [20-22]. Active Jahn–Teller effects on the copper(II) center makes the structures even more versatile [23-25]. The plasticity of the copper metal also makes it a metal of first choice.

Attention has been paid on coordination bonds and other weak chemical bonds that form coordination polymers [26] which are infinite systems build up with metal ions and organic ligands as main elementary units. The role of various weak but directional non-covalent forces, which are the foundation pillars of supramolecular self-assembly are also carefully weighed.

Though several factors like the nature of metal ion, solvent, blocking organic ligand, metal:pseudohalide ratios etc. can be stated as those that control the nature of the final product, no generalization can be arrived at and therefore in many cases called ‘Serendipitous self assembly’ [27]. The various non-covalent interactions leading to structurally aesthetic supramolecular architectures in solid state also propel us to quest after [28-30]. Although voluminous research work has been done in this arena, still researchers find it difficult to control the composition and nuclearity of the final product and this ambiguity intrigues us to pursue more. Lack of rational synthetic procedures, the difficulty in predicting the coordination mode adopted by the coligands and therefore the product – these are the major problems to be addressed in this field.

1.3. Application of metal complexes of Schiff bases

1.3.1. Transition metal complexes of Schiff bases as pharmacological agents

The novel electronic/magnetic properties with fascinating structures and the easy modulation of their DNA binding and cleavage ability has made Schiff base metal complexes an area of medicinal interest for the development of new therapeutic agents [31-33]. Development of metal-based drugs saw an upswell [34,35] with the discovery of *cis*-platin [Pt(NH₃)₂Cl₂] in 1964 and its ulterior clinical use as anticancerous agent [36]. Since then, much investigation is cornered around platinum and ruthenium ions, regarded as coordination centers of potential anticancer agents [36,37], although we could see a growing interest in the synthesis of cheaper first-row transition metal complexes as efficient DNA binders with potential cytotoxic activity [38-40].

Transition metal complexes offer two peculiar advantages as DNA-binding agents [41]. First and foremost, transition metal centers are particularly attractive moieties for reversible recognition of nucleic acids because they exhibit well-defined coordination geometries. Moreover, they often possess distinctive electrochemical or photophysical properties, thus enhancing the functionality of the binding agent [42]. DNA-binding drugs can be categorized

according to the type of association with DNA: covalent binding agents, intercalators, groove binders and most recently classified [43], phosphodiester backbone binders. Due to their high specificity, minor groove binders are prone to modulate the gene expression and this has led to their development over the intercalators [44]. Among the variety of techniques available for studying the drug-DNA interaction, UV-vis absorption and fluorescence spectrometry are most used due to their good sensitivity, reproducibility, simplicity and versatility. The absorbance and fluorescence spectra of drugs become altered upon interaction with nucleic acids, shifting the band maxima [45]. From the absorbance spectral data, we can deduce the value of intrinsic binding constant, K_b – a valuable tool to quantify the interaction affinity between small molecules and DNA [46].

Research on synthetic metal complexes as DNA cleavage agents are also appealing taken in to account their efficacy as anti-tumour agents [47]. The correlation between DNA binding and cytotoxic activity against cancer cells is still a crucial step in the search for new anticancer drugs [48-53]. DNA which is usually resistant towards the hydrolysis can be very effectively cleaved *via* oxidative pathway. Metal ions with known redox chemistry are hence used for the development of artificial nucleases. Metals like Cu(II), Fe(II) etc. under proper conditions cleave DNA by oxidative pathway [54] and their highly Lewis acidic nature compensates for the sub-optimal reactivity of synthetic agents [55]. Most of the literature focuses on DNA damage caused by only single metal ion while the situation is different for a cellular environment with many metal ions present simultaneously [56]. So it is necessary to study the rates of damage under these more complex conditions and to sketch a comprehensive picture of the processes involved.

A preliminary investigative study of the complex - DNA interaction was carried out in five of our complexes, the details of which can be referred to in Section 7.2.1.1.2. The biological studies were done at the Dept. of Biotechnology, CUSAT.

1.3.2. Third order non-linear optical studies of metal complexes of Schiff base

The NLO response can be induced in a medium by the input of intense light (often a laser), and then the medium counter acts on the light. The latter process is nonlinear and obeys Maxwell's equations [57]. Nonlinear optics (NLO) is the branch of optics that describes the behavior of light in media where the dielectric polarization responds nonlinearly to (the electric field component of) light [58,59]. The third-order NLO materials are currently of interest to a large number of research groups as they can be used for a number of photonic applications, for example, optically addressed optical switches for photonics switching, optical signal processing, optical communication etc. Compared with inorganic, organic and polymeric materials, metal complexes have the following merits:

(1) More sublevels in the energy hierarchy, which permit more allowed electronic transitions to take place and result in a larger NLO effect; (2) High damage threshold and fast response, which are important factors for their practical applications [60-62].

Coordination polymers play an important role in the family of nonlinear optical materials. The possibility of modulating the NLO property of coordination polymers is immense when compared to other systems because of the following reasons:

- a) Electronic properties can be tuned by changing the coordinated metal centre.
- b) Extended π conjugation length can be altered by modifying the ligands attached to the metal centre [63].

The NLO effect has largely to do with the valence shell structure of the central metal ion, because the empty d orbitals on the metal centers would communicate electronically with the π system of ligands and the axial groups, thereby enhancing the non-linear susceptibility [64].

Literature shows that there exists good correlation between the structure of coordination polymers and the observed NLO properties. Accordingly,

- Coordination polymers with open *d*-shell metal ions exhibit self-defocusing behaviors.
- Coordination polymers with d^{10} valence shell metal ions give strong self-focusing behaviors.
- All two-dimensional rhombohedral grid coordination polymers possess strong self-focusing effects regardless of the valence shell structures of metal ions.
- Three dimensional coordination polymers have the same relationship between the structures and the NLO properties as one dimensional coordination polymers.
- The increased π back-donation capacity of metal ions to ligands may enhance the extension of the electronic π system and improve NLO properties [65].

The third order NLO properties of the selected compounds were tested by using z-scan technique and the results are discussed in Section 7.3.3. The non-linear optical studies were carried out at the International School of Photonics, CUSAT.

1.3.3. Biomimetic activity of metal complexes of Schiff base

One of the main objectives of bio-inorganic chemist is to establish a correlation between the geometric and electronic structure with its function. The main focus is to develop catalytic reactions through which we can comprehend and mimic the enzymatic functions of the metallo-enzymes. Apart from sketching the mechanistic pathways of such reactions, the long term goal is to design complexes that would be useful as catalysts. Using the knowledge of coordination chemistry, redox potential and electronic factors [66-69], the enzyme donor sites are modelled with small molecule called ligands, which are then incorporated with metals to form complexes that are probed as structural and functional models.

The catechol oxidase enzyme has a type-III active site and catalyzes the oxidation of dioxolenes (catechols) to the corresponding *o*-quinones. This enzyme lodges a dicopper(II) moiety which acts as the active site and therefore, efforts have been channelized to design complexes with similar ligand environment [70-73]. Catecholase activity is largely based on structural factors and the researchers all over the world are trying to establish a general structure-activity correlation which is difficult. Metal-metal separation, electrochemical properties of the complexes, influence of ligand structure or exogenous bridging ligand are some of the structural parameters that affect the activity. The variation in the activity with subtle changes in the electronic factors suggests that the synergism of the ligand and the metal renders a strong effect on the affinity for substrate and in addition the change in metal also changes oxygen affinity.

In nature, copper(II) containing enzyme catechol oxidase generates water as a byproduct through four electron reduction of oxygen, while in the case of biomimetic copper(II) complexes the reaction of dioxygen with the catalyst in presence of substrate scarcely generates water and mostly performs the two electron reduction of oxygen to generate hydrogen peroxide during the oxidation of catechol to *o*-quinone [74].

1.4. Theory behind the effect of solvents on the coordination geometry of the complexes

Solvatochromic studies were carried out in order to investigate the effect of solvents on the coordination geometry of the complexes. Here, the solvents were chosen on the basis of the donor number, a parameter which actually indicates the coordinating ability of the solvent. In most of the copper complexes, the axially bound ligands will be weak compared to the equatorial ones due to the greater repulsion from the electron pair residing in $d_{x^2-y^2}$. Hence the solvents will try to occupy the axial sites and this ability is a function of the donor power of the solvents. In other words, the donor number is a measure of the (axial) ligand field strength.

The electronic spectrum of the Cu(II) complex shows one broad $d-d$ band in the visible region, corresponding to the excitation of an electron to the "hole" in $d_{x^2-y^2}$ from the remaining four orbitals. For a fixed set of axial ligands, the position (ν_{\max}) of this band is shifted to blue with an increase in ligand field strength of the equatorial ligands. Here, the repulsion between the equatorial ligands and the electron in $d_{x^2-y^2}$ increases, so that this electron will become more and more energy-rich and unstable. This electron can't escape into the d_{z^2} orbital and no other electron will occupy the orbital due to strong repulsion. Thus, more energy is required for excitation, shifting the ν_{\max} to blue in the order of increasing ligand field strength of the equatorial ligands.

For a fixed set of equatorial ligands, the band is shifted to red with increase in strength of the axial field ligands. In this case, the electron pair in d_{z^2} (and, to a lesser extent, those in d_{xz} and d_{yz}) is repelled and instabilized more strongly by the axial ligands of higher ligand field strength. As a result less energy is needed to excite electrons to hole in $d_{x^2-y^2}$ which shifts ν_{\max} to red [75].

1.4.1. Effect of solvents on square planar structure

Square planar geometry in solution phase have the solvent molecules loosely bound around Cu(II) ion in axial sites. The repulsion between the axial ligand (i.e. solvent) and the d_{z^2} electrons becomes so strong that it tends to avoid it by undergoing hybridization with the 4s and 4p orbitals. The electron pair can then occupy one of these hybrid orbitals, pointing away from the ligand. Thus the metal ion is pulled out of the plane of the chelate to yield the square pyramidal structure. The possibility of coordination of a ligand from below the plane becomes difficult due to strong repulsion between the ligand and the displaced electron pair. Therefore, on solvation the square planar geometry can become a square pyramidal one [Fig. 1.1].

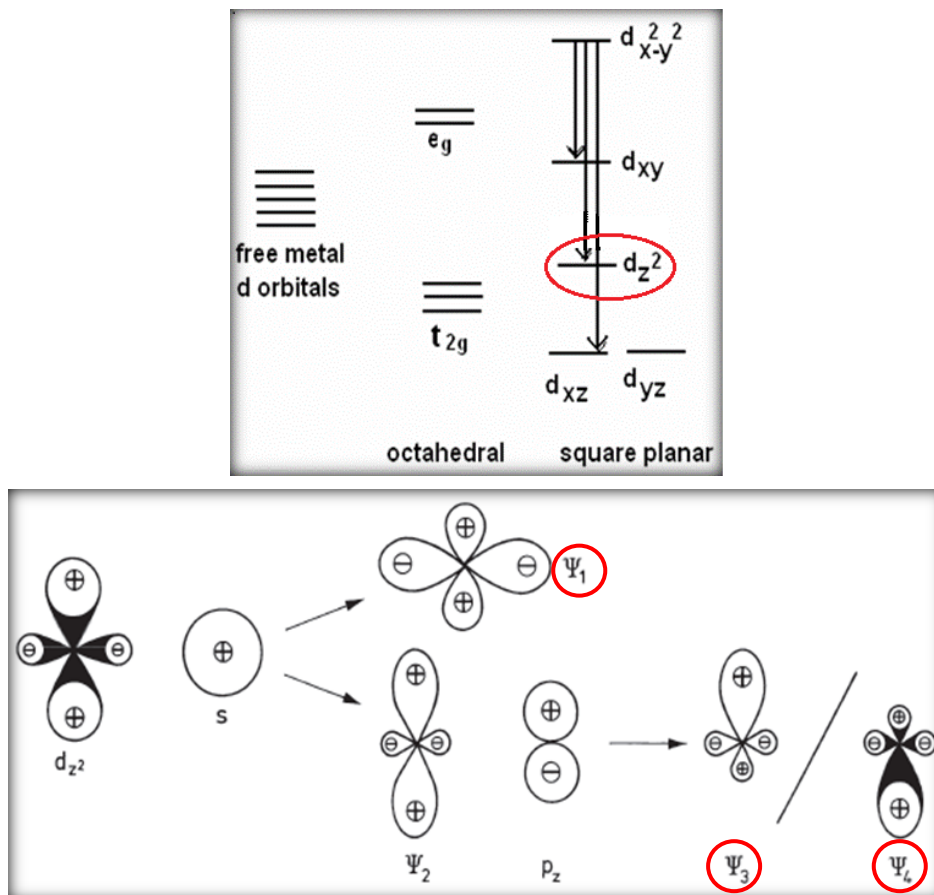


Fig. 1.1. The pictorial representation of the crystal field splitting in square planar geometry and the hybridisation of d_{z^2} orbital.

1.4.2. Effect of solvents on square pyramidal structure

Some solvent molecules will surround the X^- ion coordinated to the chelate plane, probably on top of a square pyramidal structure, and pull out the anion from the coordination sphere. Other solvent molecules will then try to attack the Cu(II) ion directly to form a solvated chelate cation [Fig. 1.2].

On dissolving the complexes in solvents of varying donor numbers, there arises a competition between the solvents and the anions for the axial site. In our complexes, the axial site is occupied by the pseudohalide ions and their linear

π conjugated structure will make them more solvated. Thus, pseudohalides are weaker ligands than the halide ions in organic solvents, [76,77] thereby making the replacement of anions by solvents easy.

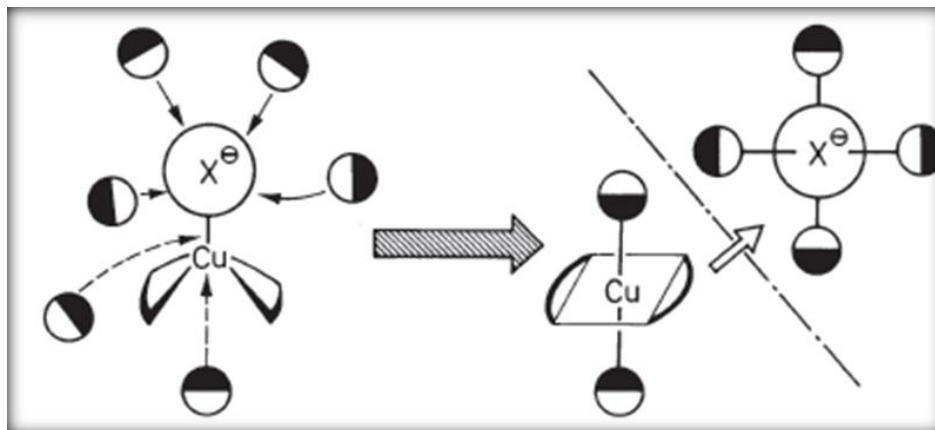


Fig. 1.2. Pictorial representation of solvation of anion followed by change in geometry.

1.5. Scope and objectives of the present study

The thesis embodies the work done to meet the following objectives -

- 1) Synthesis of copper(II) metal complexes from various N_2O tridentate Schiff base systems and various pseudohalides, with the focus laid on the isolation of single crystals.
- 2) To study the
 - a) Effect of solvents on the intra-ligand and charge-transfer transitions
 - b) Effect of solvents on the geometry of the complex species.
- 3) To study and substantiate the structural variations of the tridentate complex species on the basis of spectroscopic studies.
- 4) To assess the DNA binding and cleavage activity.
- 5) To study the third order NLO activity of the complexes.
- 6) To study the catecholase like ability of copper(II) dimeric complex.

1.6. Physical measurements

1.6.1. Spectral methods

1.6.1.1. Infrared spectroscopy

Different bonds have different vibrational frequencies and therefore the presence of such bonds can be easily identified from its characteristic frequency appearing as an absorption band in the infrared spectrum. In the case of coordination complexes, the ligand based vibrations, metal-ligand vibrations and the formation of new bonds can be easily assessed by this technique. The changes occurring as a result of complexation will affect the vibrational modes of bonds, which is reflected in the nature of the spectrum. Also, the characteristic infrared absorptions associated with each functional group can be used to deduce the presence of such groups in complexes.

Infrared spectra of the compounds were recorded on a JASCO FT-IR-5300 Spectrometer in the 4000-400 cm^{-1} range using KBr pellets at the Department of Applied Chemistry, CUSAT, Kochi, India. The azomethine bond formation, presence of pseudohalides and the mode of their coordination (monodentate/bidentate) in complexes are identified from their IR data.

1.6.1.2. Electronic spectroscopy

This is based on the fact that electronic transitions occur between levels whose energy separations correspond to wavelengths characteristic of visible and ultraviolet region of the spectrum. Factors like geometry of the complex, nature of the bonded ligands and the oxidation state of the central metal atom can alter the gap between the energy levels, thereby reflecting in the electronic spectra.

The absorption spectra of a complex can be due to any of the following reasons:

- a) Ligand spectra: These are the intraligand transitions that appear even after complexation, with a slight shift in its position and intensity from the free ligand.

- b) Charge-transfer spectra: It can be of either ligand to metal (LMCT) or metal to ligand (MLCT) type and it involves transitions between orbitals that mainly belong to metal and orbitals that belong to ligand. This is an evidence for complexation.
- c) Ligand-field spectra: The *d* orbitals of the metal which are split by the influence of the ligand field produces ligand-field spectra; these are otherwise called *d-d* spectra. The nature and the region of absorption of the *d-d* spectra can be used to identify the metal present in the complex.

The electronic spectra of the compounds were recorded in solvents of varying polarity/donor number (methanol, tetrahydrofuran, ethyl acetate, acetone, acetonitrile, toluene and chloroform, DMSO, DCM) on a Thermo Scientific Evolution 220 UV-vis Spectrophotometer in the 200-900 nm range at the Department of Applied Chemistry, CUSAT, Kochi, India. For recording the spectra in solution, quartz cuvettes with a path length of 1 cm is used. Solvatochromic studies were carried out so as to perceive the effect of solvents on the absorption spectra.

1.6.1.3. EPR spectroscopy

EPR spectroscopy is the branch of absorption spectroscopy that utilizes microwave frequency so as to probe the electronic structure of paramagnetic molecules. The ESR signature of a complex is used to gain information about the metal ligand bonding, unpaired electron distribution and spatial disposition of ligands around the central metal ion. Several microwave frequencies like S-band (3.5 GHz), X-band (9.25 GHz), K-band (20 GHz), Q-band (35 GHz) and W-band (95 GHz) are available. ESR spectrometer operating in X-band frequency is used.

EPR spectra can be recorded by two modes

- a. CW-EPR spectroscopy (CW- continuous wave)
- b. Pulsed-EPR spectroscopy

The primary coordination sphere (inner sphere) of the complex consists of the central Cu(II) ion and the directly coordinating atoms (like N, O or S). The CW-EPR spectroscopy is sensitive to the identity and the number of equatorially coordinating atoms and this interaction is reflected as a change in the CW-EPR parameters like g_{\parallel} and A_{\parallel} . Whereas the interaction between the axially coordinating atoms and the central ion is relatively weak [78].

The secondary coordination sphere (outer sphere) includes non-coordinating atoms linked to central metal ion *via* multiple chemical bond. The interactions between the central metal ion and an atom with non-zero spin in the outer sphere is detected by pulsed-EPR spectroscopy.

The number, type and the electronegativity of the equatorially aligned coordinating atoms will influence the hyperfine interaction parameters. As the number of nitrogen atoms increase, g_{\parallel} values tend to decrease and A_{\parallel} will increase. The interaction with the nuclear spins of directly coordinating atoms – known as superhyperfine interactions can also be detected in X-band frequency and is an evidence for the delocalization of the electrons.

The copper(II) ion with a d^9 configuration has an effective spin of $S = 1/2$ and is associated with a spin angular momentum $m_s = \pm 1/2$ leading to a doubly degenerate spin state in the absence of magnetic field. In a magnetic field this degeneracy is lifted and the energy difference between these states is given by $\Delta E = h\nu = g\beta B$ where h is the Planck's constant, ν is the microwave frequency for transition from $m_s = +1/2$ to $m_s = -1/2$, g is the Lande splitting factor (equal to 2.0023 for a free electron), β is the Bohr magneton and B is the magnetic field strength. The copper (II) ion, with an effective spin of $S = 1/2$ couples with nuclear spin of ^{63}Cu ($I = 3/2$) and give rise to four ($2nI + 1 = 4$) hyperfine lines.

The principal g tensor values are used to determine the geometry as well as the nature of bonding in the complexes. The coordination geometry is identified by the overall spectral shape such as the relative position of the peaks with respect to the given magnetic field strength and the splitting between two adjacent peaks [Fig. 1.3].

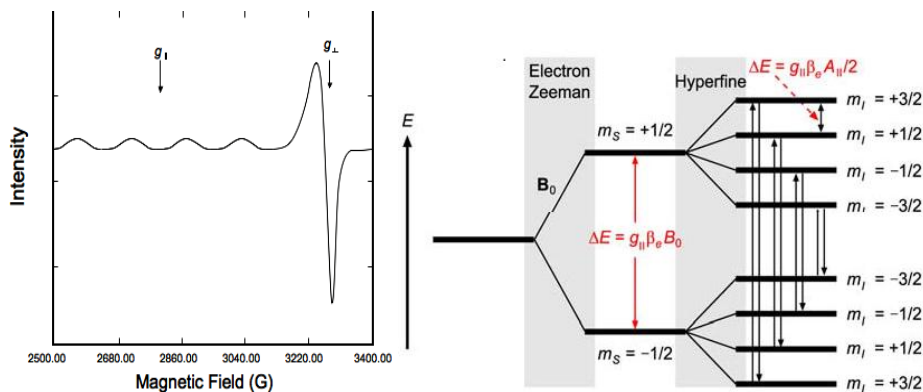


Fig. 1.3. Magnetic field position corresponding to the g tensor values in the spectrum of a Cu(II) complex (left), each of the two Zeeman eigen states further split into four due to hyperfine interaction (right).

Geometry of the complexes

- For coordination geometries corresponding to elongated octahedron, square pyramid or square planar, the ground state is $d_{x^2-y^2}$ and $g_{\parallel} > g_{\perp} > g_e$
- When it is compressed octahedron or trigonal bipyramid, the ground state becomes d_{z^2} and $g_{\perp} > g_{\parallel} > g_e$. [79].

Nature of bonding

As putforth by Kivelson and Neiman,

- $g_{\parallel} \geq 2.3$ for an ionic environment and it is less than 2.3 for covalent environment. The higher g values for our complexes are also an indication of covalent nature of bond between metal ion and ligand [80].
- The geometric parameter G , a measure of the exchange interaction between the copper centres in the polycrystalline state is calculated using the equation, $G = g_{\parallel} - 2.0023 / g_{\perp} - 2.0023$ for axial spectra and the G values less than 4.4 suggests $d_{x^2-y^2}$ ground state with considerable exchange coupling [81,82].

c) The bonding parameters α^2 , β^2 and γ^2 may be regarded as measures of covalency of the in-plane σ bonds, in-plane π bonds and out-of-plane π bonds respectively. The value of the in-plane σ bonding parameter α^2 , is a measure of the fraction of the unpaired electron density located on the copper ion and is estimated from the expression, $\alpha^2 = -A_{\parallel} / 0.036 + (g_{\parallel} - 2.0023) + 3/7 (g_{\perp} - 2.0023) + 0.04$. The values of the bonding parameters less than 1 (= 1 for pure ionic character) indicate that the metal-ligand bonds are partially ionic and partially covalent in nature.

d) The orbital reduction factors, $K_{\parallel}^2 = \alpha^2\beta^2$ and $K_{\perp}^2 = \alpha^2\gamma^2$ are calculated using the following expressions,

$$K_{\parallel}^2 = (g_{\parallel} - 2.0023) E_{d-d} / 8\lambda_o$$

$$K_{\perp}^2 = (g_{\perp} - 2.0023) E_{d-d} / 2\lambda_o$$

where λ_o represents the spin orbit coupling constant with a value of -828 cm^{-1} [83,84].

- For pure σ bonding, $K_{\parallel} \approx K_{\perp} \approx 0.77$
- For in-plane π bonding, $K_{\parallel} < K_{\perp}$
- For out of-plane π bonding, $K_{\perp} < K_{\parallel}$ [85]

The EPR spectra of the complexes in the solid state at 298 K and in DMF at 77 K were recorded on a Varian E-112 spectrometer using TCNE as the standard with 100 kHz modulation frequency, 2 G modulation amplitude and 9.1 GHz microwave frequency at the SAIF, IIT Bombay, India. Some of the EPR spectra are simulated using EasySpin [86].

1.6.1.4. Fluorescence spectroscopy

A Jablonski diagram can be used to describe the process involved in fluorescence and phosphorescence [Fig. 1.4].

The singlet ground, first and second excited states are depicted as S_0 , S_1 and S_2 respectively and each of these levels have a number of vibrational states,

labelled 0, 1, 2 etc. and the fluorophores can exist in these states. Transitions between the levels occur in a time of about 10^{-15} s, a time too short for the displacement of nuclei (Franck-condon principle) to take place. Absorption and emission typically occur from molecules with the lowest vibrational energy.

Processes involved

Light absorption excites the fluorophore to some higher vibrational levels of either S_1 or S_2 . The excited molecules usually relax to the lowest vibrational state of S_1 , by a process called internal conversion (occurs in 10^{-12} s) and fluorescence occurs from this lowest state.

Return from the lowest vibrational state of S_1 to that of the ground state results in emission spectrum and the relaxation to the excited vibrational levels of the ground state (S_0) is the reason for the vibrational structure in the emission spectrum.

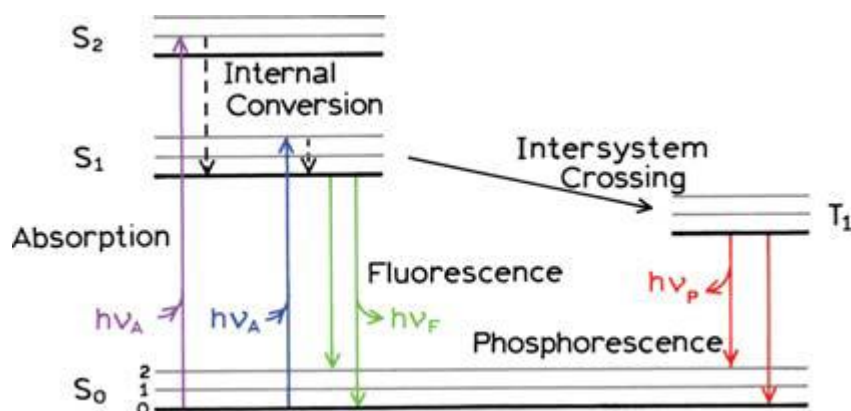


Fig. 1.4. One form of a Jablonski diagram.

By examining the energy and the intensity of the emitted photons as it drops down to the ground state, we can draw a picture about the structure of the vibrational levels. Fluorescence spectral data are presented as the emission spectra. A fluorescence emission spectra is a plot of the fluorescence intensity versus wavelength (nm).

Excitation spectrum: The excitation light is scanned through different wavelengths while keeping the emission light at constant wavelength.

Emission spectrum: The different wavelengths of fluorescent light emitted by a sample are experimentally measured by maintaining a constant excitation wavelength.

The photoluminescence spectra were recorded in Thermo-Fischer Variaskan Flash at the Department of Chemical Oceanography and in Horiba Scientific Fluoromax-4 Spectrofluorimeter at the School of Pure and Applied Physics, M. G. University, Kottayam. Quantum yield studies were done in Shimadzu RF-5301 PC spectrofluorimeter at the School of Environmental Sciences, CUSAT.

The fluorescence quantum yield was determined using 9,10-diphenylanthracene (0.90) in cyclohexane (refractive index, $\eta = 1.4266$) as a reference. The complexes were dissolved in acetonitrile medium (refractive index, $\eta = 1.3441$). The emission spectra was recorded by exciting the samples as well as the reference at the same wavelength, maintaining nearly equal absorbance (~ 0.06). The area of the emission spectrum was integrated using the software available in the instrument and the quantum yield was calculated according to the equation,

$$\Phi_s = \Phi_r \frac{A_s I_r \eta_s^2}{A_r I_s \eta_r^2}$$

Where Φ_s and Φ_r are the fluorescence quantum yield of the sample and reference, respectively. A_s and A_r are the respective absorbances at the wavelength of excitation, I_s and I_r correspond to the areas under the fluorescence curve; η_s and η_r are the refractive index values for the sample and reference, respectively.

1.6.2. Elemental analysis

Elemental analyses of carbon, hydrogen and nitrogen present in all the compounds were done on a Vario EL III CHNS elemental analyzer at the Sophisticated Analytical Instrument Facility, Cochin University of Science and Technology, Kochi-22, Kerala, India. This information is important to determine the purity of synthesized compounds.

1.6.3. Thermal analysis

Thermal methods of analysis involves those techniques in which a change in physical or chemical properties of a substance are measured as a function of temperature.

i) Thermogravimetric Analysis (TGA)

Here, the mass of the sample in a controlled atmosphere is recorded continuously as a function of temperature or time as the temperature of the sample is increased. A plot of mass or mass percentage as a function of time is called a thermogram or thermal decomposition curve. TGA gives a quantitative information about the mass loss associated with a transition. The changes in mass are as a result of the rupture or formation of chemical bonds at elevated temperatures and loss of some volatile products. TGA is useful in determining the

- Moisture content
- Decomposition, oxidation process
- Physical processes like vaporization, sublimation and desorption.

ii) Differential Thermal Analysis (DTA)

Here, the first derivative of mass change with respect to time is recorded as a function of time or temperature. The derivative curve is obtained from TG curve either by manual differentiation or the electronic differentiation of the TG signals and the area of the DTG curve at any temperature gives the rate of mass change at that temperature. DTA is a qualitative technique where difference in temperature is measured. It is used to study decomposition temperatures, phase transitions, melting, crystallization points and thermal stability.

iii) Differential Scanning Calorimetry (DSC)

This is a quantitative technique, which measures the difference in energy. The heat flow into the sample and reference is measured while the sample temperature is changed at a constant rate. A typical DSC

thermogram displays several processes that occur as the temperature is changed. An increase in heat flow signifies an exothermic process and a decrease indicates an endothermic process.

TG-DTG analyses of the complexes were carried out in a Perkin Elmer Pyris Diamond TG/DTA analyzer under nitrogen at a heating rate of 10 °C min⁻¹ in the 50-700 °C range at the Sophisticated Analytical Instrument Facility, CUSAT, Kochi, India.

1.6.4. Single crystal X-ray diffraction studies

The experimental technique which is of greatest importance in revealing the structure of crystals is X-ray diffraction. Single-crystal X-ray diffraction is a non-destructive analytical technique which provides detailed information about the internal lattice of crystalline substances, including unit cell dimensions, bond-lengths, bond-angles and details of site-ordering. Directly related is single-crystal refinement, where the data generated from the X-ray analysis is interpreted and refined to obtain the crystal structure. X-ray diffraction is now a common technique for the study of crystal structures and atomic spacing. X-ray diffraction is based on the constructive interference of monochromatic X-rays on a crystalline sample and it happens when conditions satisfy Bragg's Law ($n\lambda = 2d \sin\theta$). It relates the wavelength of the electromagnetic radiation to the diffraction angle and the lattice spacing in the crystalline sample.

Single crystal X-ray diffraction studies of the compounds were carried out using Bruker SMART APEXII CCD diffractometer equipped with a graphite crystal, incident-beam monochromator and a fine focus sealed tube with Mo K α ($\lambda = 0.71073 \text{ \AA}$) as the X-ray source at the SAIF, Cochin University of Science and Technology, Kochi, Kerala, India. The unit cell dimensions were measured and the data collections were performed at 296(2) K. Bruker SMART software was used for data acquisition and Bruker SAINT software for data integration [87]. Absorption corrections were carried out using SADABS based on Laue symmetry using equivalent reflections [88]. The structure was solved by direct methods and refined by full-matrix least-squares calculations with the WinGX

[89a] and the SHELXL-97 software package [89b]. The molecular and crystal structures were plotted using DIAMOND version 3.2g [89c] and ORTEP-3 for Windows [89a].

References

- [1] E. Sinn, C.M. Harris, *Coord. Chem. Rev.* **1969**, *4*, 391.
- [2] S.A. Kuby, *Mechanism of Enzyme Action*; CRC Press: Boca Raton, FL, **1990**, *2*.
- [3] H. Nozaki, H. Takaya, S. Moriuti, R. Noyori, *Tetrahedron* **1968**, *24*, 3655.
- [4] B.J. Holliday, C.A. Mirkin, *Angew. Chem. Int. Ed.* **2001**, *40*, 2022.
- [5] P.K. Bhaumik, K. Harms, S. Chattopadhyay, *Polyhedron* **2014**, *67*, 181.
- [6] P.K. Bhaumik, K. Harms, S. Chattopadhyay, *Inorg. Chim. Acta* **2013**, *405*, 400.
- [7] C. Biswas, S. Chattopadhyay, M.G.B. Drew, A. Ghosh, *Polyhedron* **2007**, *26*, 4411.
- [8] S. Jana, P.K. Bhaumik, K. Harms, S. Chattopadhyay, *Polyhedron* **2014**, *78*, 94.
- [9] (a) P. Metrangolo, G. Resnati, *Halogen Bonding : Fundamentals and Applications*; ed. *Structure and Bonding*, Springer Verlag: Berlin Heidelberg, **2008**, *126*.
(b) P. Metrangolo and G. Resnati, *Science* **2008**, *321*, 918.
- [10] Y. Nair, M. Sithambaresan, M.R.P. Kurup, *Acta Crystallogr., Sect. E: Struct. Rep. Online* **2012**, *68*, 2709.
- [11] P. Bhowmik, S. Chattopadhyay, M.G.B. Drew, A. Ghosh, *Inorg. Chim. Acta* **2013**, *395*, 24.
- [12] P. Bhowmik, S. Chattopadhyay, A. Ghosh, *Inorg. Chim. Acta* **2013**, *396*, 66.
- [13] L. Wang, R.B. Huang, L.S. Long, L.S. Zheng, E.B. Wang, Z.X. Xie. *J. Coord. Chem.* **2005**, *58*, 1439.

- [14] B. Sarkar, M.S. Ray, M.G.B. Drew, C.Z. Lu, A. Ghosh. *J. Coord. Chem.* **2007**, *60*, 2165.
- [15] Z.L. You, X.L. Ma, S.Y. Niu. *J. Coord. Chem.* **2008**, *61*, 3297.
- [16] S. Sasmal, S. Hazra, P. Kundu, S. Dutta, G. Rajaraman, E.C. Sañudo, S. Mohanta, *Inorg. Chem.* **2011**, *50*, 7257.
- [17] S. Sasmal, S. Hazra, P. Kundu, S. Majumder, N. Aliaga-Alcalde, E. Ruiz, S. Mohanta, *Inorg. Chem.* **2010**, *49*, 9517.
- [18] C. Adhikarya, S. Koner, *Coord. Chem. Rev.* **2010**, *254*, 2933.
- [19] A. Matuz, M. Giorgi, G. Speier, J. Kaizer, *Polyhedron* **2013**, *63*, 41.
- [20] K.D. Karlin, Z. Tyeklar, *Bioinorganic Chemistry of Copper*, Chapman & Hall, New York, **1993**.
- [21] R.C. Maji, S.K. Barman, S. Roy, S.K. Chatterjee, F.L. Bowles, M.M. Olmstead, A.K. Patra, *Inorg. Chem.* **2013**, *52*, 11084.
- [22] G. Csire, J. Demjen, S. Timari, K. Varnagy, *Polyhedron* **2013**, *61*, 202.
- [23] Q. Gao, Y.B. Xie, M. Thorstad, J.H. Sun, Y. Cui, H.C. Zhou. *Cryst. Eng. Comm*, **2011**, *13*, 6787.
- [24] C. Biswas, M.G.B. Drew, E. Ruiz, M. Estrader, C. Diaz, A. Ghosh. *Dalton Trans.* **2010**, *39*, 7474.
- [25] M. Zbiri, S. Saha, C. Adhikary, S. Chaudhuri, C. Daul, S. Koner. *Inorg. Chim. Acta* **2006**, *359*, 1193.
- [26] A.Y. Robin, K.M. Fromm, *Coord. Chem. Rev.* **2006**, *250*, 2127.
- [27] S. Mukherjee, P.S. Mukherjee, *Acc. Chem. Res.* **2013**, *46*, 2556.
- [28] M. Layek, M. Ghosh, S. Sain, M. Fleck, P.T. Muthiah, S.J. Jenniefer, J. Ribas, D. Bandyopadhyay. *J. Mol. Struct.* **2013**, *422*, 1036.
- [29] S. Sain, R. Saha, G. Pilet, D. Bandyopadhyay. *J. Mol. Struct.* **2010**, *350*, 984.
- [30] J.W. Steed, J.L. Atwood. *Supramolecular Chemistry*, Wiley, New York **2000**.
- [31] C. Metcalfe, J.A. Thomas, *Chem. Soc. Rev.* **2003**, *32*, 215.

- [32] A. Silvestri, G. Barone, G. Ruisi, M.T. Lo Giudice, S. Tumminello, *J. Inorg. Biochem.* **2004**, *98*, 589.
- [33] F. Liang, P. Wang, X. Zhou, T. Li, Z. Li, H. Lin, D. Gao, C. Zheng, C. Wu, *Bioorg. Med. Chem. Lett.* **2004**, *14*, 1901.
- [34] C. Jones, J. Thornback, *Medicinal Applications of Coordination Chemistry*, Royal Society of Chemistry, Cambridge, **2007**.
- [35] B. Garcia, J. Garcia-Tojal, R. Ruiz, R. Gil-Garcia, S. Ibeas, B. Donnadieu, J.M. Leal, *J. Inorg. Biochem.* **2008**, *102*, 1892.
- [36] W. Han Ang, P.J. Dyson, *Eur. J. Inorg. Chem.* **2006**, *2006*, 4003.
- [37] N. Busto, J. Valladolid, C. Aliende, F.A. Jalon, B.R. Manzano, A.M. Rodriguez, J.F. Gaspar, C. Martins, T. Biver, G. Espino, J.M. Leal, B. Garcia, *Chem.-Asian J.* **2012**, *7* 788.
- [38] M. del, C. Mejia Vazquez, S. Navarro, *New Approaches in the Treatment of Cancer*, Nova Science Publishers, New York, **2010**.
- [39] A.E.-M.M. Ramadan, *J. Mol. Struct.* **2012**, *56*, 1015.
- [40] K. Pothiraj, T. Baskaran, N. Raman, *J. Coord. Chem.* **2012**, *65*, 2110.
- [41] B.M. Zeglis, V.C. Pierre, J.K. Barton, *Chem. Commun.* **2007**, 4565.
- [42] N. Farrell, in: J.A. McCleverty, T.J. Meyer (Eds.), *Comprehensive Coordination Chemistry II*, Pergamon, Oxford, **2003**, 809.
- [43] S. Komeda, T. Moulaei, K.K. Woods, M. Chikuma, N.P. Farrell, L.D. Williams, *J. Am. Chem. Soc.* **2006**, *128*, 16092.
- [44] R. Ruiz, B. Garcia, J. Garcia-Tojal, N. Busto, S. Ibeas, J.M. Leal, C. Martins, J.F. Gaspar, J. Borrás, R. Gil-Garcia, M. Gonzalez-Alvarez, *J. Biol. Inorg. Chem.* **2010**, *15*, 515.
- [45] N. Busto, B. Garcia, J.M. Leal, J.F. Gaspar, C. Martins, A. Boggioni, F. Secco, *Phys. Chem. Chem. Phys.* **2011**, *13*, 19534.
- [46] N.D. Hadjiliadis, E. Sletten, *Metal Complexes-DNA Interactions* Wiley-Blackwell, Chichester, **2009**.

- [47] D. Desbouis, I.P. Troitsky, M.J. Belousoff, L. Spiccia, B. Graham, *Coord. Chem. Rev.* **2012**, 256, 897.
- [48] A.A. Holder, *Annu. Rep. Prog. Chem. Sect. A: Inorg. Chem.* **2012**, 108, 350.
- [49] E. Alessio, *Bioinorganic Medicinal Chemistry*, Wiley-VCH, Weinheim, **2011**.
- [50] F.R. Keene, J.A. Smith, J.G. Collins, *Coord. Chem. Rev.* **2009**, 253, 2021.
- [51] I. Ott, *Coord. Chem. Rev.* **2009**, 253, 1670.
- [52] P. Yang, M. Guo, *Coord. Chem. Rev.* **1999**, 189, 185.
- [53] C. Avendaño, J.C. Menendez, in: *Medicinal Chemistry of Anticancer Drugs*, Elsevier, Amsterdam, **2008**, 199.
- [54] (a) Q. Jiang, N. Xiao, P. Shi, Y. Zhu, Z. Guo, *Coord. Chem. Rev.* **2007**, 251, 1951.
- (b) D.S. Sigman, A. Mazumder, D.M. Perrin, *Chem. Rev.* **1993**, 93, 2295.
- (c) J.C. Joyner, J. Reichfield, J.A. Cowan, *J. Am. Chem. Soc.* **2011**, 133, 15613.
- [55] F. Mancin, P. Scrimin, P. Tecilla, *Chem. Commun.* **2012**, 48, 5545.
- [56] C. Angelé-Martínez, C. Goodman, J. Brumaghim *Metallomics* **2014**, 6, 1358.
- [57] Y.R. Shen, *The Principles of Nonlinear Optics*, S.J. Gu, Translator; Science, China, **1987**.
- [58] F. Castet, V. Rodriguez, J.-L. Pozzo, L. Ducasse, A. L. Plaquet and B. Champagne, *Acc. Chem. Res.* **2013**, 46, 2656.
- [59] P.C. Ray, *Chem. Rev.* **2010**, 110, 5332.
- [60] D. Espa, L. Pilia, L. Marchiò, M. Pizzotti, N. Robertson, F. Tessore, M. L. Mercuri, A. Serpe, P. Deplano, *Dalton Trans.* **2012**, 41, 12106.
- [61] K.A. Green, M.P. Cifuentes, M. Samoc, M.G. Humphrey, *Coord. Chem. Rev.* **2011**, 255, 2530.
- [62] J.C. Tan, A.K. Cheetham, *Chem. Soc. Rev.* **2011**, 40, 1059.

- [63] (a) H.W. Hou, Y.L. Wei, Y.T. Fan, C.X. Du, Y. Zhu, Y.L. Song, Y.Y. Niu, X.Q. Xin, *Inorg. Chim. Acta* **2001**, 319, 212.
- (b) O.R. Evans, W.B. Lin, *Chem. Mater.* **2001**, 13, 3009.
- (c) O.R. Evans, W.B. Lin, *Chem. Mater.* **2001**, 13, 2705.
- (d) H.W. Hou, X.R. Meng, Y.L. Song, Y.T. Fan, Y. Zhu, H.G. Lu, C.X. Du, W.H. Shao, *Inorg. Chem.* **2002**, 41, 4068.
- (e) H.W. Hou, Y.L. Wei, Y.L. Song, Y. Zhu, L.K. Li, Y.T. Fan, *J. Mater. Chem.* **2002**, 12, 838.
- [64] (a) D. Narayana Rao, *Opt. Mater.* **2002**, 21, 45.
- (c) Y.Z. Gu, F.X. Gan, S.Q. Wang, H.J. Xu, *Opt. Commun.* **2001**, 197, 501.
- [65] H. Chao, R.H. Li, B.H. Ye, H. Li, X.L. Feng, J.W. Cai, J.Y. Zhou, L.N. Ji, *J. Chem. Soc., Dalton Trans.* **1999**, 3711.
- [66] M. Rolff, J. Schottenheim, H. Decker, F. Tuzcek, *Chem. Soc. Rev.* **2011**, 40, 4077.
- [67] S. Friedle, E. Reisner, S.J. Lippard, *Chem. Soc. Rev.* **2010**, 39, 2768.
- [68] L. Que Jr., W.B. Tolman, *Nature* **2008**, 455, 333.
- [69] P.C.A. Bruijninx, G. van Koten, R.J.M. Klein Gebbink, *Chem. Soc. Rev.* **2008**, 37, 2716.
- [70] A. Martinez, I. Membrillo, V.M. Ugalde-Saldivar, L. Gasque, *J. Phys. Chem. B* **2012**, 116, 8038.
- [71] A. Banerjee, R. Singh, E. Colacio, K.K. Rajak, *Eur. J. Inorg. Chem.* **2009**, 2009, 277.
- [72] A. Banerjee, S. Sarkar, D. Chopra, E. Colacio, K.K. Rajak, *Inorg. Chem.* **2008**, 47, 4023.
- [73] I.A. Koval, C. Belle, K. Selmecezi, C. Philouze, E. Saint-Aman, A.M. Schuitema, P. Gamez, J.L. Pierre, J. Reedijk, *J. Biol. Inorg. Chem.* **2005**, 10, 739.
- [74] S.K. Dey, A. Mukherjee, *Coord. Chem. Rev.* **2016**, 310, 80.

- [75] K. Sane, Y. Fukuda, *Inorganic Thermochemistry in Inorganic Chemistry Concepts*, Springer-Verlag, Berlin, **1987**, 10, 1.
- [76] S. Ahrland, *The Chemistry of Nonaqueous Solvents*, Academic Press, New York **1978**, V A, 1.
- [77] (a) S. Ahrland, *Pure and Appl. Chem.* **1982**, 54, 1451.
(b) S. Ahrland, N. Bjork, *Coord. Chem. Rev.* **1975**, 16, 113.
- [78] J. Peisach, Blumberg, *Arch. Biochem. Biophys.* **1974**, 165, 691.
- [79] E. Garribba, G. Micera, *J. Chem. Educ.* **2006**, 83, 1229.
- [80] D. Kivelson, R. Neiman, *J. Chem. Soc., Dalton Trans.* **1961**, 35, 149.
- [81] E. Manoj, M.R.P. Kurup, A. Punnoose, *Spectrochim. Acta* **2009**, 72, 474.
- [82] B.J. Hathaway, D.E. Billing, *Coord. Chem. Rev.* **1970**, 5, 143.
- [83] B.J. Hathaway, *Structure and Bonding*, Springer Verlag, Heidelberg, **1973**, 60.
- [84] U.L. Kala, S. Suma, S. Krishnan, M.R.P. Kurup, R.P. John, *Polyhedron* **2007**, 26, 1427.
- [85] B.J. Hathaway, *J. Chem. Soc., Dalton Trans.* **1972**, 1196.
- [86] S. Stoll, *Spectral Simulations in Solid-State Electron Paramagnetic Resonance, Ph. D. Thesis*, ETH, Zurich, **2003**.
- [87] SMART and SAINT, Area Detector Software Package and SAX Area Detector Integration Program, Bruker Analytical X-ray; Madison, WI, USA, **1997**.
- [88] SADABS, Area Detector Absorption Correction Program; Bruker Analytical X-ray; Madison, WI, **1997**.
- [89] (a) L.J. Farrugia, *J. Appl. Cryst.* **2012**, 45, 849.
(b) G.M. Sheldrick, *Acta Cryst. A* **2008**, 64, 112.
(c) K. Brandenburg, *Diamond Version 3.2g*, Crystal Impact GbR, Bonn, Germany, **2010**.



Polymeric polymorphs and monomers of pseudohalide incorporated Cu(II) complexes of *N,N*-dimethylethylenediamine and 3,5-dichlorosalicylaldehyde

- 2.1. Introduction
- 2.2. Experimental
- 2.3. Results and discussion

Conspectus

In the present investigation, copper(II) complexes of tridentate [2,4-dichlorido-6-((2-dimethylamino)ethylimino)methyl]phenol] (HL^1) Schiff base system incorporating azido $[Cu(L^1)(N_3)]_n$ (**1a** and **1b**), cyanato $[Cu(L^1)(NCO)]$ (**2**) and thiocyanato $[Cu(L^1)(NCS)]$ (**3**) groups are prepared and characterized by elemental analysis, IR, UV-vis and single crystal X-ray diffraction studies. While the polymeric polymorphs, **1a** and **1b** have a square-pyramidal geometry for the basic unit, complexes **2** and **3** exhibit square planar topology. The polymorphs are one-dimensional helical coordination polymers with azido group in single asymmetric equatorial-axial end-on bridging mode. The interestingly different combinations of intermolecular interactions have resulted in polymorphs **1a** and **1b**. Based on the angular preference, intermolecular distance and the size of Cl atom, type I halogen interactions which are rather rarely observed is also discussed. Solvent effect on the charge-transfer bands and d-d bands are analysed and the former exhibits negative solvatochromic effect while latter a red shift with increasing polarity of solvents.

Solid and solution state optical emission properties are analysed. All the copper complexes emit in the blue region. Thermal analyses have been performed in order to understand the thermal decomposition pattern of the complexes. Spin Hamiltonian and bonding parameters have been calculated from EPR analysis. The g values, calculated for the complexes **1a**, **1b** and **2** in frozen DMF, indicate the presence of an unpaired electron in the $d_{x^2-y^2}$ orbital consistent with a square pyramidal topology whereas that of complex **3** corresponds to a rhombic symmetry.

2.1. Introduction

Herein, we have used the N₂O tridentate Schiff base derived from refluxing *N,N*-substituted ethylenediamine and 3,5-dichlorosalicylaldehyde along with azido, cyanato and thiocyanato ligands. We have obtained two azido linked polymeric polymorphs and two monomeric complexes from 2,4-dichlorido-6-((2-(dimethylamino)ethylimino)methyl)phenol. Only azido ligand produced polymeric complexes revealing its greater ability to bridge over the other. Since not much of experimental work highlighting the halogen interaction is known, our group employed halogen substituted salicylaldehydes to explore more on halogen interactions [1], a new tool for crystal engineers and to discuss the role of various other weak interactions in stabilizing a specific crystal system. The synthesis, spectral characterization, crystal structures, packing interactions (supramolecular assemblies including halogen interactions), photophysical studies and EPR spectral studies are discussed here.

2.2. Experimental

2.2.1. Materials

All chemicals were of reagent grade and purchased from commercial sources. The solvents were purified according to standard procedures. 3,5-Dichlorosalicylaldehyde (Aldrich), *N,N*-dimethyl-1,2-diaminoethane (Aldrich), CuCl₂·2H₂O, CuSO₄·5H₂O, NaN₃, NaCNO, NaSCN (all are BDH, AR quality) were used as received.

The Schiff bases were formed *in situ*.

Caution! Azido compounds are potentially explosive. Although no problems were encountered in the present study, it should be prepared only in small quantities and handled with care.

2.2.2. Synthesis of copper(II) complexes

2.2.2.1. Synthesis of [Cu(L¹)(N₃)]_n (1a)

[HL¹= 2,4-dichlorido-6-((2-(dimethylamino)ethylimino)methyl)phenol]

3,5-Dichlorosalicylaldehyde (0.191 g, 1 mmol) and *N,N*-dimethyl-1,2-diaminoethane (0.088 g, 1 mmol) were dissolved in 10 mL methanol and

refluxed for about an hour. A methanolic solution (10 mL) of copper(II) chloride dihydrate (0.170 g, 1 mmol) was added to the hot reaction mixture. To the resulting deep green solution, sodium azide (0.130 g, 2 mmol) in a MeOH/H₂O (1:9) mixture was added dropwise with continuous stirring and filtered. Suitable single crystals for structure determination by X-ray diffraction were obtained by slow evaporation of the mother liquor in air.

Yield: 0.297 g (81%). *Anal.* Calc. for C₁₁H₁₃Cl₂CuN₅O (365.70): C, 36.13; H, 3.58; N, 19.15 Found C, 36.09; H, 3.55; N, 19.10%.

UV-vis, λ_{\max} /nm ($\epsilon_{\max}/10^3 \text{ M}^{-1}\text{cm}^{-1}$) (acetonitrile): 376 (7.60), 238 (28.54).

2.2.2.2. Synthesis of [Cu(L¹)(N₃)_n] (1b)

[HL¹=2,4-dichlorido-6-((2-(dimethylamino)ethylimino)methyl)phenol]

Complex **1b** was prepared by a method similar to that of complex **1a** except that copper(II) sulfate pentahydrate (0.249 g, 1 mmol) was added to the hot reaction mixture instead of copper(II) chloride dihydrate. To the resulting deep green solution, sodium azide (0.130 g, 2 mmol) in a MeOH/H₂O (1:9) mixture was added dropwise with continuous stirring and filtered. Suitable single crystals for structure determination by X-ray diffraction were obtained by slow evaporation of the mother liquor in air. Complex **1b** was found to be a polymorph of **1a**.

Yield: 0.2123 g (66%). *Anal.* Calc. for C₁₁H₁₃Cl₂CuN₅O (365.70): C, 36.13; H, 3.58; N, 19.15 Found C, 36.11; H, 3.58; N, 19.14%.

UV-vis, λ_{\max} /nm ($\epsilon_{\max}/10^3 \text{ M}^{-1}\text{cm}^{-1}$) (acetonitrile): 376 (8.12), 237 (31.27).

2.2.2.3. Synthesis of [Cu(L¹)(NCO)] (2) & [Cu(L¹)(NCS)] (3)

[HL¹=2,4-dichlorido-6-((2-(dimethylamino)ethylimino)methyl)phenol]

Complexes **2** and **3** were prepared by a similar method except for the pseudohalides used. A methanolic solution of copper(II) chloride dihydrate (0.170 g, 1 mmol) was used for the synthesis of both complexes. For the preparation of complex **2**, sodium cyanate (0.130 g, 2 mmol) in a MeOH/H₂O

mixture was added dropwise and the resulting solution further stirred for *ca.* 2 h and filtered whilst sodium thiocyanate (0.194 g, 2 mmol) was used for the synthesis of complex **3**. Diffraction quality single crystals for structure determination were obtained by slow evaporation of this mother liquor in air.

Complex 2

Yield: 0.2081 g (54%). *Anal.* Calc. for $C_{11}H_{13}Cl_2CuN_5O$ (365.70): C, 39.41; H, 3.58; N, 11.49.

Found C, 39.20; H, 3.50; N, 11.52%.

UV-vis, λ_{max}/nm ($\epsilon_{max}/10^3 M^{-1}cm^{-1}$) (acetonitrile): 389 (5.16), 238 (25.16).

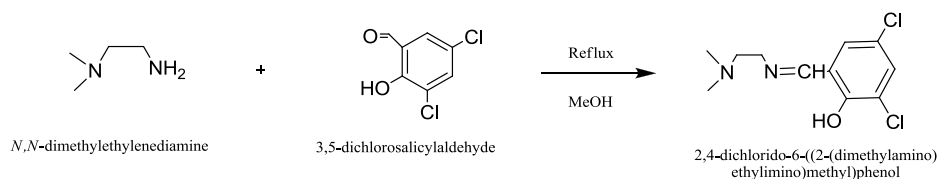
Complex 3

Yield: 0.2368 g (62%). *Anal.* Calc. for $C_{12}H_{13}Cl_2CuN_3OS$ (381.76): C, 37.75; H, 3.43; N, 11.01; S 8.40. Found C, 37.70; H, 3.48; N, 11.05, S 8.35%.

UV-vis, λ_{max}/nm ($\epsilon_{max}/10^3 M^{-1}cm^{-1}$) (acetonitrile): 383 (5.96), 236 (31.45).

2.3. Results and discussion

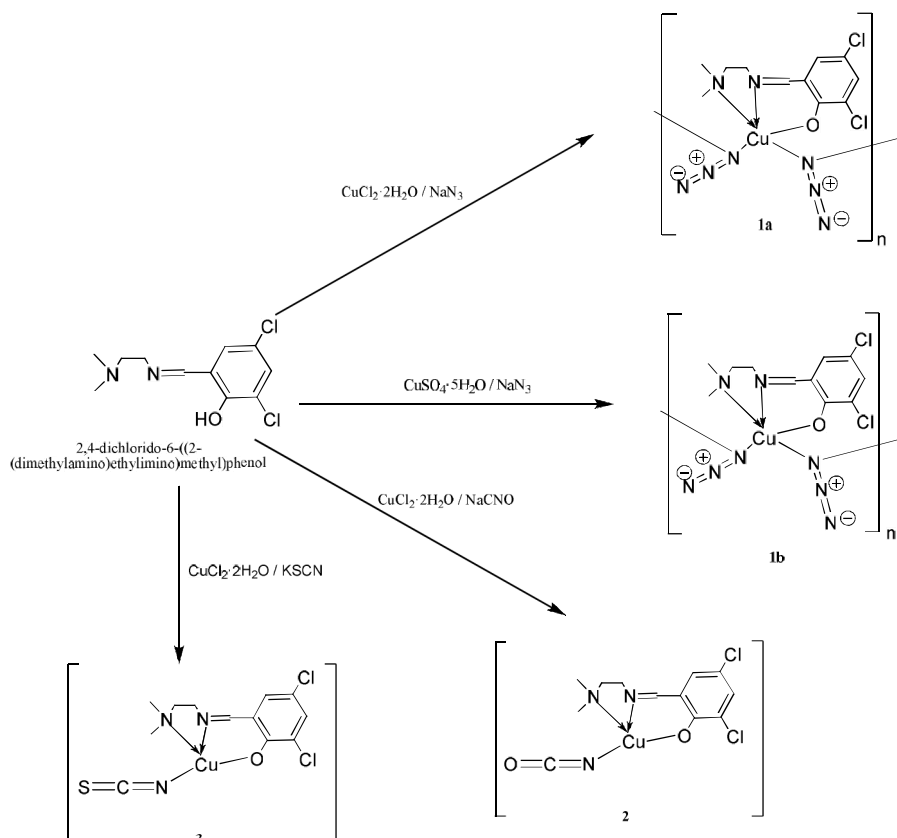
Facile condensation of 3,5-dichlorosalicylaldehyde with *N,N*-dimethyl-1,2-diaminoethane in equimolar ratio (1:1) resulted in the formation of the tridentate Schiff base ligand [Scheme 2.1]. Since the isolation of the Schiff base was difficult, one-pot synthetic strategy was adopted for the preparation of all complexes.



Scheme 2.1. Formation of tridentate Schiff base ligand.

The Schiff-base on reaction with copper(II) chloride dihydrate and copper(II) sulfate pentahydrate, followed by the addition of sodium azide in the ratio 1:1:2 yielded the polymeric polymorphs **1a** and **1b** respectively whereas

the monomeric complexes **2** and **3** were obtained by adding sodium cyanate and sodium thiocyanate respectively, in the same ratio [Scheme 2.2]. The polymorphic complexes showed variation in the cell parameters.



Scheme 2.2. Synthetic route to the complexes.

All the complexes are analytically pure as confirmed from their elemental analysis. They are soluble in polar solvents like methanol, DMF and DMSO.

2.3.1. Spectral characterization

2.3.1.1. IR and electronic spectra

The C=N stretching vibrations for all the four complexes lie in the region $1625\text{--}1634\text{ cm}^{-1}$ [2]. The polymorphic pair shows a single band consistent with the presence of only one type of azido bridge in the structures and this

characteristic strong band at 2045 cm^{-1} can be ascribed to the presence of asymmetric bridging [3a,b]. Moreover, the IR spectra also exhibit peaks at 1319 and 758 cm^{-1} corresponding to symmetric stretching, $\nu_s(\text{N}_3)$ and bending mode $\delta(\text{N}_3)$ of the pseudohalide present [4a]. One sharp and strong band at 2234 cm^{-1} in the IR spectrum of complex **2** indicates the presence of N bonded cyanato group [2]. A band at 2091 cm^{-1} [$\nu_{\text{as}}(\text{NCS})$] along with bands at 1454 cm^{-1} [$\nu_s(\text{NCS})$] are typical of a N-bonded thiocyanato group [4b]. The IR band in the region $2918\text{--}2930\text{ cm}^{-1}$ seen in complexes is assignable to alkyl C–H stretching vibrations [5]. The spectra showing the characteristic peaks are shown in Fig. 2.1.

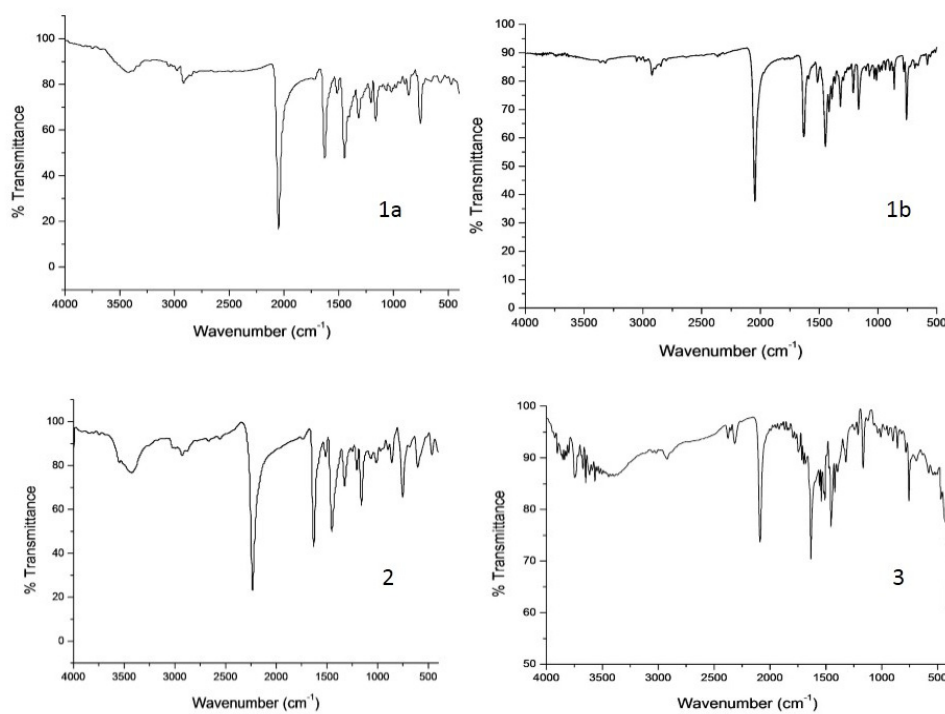


Fig. 2.1. The IR spectra of the complexes **1a**, **1b**, **2** and **3**.

The electronic spectra of all the four complexes were recorded in acetonitrile in the 200-1000 nm region at room temperature. The electronic spectra of all complexes showed broad bands in the high energy 370-390 nm region consistent with the LMCT bands comprising of transitions from the coordinating atoms of respective pseudohalides to the metal centre [3b,6] apart from O→Cu, N→Cu transitions. The bands *ca.* 235 nm correspond to intraligand transitions [7a,b]. The high ϵ values for these bands are supportive of the charge transfer and intraligand transitions [Table 2.17]. The absorption at low energy region, 590-650 nm corresponds to *d-d* transition. For complexes **1a** and **1b**, peak at 593 nm typical of a square pyramidal environment of the Cu(II) centre is seen, enclosing ${}^2A_{1g} \leftarrow {}^2B_{1g}$, ${}^2B_{2g} \leftarrow {}^2B_{1g}$, and ${}^2E_g \leftarrow {}^2B_{1g}$ transitions [8,9a,b] and peak *ca.* 630 nm can be assigned to a square-planar environment with transitions ${}^2B_{2g} \leftarrow {}^2B_{1g}$, ${}^2A_{1g} \leftarrow {}^2B_{1g}$ and ${}^2E_g \leftarrow {}^2B_{1g}$ [9a]. It is difficult to interpret the electronic spectra of Cu(II) complexes as they possess flexible stereochemistry due to Jahn-Teller distortion [10].

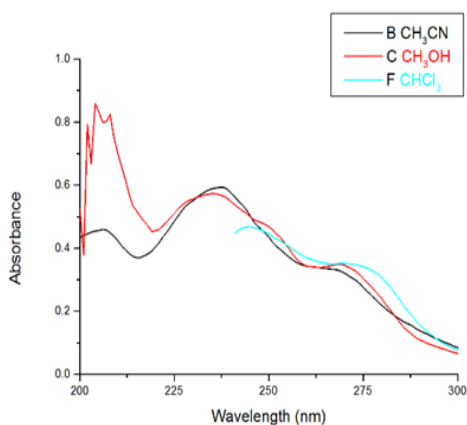
2.3.1.2. Solvatochromic studies

The electronic spectra of all the four complexes were recorded in different solvents of varying polarity to investigate the effect of solvents on the absorption bands (CT and *d-d*) of the copper complexes. Solvents chosen for the study included polar protic (methanol), polar aprotic (tetrahydrofuran, ethyl acetate, acetone and acetonitrile) and non-polar solvents (toluene, chloroform). All the four complexes exhibited interesting solvatochromic behavior.

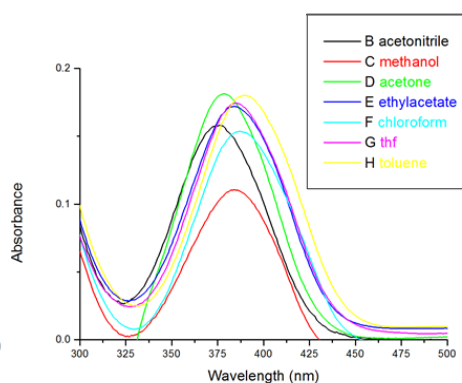
All the complexes were soluble in a wide range of organic solvents that made their solvatochromic study easy. Both charge transfer bands and *d-d* bands exhibited solvatochromism although significant shift in energy was seen for the *d-d* bands.

The charge-transfer and intraligand transitions exhibited negative solvatochromism [Fig. 2.2], though the variation occurs within a narrow range. With increasing solvent polarity, within each classification of solvents (polar

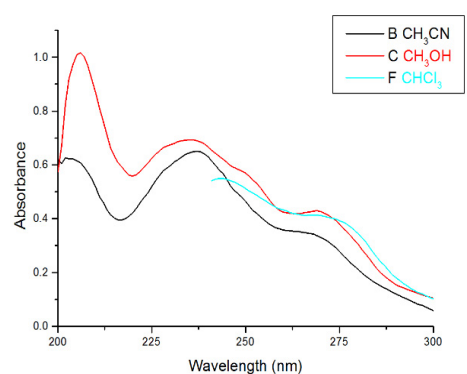
protic, polar aprotic and non-polar), hypsochromic (or blue) shift of these bands were observed. This is called “negative solvatochromism” and it occurs due to differential solvation of the ground and first excited state of the light-absorbing molecule (or its chromophore) : if, with increasing solvent polarity, the ground state molecule is better stabilized by solvation than the molecule in the excited state, negative solvatochromism will result [11]. This is due to a solvent-induced change of the electronic ground state structure from a less dipolar (in non-polar solvents) to a more dipolar chromophore (in polar solvents) with increasing solvent polarity. The λ_{\max} (nm) along with their ϵ ($M^{-1}cm^{-1}$) values in various solvents are tabulated [Table 2.1].



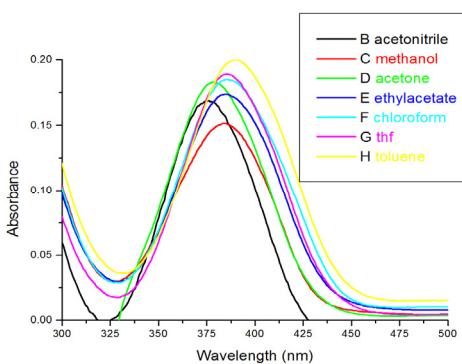
(1a)



(1a)



(1b)



(1b)

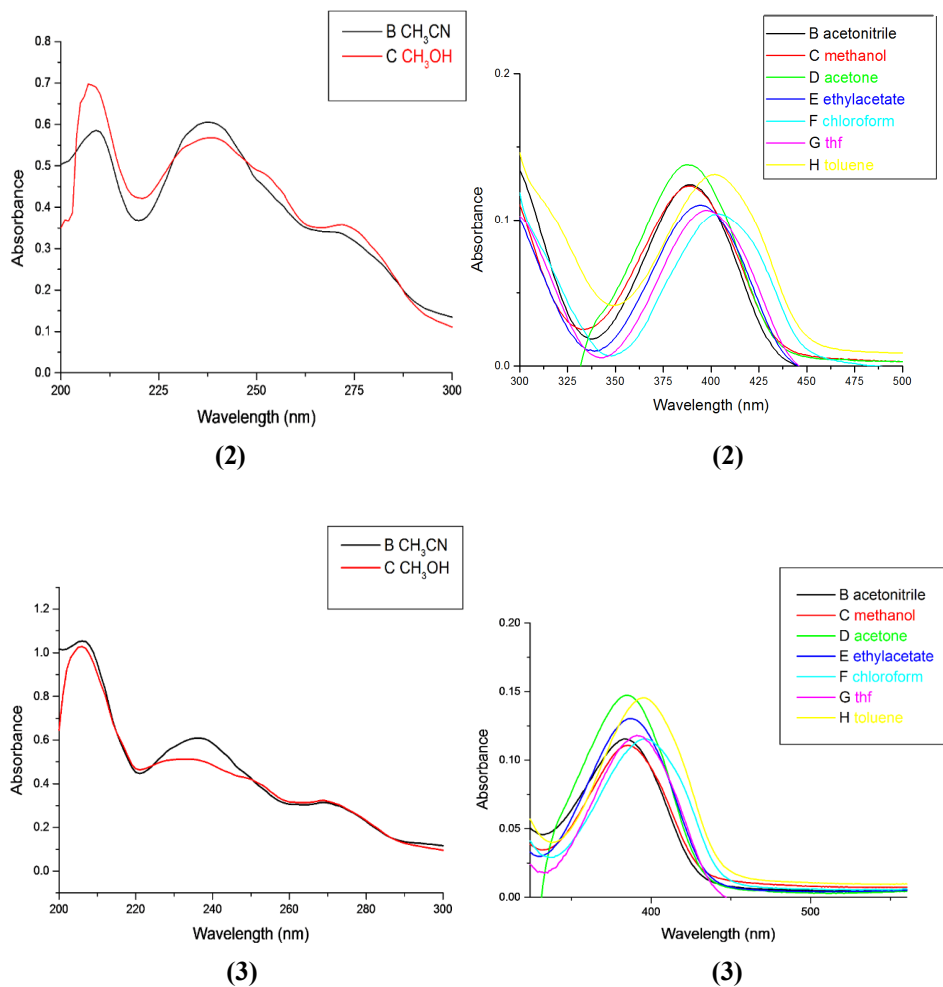


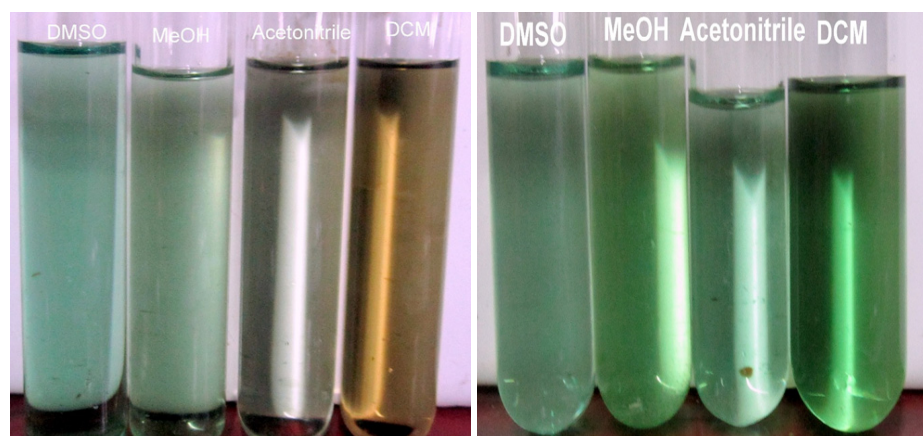
Fig. 2.2. Spectra showing the solvatochromic effects on the intraligand (left) and charge-transfer (right) transitions of the complexes, con: $1 \cdot 10^{-3}$ M).

Table 2.1. The λ_{\max} (nm) values along with their ϵ ($M^{-1}cm^{-1}$) in various solvents

| Polarity Index* | Solvents (decreasing order of polarity) | Complex 1a | | Complex 1b | | Complex 2 | | Complex 3 | |
|-----------------|---|-----------------------|---------------------------------------|-----------------------|---------------------------------------|-----------------------|---------------------------------------|-----------------------|---------------------------------------|
| | | λ_{\max} (nm) | $\epsilon * 10^3$ ($M^{-1}cm^{-1}$) | λ_{\max} (nm) | $\epsilon * 10^3$ ($M^{-1}cm^{-1}$) | λ_{\max} (nm) | $\epsilon * 10^3$ ($M^{-1}cm^{-1}$) | λ_{\max} (nm) | $\epsilon * 10^3$ ($M^{-1}cm^{-1}$) |
| 5.1 | Methanol | 384 | 5.32 | 385 | 7.29 | 389 | 5.12 | 386 | 5.72 |
| | | 235 | 27.56 | 235 | 30.32 | 238 | 23.61 | 233 | 26.35 |
| | | | | | | 209 | 24.32 | | |
| 5.8 | Acetonitrile | 376 | 7.60 | 376 | 8.12 | 389 | 5.16 | 383 | 5.96 |
| | | 238 | 28.54 | 237 | 31.27 | 238 | 25.16 | 236 | 31.45 |
| 5.1 | Acetone | 378 | 8.73 | 378 | 8.80 | 388 | 5.73 | 385 | 7.60 |
| 4.4 | Ethylacetate | 384 | 8.27 | 385 | 8.35 | 395 | 4.58 | 387 | 6.72 |
| 4.0 | Tetrahydrofuran | 385 | 8.39 | 385 | 9.09 | 398 | 4.43 | 391 | 6.09 |
| 4.1 | Chloroform | 387 | 7.39 | 387 | 8.89 | 404 | 4.33 | 397 | 5.96 |
| | | 245 | 22.52 | 245 | 26.44 | 273 | 14.75 | 262 | 46.22 |
| 2.4 | Toluene | 390 | 8.66 | 390 | 9.62 | 402 | 5.45 | 395 | 7.51 |

*Relative measure of degree of interaction of the solvents with various polar test solutes

The solvents apart from influencing the chromophoric groups also affects the coordination environment of the metal centre which is reflected as a shift in the $d-d$ absorption band. The color change of the complexes can be attributed to this shift. Pseudohalogeno complexes appear in various shades of green [12] [Fig. 2.3].

**Fig. 2.3.** Snapshot of complex 1a and 2 in various solvents.

The influence of the donor power of the solvent on the λ_{max} values of the $d-d$ bands of the complexes have been investigated by means of visible spectroscopy. Four solvents of varying donor powers – DMSO, MeOH, CH₃CN and DCM were chosen for the study and it was found that the $d-d$ bands shift to red with increasing donor number of the solvents. Observed shifts in this region as a function of donor power of chosen solvents was significant and a red shift was noted [Fig. 2.4, Table 2.2].

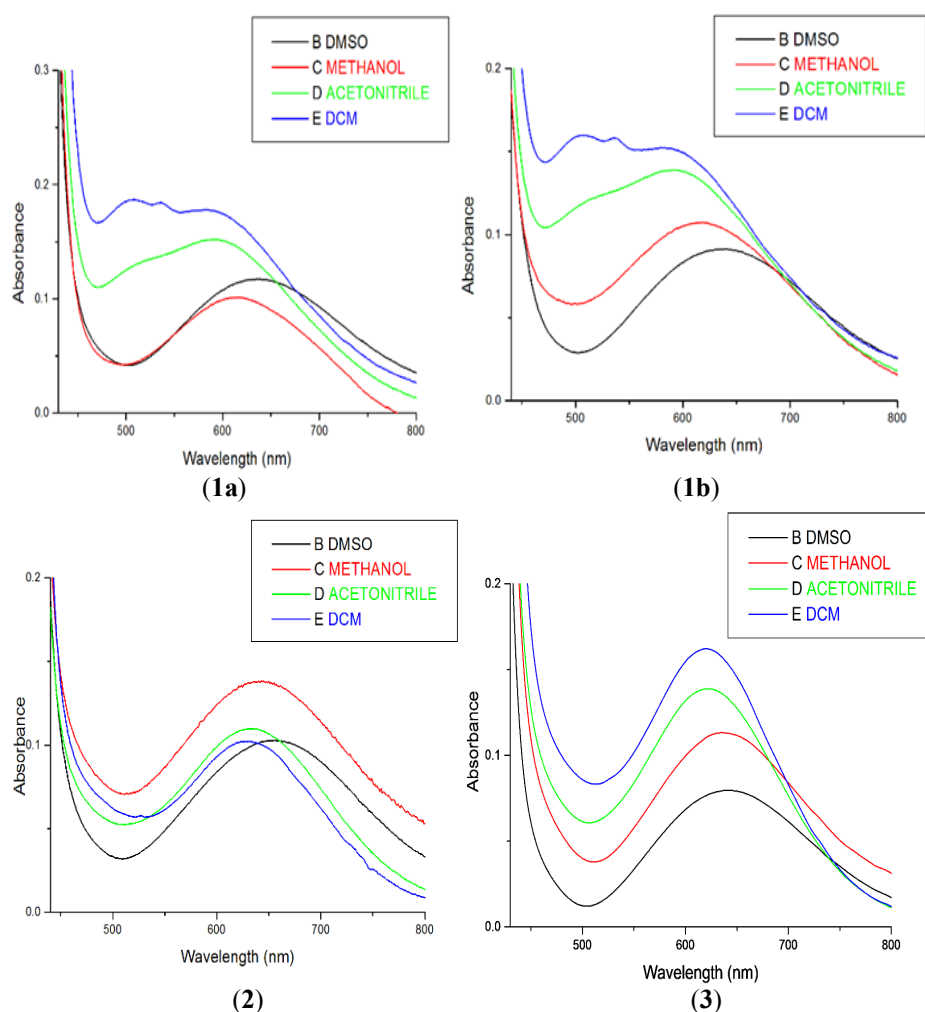


Fig. 2.4. The spectra showing solvatochromic behavior of $d-d$ transitions (con: $2 \cdot 10^{-3}$ M) of complexes in various solvents.

Table 2.2. The λ_{\max} (nm) values along with their ϵ ($M^{-1}cm^{-1}$) of *d-d* bands in various solvents

| Solvents | Donor number of solvents (DN) | Complex 1a | | Complex 1b | | Complex 2 | | Complex 3 | |
|--------------|-------------------------------|-----------------------|--------------------------------|-----------------------|--------------------------------|-----------------------|--------------------------------|-----------------------|--------------------------------|
| | | λ_{\max} (nm) | ϵ ($M^{-1}cm^{-1}$) | λ_{\max} (nm) | ϵ ($M^{-1}cm^{-1}$) | λ_{\max} (nm) | ϵ ($M^{-1}cm^{-1}$) | λ_{\max} (nm) | ϵ ($M^{-1}cm^{-1}$) |
| DMSO | 29.8 | 639 | 164 | 639 | 128 | 656 | 152 | 640 | 119 |
| Methanol | 19.0 | 613 | 142 | 619 | 151 | 640 | 204 | 636 | 169 |
| Acetonitrile | 14.1 | 593 | 213 | 591 | 195 | 633 | 162 | 621 | 207 |
| DCM | 0.0 | 583 | 250 | 583 | 214 | 632 | 151 | 619 | 242 |
| | | 535 | 259 | 535 | 223 | | | | |
| | | 509 | 262 | 509 | 225 | | | | |

The *d-d* band spectra of all the three complexes showed almost a broad band in the visible region assignable to the promotion of electron in the low energy orbitals to the hole in $d_{x^2-y^2}$ orbital of the copper(II) ion (d^9). The position of this band is shifted to longer wavelengths as the DN (donor number) of the solvent increases. As the solvent molecules approach along the *z* axis of the complex the ligands in the *xy* plane move out and the interactions become more with orbitals that have *z* characters (d_{z^2} , d_{xz} , and d_{yz}). These orbitals are thus destabilized, while the other orbitals energetically decrease and eventually a typical octahedral *d* orbital splitting is formed and in this process the *d-d* bands shift to red region. The change in the color of the complex with solvent molecules is because of weak coordination of the solvent molecules which is attributable to a strong Jahn–Teller effect of the Cu(II) center with a d^9 configuration [13a,b].

Among the four complexes, greatest solvatochromic effect is seen for the azido pair and there is a difference of 1500 cm^{-1} as we move from DCM to DMSO whereas for **2** that difference is only around 580 cm^{-1} . It is observed that in solvent with the highest donor number (DMSO), the absorption maxima for the complexes is hardly noticeable (406 cm^{-1}) and in weakly coordinating solvent like DCM, there is considerable difference (1330 cm^{-1}).

2.3.2. X-ray crystallography and structural description

Single crystals of compounds $[Cu(L^1)(N_3)]_n$ (**1a**), $[Cu(L^1)(N_3)]_n$ (**1b**), $[Cu(L^1)(NCO)]$ (**2**), $[Cu(L^1)(NCS)]$ (**3**) suitable for X-ray diffraction studies

were grown from their methanol solutions by slow evaporation at room temperature. The crystallographic data along with details of structure solution refinements are given in Tables 2.3 and 2.4.

Table 2.3. Crystal data and refinement details of complexes **1a** and **1b**

| Parameters | 1a | 1b |
|-----------------------------------|--|--|
| Empirical formula | C ₁₁ H ₁₃ Cl ₂ CuN ₅ O | C ₂₂ H ₂₆ Cl ₄ Cu ₂ N ₁₀ O ₂ |
| Formula weight | 365.71 | 731.43 |
| Temperature (T) | 293(2) K | 296(2) K |
| Wavelength | 0.71073 Å | 0.71073 Å |
| Crystal system | Monoclinic | Monoclinic |
| Space group | <i>P</i> 2 ₁ / <i>c</i> | <i>P</i> 2 ₁ / <i>n</i> |
| Unit cell dimensions | a = 11.0792(5) Å α = 90° b = 6.8477(3) Å β = 101.826(2)° c = 19.5346(8) Å γ = 90° | a = 6.9187(2) Å α = 90° b = 19.2758(7) Å β = 97.682(2)° c = 21.3470(7) Å γ = 90°. |
| Volume | 1450.58(11) Å ³ | 2821.36(16) Å ³ |
| Z | 4 | 4 |
| Density (calculated) | 1.675 Mg m ⁻³ | 1.722 Mg m ⁻³ |
| Absorption coefficient | 1.875 mm ⁻¹ | 1.928 mm ⁻¹ |
| F(000) | 740 | 1480 |
| Crystal size | 0.41 × 0.13 × 0.10 mm ³ | 0.40 × 0.35 × 0.35 mm ³ |
| θ range for data collection | 3.12 to 27.77° | 1.43 to 26.50° |
| Limiting indices | -14 ≤ h ≤ 14, 0 ≤ k ≤ 8, 0 ≤ l ≤ 25 | -8 ≤ h ≤ 8, -24 ≤ k ≤ 20, -26 ≤ l ≤ 26 |
| Reflections collected | 10989 | 18807 |
| Unique reflections | 6794 [R(int) = 0.0000] | 5861 [R(int) = 0.0307] |
| Refinement method | Full-matrix least-squares on F ² | Full-matrix least-squares on F ² |
| Data / restraints / parameters | 3356 / 0 / 182 | 5853 / 0 / 366 |
| Goodness-of-fit on F2 | 1.084 | 1.014 |
| Final R indices [I > 2σ(I)] | R ₁ = 0.0538, wR ₂ = 0.1172 | R ₁ = 0.0299, wR ₂ = 0.0790 |
| R indices (all data) | R ₁ = 0.0937, wR ₂ = 0.1354 | R ₁ = 0.0444, wR ₂ = 0.0901 |
| Largest diff. peak and hole | 0.764 and -0.591 e.Å ⁻³ | 0.341 and -0.480 e.Å ⁻³ |
| CCDC | 1407849 | 1407850 |

$$R_1 = \frac{\sum ||F_o| - |F_c||}{\sum |F_o|}$$

$$wR_2 = [\frac{\sum w(F_o^2 - F_c^2)^2}{\sum w(F_o^2)^2}]^{1/2}$$

Table 2.4. Crystal data and refinement details of complexes **2** and **3**

| Parameters | 2 | 3 |
|-----------------------------------|---|--|
| Empirical formula | C ₁₂ H ₁₈ Cl ₂ CuN ₃ O ₂ | C ₁₃ H ₁₅ Cl ₂ CuN ₃ OS |
| Formula weight | 366.71 | 395.80 |
| Temperature | 296(2) K | 296(2) K |
| Wavelength | 0.71073 Å | 0.71073 Å |
| Crystal system | Orthorhombic | Orthorhombic |
| Space group | <i>Pnma</i> | <i>Pnma</i> |
| Unit cell dimensions | a = 18.5526(12) Å α = 90° b = 6.8128(3) Å β = 90° c = 11.1901(6) Å γ = 90° | a = 19.291(3) Å α = 90° b = 6.9499(7) Å β = 90° c = 11.1624(11) Å γ = 90° |
| Volume | 1414.37(13) Å ³ | 1496.6(3) Å ³ |
| Z | 4 | 4 |
| Density (calculated) | 1.722 Mg m ⁻³ | 1.757 Mg m ⁻³ |
| Absorption coefficient | 1.925 mm ⁻¹ | 1.956 mm ⁻¹ |
| <i>F</i> (000) | 744.0 | 804 |
| Crystal size | 0.35 × 0.25 × 0.20 mm ³ | 0.30 × 0.25 × 0.20 mm ³ |
| θ range for data collection | 2.85 to 28.25° | 2.79 to 25.99° |
| Limiting indices | -24 ≤ h ≤ 24, -8 ≤ k ≤ 9, -14 ≤ l ≤ 14 | -23 ≤ h ≤ 12, -8 ≤ k ≤ 8, -13 ≤ l ≤ 13 |
| Reflections collected | 10832 | 9332 |
| Unique reflections | 1892 [R(int) = 0.0342] | 1599 [R(int) = 0.0959] |
| Refinement method | Full-matrix least-squares on F ² | Full-matrix least-squares on F ² |
| Data / restraints / parameters | 1882 / 2 / 145 | 1600 / 0 / 123 |
| Goodness-of-fit on F ² | 1.044 | 1.148 |
| Final R indices [I > 2σ(I)] | R ₁ = 0.0300, wR ₂ = 0.0715 | R ₁ = 0.0606, wR ₂ = 0.1635 |
| R indices (all data) | R ₁ = 0.0407, wR ₂ = 0.0774 | R ₁ = 0.0701, wR ₂ = 0.1772 |
| Largest diff. peak and hole | 0.544 and -0.450 e.Å ⁻³ | 0.709 and -1.037 e.Å ⁻³ |
| CCDC | 1407851 | -- |

$$R_1 = \frac{\sum ||F_o| - |F_c||}{\sum |F_o|}$$

$$wR_2 = [\sum w(F_o^2 - F_c^2)^2 / \sum w(F_o^2)^2]^{1/2}$$

The crystal of **1a** is a non-merohedral twin, and the diffraction intensities were separated into two sets by using PLATON [14]. The minor component refined to 17.8(2)%. Complex **2** possess a crystallographic mirror symmetry with all the atoms lying on a mirror plane and hence enjoys an occupancy factor of 0.50 (special position constraint). The occupation site in disorder refinement is 50:50. For the thiocyanato complex, all non-H atoms except C9 and C10 lie along the crystallographic mirror symmetry. The H atoms were placed in idealized positions and constrained to ride on their parent atoms, with C–H distances in the range 0.93–0.97 Å, and with $U_{\text{iso}}(\text{H}) = 1.2$ or $1.5U_{\text{eq}}(\text{C})$.

2.3.2.1. $[\text{Cu}(\text{L}^1)(\text{N}_3)]_n$ (**1a**)

Compound crystallizes in monoclinic $P2_1/c$ space group. A perspective view of the complex with atom labelling scheme is shown in Fig. 2.5. Selected bond lengths and angles are given in Table 2.5.

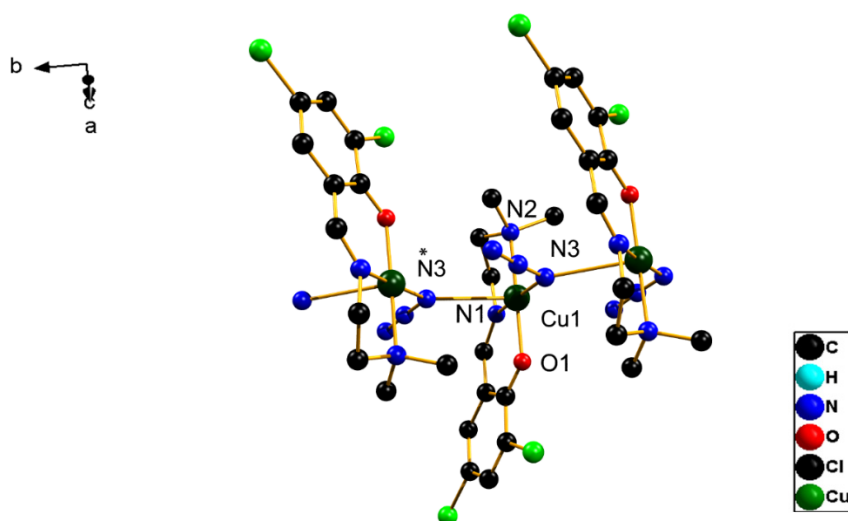


Fig. 2.5. Perspective view of complex **1a**. Only relevant atoms are labelled. Symmetry element: * = x, 5.5-y, -0.5+z. (Hydrogen atoms are omitted for clarity)

Table 2.5. Selected bond lengths (Å) and bond angles (°) for [Cu(L¹)(N₃)_n]**(1a)**

| Bond lengths (Å) | | Bond angles (°) | |
|------------------|----------|------------------|------------|
| Cu(1)–O(1) | 1.924(3) | O(1)–Cu(1)–N(1) | 92.44(17) |
| Cu(1)–N(1) | 1.951(4) | O(1)–Cu(1)–N(3a) | 89.76(17) |
| Cu(1)–N(3) | 1.975(4) | N(1)–Cu(1)–N(3) | 173.8(2) |
| Cu(1)–N(2) | 2.071(4) | O(1)–Cu(1)–N(2) | 176.89(15) |
| Cu(1)–N(3a) | 2.694(5) | N(1)–Cu(1)–N(2) | 84.53(17) |
| O(1)–C(1) | 1.296(7) | N(3)–Cu(1)–N(2) | 92.84(19) |
| Cl(1)–C(2) | 1.737(6) | N(4)–N(3)–Cu(1) | 111.7(4) |
| Cl(2)–C(4) | 1.745(6) | N(5)–N(4)–N(3) | 177.0(6) |
| N(1)–C(7) | 1.272(7) | C(11)–N(2)–C(10) | 108.2(5) |
| N(1)–C(8) | 1.470(7) | Cu(1)–N(3)–Cu(1) | 130.8(2) |
| N(2)–C(9) | 1.482(7) | N(3)–Cu(1)–N(3a) | 99.0(1) |
| N(3)–N(4) | 1.200(6) | N(1)–Cu(1)–N(2) | 84.53(17) |

The single crystal X-ray analysis reveals the asymmetric unit as a crystallographically distinct square planar Cu(II) centre with its plane accommodated by amino nitrogen (N2), imine nitrogen (N1), phenoxo oxygen (O1) and the N3 of the azido group [Fig. 2.6] although in the entire polymeric structure, each unit has pentacoordinated (4+1) geometry, with the fifth coordination site being satisfied by the nitrogen of the azido group of the adjacent unit *via* $\mu_{1,1}$ -bridging. In brief, the coordination modes are satisfied by tridentate monoanionic Schiff base system and two azido ions, both of which are involved in *end-on* bridging [Fig. 2.5].

The pattern of propagation of the chain is in such a manner that each azido group exhibits dual nature - while it is axially disposed with respect to one metal ion, the same N₃⁻ is equatorially aligned with respect to the adjacent metal ion. Bridging Cu–N bond lengths are significantly different with values 1.975(4)/2.694(5) for basal/axial bonds. Therefore the mode of *end-on* azido bridging is asymmetric in terms of the type of the coordination position it occupies [15].

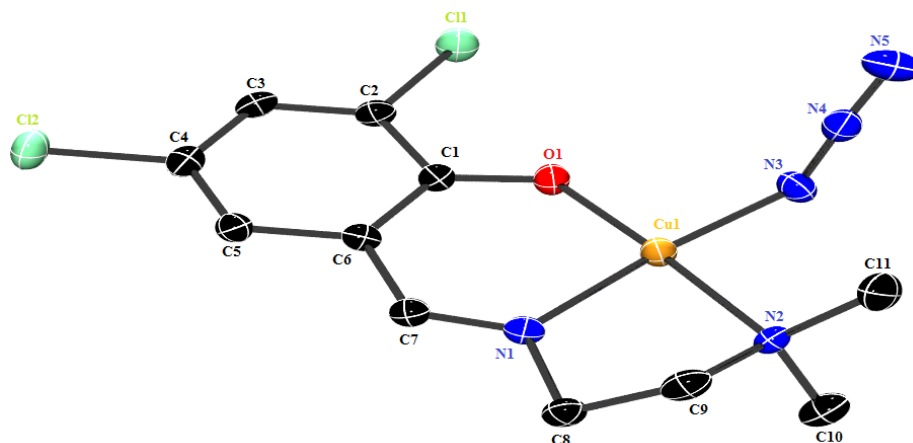


Fig. 2.6. ORTEP diagram showing the atom labelling of the asymmetric unit of the complex **1a** (drawn with 30% ellipsoid probability and the hydrogen atoms are omitted for clarity).

The extent of distortion of the pentacoordinated geometry can be conveniently measured by Addison parameter, given by the equation $\tau = (\beta - \alpha)/60$ [16] (for perfect square pyramidal and trigonal bipyramidal geometries the values of τ are zero and unity respectively). The value of τ - the angular structural parameter, an index of degree of trigonality is 0.051, suggestive of an almost square pyramidal geometry. Also the metal centre deviates from the least squares plane by a distance of 0.0442 Å towards apical donor atom and amongst the other donor atoms, the imino nitrogen deviates the most (0.0533 Å) from the plane.

The *trans*- $\mu_{1,1}$ bridging mode of azido group constructs the whole molecule into a one-dimensional polymeric structure along 'b' axis. Also, each monomeric unit is related to its adjacent one by a 2_1 screw axis. This translational element of symmetry coupled with the *trans* bridging mode of N_3^- generates a helical chain [Fig. 2.7].

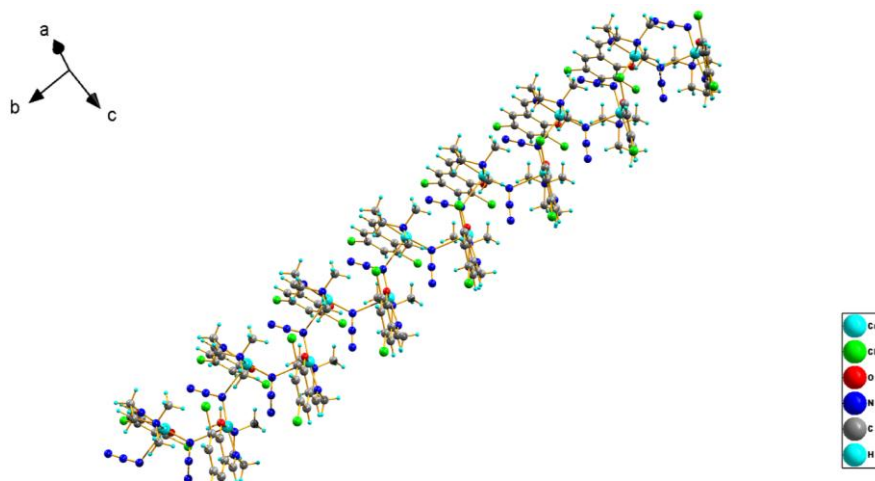


Fig. 2.7. Helical propagation of polymeric complex **1a**.

It is interesting to note that although several $\mu_{1,3}\text{-N}_3$ bridged helical chains have been reported, there are very few examples reported for helical *trans*- $\mu_{1,1}$ chains with Cu(II) [17a,b,c]

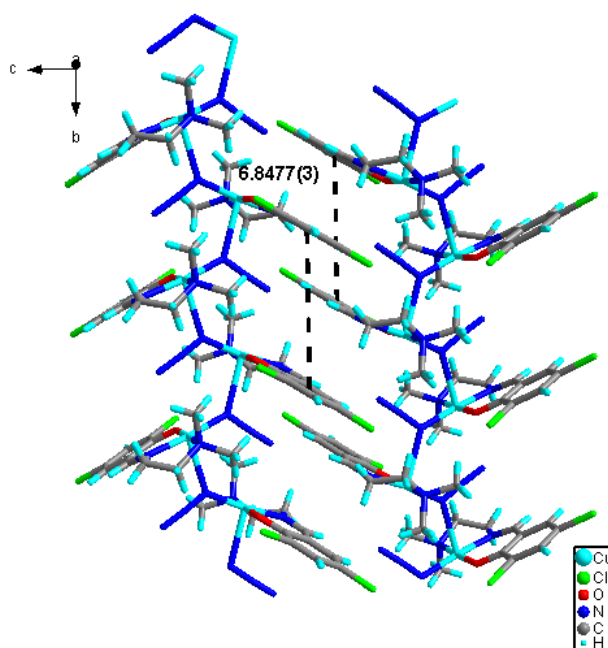


Fig. 2.8. The two adjacent chains of complex **1a** fit to form a zipper-like structure with teeth tilted.

The *trans* $\mu_{1,1}$ -azido ligand packs the succeeding units in such a fashion that the alternate units can be stacked one over the other with a dihedral angle of 0° between them, further evidencing the piling of the units. Two adjacent 1-D strands fit in to a zipper-like structure where the alternate teeth are spaced at a distance of 6.8477(3) Å [Fig. 2.8].

The Cu...Cu non-bonded distance along a chain is 4.2548(10) Å and the interchain Cu...Cu distance is 10.1471(10) Å. The bridging pseudo-halide is quasi-linear as revealed by the N–N–N bond angle of $177.0(6)^\circ$.

The metrical parameters like metal-N-metal bridge angle (Cu1–N3–Cu1) in this metal-azido complex is $130.8(2)^\circ$ and the N3–Cu1–N3 bond angle emerges to $99.0(1)^\circ$. The bond distances in the azido complex follow the order metal-axial azido nitrogen (2.694(5) Å) > metal-amino nitrogen (2.071(4) Å) > metal-equatorial azido nitrogen (1.975(4) Å) > metal-imino nitrogen (1.951(4) Å) > metal-phenoxo oxygen (1.924(3) Å). The Cu–N distance in apical position is longer than the basal distance, which is an obvious consequence of Jahn-Teller distortion in a d^9 copper(II) system [Table 2.5]. Also the metal-imine bond distance is shorter than metal-amino nitrogen, as seen in many other similar systems [18a,b]. The five membered chelate ring incorporating the amino fragment *i.e.* Cg(1) [Cu1/N1/C8/C9/N2] adopts an envelope conformation with C(9) as the flap atom of the envelope, with a puckering amplitude of $Q = 0.422(6)$ Å and $\varphi = 108.8(6)^\circ$ [19]. The puckering of the metallocycle is also calculated in terms of pseudorotation parameters P and τ_m [20] and the envelope conformation was confirmed with $P = 264.6(3)^\circ$ and $\tau = 47.3(3)^\circ$ for reference bond Cu(1)–N(1). The six membered chelate ring formed by the aldehydic moiety, Cg(2) [Cu1/O1/C1/C6/C7/N1] also assumes an envelope conformation with puckering amplitude, $Q = 0.163(4)$ Å and $\varphi = 182(2)^\circ$.

2.3.2.2. [Cu(L¹)(N₃)_n] (1b)

The polymorphic counterpart crystallizes in monoclinic $P2_1/n$ space group. The asymmetric unit of this polymeric polymorph houses two crystallographically distinct molecules, with both the Cu(II) centres, (Cu1 and Cu2) disposing in square

planar topology [Fig. 2.9] and the polymeric one dimensional chain constituting both Cu1 and Cu2 [Fig. 2.10] units are built by the *end-on* bridging of azido group in axial-equatorial fashion along 'a' axis [Fig. 2.11].

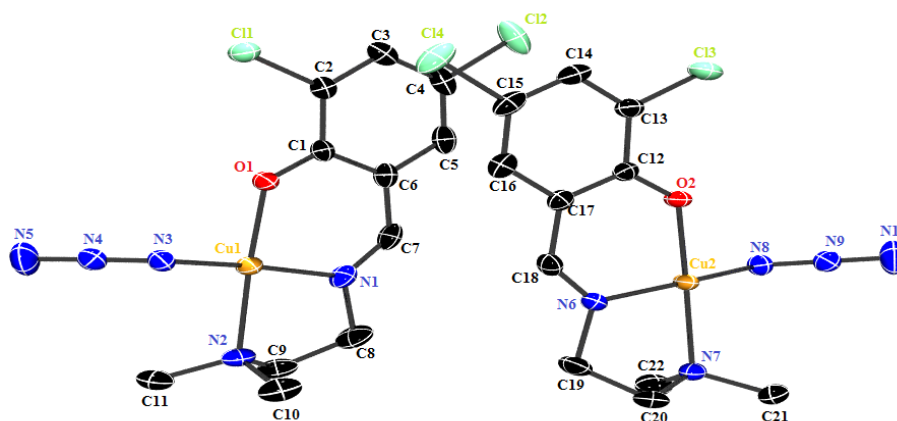


Fig. 2.9. ORTEP diagram showing the atom labelling of asymmetric unit of complex **1b** (drawn with 30% ellipsoid probability and the hydrogen atoms are omitted for clarity).

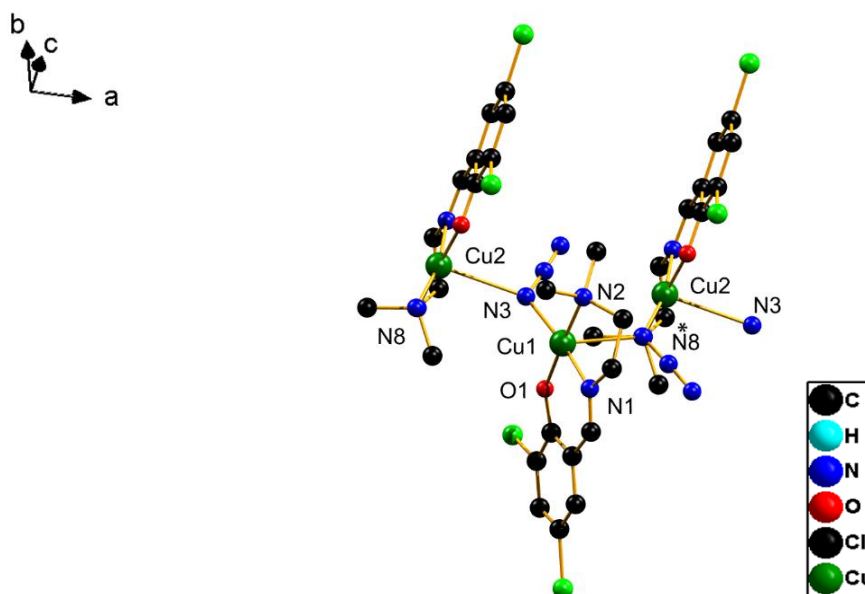


Fig. 2.10. Perspective view of complex **1b**. Only relevant atoms are labelled. Symmetry element: * = 4-x, 2-y, 2-z. (Hydrogen atoms are omitted for clarity).

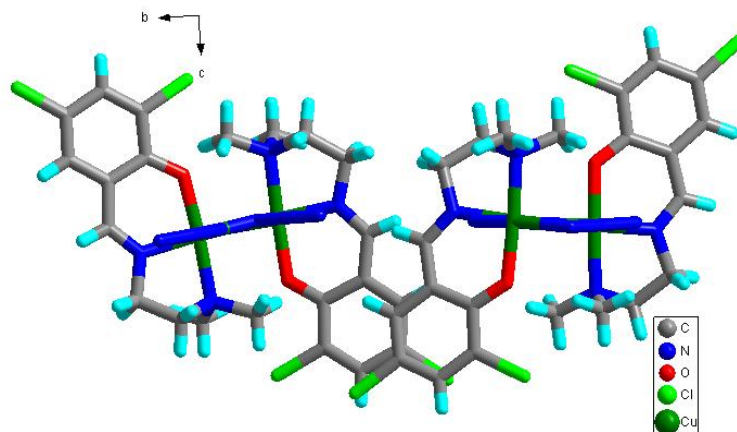


Fig. 2.11. Propagation of polymeric complex **1b** along 'a' axis.

The asymmetric alignment of the pseudohalide is further evidenced by the metrical parameters like metal-nitrogen distance, metal-N-N bond angle, metal-N-metal bridge angle etc. [Table 2.6].

Table 2.6. Metrical parameters with respect to Cu1 and Cu2

| Metrical parameters | With respect to Cu1 | | With respect to Cu2 | |
|--------------------------------|------------------------------|------------|------------------------------|------------|
| Metal-nitrogen distance (Å) | Cu1–N3 ^a basal | 1.980(2) | Cu2–N3 ^c axial | 2.713(2) |
| | Cu1–N8 ^b axial | 2.629(2) | Cu2–N8 ^b basal | 1.967(2) |
| Metal-N-N bond angle (°) | Cu1–N3–N4 | 120.1(1) | Cu2–N3–N4 | 106.97(16) |
| | Cu1–N8–N9 | 110.29(16) | Cu2–N8–N9 | 117.7(1) |
| Metal-N-metal bridge angle (°) | Cu1–N3–Cu2 | 132.01(10) | Cu1–N8–Cu2 | 131.93(10) |

$$a = 1.5-x, -0.5+y, 0.5-z ; b = -1+x, -1+y, -1+z ; c = 0.5-x, -0.5+y, 0.5-z$$

The azido groups in the crystallographically distinct units are quasi-linear with N–N–N bond angle of 177.3(3)°. The non-bonded distances of Cu1 with the symmetrically related copper centres [Cu2 (x, -1+y, -1+z)] along this

chain are 4.2061(5) and 4.2965(5) Å respectively. This complex is much more closely packed as revealed by the comparatively lower interchain Cu...Cu distances of 9.7985(6) and 9.8565(6) Å, with respect to **1a**. The polymorphic form also exhibits a zipper like structure with a spacing of 6.9187(2) Å between alternate teeth [Fig. 2.12].

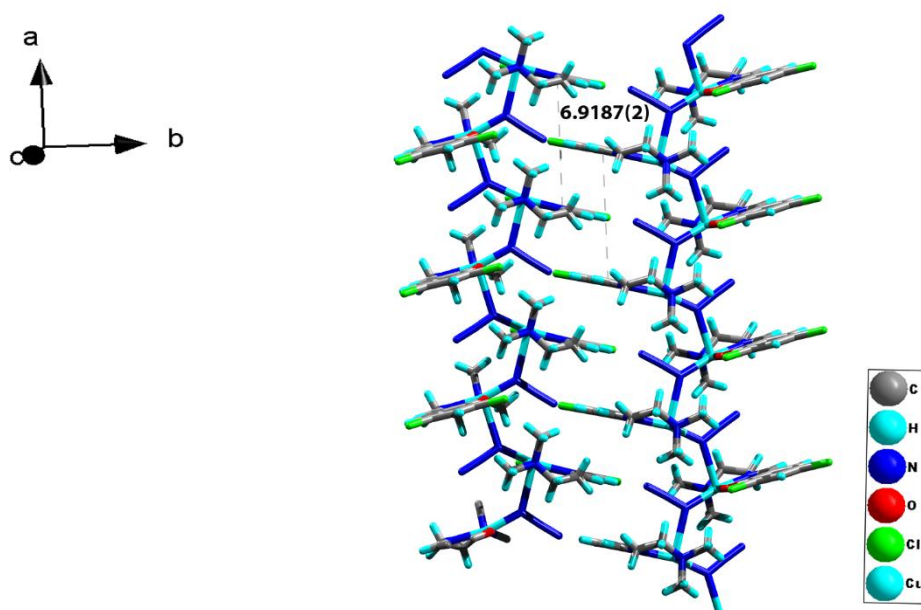


Fig. 2.12. The two adjacent chains of complex **1b** fit to form a zipper-like structure.

The central metal atoms, Cu1 and Cu2 deviate by 0.0720 and 0.0724 Å from the respective least square planes. Though both forms have axially elongated pentacoordinated environment, this crystallographic form with two different copper centres exhibit a greater distortion as revealed by a trigonality index value of 0.11 and 0.1565 respectively, which is almost and more than twice of its counterpart. A closer examination of the transoid angles unveil the fact that the higher value of Addison parameter is due to variation in the non-linear *trans* angle value involving azido nitrogen atoms (N1–Cu1–N3, 169.73(9)°/ N6–Cu2–N8, 167.39(9)° over N1–Cu1–N3, 173.8(2)° of former crystal). A measure of the relative strength of bonding follows the same order

as that of **1a** *i.e.* metal-phenoxo oxygen > metal-imino nitrogen > metal-equatorial azido nitrogen > metal-amino nitrogen > metal-axial azido nitrogen although slight variations do exist in the bonding distances [Table 2.7].

Table 2.7. Selected bond lengths (Å) and bond angles (°) for [Cu(L¹)(N₃)_n (**1b**)

| Bond lengths (Å) | | Bond angles (°) | | | |
|------------------|------------|-----------------|-----------|-----------------|-----------|
| Cu(1)–N(1) | 1.943(2) | N(1)–Cu(1)–O(1) | 92.25(8) | N(3)–Cu(2)–N(6) | 91.22(8) |
| Cu(1)–N(2) | 2.053(2) | N(1)–Cu(1)–N(2) | 84.08(9) | N(3)–Cu(2)–N(7) | 89.50(7) |
| Cu(1)–N(3) | 1.980(2) | N(1)–Cu(1)–N(3) | 169.73(9) | N(3)–Cu(2)–N(8) | 101.33(8) |
| Cu(1)–N(8) | 2.629(2) | N(1)–Cu(1)–N(8) | 88.60(8) | N(3)–Cu(2)–O(2) | 88.60(8) |
| Cu(1)–O(1) | 1.9069(17) | N(2)–Cu(1)–N(3) | 93.00(9) | N(6)–Cu(2)–N(7) | 84.70(8) |
| Cu(2)–N(3) | 2.713(2) | N(2)–Cu(1)–N(8) | 91.33(8) | N(6)–Cu(2)–N(8) | 167.39(9) |
| Cu(2)–N(6) | 1.931(2) | N(2)–Cu(1)–O(1) | 176.32(9) | N(6)–Cu(2)–O(2) | 92.67(8) |
| Cu(2)–N(7) | 2.051(1) | N(3)–Cu(1)–O(1) | 90.56(8) | N(7)–Cu(2)–N(8) | 92.75(9) |
| Cu(2)–N(8) | 1.967(2) | N(8)–Cu(1)–O(1) | 88.88(8) | N(7)–Cu(2)–O(2) | 176.72(8) |
| Cu(2)–O(2) | 1.9067(17) | N(3)–Cu(1)–N(8) | 101.33(8) | N(8)–Cu(2)–O(2) | 90.24(8) |

In complex **1b**, the five membered ring involving amine is twisted on C9–N2 bond with puckering parameters, $Q = 0.443(3)$ Å and $\varphi = 120.9(3)^\circ$. The metallocycle (Cu2–N6–C19–C20–N7) assumes an envelope conformation with C20 as the flap atom of the envelope with parameters $Q = 0.419(3)$ Å and $\varphi = 113.2(3)^\circ$. Puckering of both metallocycles is further confirmed by the pseudorotation parameters – *i.e.* $P = 274.5(2)^\circ$ and $\tau_m = 47.2(2)^\circ$ for reference bond Cu(1)–N(1) in Cg(1) [Cu1/N1/C8/C9/N2] and $P = 267.9(2)^\circ$ and $\tau_m = 46.3(2)^\circ$ for reference bond Cu(2)–N(6) in Cg(2) [Cu2/N6/C19/C20/N7]. No puckering was found for the six membered ring unlike seen in its polymorphic counterpart.

2.3.2.2.1. Comparison of the polymorphic structures

An overall comparison brings out that the strongest axial bond and the strongest equatorial bonds are seen in complex **1b** [Table 2.8]. The value of Addison parameter, τ and the deviation of metal centre from the least squares

plane are taken as indicators of the relative extent of distortion of a square-pyramidal environment [15]. In the case of polymorphic compounds obtained, the τ/d (Å) values are 0.051/0.0442 (**1a**), 0.11/0.0720 (Cu1 of **1b**), 0.1565/0.0724 (Cu2 of **1b**) from which the extent of distortion follows the order Cu2(**1b**) > Cu1(**1b**) > Cu1(**1a**). Coupled to the above values, the wide variation in transoid bond angle values [(176.72(8)°/167.39(9)°)] also contribute to the greater distortion of Cu2 environment of complex **1b**.

Table 2.8. Comparative analysis of metal-donor atom bond distances in the polymorphic forms

| | Crystallographic distinct form (1) | Two distinct crystallographic entities (2) | |
|------------------------------------|---------------------------------------|---|----------------------------------|
| metal-axial azido nitrogen | Cu1–N3 ^{1a} 2.694(5) | Cu1–N8 ^{2b} 2.629(2) | Cu2–N3 ^{2a} 2.713(2) |
| metal-amino nitrogen | Cu1–N2 2.071(4) | Cu1–N2 2.053(2) | Cu2–N7 2.051(1) |
| metal-equatorial azido nitrogen | Cu1–N3 ^{1b} 1.975(4) | Cu1–N3 ^{2a} 1.980(2) | Cu2–N8 ^{2b} 1.967(2) |
| metal-imino nitrogen | Cu1–N1 1.951(4) | Cu1–N1 1.943(2) | Cu2–N6 1.931(2) |
| metal-phenoxo oxygen | Cu1–O1 1.924(3) | Cu1–O1 1.9069(17) | Cu2–O2 1.9067(17) |

1a = 1-x, 1-y, 1-z ; 1b = x, 0.5-y, -0.5+z

2a = 1.5-x, -0.5+y, 0.5-z ; 2b = -1+x, -1+y, -1+z ; 2c = 0.5-x, -0.5+y, 0.5-z

2.3.2.3. [Cu(L¹)(NCO)] (2)

Complex **2** crystallizes in the orthorhombic space group *Pnma*. The complex assumes a square planar geometry, with the tetracoordination of Cu(II) being satisfied by the imino nitrogen (N1), amino nitrogen (N2), phenoxo oxygen (O1) of the tridentate Schiff base ligand (L¹) and N3 atom of the cyanato group [Fig. 2.13].

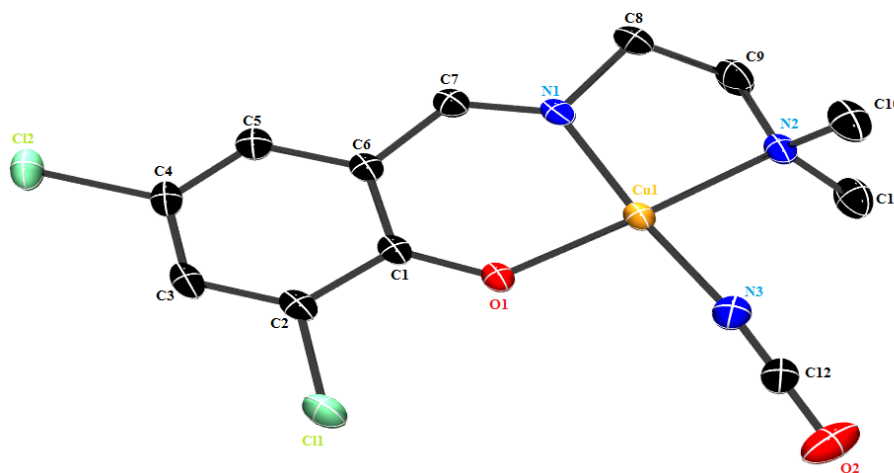


Fig. 2.13. ORTEP diagram showing the atom labelling of asymmetric unit of complex **2** (drawn with 30% ellipsoid probability, Hydrogen atoms and disordered atoms are omitted for clarity).

The extent of deformation in a tetracoordinated complex is given by the τ_4 index, a measure of the extent of distortion between a perfect tetrahedron ($\tau_4 = 1$) and perfect square planar geometry ($\tau_4 = 0$), given by the formula: $\tau_4 = [360^\circ - (\alpha + \beta)]/141^\circ$, α and β being the two largest angles around the central metal atom in the complex [21]. The τ_4 value of 0.1084, for this complex confirms a slightly distorted square planar geometry. Moreover, the different angles around the copper metal summate to 359.36° indicating negligible deviation from the coordination polyhedron. Of the various coordinating atoms O1, N1, N2 and N3, imino nitrogen (N1) and amino nitrogen (N2) shows 0.2081 and 0.2299 Å deviation from the least square mean plane whereas O1 and N3 lies exactly in the plane. No deviation was found for Cu(II) from the reference plane. The metal-donor bond strength follows the order Cu1–N3 (cyanato nitrogen) > Cu1–O1 (phenoxo oxygen) > Cu1–N1 (amino nitrogen) > Cu1–N2 (imino nitrogen) which in turn reflects the reverse order of the metal-donor bond distances [Table 2.9]. The pseudolinearity of the cyanato ligand is evidenced by the bond angle value of $179.6(4)^\circ$ for N(3)–C(12)–O(2). The tridentate ligand forms six and five membered metallocycles with chelate bite angles of $91.59(6)^\circ$ and $84.51(13)^\circ$ for the rings respectively.

Table 2.9. Selected bond lengths (Å) and bond angles (°) for **2**

| Bond lengths (Å) | | Bond angles (°) | |
|------------------|----------|-----------------|-----------|
| Cu(1)–O(1) | 1.914(1) | O(1)–Cu(1)–N(2) | 172.11(1) |
| Cu(1)–N(1) | 1.931(3) | O(1)–Cu(1)–N(3) | 92.46(12) |
| Cu(1)–N(2) | 2.075(3) | O(1)–Cu(1)–N(1) | 91.59(9) |
| Cu(1)–N(3) | 1.897(3) | N(1)–Cu(1)–N(2) | 84.51(13) |
| N(1)–C(7) | 1.272(5) | N(1)–Cu(1)–N(3) | 172.6(2) |
| N(3)–C(12) | 1.140(4) | N(2)–Cu(1)–N(3) | 92.18(14) |
| O(2)–C(12) | 1.185(4) | N(3)–C(12)–O(2) | 179.6(4) |

Ring puckering analyses and least square plane calculations show that the five membered metallocycle, Cg(1) is twisted on C(8)–C(9) bond with puckering amplitude, $Q = 0.400(6)$ Å and $\phi = 97.8(7)^\circ$. A boat conformation is found for the six membered metallocycle, Cu1-N1-C7-C6-C7a-N1a [C7a, N1a stands for the disordered atoms] with puckering parameters $Q = 1.524(8)$ Å, and $\phi = 180.0(5)^\circ$. Another six membered metallocycle, Cg(3) [Cu1/N1/C7/C6/C1/O1] is also puckered with an amplitude of $Q = 0.106(6)$ Å and $\phi = 165(5)^\circ$.

2.3.2.4. [Cu(L¹)(NCS)] (**3**)

The thiocyanato complex also crystallizes in the same orthorhombic space group with a similar coordination polyhedron [Fig. 2.14].

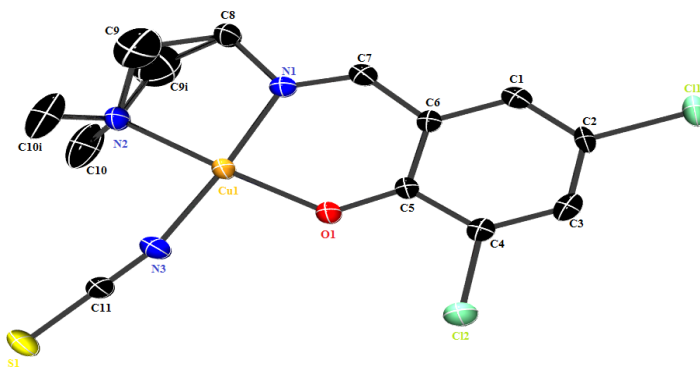


Fig. 2.14. ORTEP diagram showing the atom labelling of asymmetric unit of complex **3** (drawn with 30% ellipsoid probability and the hydrogen atoms are omitted for clarity).

The τ_4 value of 0.0531, highlights the distortion in the square planar geometry. The chelate bite angles summate to a total of 360.1° around the central copper atom. The thiocyanato group is linear as evidenced by its bond angle value of $180.0(6)^\circ$. The selected bond lengths (Å) and bond angles ($^\circ$) for **3** are given in Table 2.10.

Table 2.10. Selected bond lengths (Å) and bond angles ($^\circ$) for **3**

| Bond lengths (Å) | | Bond angles ($^\circ$) | |
|------------------|-----------|--------------------------|----------|
| Cu(1)–O(1) | 1.910(4) | O(1)–Cu(1)–N(1) | 92.7(2) |
| Cu(1)–N(1) | 1.927(6) | O(1)–Cu(1)–N(3) | 92.0(2) |
| Cu(1)–N(3) | 1.919(7) | N(1)–Cu(1)–N(3) | 175.4(2) |
| Cu(1)–N(2) | 2.053(6) | O(1)–Cu(1)–N(2) | 177.1(2) |
| O(1)–C(5) | 1.282(8) | N(1)–Cu(1)–N(2) | 84.4(2) |
| Cl(1)–C(2) | 1.731(6) | N(3)–Cu(1)–N(2) | 91.0(3) |
| Cl(2)–C(4) | 1.719(7) | N(3)–C(11)–S(1) | 180.0(6) |
| N(1)–C(7) | 1.268(9) | C(11)–N(3)–Cu(1) | 166.0(6) |
| N(1)–C(8) | 1.460(8) | C(10)–N(2)–C(10A) | 107.3(8) |
| N(2)–C(9) | 1.522(12) | | |
| S(1)–C(11) | 1.612(7) | | |
| N(3)–C(11) | 1.161(10) | | |

The four membered ring, N(2)/C(8)/C(9) and C(9a) involving the disordered atoms, C(9) and C(9a) forms a chair conformation with a puckering amplitude of $0.612(10)$ Å. Also, the five membered and six membered metallocycles – Cg(4) & Cg(7), adopts envelope and half-chair conformation respectively. Since the crystal structure of the complex has been already published [22], we have focused more on the spectral characterization of the complex.

2.3.2.5. Supramolecular features as structural adhesives

Whilst one of the hydrogen atoms, H(11B) borne by the C(11) atom of the methyl group forms an (intermolecular) intrachain hydrogen bonding interaction with the deprotonated phenoxy oxygen atom (O1), the other hydrogen atom H(11C) of the same carbon is involved in two intramolecular interactions with N(3) and N(4) of the azido group, thus forming a bifurcated, three centre hydrogen bonding interaction [Fig. 2.15], leading to S(3) ring motif. Due to the

involvement of azido nitrogens in hydrogen bonding, S(5) and S(6) motifs are also formed.

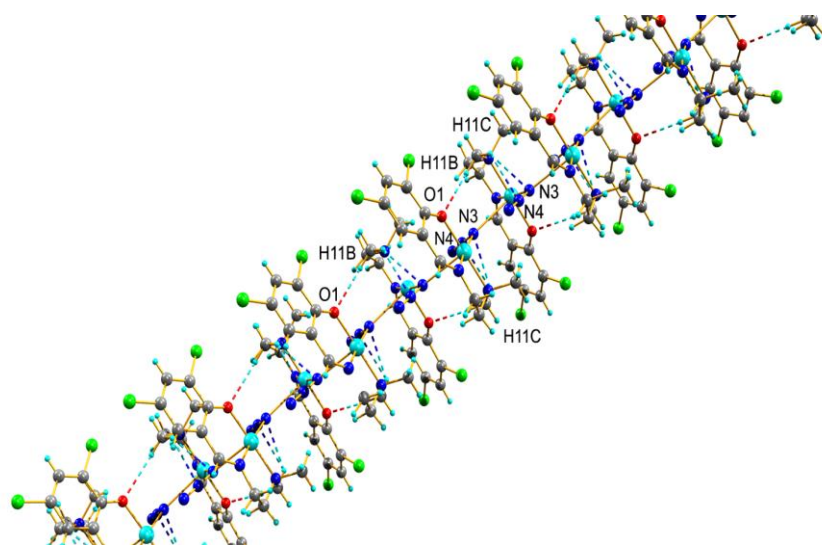


Fig. 2.15. Intrachain intermolecular and intramolecular hydrogen bonding interactions in complex **1a**.

The hydrogen bonding between H(5) atom on C(5) with that of the N(5) of the azido group of a similar molecule in the adjacent chain stitches the neighbouring one-dimensional polymeric chains in such a manner that the molecules pack in 'bc' plane [Table 2.11, Fig. 2.16]. No significant ring interactions are found in the complex.

Table 2.11. Non-conventional hydrogen bonding interactions in the complex $[\text{Cu}(\text{L}^1)(\text{N}_3)]_n$ (**1a**)

| D–H···A | D–H (Å) | H···A (Å) | D···A (Å) | D–H···A (°) |
|--|---------|-----------|-----------|-------------|
| Intermolecular hydrogen bonding | | | | |
| C(5)–H(5)···N(5) ^a | 0.93 | 2.52 | 3.371(9) | 153 |
| C(11)–H(11B)···O(1) ^b | 0.96 | 2.48 | 3.405(8) | 163 |
| Intramolecular hydrogen bonding | | | | |
| C(11)–H(11C)···N(3) | 0.96 | 2.59 | 3.097(9) | 113 |
| C(11)–H(11C)···N(4) | 0.96 | 2.50 | 3.096(8) | 120 |

Equivalent position codes: a = 1-x, -1/2+y, 3/2-z ; b = x, -1/2-y, -1/2+z

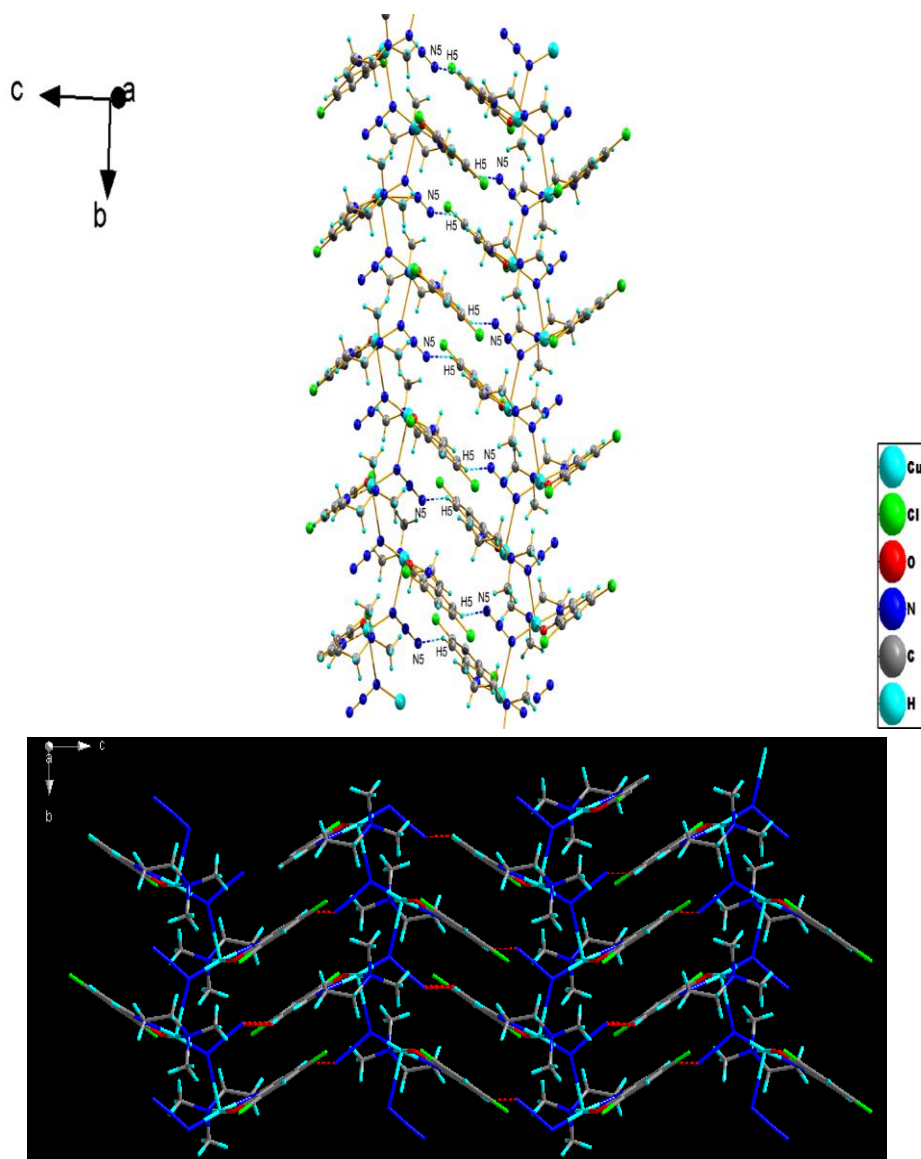


Fig. 2.16. Plot showing hydrogen bonding interaction between two adjacent chains in complex **1a** and the stacking in '*bc*' plane.

In the polymorphic form, the three intermolecular interactions, namely C(7)–H(7)···N(5), C(16)–H(16)···N(10) and C(18)–H(18)···N(10) sew together adjacent one-dimensional chains and pack the molecules in '*ab*' plane [Fig. 2.17].

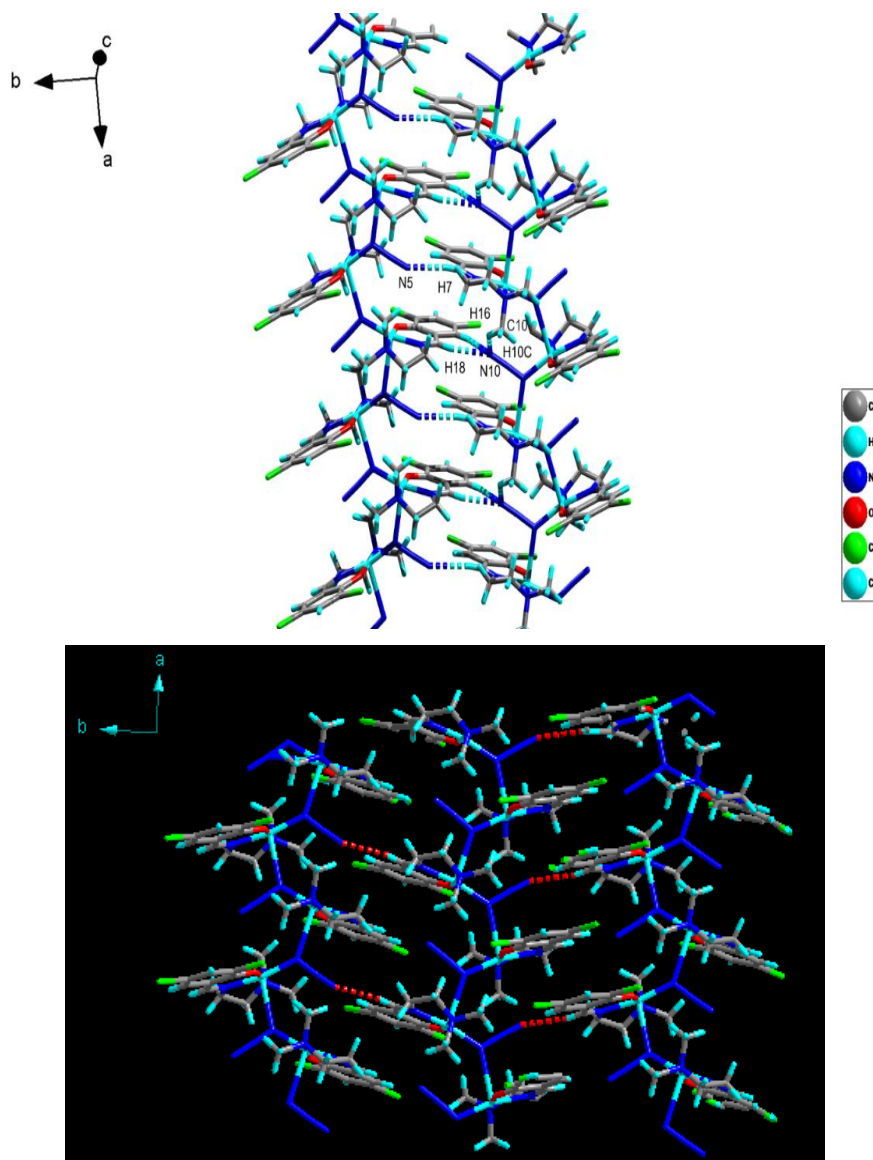


Fig. 2.17. Plot showing the hydrogen bonding interaction between two adjacent chains of complex **1b** and the stacking in 'ab' plane.

A trifurcated hydrogen bonding interaction is established by H(10C), H(18) and H(16) with a common acceptor, N(10) [Fig. 2.18]. A $R_2^1(6)$ pattern

is generated considering only the hydrogen bond interaction of H(18) and H(16) with the common acceptor, N(10) [bifurcated interaction, Fig. 2.18].

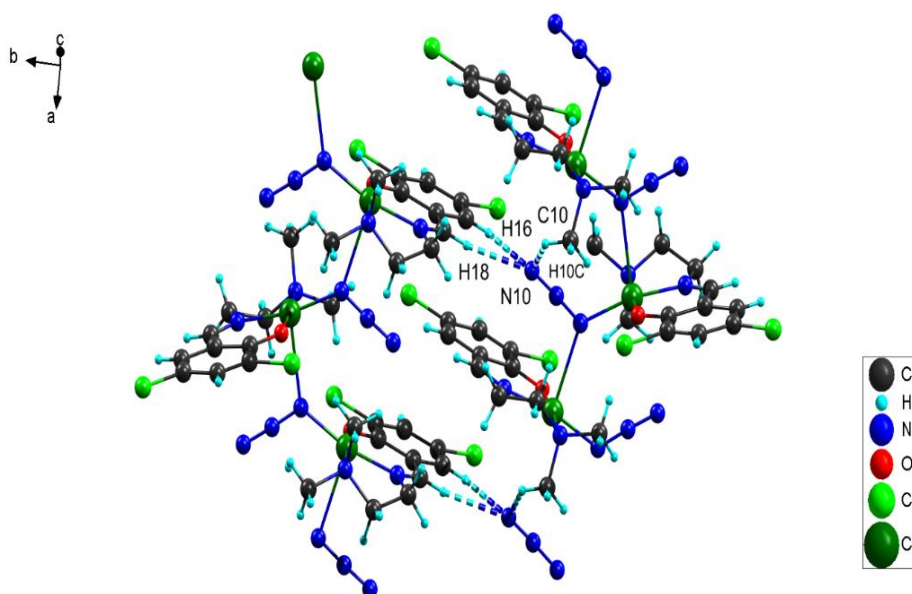


Fig. 2.18. Plot highlighting the trifurcated and bifurcated hydrogen bonding interaction in complex **1b**.

One of the phenoxy oxygens, O(1) is engaged in an intermolecular H bonding with the hydrogen [H(21A)] of the methyl carbon C(21). The other phenoxy oxygen O(2), is involved in an intrachain intermolecular hydrogen bonding with the hydrogens (H10B & H11A) of methyl carbons, C(10) and C(11) of two different adjacent units, creating a bifurcated interaction and bringing them closer together. Apart from this, an intramolecular hydrogen bond is formed by the nitrogen of azido functional group, N(4) with the hydrogen [H(11B)] borne by the methyl carbon, C(11) thus forming a S(6) ring motif [Fig. 2.19]. The two interactions arising from H(10B) and H(10C) of C(10) to O(2) and N(10) forms a $R_2^2(8)$ pattern [Fig. 2.19, Table 2.12]. No classic hydrogen bonds are present in the complexes.

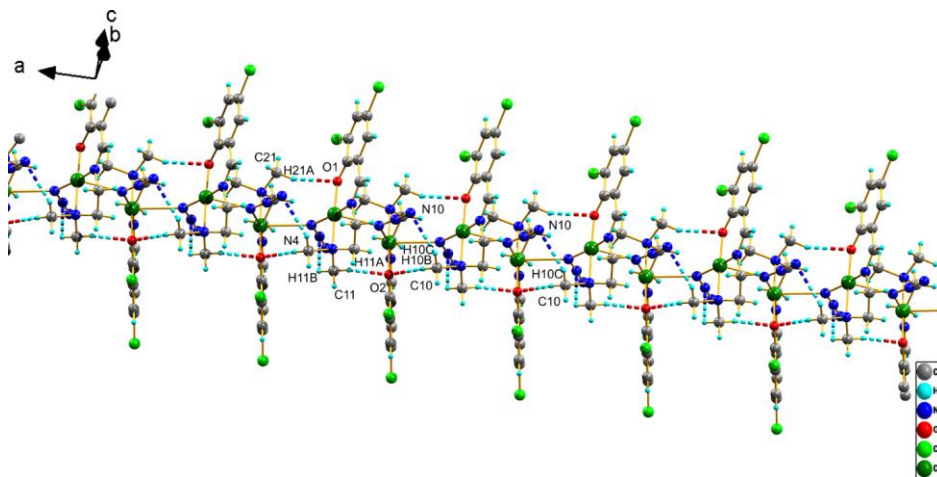


Fig. 2.19. Plot highlighting the intra and inter hydrogen bonding interaction in complex **1b**.

Table 2.12. Hydrogen bonding interactions in the complex $[\text{Cu}(\text{L}^1)(\text{N}_3)]_n$ (**1b**)

| D–H···A | D–H (Å) | H···A (Å) | D···A (Å) | D–H···A (°) |
|--|---------|-----------|-----------|-------------|
| Intermolecular hydrogen bonding | | | | |
| C(7)–H(7)···N(5) ^h | 0.93 | 2.47 | 3.382(4) | 169 |
| C(10)–H(10B)···O(2) ⁱ | 0.96 | 2.60 | 3.549(4) | 171 |
| C(11)–H(11A)···O(2) ^j | 0.96 | 2.49 | 3.439(4) | 170 |
| C(10)–H(10C)···N(10) ⁱ | 0.93 | 2.62 | 3.236(5) | 122 |
| C(16)–H(16)···N(10) ⁱ | 0.93 | 2.55 | 3.402(4) | 152 |
| C(18)–H(18)···N(10) ⁱ | 0.93 | 2.46 | 3.345(4) | 159 |
| C(21)–H(21A)···O(1) ^k | 0.96 | 2.57 | 3.491(4) | 160 |
| Intramolecular hydrogen bonding | | | | |
| C(11)–H(11B)···N(4) | 0.96 | 2.61 | 3.118(4) | 113 |

Equivalent position codes: h = 5/2-x, -1/2+y, 3/2-z; i = 3/2-x, -1/2+y, 3/2-z;
j = 5/2-x, -1/2+y, 3/2-z; k = 3/2-x, 1/2+y, 3/2-z

In form **1b**, the halogen bearing aromatic ring of one copper unit is involved in a face to face $\pi \cdots \pi$ [Cg(5)–Cg(6)] interaction [3.632(4)] with a similar ring of the adjacent unit in the nearby polymeric chain [Fig. 2.20, Table 2.13].

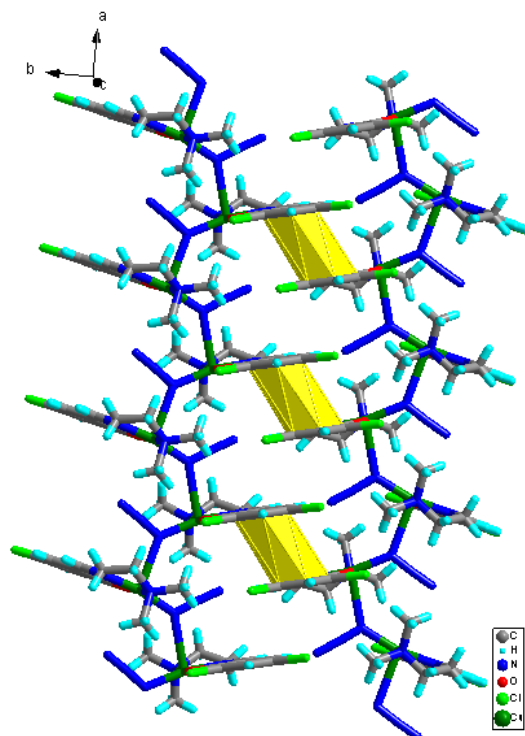


Fig. 2.20. Cg(5)···Cg(6) interaction in **1b**.

Table 2.13. Short ring interactions in $[\text{Cu}(\text{L}^1)(\text{N}_3)]_n$ (**1b**)

| Cg(I)···Cg(J) | Cg···Cg | α (°) | β (°) | γ (°) |
|-----------------------------|------------|--------------|-------------|--------------|
| Cg(5)··· Cg(6) ^a | 3.7106(15) | 1.11(12) | 23.0 | 24.1 |
| Cg(6)··· Cg(5) ^a | 3.7106(15) | 1.11(12) | 24.1 | 23.0 |

Equivalent position code: a = x, y, z

Cg(5) = C(1), C(2), C(3), C(4), C(5), C(6)

Cg(6) = C(12), C(13), C(14), C(15), C(16), C(17)

α = Dihedral angle between planes I and J (°)

β = Angle between Cg···Cg and normal to plane I

γ = Angle between Cg···Cg and normal to plane J

The azido nitrogens, N(5) and N(10) establish a non-covalent interaction with the six membered metallocycles, Cg(4) and Cg(3) respectively. Also the

halogen atom, Cl(4) establishes a contact with the halogen bearing aromatic ring, [Cg(5)] of the nearby one dimensional chain [Fig. 2.21, Table 2.14].

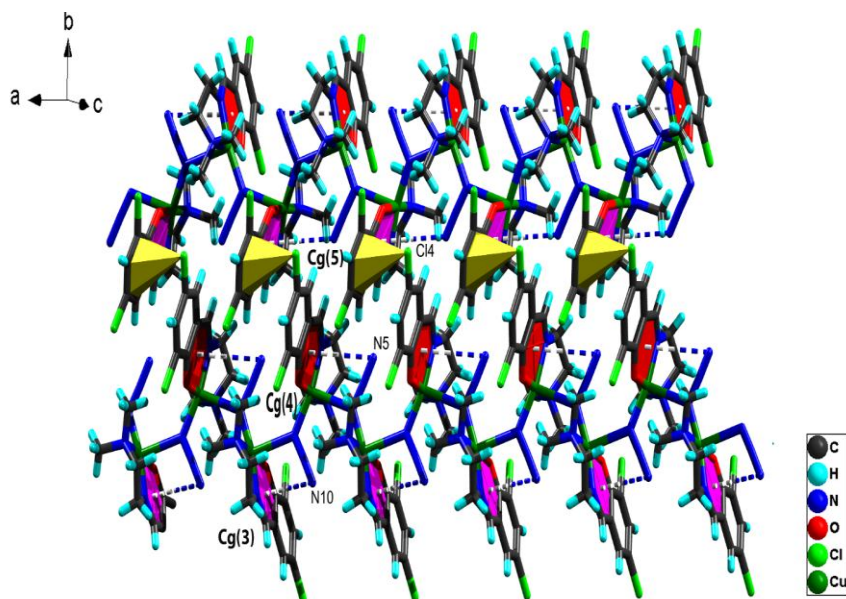


Fig. 2.21. Y–X⋯Cg interactions in **1b**.

Table 2.14. Y–X⋯Cg interactions in $[\text{Cu}(\text{L}^1)(\text{N}_3)]_n$ (**1b**)

| Y–X(I)⋯Cg(J) | X⋯Cg (Å) | Y⋯Cg (Å) | Y–X⋯Cg (°) |
|--------------------------------|------------|----------|------------|
| C(15)–Cl(4)⋯Cg(5) ^b | 3.6824(13) | 3.881(2) | 83.14(8) |
| C(15)–Cl(4)⋯Cg(5) ^c | 3.8309(13) | 3.430(2) | 63.55(8) |
| N(4)–N(5)⋯Cg(4) ^d | 3.624(4) | 3.287(2) | 63.9(1) |
| N(4)–N(5)⋯Cg(4) ^e | 3.679(4) | 4.361(2) | 119.8(2) |
| N(9)–N(10)⋯Cg(3) ^f | 3.666(4) | 4.407(2) | 124.0(2) |
| N(9)–N(10)⋯Cg(3) ^g | 3.632(4) | 3.243(3) | 61.3(1) |

Equivalent position codes: b = $-1 + x, y, z$; c = x, y, z ; d = $3/2 - x, -1/2 + y, 3/2 - z$;

e = $5/2 - x, -1/2 + y, 3/2 - z$; f = $3/2 - x, 1/2 + y, 3/2 - z$; g = $5/2 - x, 1/2 + y, 3/2 - z$

Cg(3) = Cu(1), O(1), C(1), C(6), C(7), N(1)

Cg(4) = Cu(2), O(2), C(12), C(17), C(18), N(6)

Cg(5) = C(1), C(2), C(3), C(4), C(5), C(6)

Complex **1a** doesn't have any halogen...halogen interaction whereas two intermolecular halogen interactions are seen in its polymorphic counterpart. Halogen interaction is seen between Cl(1)...Cl(1) and Cl(2)...Cl(3) atoms with distances, 3.266 and 3.6222(11) Å respectively between them which is definitely less than the sum of their van der Waals radii [Fig. 2.22]. According to Desiraju *et al.* [23,24], halogen interactions are classified as Type I and II based on bond angles 'θ1' and 'θ2' made at the halogen atoms and the intermolecular distances. So considering the angular preference, intermolecular distance and the size of Cl atom [24], we conclude these to be Type I halogen interaction where $0^\circ \leq |\theta_1 - \theta_2| \leq 15^\circ$ [Table 2.15]. Type I interaction is geometry based contact that arises from close packing and this is most effective in Cl due to its small polarisability over other halogens.

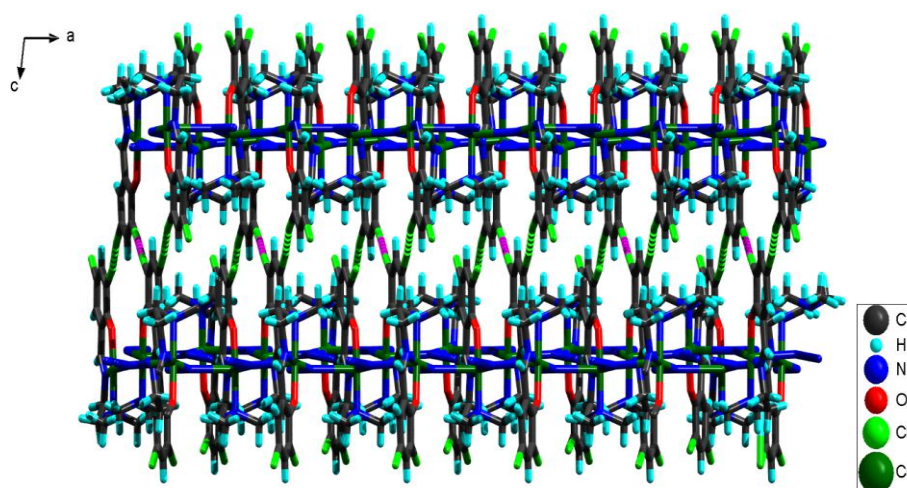


Fig. 2.22. Intermolecular Cl(1)...Cl(1) (pink) and Cl(2)...Cl(3) (green) interactions in **1b**.

Table 2.15. Type I halogen contacts in complex **1b**

| Interaction | θ1 (°) | θ2 (°) | (θ1- θ2) | X...X (Å) |
|---------------|-----------------------------------|------------------------------------|----------|-----------|
| Cl(1)...Cl(1) | C(2)- Cl(1)...Cl(1) 162.66(9) | Cl(1)...Cl(1)-C(2) 162.66(9) | 0 | 3.266 |
| Cl(2)...Cl(3) | C(4)- Cl(2)...Cl(3) 165.57(11) | Cl(3)- Cl(3)...Cl(2) 170.07(11) | 4.5 | 3.622 |

An intramolecular interaction C(2)–Cl(1)···O(1) is seen in the complex **1a** with a donor-acceptor distance of 2.912(4) Å [Fig. 2.23]. Similar interactions, C(2)–Cl(1)···O(1) and C(13)–Cl(3)···O(2) with X···B distances of 2.889(1) and 2.906(1) Å respectively are seen in the complex **1b** [Fig. 2.23]. Still they cannot be categorized as halogen bonding since the halogen in both cases are bonded to a less electronegative carbon and hence chances for chlorine to become electrophilic is meagre [25].

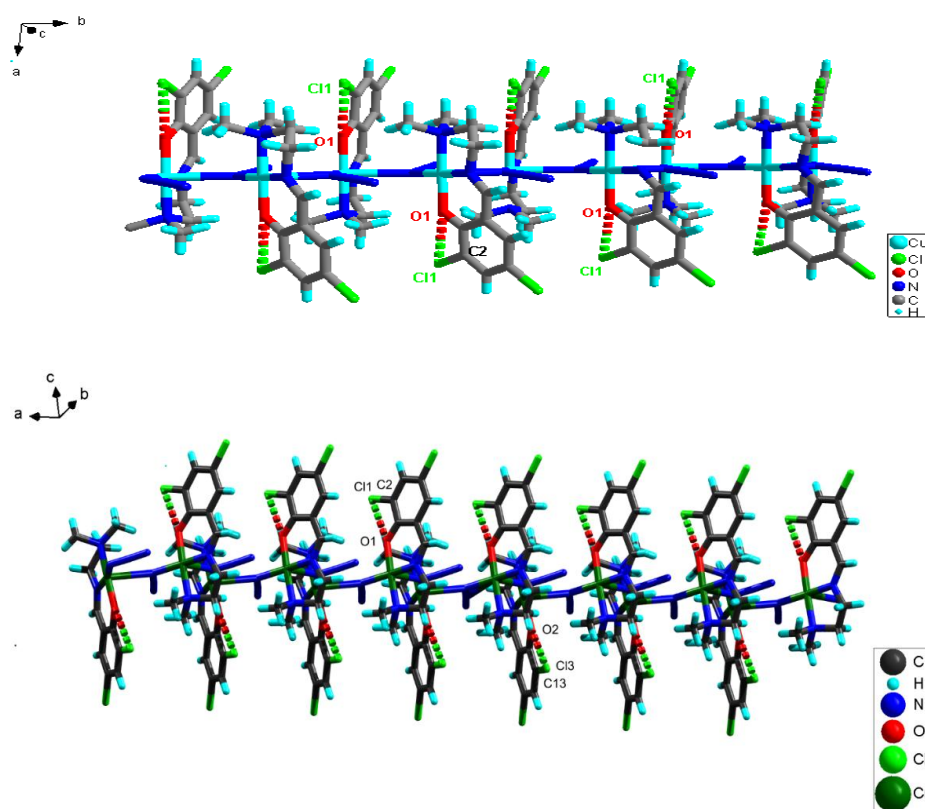


Fig. 2.23. Plot showing the intra C–Cl···O bonding interaction in complex **1a** and **1b**.

The difference in the intermolecular interactions present in complexes enabled a variation in the packing motifs, thus resulting in packing polymorphism [26]; polymorph **1a** and **1b**. The various packing interactions

and the calculated density values (1.675 and 1.722 Mgm⁻³ for **1a** and **1b** respectively), is supportive of the greater close packing of molecules in form **1b** as compared to that of **1a**. Apart from the Cg...Cg stacking interaction between rings and the hydrogen bonding interactions, these polymorphs are characterized by a difference in the halogen bonding interactions.

In the cyanato complex **2**, an intramolecular hydrogen bonding between the nitrogen (N3) of the cyanato group and the methyl carbon, C(10) generates a S(5) ring motif. A bifurcated, 3c-2 electron bond is seen between the phenoxy oxygen, O(2) [acceptor] and H(7) and H(8B) of the donor atoms C(7) [azomethine carbon] and C(8) respectively which creates a R₂¹(6) pattern [Fig. 2.24, Table 2.16] and interconnects the molecules along 'a' axis.

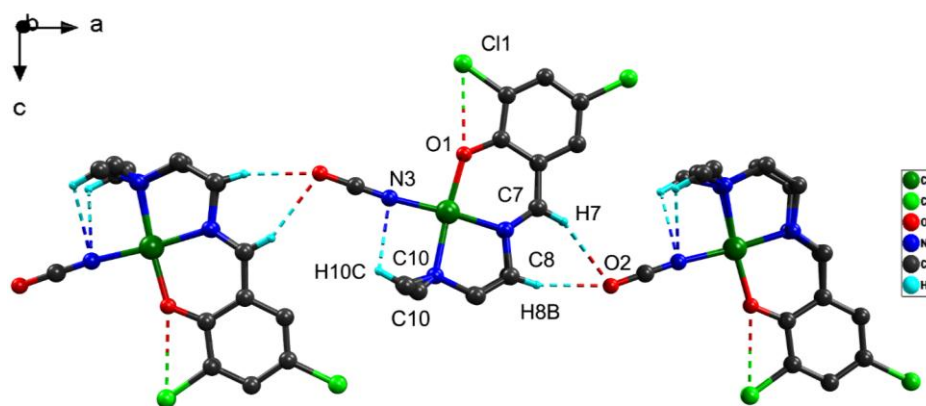


Fig. 2.24. Hydrogen bonding interactions in **2** (The C10 and H10C atoms are disordered and treated).

Table 2.16. Non-conventional hydrogen bonding interactions in the complex **2**

| D-H...A | D-H (Å) | H...A (Å) | D...A (Å) | D-H...A (°) |
|--|---------|-----------|-----------|-------------|
| Intermolecular hydrogen bonding | | | | |
| C(7)-H(7)...O(2) ^a | 0.93 | 2.57 | 3.432(5) | 154 |
| C(8)-H(8B)...O(2) ^b | 0.97 | 2.39 | 3.296(5) | 155 |
| Intramolecular hydrogen bonding | | | | |
| C(10)-H(10C)...N(3) | 0.96 | 2.58 | 3.089(16) | 113 |

Equivalent position codes:

$$a = 1/2 + x, 1/2 - y, 1/2 - z, b = 1/2 + x, y, 1/2 - z$$

Ring interactions exist between the halogen bearing ring, Cg(6) and metallocycles Cg(3) and Cg(4). Also aromatic rings, Cg(6) interact face to face with each other [Fig. 2.25, Table 2.17].

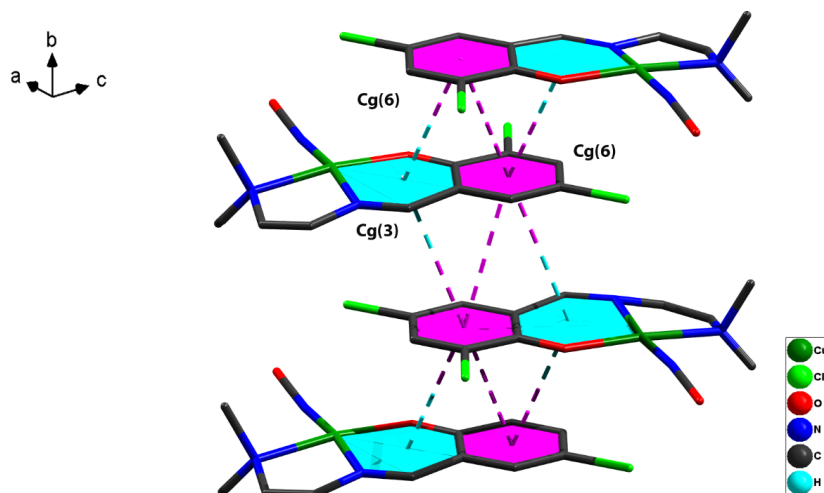


Fig. 2.25. Ring interactions in complex **2** (disordered atoms are omitted for clarity).

Table 2.17. Short ring interactions in complex **2**

| Cg(I)···Cg(J) | Cg···Cg | α (°) | β (°) | γ (°) |
|-----------------------------|-----------|--------------|-------------|--------------|
| Cg(4)··· Cg(6) ^a | 3.733(4) | 3.8(3) | 26.8 | 26.2 |
| Cg(6)··· Cg(3) ^a | 3.733(4) | 3.8(3) | 26.2 | 23.8 |
| Cg(6)··· Cg(6) ^a | 3.7076(7) | 0.0 | 23.3 | 23.3 |

Equivalent position code: $a = 1 - x, -1/2 + y, -z$

Cg(3) = Cu1,O1,C1,C6,C7,N1

Cg(4) = Cu1,O1,C1,C6,C7a,N1a

Cg(6) = C1,C2,C3,C4,C5,C6

α = Dihedral angle between planes I and J (°)

β = Angle between Cg···Cg and normal to plane I

γ = Angle between Cg···Cg and normal to plane J

There is the presence of C–X···Cg interaction between the halogen, Cl(2) and aromatic rings Cg(3) and Cg(4) [Fig. 2.26, Table 2.18].

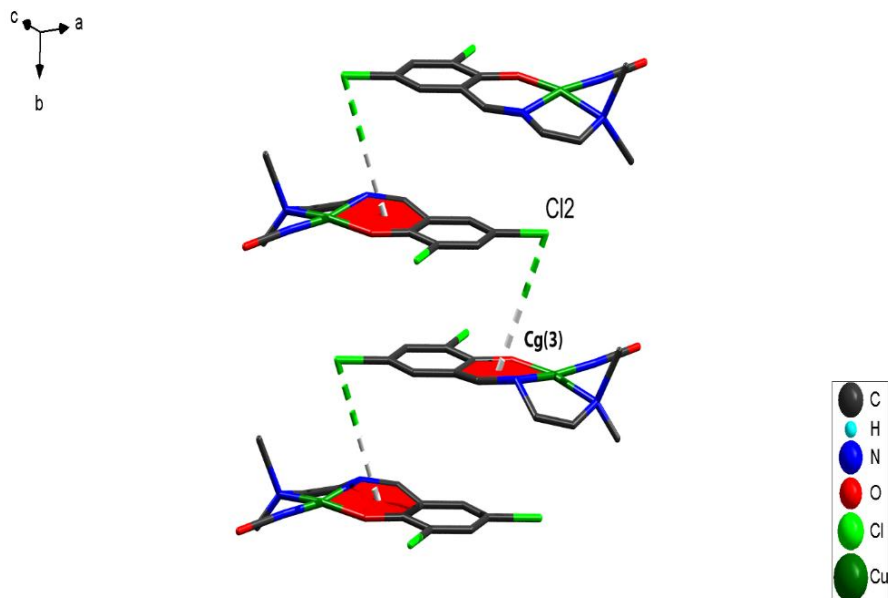


Fig. 2.26. C–X...Cg interactions in complex **2** (disordered atoms are omitted for clarity).

Table 2.18. C–X...Cg interactions in complex **2**

| C–X(I)...Cg(J) | X...Cg (Å) | C...Cg (Å) | C–X...Cg (°) |
|---------------------------------|------------|------------|--------------|
| C(4)–Cl(2)...Cg(3) ^b | 3.663(4) | 3.361(5) | 66.19(4) |
| C(4)–Cl(2)...Cg(4) ^b | 3.768(4) | 3.475(5) | 66.90(3) |

Equivalent position code: a = 1-x, -1/2+y, -z

Cg(3) = Cu1,O1,C1,C6,C7,N1

Cg(4) = Cu1,O1,C1,C6,C7a,N1a

In the thiocyanato complex **3**, Cl(1) accepts H atoms from the methyl carbons, C(10) of the adjacent units, thereby steering the monomeric units into a one-dimensional supramolecular chain along 'b' axis [Fig. 2.27, Table 2.19].

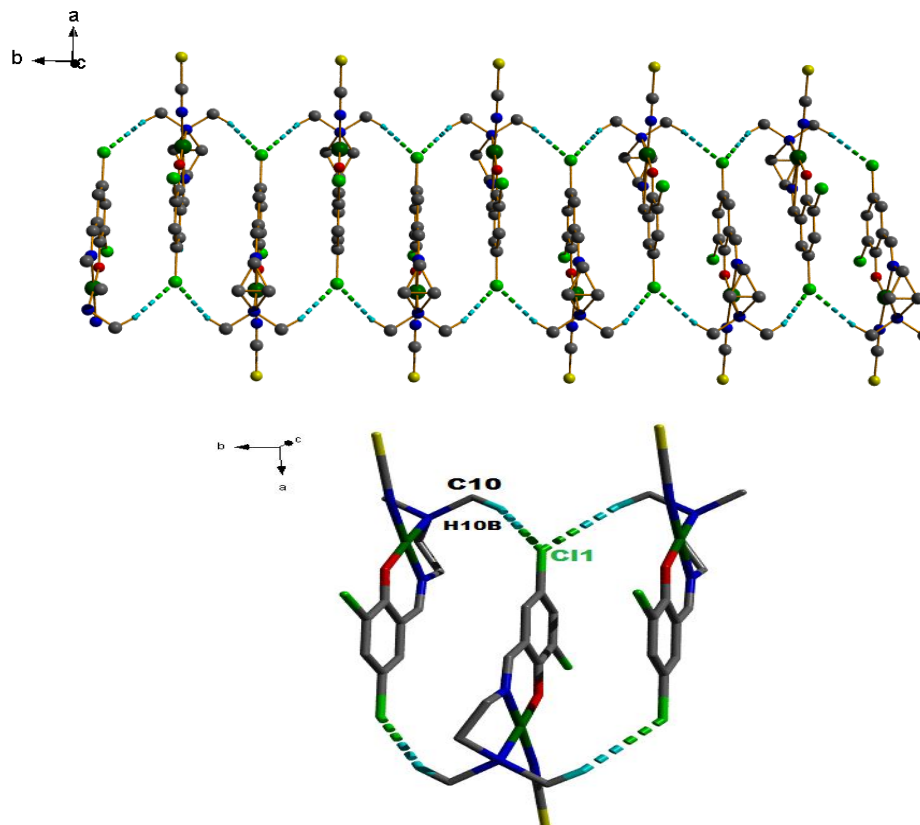


Fig. 2.27. Hydrogen bonding interactions in complex **3**, propagating the monomeric units into a supramolecular chain.

Table 2.19. Non-conventional hydrogen bonding interactions in the complex **3**

| D-H···A | D-H (Å) | H···A (Å) | D···A (Å) | D-H···A (°) |
|--|---------|-----------|-----------|-------------|
| Intermolecular hydrogen bonding | | | | |
| C(10)–H(10B)···Cl(1) ^a | 0.96 | 2.82 | 3.699(8) | 153 |

Apart from the above mentioned hydrogen bond interaction involving halogen as acceptor, there are also the presence of stacking interactions [Fig. 2.28, Table 2.20] and the halogen atom is observed to satisfy its electrophilicity by being involved in ring interaction [Fig. 2.29, Table 2.21].

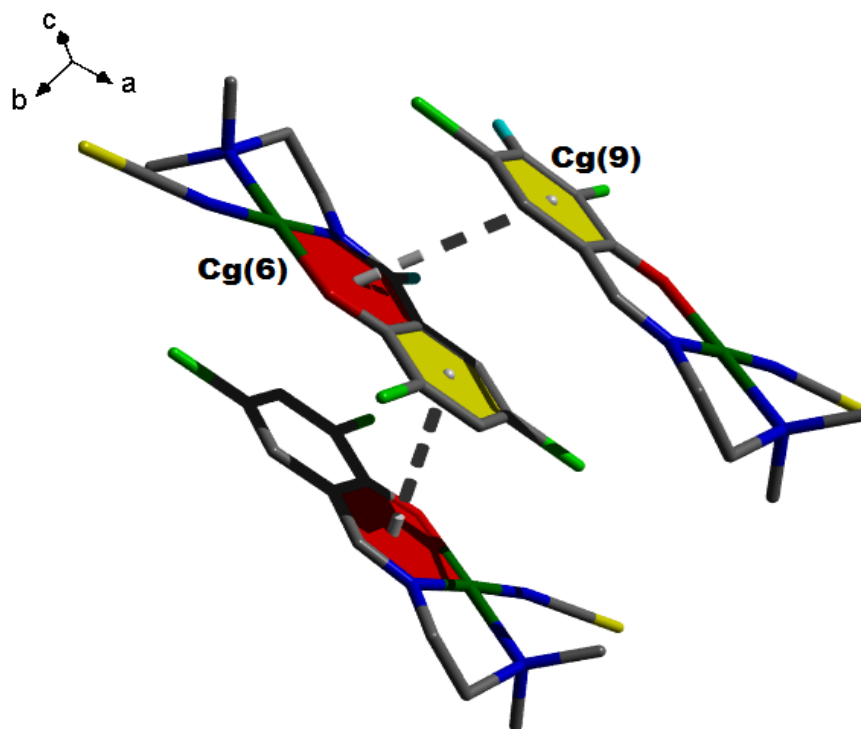


Fig. 2.28. Aromatic ring interactions in complex 3.

Table 2.20. Short ring interactions in complex 3

| Cg(I)···Cg(J) | Cg···Cg | α (°) | β (°) | γ (°) |
|-----------------------------|----------------|--------------------------------|-------------------------------|--------------------------------|
| Cg(6)··· Cg(9) ^a | 3.8368(16) | 0 | 25.1 | 25.1 |
| Cg(9)··· Cg(6) ^b | 3.8(4) | 3.8366(13) | 25.1 | 25.1 |
| Cg(9)··· Cg(9) ^c | 3.8225(16) | 0.0 | 24.6 | 24.6 |

Equivalent position codes: a = 1-x, -1/2+y, -z; b = 1-x, 1/2+y, -z; c = 1-x, -y, -z

Cg(6) = Cu1,O1,C5,C6,C7,N1

Cg(9) = C1,C2,C3,C4,C5,C6

α = Dihedral angle between planes I and J (°)

β = Angle between Cg···Cg and normal to plane I

γ = Angle between Cg···Cg and normal to plane J

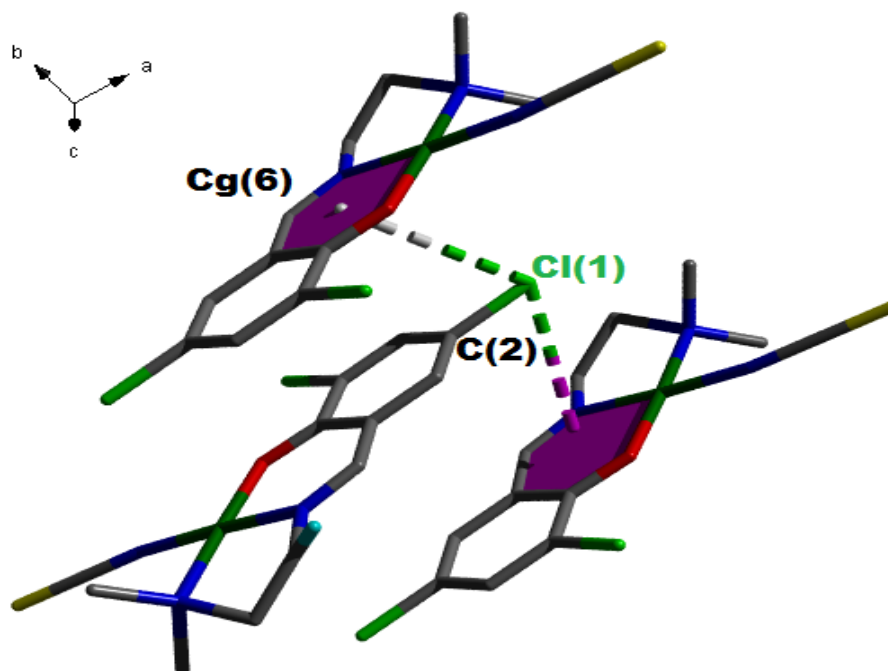


Fig. 2.29. C–Cl...Cg(6) interaction in complex **3**.

Table 2.21. C–X...Cg interaction in complex **3**

| C–X(I)...Cg(J) | X...Cg (Å) | C...Cg (Å) | C–X...Cg (°) |
|---------------------------------|------------|------------|--------------|
| C(2)–Cl(1)...Cg(6) ^d | 3.663(4) | 3.361(5) | 66.19(4) |

Equivalent position code: d = 1-x, -1/2+y, -z.

Cg(6) = Cu1,O1,C5,C6,C7,N1

2.3.3. Photoluminescence studies

Spectral analysis of the optical emission of all the four complexes were investigated in acetonitrile solution and in solid state at room temperature. The fluorescent emission spectra are shown in Fig. 2.30. The luminescent data of the complexes are summarized in Table 2.22. All copper(II) complexes showed fluorescence behavior. Complexes **1a**, **1b**, **2** and **3** on photoexcitation in the range 386-400 nm in their solid state, showed almost same behavior with an emission in the blue region (*ca.* 465 nm). The solution state emission of the

same complexes showed only violet luminescence (*ca.* 420 nm) when excited at 345 nm. There is a red shift in the major emissive peak in solid state when compared with that of solution state. The possibility of greater stacking due to the presence of stronger non-covalent interactions between molecules may be responsible for the larger red shifts of the solid state emission bands compared to their respective counterparts in solution [27]. The coordination of a metal ion with the ligand produces metallocycles which increases the conjugation length and conformational coplanarity thereby reducing transition energy of intraligand charge transfer [28].

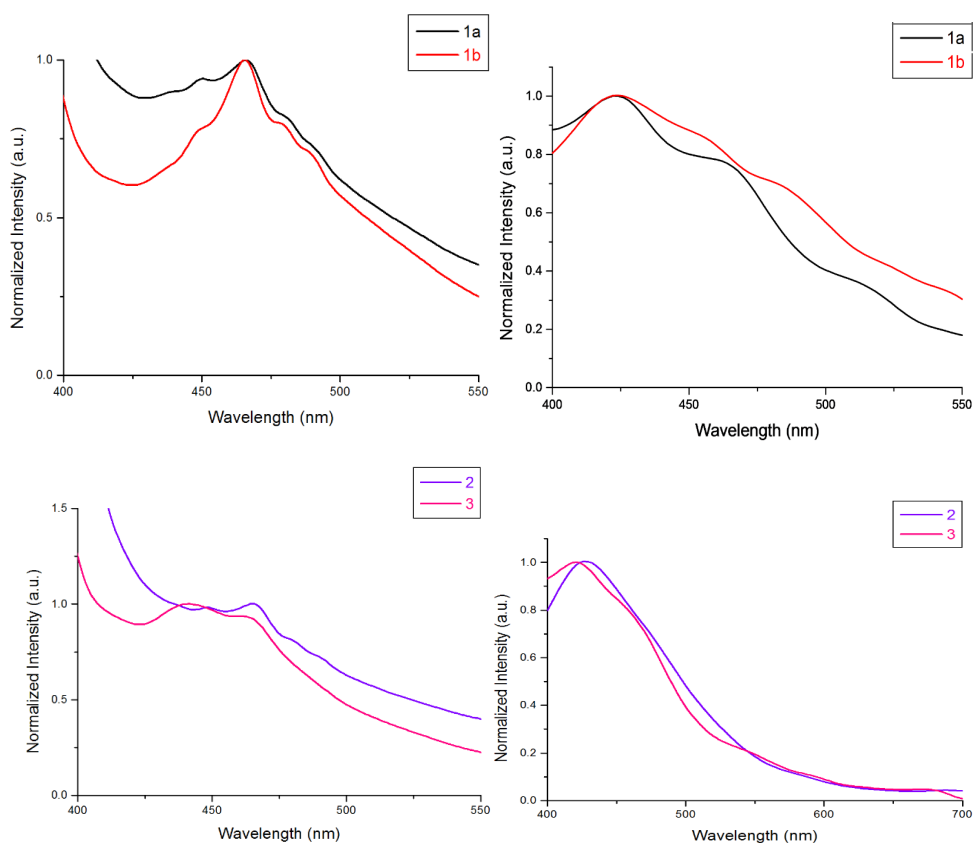


Fig. 2.30. Solid state (left) and solution state (right) [acetonitrile, 1×10^{-3} M concentration] fluorescence spectra of the complexes.

Table 2.22. Photophysical data of complexes

| Complex | Excitation (nm) | Solid state emission (nm) | Solution state emission (nm) at excitation of 345 nm |
|-----------|-----------------|---------------------------|--|
| 1a | 386 | 466 | 424 |
| 1b | 386 | 465 | 424 |
| 2 | 399 | 464 | 428 |
| 3 | 399 | 442 | 422 |

2.3.4. Thermal analysis

The thermogravimetric analysis of complex **1a** showed a single weight loss of 25.50% (calcd. 23.70%) in the temperature range of 230-260 °C corresponding to the loss of amine part. The process is exothermic as seen in DSC curves [Fig. 2.30-1a]. Beyond 400 °C a gradual weight loss occurs due to the thermal degradation of the remaining part of the complex and the decomposition is not completed even at 700 °C. Whilst its polymorphic counterpart exhibits three stage decomposition – an initial weight loss of 7.45% (calcd. 7.65%) corresponding to the loss of nitrogen from the amine portion in the range 220-240 °C, then the decomposition of azide group as N_3H coinciding with a mass loss of 13.99% (calcd. 12.43%) in the 240-271 °C range and finally there is a loss of chloride ion as HCl in 320–360 °C fitting to a 12.66% (calcd. 12.72%) mass loss. Unlike seen in complex **1a**, here a plateau like formation is observed at higher temperatures indicating the formation of a stable metal oxide. The DSC curves show exothermic peaks for all the three stages [Fig. 2.30-1b].

The thermogram of complex **2** shows a 29.54% (calcd. 30.89%) weight loss (230-263 °C), exothermically corresponding to the loss of HCN and Cl_2O [Fig. 2.30-2] after which a stable metal oxide is formed.

Complex **3** exhibits a double stage exothermic decomposition pattern with an initial loss of nitrogen, corresponding to a mass degradation of 6.31% (calcd. 7.91%) followed by a loss of Cl_2O (27.18%, calcd. 26.70%). At higher temperatures, formation of a stable metal oxide is observed [Fig. 2.30-3].

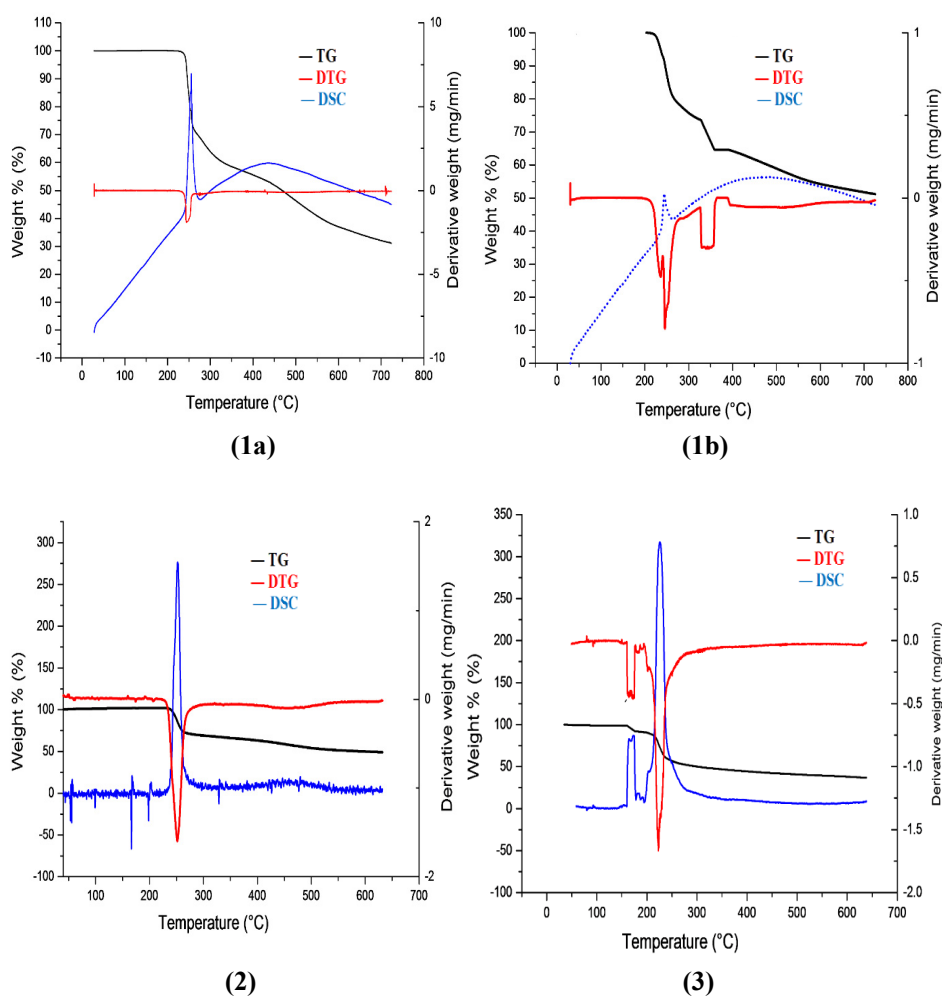


Fig. 2.30. Thermogram of the complexes.

2.3.5. EPR spectral studies

The EPR spectra of the polycrystalline polymeric complexes **1a** and **1b** at room temperature are of axial type giving rise to two g values, g_{\parallel} and g_{\perp} with $g_{\parallel} > g_{\perp} > g_e$ (2.0023), with no hyperfine lines in the parallel and perpendicular region. The variation in the g_{\parallel} and g_{\perp} values indicate that in the solid state, the

geometry of the compounds is affected by the nature of coordinating ligands [Fig. 2.32]. The EPR spectra are simulated using EasySpin package [29] and the experimental (red) and simulated (blue) best fits are included.

The g -values in axial symmetry are correlated by the expression,

$$G = (g_{\parallel} - 2.0023) / (g_{\perp} - 2.0023) \quad [30]$$

which reflects the exchange interaction between Cu(II) centers in the solid polycrystalline complexes. Accordingly, if G is greater than 4, the exchange interaction may be negligible; however, if G is less than 4, a considerable exchange interaction is indicated in the solid complex [31]. The G values for the polymer complexes were found to be less than 4.0, indicative of considerable exchange interaction between the copper centers in the solid.

The EPR spectra of the complexes recorded in frozen state at 77 K gives more information on the geometry of the complexes. Both the complexes, **1a** and **1b** display axial features [$(g_{\parallel} = 2.232, g_{\perp} = 2.085)$ and $(g_{\parallel} = 2.202, g_{\perp} = 2.120)$] with well resolved hyperfine splittings in parallel and perpendicular region due to the interaction of the odd electron with the nuclear spin ($^{63,65}\text{Cu}, I = 3/2$). Although expected superhyperfine splittings are not seen for complex **1a**, its polymorphic counterpart shows quintet splittings in the perpendicular regions due to the coupling of electron spin with the nuclear spin of the two nitrogen atoms ($I = 1$) with super exchange splitting constant, $A_{\text{N}_a} = 15.83 \times 10^{-4} \text{ cm}^{-1}$. However, the superhyperfine splittings are not visible in the parallel region.

For these pentacoordinate complexes **1a** and **1b**, the fact that g_{\parallel} is greater than g_{\perp} suggests a distorted square-pyramidal structure consistent with the X-ray structural analysis and rules out the possibility of a trigonal bipyramidal structure, which would be expected to have $g_{\perp} > g_{\parallel}$.

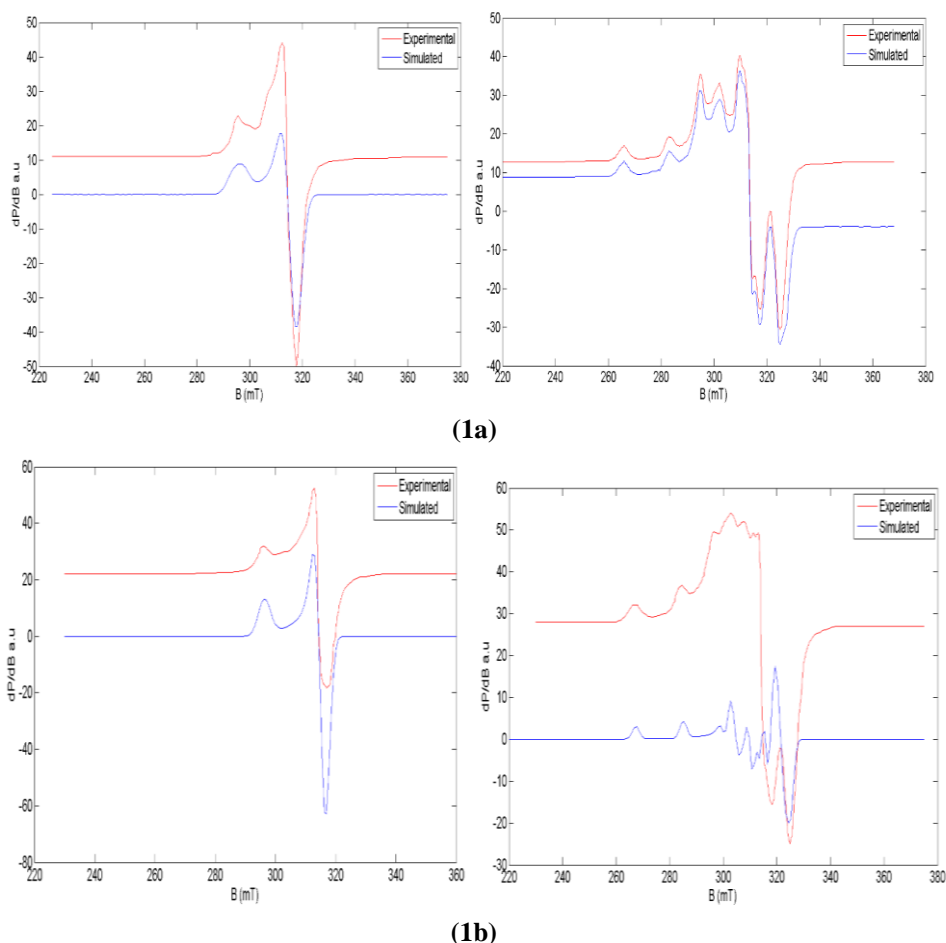


Fig. 2.32. EPR spectra of complexes **(1a)** and **(1b)** in polycrystalline state (left) and in DMF at 77 K (right).

Complex **2** presents a typical axial spectra in the polycrystalline state with well-defined g_{\parallel} and g_{\perp} values. The spectra is broad because of the fast spin lattice relaxation and exchange coupling. Eventhough axial features are displayed, since it is magnetically concentrated, hyperfine splitting was not clear both in parallel and perpendicular regions. Calculated G values for complex **2** is slightly greater than 4 ruling out the possibility of an exchange interaction. The spectrum of compound **2** in DMF gave three g values, *viz.* $g_1 = 2.056$, $g_2 = 2.180$ and $g_3 = 2.293$, indicating a rhombic distortion in the geometry [Fig. 2.33].

Complex **3** has g values - $g_{\parallel} = 2.125$ and $g_{\perp} = 2.117$, characteristic of an axial spectrum and the G value is indicative of a possible exchange interaction in polycrystalline state. The spectra of the complex at 77 K shows four hyperfine splittings in the parallel region although they are not observed in the perpendicular region [Fig. 2.33].

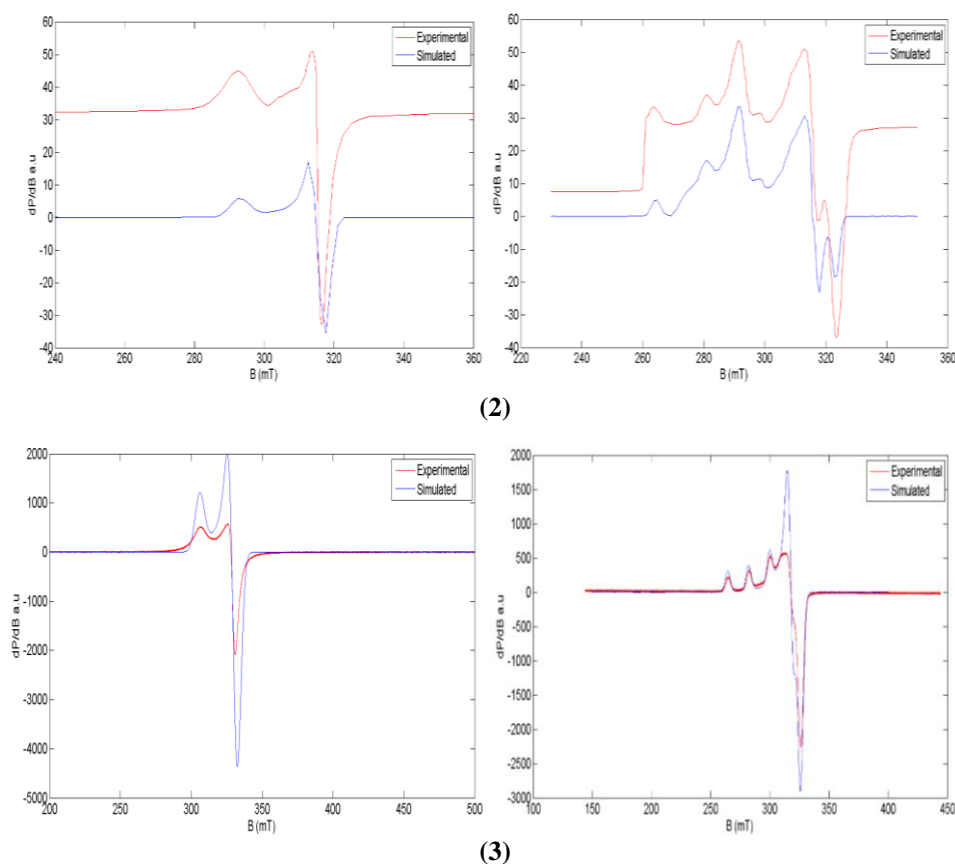


Fig. 2.33. EPR spectra of complexes (**2** and **3**) in polycrystalline state (left) and in DMF at 77 K (right).

The bonding parameters α^2 , β^2 and γ^2 , considered to be the measure of the covalency of in-plane σ -bonds, in-plane π -bonds and out-of-plane π -bonds respectively are evaluated using the EPR parameters g_{\parallel} , g_{\perp} , g_{av} , A_{\parallel} (Cu) and A_{\perp} (Cu) along with the energies of $d-d$ transition.

The value of in-plane sigma bonding parameter α^2 was estimated from the expression [32]

$$\alpha^2 = -A_{\parallel} / 0.036 + (g_{\parallel} - 2.0023) + 3/7 (g_{\perp} - 2.0023) + 0.04$$

The following simplified expressions were used to calculate the bonding parameters

$$K_{\parallel}^2 = (g_{\parallel} - 2.0023) E_{d-d} / 8\lambda_0$$

$$K_{\perp}^2 = (g_{\perp} - 2.0023) E_{d-d} / 2\lambda_0$$

$$K_{\parallel}^2 = \alpha^2 \beta^2$$

$$K_{\perp}^2 = \alpha^2 \gamma^2$$

Where K_{\parallel} and K_{\perp} are orbital reduction factors and λ_0 represents the one electron spin orbit coupling constant which equals -828 cm^{-1} .

Hathaway [33] has pointed out that for pure sigma bonding $K_{\parallel} \approx K_{\perp} \approx 0.77$, for in plane π -bonding $K_{\parallel} < K_{\perp}$ and for out-of-plane π -bonding, $K_{\perp} < K_{\parallel}$. For complexes **1a**, **1b**, **2** and **3**, it is observed that $K_{\parallel} < K_{\perp}$ which indicates the presence of significant in-plane π -bonding. The nature of metal-ligand bond is evaluated by comparing the value of in-plane sigma bonding parameter α^2 *i.e.* if the M-L bond is purely ionic, the value of α^2 is unity and it is completely covalent, if $\alpha^2 = 0.5$ [33]. Here α^2 values calculated for all the complexes lie between 0.5 and 1, which means that the metal-ligand bonds in the complexes under study are partially ionic and partially covalent in nature.

The g_{\parallel} values also provide information regarding the nature of metal-ligand bond [34]. The g_{\parallel} value is normally 2.3 or larger for ionic and less than 2.3 for covalent metal-ligand bonds. The g_{\parallel} values obtained for our complexes indicate a significant degree of covalency in the metal-ligand bonds [35]. The index of tetragonal distortion f is calculated as $f = g_{\parallel} / A_{\parallel}$, whose value may vary from 105-135 for small to medium distortion and depends on the nature of the coordinated atom [36]. In all complexes distortion is medium and is found to be in the range 105-115 cm [37]. EPR parameters of the copper(II) complexes are presented in Table 2.23.

Table 2.23. Spin Hamiltonian and bonding parameters of copper(II) complexes

| Compounds | Polycrystalline state (298 K) | | | | | | | | | | DMF solution (77 K) | | | | | | | | | |
|--|-------------------------------|-----------------|-------------|--------|--------------------|---------------------|-----------------|-----------------|-------------|-----------------|---------------------|-----------|------------|-----------------|-------------|--------|--|--|--|--|
| | g_{iso} | g_{\parallel} | g_{\perp} | G | $g_{\parallel}g_s$ | $g_{\perp}g_1, g_2$ | g_{sw} | A_{\parallel} | A_{\perp} | A_{sw} | α^2 | β^2 | γ^2 | K_{\parallel} | K_{\perp} | f | | | | |
| $[\text{Cu}(\text{L}^1)(\text{N}_3)]_n$ (1a) | -- | 2.200 | 2.056 | 3.6816 | 2.252 | 2.085 | 2.1337 | 200 | 83 | 122 | 0.8602 | 0.8890 | 1.0668 | 0.7647 | 0.9177 | 111.60 | | | | |
| $[\text{Cu}(\text{L}^1)(\text{N}_3)]_n$ (1b) | -- | 2.195 | 2.060 | 3.3397 | 2.202 | 2.120 | 2.1471 | 214 | 40 | 98 | 0.8863 | 0.8058 | 1.2373 | 0.7142 | 1.0966 | 102.48 | | | | |
| $[\text{Cu}(\text{L}^1)(\text{NCO})]_n$ (2) | -- | 2.220 | 2.056 | 4.054 | 2.293 | 2.056, | 2.1384 | 208 | 35 | 93 | 0.8982 | 0.3985 | 1.4496 | 0.3579 | 1.3020 | 110.10 | | | | |
| | | | | | | 2.180 | | | | | | | | | | | | | | |
| $[\text{Cu}(\text{L}^1)(\text{NCS})]_n$ (3) | --- | 2.125 | 2.117 | 1.069 | 2.234 | 2.045 | 2.1077 | 205 | -- | -- | 0.8601 | 0.8726 | 0.7492 | 0.7505 | 0.6444 | 108.00 | | | | |

 A values in 10^{-4} cm^{-1}

References

- [1] Y. Nair, M. Sithambaresan, M.R.P. Kurup, *Acta Crystallogr., Sect. E: Struct. Rep. Online* **2012**, *68*, 2709.
- [2] P. Bhowmik, A. Bhattacharyya, K. Harms, S. Sproules, S. Chattopadhyay, *Polyhedron* **2015**, *85*, 221.
- [3] a) M. Das, S. Chattopadhyay, *Transit. Met. Chem.* **2013**, *38*, 191.
b) T.A. Reena, E.B. Seena, M.R.P. Kurup, *Polyhedron* **2008**, *27*, 1825.
- [4] a) S. Sasi, M. Sithambaresan, M.R.P. Kurup, H-K. Fun, *Polyhedron* **2010**, *29*, 2643.
b) R.J. Kunnath, M. Sithambaresan, A.A. Aravindakshan, A. Natarajan, M.R.P. Kurup, *Polyhedron* **2016**, *113*, 73.
- [5] P. Bhowmik, S. Chatterjee, S. Chattopadhyay, *Polyhedron* **2013**, *63*, 214.
- [6] B. Shaabani, A.A. Khandar, M. Dusek, M. Pojarova, F. Mahmoudi, *Inorg. Chim. Acta* **2013**, *394*, 563.
- [7] a) S. Biswas, A. Ghosh, *Polyhedron* **2013**, *65*, 322.
b) R. Gup, B. Kirkan, *Spectrochim. Acta A* **2005**, *62*, 1188.
- [8] S.-Q. Bai, E.-Q. Gao, Z. He, C.-J. Fang and C.-H. Yan, *New J. Chem.* **2005**, *29*, 935.
- [9] a) B.J. Hathaway, in: G. Wilkinson, R.D. Gillard, J.A. McCleverty (Eds.), *Comprehensive Coordination Chemistry*, Vol. 5, Pergamon, Oxford, **1987**, p. 533.
b) P. Mukherjee, O. Sengupta, M.G.B. Drew, A. Ghosh, *Inorg. Chim. Acta* **2009**, *362*, 3285.
- [10] N.A. Mangalam, S. Sivakumar, M.R.P. Kurup, E. Suresh, *Spectrochim. Acta A* **2010**, *75*, 686.
- [11] C. Reichardt, *Chem. Rev.* **1994**, *94*, 2319.
- [12] K. Sone, Y. Fukuda, *Inorganic Thermochemistry in Inorganic Chemistry Concepts*, Vol. 10, Springer-Verlag, Berlin, **1987**, 72.

- [13] a) H. Golchoubian, G. Moayyedi, G. Bruno, H. Amiri, *Polyhedron* **2011**, *30*, 1027.
b) H. Golchoubian, G. Moayyedi, E. Rezaee, G. Bruno, *Polyhedron* **2015**, *96*, 71.
- [14] A.L. Spek, *Acta Cryst. C*, **2015**, *71*, 9.
- [15] S. Mondal, P. Chakraborty, N. Aliaga-alcalde, S. Mohanta, *Polyhedron* **2013**, *63*, 96.
- [16] A.W. Addison, T.N. Rao, J. Reedijk, J. Van Rijn, G.C. Verschoor, *J. Chem. Soc., Dalton Trans.* **1984**, 1349.
- [17] a) C. Biswas, M.G.B. Drew, E. Ruiz, M. Estrader, A. Ghosh, *Dalton Trans.* **2010**, *39*, 7474.
b) J.M. Clemente-juan, S. Naiya, C. Biswas, M.G.B. Drew, J.G. Carlos, *Inorg. Chem.* **2010**, *49*, 6616.
c) S. Sasmal, S. Sarkar, *Inorg. Chem.* **2011**, *50*, 5687.
- [18] a) P. Bhowmik, A. Bhattacharyya, K. Harms, S. Sproules, S. Chattopadhyay, *Polyhedron* **2015**, *85*, 221.
b) P.K. Bhaumik, K. Harms, S. Chattopadhyay, *Polyhedron* **2013**, *62*, 179.
- [19] D. Cremer, J.A. Pople, *J. Am. Chem. Soc.* **1975**, *97*, 1354.
- [20] S.T. Rao, E. Westhof, M. Sundaralingam, *Acta Crystallogr., Sect. A: Struct. Rep. Online* **1981**, *37*, 421.
- [21] L. Yang, D.R. Powell, R.P. Houser, *Dalton Trans.* **2007**, 955.
- [22] Z. You, *Acta Cryst.* **2005**, *E61*, m2226.
- [23] S. Tothadi, S. Joseph, G.R. Desiraju, *Cryst. Growth Des.* **2013**, *13*, 3242.
- [24] A. Mukherjee, S. Tothadi, G.R. Desiraju, *Acc. Chem. Res.* **2014**, *47*, 2514.
- [25] P. Politzer, J.S. Murray, *Chem. Phys. Chem.* **2013**, *1*.

- [26] U. Mukhopadhyay, I. Bernal, D.S. Yufit, J.A.K. Howard, L. Massa, A. Gindulyte, L. Todaro, S.S. Massoud, *Inorg. Chim. Acta* **2004**, 357, 4121.
- [27] Y. He, C. Zhong, Y. Zhou, H. Zhang, *J. Chem. Sci.* **2009**, 121, 407.
- [28] M. Barwiolek, E. Szlyk, T.M. Muzioł, T. Lis, *Dalton Trans.* **2011**, 40, 11012.
- [29] S. Stoll, *Spectral Simulations in Solid-State Electron Paramagnetic Resonance*, Ph.D. thesis, ETH, Zurich, **2003**.
- [30] I.M. Procter, B.J. Hathaway, P. Nicholis, *J. Chem. Soc. A* **1968**, 1678.
- [31] X. Wang, J. Ding, J.D. Ranford, J.J. Vittal, *J. Appl. Phys.* **2003**, 93, 7819.
- [32] B.N. Figgis, *Introduction to Ligand fields*, Interscience, New York, **1996**, 295.
- [33] B.J. Hathaway, in: G. Wilkinson, R.D. Gillard, J.A. McCleverty (Eds.), *Comprehensive Coordination Chemistry*, Vol. 5, Pergamon, Oxford, **1987**, p. 533.
- [34] T.D. Smith, J. Pilbrow, *Coord. Chem. Rev.* **1974**, 13, 173.
- [35] D. Kivelson, R. Neiman, *J. Chem. Phys.* **1961**, 35, 149.
- [36] L. Latheef, M.R.P Kurup, *Spectrochim. Acta A* **2008**, 70, 86.
- [37] R.P. John, A. Sreekanth, V. Rajakannan, T.A. Ajith, M.R.P. Kurup, *Polyhedron* **2004**, 23, 2549.

.....✂.....

Chapter 3

Coordination polymers derived from *N,N*-dimethyl-1,3-propanediamine and 3,5-dichlorosalicylaldehyde

Contents

- 3.1. Introduction
- 3.2. Experimental
- 3.3. Results and discussion

Conspectus

Two copper(II) complexes based on *N,N*-dimethyl-1,3-propanediamine and 3,5-dichlorosalicylaldehyde are synthesized, both of which are coordination polymers with azido and dicyanamido groups in an end-to-end bridging mode. As a sequel to the earlier chapter, we have adopted the same synthetic protocol except for the amine used – *N,N*-dimethyl-1,3-propanediamine instead of *N,N*-dimethylethylenediamine. We have successfully isolated single crystals of both the complexes. The azido complex is a coordination polymer along 'a' axis of the orthorhombic unit cell whilst the dicyanamido complex propagates as a chain along 'b' axis of the triclinic unit cell. Although the azido complex is a 1-D polymer, the involvement of non-covalent forces develop it into a 3-D supramolecular network. In the case of dicyanamido complex, there is no such self-assembling forces observed, making it purely one dimensional. Apart from the preliminary characterization studies, we have done solvatochromic studies of the complexes so as to study the effect of solvents on charge-transfer/intra-ligand transitions as well as on the d-d bands. The former showed negative solvatochromic effect and the latter showed a red shift. The photoluminescence study, thermal analysis and solution-state EPR analysis of the samples are also carried out.

3.1. Introduction

Coordination polymers are infinite systems build up with metal ions and organic ligands as main elementary units linked *via* coordination bonds and other weak chemical bonds [1]. In coordination polymers, the main synthons are the coordination bonds and the tectons are the copper(II) ions and the ligands [2].

We have used HL type of ligand system, whereby one of the charges of copper(II) is satisfied by the phenolate oxygen and the other by the pseudohalide coligand. In the complexes that we isolated, the linear azide and the polynitrile bent ligand, dicyanamide act as linkers. In both the complexes, the ambidenticity of the linkers are revealed as both the nitrogen atoms of the spacer group simultaneously engage in bonding - $\mu_{1,3}$ in case of azide and $\mu_{1,5}$ for dicyanamide.

3.2. Experimental

3.2.1. Materials

All chemicals were of reagent grade and purchased from commercial sources. The solvents were purified according to standard procedures. 3,5-Dichlorosalicylaldehyde (Aldrich), *N,N*-dimethyl-1,3-propanediamine (Aldrich), $\text{CuCl}_2 \cdot 2\text{H}_2\text{O}$, $\text{Cu}(\text{OAc})_2 \cdot \text{H}_2\text{O}$, NaN_3 , $\text{Na}[\text{N}(\text{CN})_2]$ (all are BDH, AR quality) were used as received.

The Schiff bases were formed *in situ*.

Caution! Azido compounds are potentially explosive. Although no problems were encountered in the present study, it should be prepared only in small quantities and handled with care.

3.2.2. Synthesis of copper(II) complexes

3.2.2.1. Synthesis of complexes, $[\text{Cu}(\text{L}^2)(\text{X})]_n$ (4 and 5)

**$[\text{HL}^2 = 2,4\text{-dichlorido-6-}((3\text{-(dimethylamino)propylimino)methyl)phenol}$
($\text{X} = \text{N}_3^-$, $\text{N}(\text{CN})_2^-$)**

3,5-Dichlorosalicylaldehyde (0.205 g, 1 mmol) and *N,N*-dimethyl-1,3-propanediamine (0.102 g, 1 mmol) were dissolved in 10 mL methanol and refluxed for about an hour. After heating the reaction mixture with methanolic

solution (10 mL) of copper(II) chloride dihydrate (0.170 g, 1 mmol) for about half an hour, sodium azide (0.130 g, 2 mmol) in a MeOH/H₂O (1:9) mixture was added dropwise with continuous stirring and refluxed further for about two hours. The procedure was repeated as such except for the addition of copper(II) acetate monohydrate (0.199 g, 1 mmol) followed by sodium dicyanamide (0.130 g, 2 mmol) in a MeOH/H₂O (1:9) mixture to prepare complex 5. Suitable single crystals for structure determination by X-ray diffraction were obtained by slow evaporation of the mother liquor in air.

Complex 4:

Yield: 0.3408 g (78%). *Anal.* Calc. for C₁₃H₁₈Cl₂CuN₈O (436.79): C, 35.75; H, 4.15; N, 25.65 Found C, 35.73; H, 4.18; N, 25.67%.

UV-vis, λ_{\max} /nm ($\epsilon_{\max}/10^3 \text{ M}^{-1}\text{cm}^{-1}$) (acetonitrile): 383 (8.73), 268 (20.53), 232 (34.05)

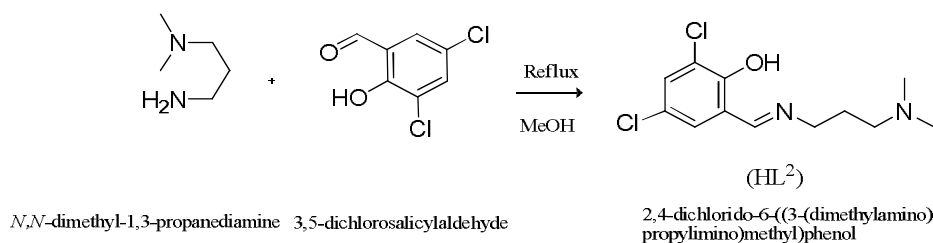
Complex 5:

Yield: 0.3640 g (70%). *Anal.* Calc. for C₂₀H₂₇Cl₂CuN₈O (529.00): C, 44.73; H, 6.38; N, 20.87 Found C, 44.76; H, 6.40; N, 20.85%.

UV-vis, λ_{\max} /nm ($\epsilon_{\max}/10^3 \text{ M}^{-1}\text{cm}^{-1}$) (acetonitrile): 384 (5.83), 272 (14.83), 234 (26.97)

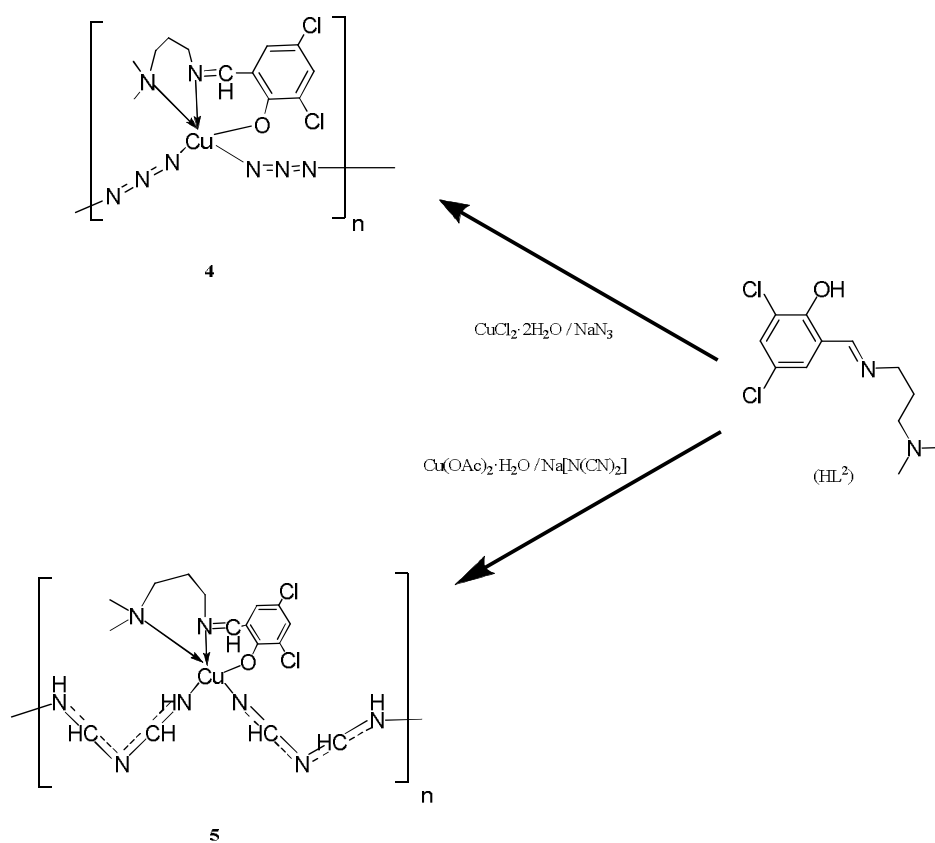
3.3. Results and discussion

The simple 1:1 condensation reaction between *N,N*-dimethyl-1,3-propanediamine and dichlorosubstituted aldehyde resulted in the formation of tridentate Schiff base ligand [Scheme 3.1]. The isolation of Schiff base being difficult, we followed an *in-situ* generation of ligand for the preparation of complex [Scheme 3.2].



Scheme 3.1. Formation of tridentate Schiff base.

The ligand thus generated was treated with copper salts followed by the addition of pseudohalides like sodium azide and sodium dicyanamide in 1:2 ratio. We could isolate single crystals of a polymeric azide and dicyanamide from 2,4-dichlorido-6-((3-(dimethylamino)propylimino)methyl)phenol (HL^2).



The elemental analysis confirmed the purity of all complexes. They are soluble in polar solvents like methanol, DMF and DMSO.

3.3.1. Spectroscopic features

3.3.1.1. IR and electronic spectra

Distinct bands due to azomethine ($C=N$) group within $1580-1630\text{ cm}^{-1}$ are customarily observed in the complexes confirming the process of

complexation [3]. The stretching frequency at 2075 cm^{-1} corroborates the *end-to-end* azide linkage as seen in X-ray diffraction studies [4]. In the case of dicyanamido complex, the slight shift in frequency from that of the free dca anion [$\nu_{\text{as}} + \nu_{\text{s}}(\text{C}=\text{N})$ combination modes (2286 cm^{-1}), $\nu_{\text{as}}(\text{C}=\text{N})$ (2232 cm^{-1}) and $\nu_{\text{s}}(\text{C}=\text{N})$ (2179 cm^{-1})] to 2296 , 2243 and 2171 cm^{-1} respectively is indicative of the bridging bidentate dca [5]. The band at 2046 cm^{-1} is consistent with the presence of only single type of azido bridge in the complex [6]. The IR spectra of the complexes is shown in Fig. 3.1.

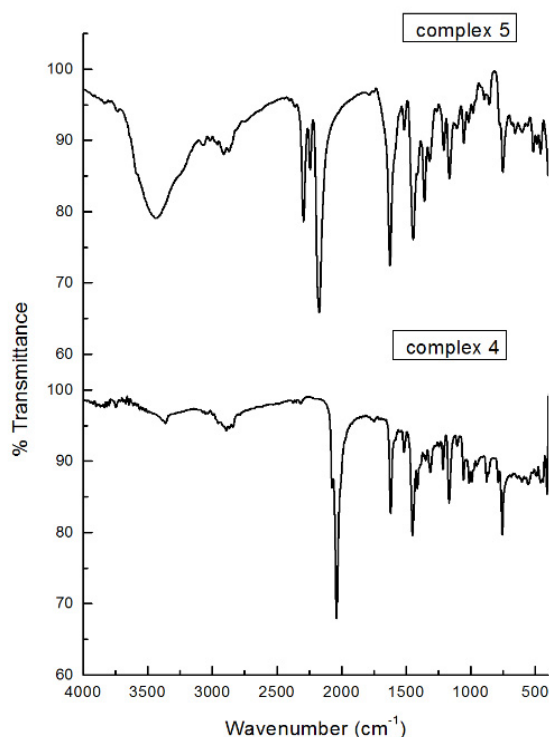


Fig. 3.1. IR spectra of the complexes 4 and 5.

The linear optical properties of the compounds were scanned in the UV-vis region in acetonitrile medium. The NNO tridentate complexes exhibit almost similar spectroscopic pattern with high intense bands [with $\epsilon > 5000\text{ M}^{-1}\text{cm}^{-1}$] at $\lambda < 400\text{ nm}$ corresponding to charge-transfer and intra-ligand transitions and a single broad band in the visible region at $\lambda = 570 - 650\text{ nm}$ with ϵ values

ranging from 230 to 300 $M^{-1}cm^{-1}$, consistent with non resolved $d-d$ transitions from low lying orbitals to the half-filled d orbital. The presence of extended π -system resulting in a high degree of π -delocalisation between the metal centre and the ligand is reflected in the ϵ values.

3.3.1.2. Solvatochromic studies

The interaction of solvents with solute's ground and excited states are different. This variation in solvation energy between the two states result in change of optical transition energy of solutes, called solvatochromic shift [7].

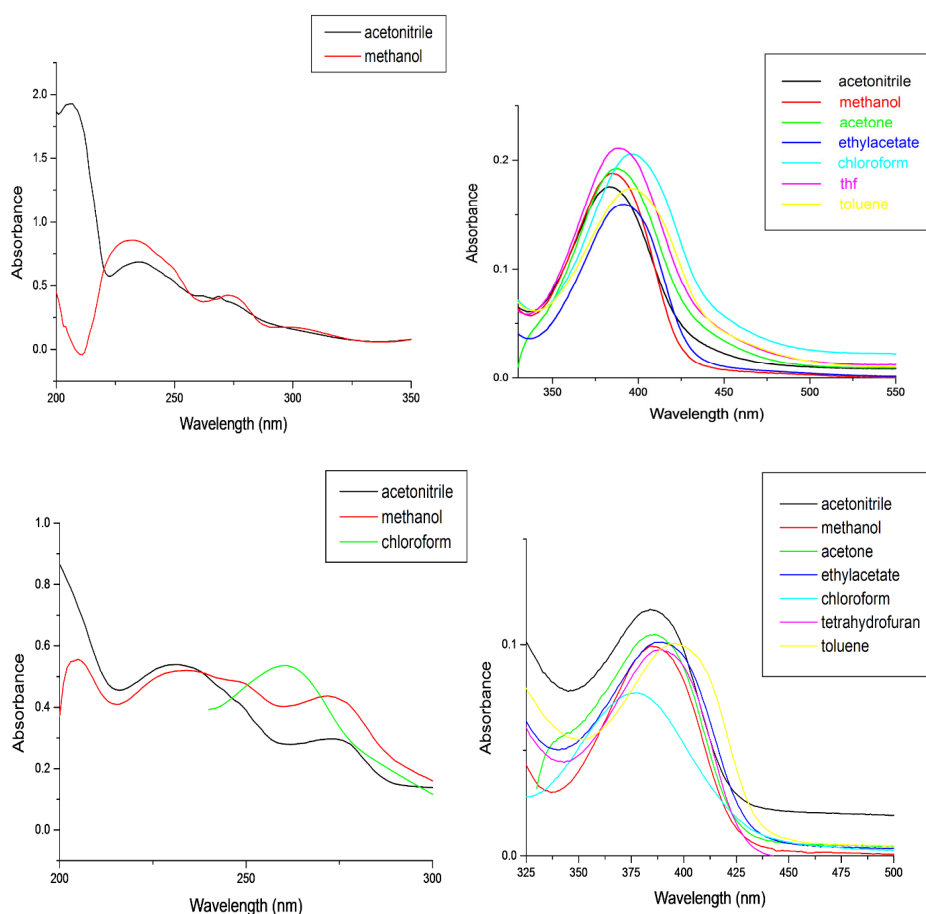


Fig. 3.2. Spectra showing the effect of solvents on the intraligand and CT bands of complexes **4** (top) and **5** (bottom).

Solvents classifiable to polar protic, polar aprotic and non-polar were chosen for our study so as to find the effect of solvents on the electronic spectra of complexes. As seen for other complexes, a negative solvatochromic trend is observed for these compounds also. Within each category, with rise in polarity, there is a decrease in the λ_{max} values for the charge-transfer bands of the complexes due to solvent induced stabilization of the electronic ground state. The λ_{max} (nm) along with their ϵ ($\text{M}^{-1}\text{cm}^{-1}$) values in various solvents are tabulated [Fig. 3.2, Table 3.1].

Table 3.1. The λ_{max} (nm) along with their ϵ ($\text{M}^{-1}\text{cm}^{-1}$) values of complexes **4** and **5** in various solvents

| Polarity Index* | Solvents (decreasing order of polarity) | Complex 4 | | Complex 5 | |
|-----------------|---|-----------------------------|---|-----------------------------|---|
| | | λ_{max} (nm) | $\epsilon * 10^3$ ($\text{M}^{-1}\text{cm}^{-1}$) | λ_{max} (nm) | $\epsilon * 10^3$ ($\text{M}^{-1}\text{cm}^{-1}$) |
| 5.1 | Methanol | 385 | 9.34 | 384 | 4.95 |
| | | 272 | 21.10 | 272 | 21.83 |
| | | 232 | 42.57 | 234 | 25.99 |
| 5.8 | Acetonitrile | 383 | 8.73 | 384 | 5.83 |
| | | 268 | 20.53 | 272 | 14.83 |
| | | 232 | 34.05 | 234 | 26.97 |
| 5.1 | Acetone | 387 | 9.55 | 386 | 5.24 |
| 4.4 | Ethylacetate | 392 | 7.93 | 390 | 4.87 |
| 4.0 | Tetrahydrofuran | 389 | 10.46 | 389 | 5.05 |
| 4.1 | Chloroform | 396 | 10.20 | 377 | 3.85 |
| 2.4 | Toluene | 396 | 8.65 | 396 | 5.03 |

*Relative measure of degree of interaction of the solvents with various polar test solutes

The solvent environment is also found to have a profound influence on the rather low energy metal based *d-d* transitions. The spectral trend observed for the charge transfer bands highlight the solute-solvent interactions and various hydrogen bonding interactions and other bulk solvent properties [8] whilst their effect on *d-d* bands brings out the lability of ligands around the central metal and also unveils the solid to solution phase change over of the coordination geometry of the complexes.

DMSO, MeOH, CH₃CN and DCM were chosen for the study based on the donor number variation. Unlike the CT bands, observed shift as a function

of donor power of chosen solvents showed positive solvatochromic effect which was substantial. As we move up from the least donating solvent, DCM to the highest, DMSO, the dicyanamido species is found to have the largest variation in energy – 5226 cm^{-1} i.e. an impression for the change in environ of the metal complex with solvent [Fig. 3.3, Table 3.2].

Complexes with square-pyramidal geometry in the solid state is susceptible to a change in its surroundings as well as geometry depending up on the solvent. Pseudohalides with linear conjugated structure is easily solvated and therefore solvents substitute them effectively. When the solvent molecules approach along the z axis of the complex the ligands in the x,y plane move out and the interactions become more with orbitals that have z characters (d_{z^2} , d_{xz} , and d_{yz}). These orbitals are thus destabilized, while the other orbitals energetically decreases and in this process the $d-d$ bands shift to red region.

The following two phenomena observed during solvatochromic studies underscores the existence of polymeric species as discrete molecules in solution phase.

- Pseudohalides acting as linkers are easily substituted.
- Various packing forces responsible for the stability of crystals in solid state vanish in solvents as they are distance dependant.

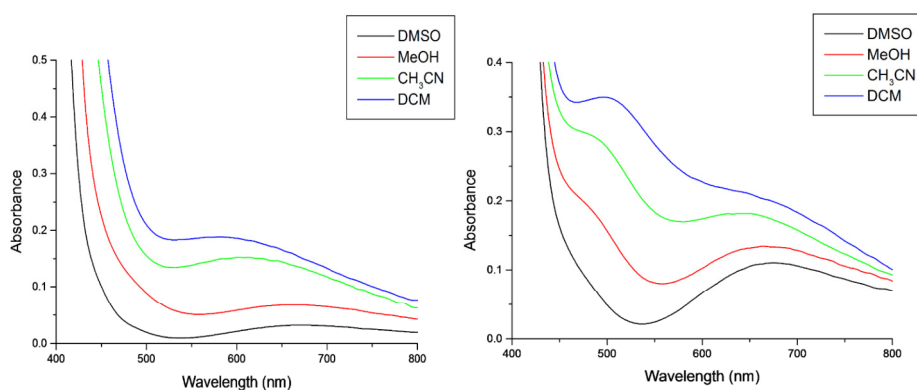


Fig. 3.3. Spectra showing the effect of solvents on the $d-d$ bands of complexes **4** (left) and **5** (right).

Table 3.2. The λ_{\max} (nm) along with their ε ($M^{-1}cm^{-1}$) values of *d-d* bands of complexes **4** and **5** in various solvents

| Solvents | Donor number of solvents (DN) | Complex 4 | | Complex 5 | |
|----------|-------------------------------|-----------------------|-----------------------------------|-----------------------|-----------------------------------|
| | | λ_{\max} (nm) | ε ($M^{-1}cm^{-1}$) | λ_{\max} (nm) | ε ($M^{-1}cm^{-1}$) |
| DMSO | 29.8 | 675 | 49 | 675 | 166 |
| MeOH | 19.0 | 662 | 104 | 663 | 205 |
| AcN | 14.1 | 603 | 236 | 642 | 276 |
| DCM | 0.0 | 579 | 291 | 499 | 524 |

3.3.2. X-ray crystallography and structural description

Single crystals of compounds $[Cu(L^2)(N_3)]_n$ (**4**) and $[Cu(L^2)(N(CN)_2)]_n$ (**5**) suitable for X-ray diffraction studies were grown from their methanol solutions by slow evaporation at room temperature. The snapshot of the crystal (complex **4**) mounted for XRD analysis is shown in Fig. 3.4.

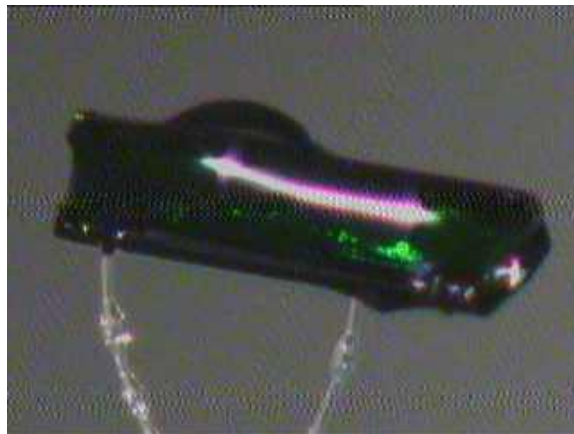


Fig. 3.4. Single crystal of complex **4**.

In complexes **4** and **5**, all non-hydrogen atoms were refined anisotropically and all H atoms on C were placed in calculated positions guided by difference maps with C–H bond distances 0.95-0.99 Å in **4** and 0.93-0.97 Å in **5**. The H atoms were assigned as $U_{iso}=1.2U_{eq}$ (1.5 for Me).

3.3.2.1. $[\text{Cu}(\text{L}^2)(\text{N}_3)]_n$ (4)

The perspective view of the complex along with atom numbering scheme is shown in Fig. 3.5. Bond parameters are given in Table 3.3.

Table 3.3. Crystal data and refinement details of complexes 4 and 5

| Parameters | 4 | 5 |
|--|--|---|
| Empirical formula | $\text{C}_{12}\text{H}_{15}\text{N}_5\text{OCl}_2\text{Cu}$ | $\text{C}_{28}\text{H}_{30}\text{Cl}_4\text{Cu}_2\text{N}_{10}\text{O}_2$ |
| Formula weight | 379.73 | 807.50 |
| Temperature | 173(2) K | 296(2) K |
| Wavelength | 1.54184 Å | 0.71073 Å |
| Crystal system | Orthorhombic | Triclinic |
| Space group | <i>Pbca</i> | $P\bar{1}$ |
| Unit cell dimensions | a = 10.1800(2) Å $\alpha = 90^\circ$ b = 13.4277(3) Å $\beta = 100.906(3)^\circ$ c = 22.4252(5) Å $\gamma = 90^\circ$ | a = 10.7128(6) Å $\alpha = 89.305(2)^\circ$ b = 11.2092(6) Å $\beta = 72.250(2)^\circ$ c = 14.2763(7) Å $\gamma = 84.965(3)^\circ$ |
| Volume | 3065.41(11) Å ³ | 1626.22(15) Å ³ |
| Z | 8 | 2 |
| Density (calculated) | 1.646 Mg m ⁻³ | 1.670 Mg m ⁻³ |
| Absorption coefficient | 5.274 mm ⁻¹ | 1.682 mm ⁻¹ |
| <i>F</i> (000) | 1544.0 | 820 |
| Crystal size | 0.48 × 0.22 × 0.14 mm ³ | 0.250 × 0.250 × 0.200 mm ³ |
| θ range for data collection | 7.884 to 142.732° | 2.683 to 28.453° |
| Limiting indices | -12 ≤ <i>h</i> ≤ 12, -16 ≤ <i>k</i> ≤ 10, -27 ≤ <i>l</i> ≤ 27 | -14 ≤ <i>h</i> ≤ 14, -14 ≤ <i>k</i> ≤ 15, -19 ≤ <i>l</i> ≤ 19 |
| Reflections collected | 21998 | 19398 |
| Unique reflections | 2969 [R(int) = 0.0420] | 7876 [R(int) = 0.0382] |
| Refinement method | Full-matrix least-squares on <i>F</i> ² | Full-matrix least-squares on <i>F</i> ² |
| Data / restraints / parameters | 2969 / 0 / 192 | 8215 / 0 / 419 |
| Goodness-of-fit on <i>F</i> ² | 1.038 | 0.981 |
| Final R indices [<i>I</i> > 2σ(<i>I</i>)] | R ₁ = 0.0322, wR ₂ = 0.0858 | R ₁ = 0.0436, wR ₂ = 0.0970 |
| R indices (all data) | R ₁ = 0.0361, wR ₂ = 0.0905 | R ₁ = 0.0806, wR ₂ = 0.1139 |
| Largest diff. peak and hole | 0.550 and -0.250 e.Å ⁻³ | 0.834 and -0.369 e.Å ⁻³ |

$$R_1 = \frac{\sum ||F_o| - |F_c||}{\sum |F_o|}$$

$$wR_2 = [\sum w(F_o^2 - F_c^2)^2 / \sum w(F_o^2)^2]^{1/2}$$

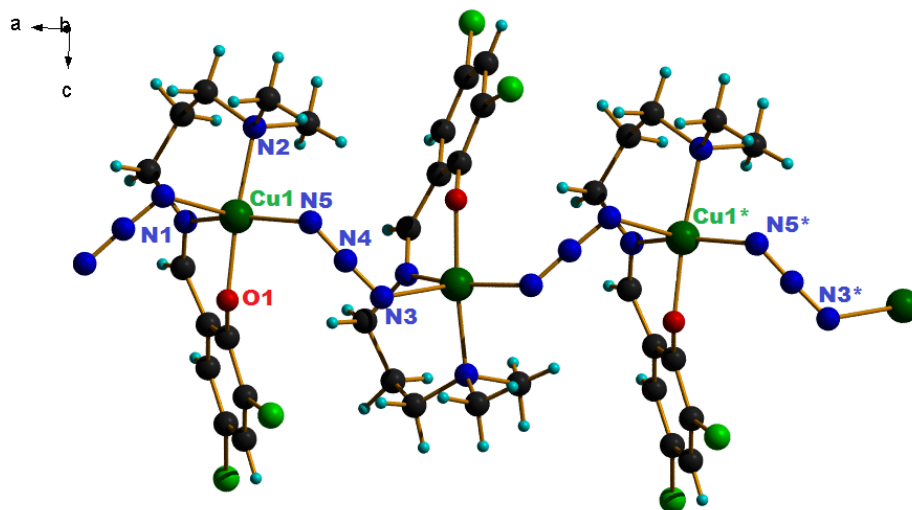


Fig. 3.5. Perspective view of the complex **4**.

The azido complex has a pentacoordinated geometry with the basal plane being occupied by the NNO atoms of the deprotonated Schiff base and the nitrogen atom of the *end-to-end* bridging azido group while the nitrogen of the other $\mu_{1,3}$ bridging azido group houses the axial site of the topology. The *end-to-end* bridging pseudohalide propagates the molecular chain along 'a' axis of the orthorhombic unit cell. The ligand is ambidentate with both the nitrogens involved in coordination and is asymmetric in its bonding pattern with one nitrogen in the basal position [2.018 Å] of the complex entity and the other nitrogen of the same ligand in the apical position [2.2969 Å] of the adjacent unit. Selected bond lengths (Å) and bond angles (°) for the complex are given in Table 3.4.

The chelate bite angles involving the donor atoms in the basal plane summate to a value of 358.5° which is slightly deviated from the perfect value. Also, the large difference in the *trans* basal angle values result in Addison parameter of 0.29 indicating a distortion from square pyramidal geometry. The pseudohalide is quasi-linear with an N–N–N angle of 176.9(2)°. The *end-to-end* linkage *via* the azide separates the adjacent centres by a distance of 5.2531(5) Å which is larger when compared to an *end-on* bridged complex.

Table 3.4. Selected bond lengths (Å) and bond angles (°) for the complex **4**

| Bond lengths (Å) | | Bond angles (°) | |
|------------------|------------|-----------------|------------|
| Cu(1)–O(1) | 1.9317(16) | O(1)–Cu(1)–N(1) | 89.06(7) |
| Cu(1)–N(1) | 2.0052(18) | N(1)–Cu(1)–N(3) | 97.83(7) |
| Cu(1)–N(3) | 2.2969(19) | N(3)–Cu(1)–N(2) | 91.77(7) |
| Cu(1)–N(2) | 2.0836(18) | N(2)–Cu(1)–N(5) | 88.27(8) |
| Cu(1)–N(5) | 2.018(2) | N(5)–Cu(1)–O(1) | 87.24(8) |
| N(3)–N(4) | 1.169(3) | O(1)–Cu(1)–N(2) | 174.55(7) |
| N(4)–N(5) | 1.182(3) | O(1)–Cu(1)–N(3) | 92.34(7) |
| O(1)–C(6) | 1.286(3) | N(5)–Cu(1)–N(1) | 157.45(8) |
| Cl(1)–C(7) | 1.736(2) | N(1)–Cu(1)–N(2) | 93.93(7) |
| Cl(2)–C(9) | 1.749(2) | N(3)–Cu(1)–N(5) | 104.54(7) |
| | | N(5)–N(4)–N(3) | 176.9(2) |
| | | Cu(1)–N(5)–N(4) | 124.73(16) |
| | | Cu(1)–N(3)–N(4) | 116.76(15) |

The metrical parameters like metal-N-N angles (Cu1–N3–N4/Cu1–N5–N4) in this metal-azido complex are 116.76(15) and 124.73(16)° respectively and the N3–Cu1–N5 bond angle is observed to be 104.54(7)°. The bond strength follows the same order as seen in other azido complexes: metal-phenoxo oxygen > metal-imino nitrogen > metal-equatorial azido nitrogen > metal-amino nitrogen > metal-axial azido nitrogen.

The six membered metallocycles Cg(1) and Cg(2) are puckered with the values $Q(2) = 0.4022(18) \text{ \AA}$, $\Phi(2) = 192.0(3)^\circ$, $Q(3) = -0.1930(19) \text{ \AA}$, $Q = 0.4462(15) \text{ \AA}$ and $\theta = 115.6(2)^\circ$ for the first ring and $Q(2) = 0.1404(19) \text{ \AA}$, $\Phi(2) = 190.9(9)^\circ$, $Q(3) = 0.533(2) \text{ \AA}$, $Q = 0.551(2) \text{ \AA}$ and $\theta = 14.7(2)^\circ$ for the latter. A $R_2^2(8)$ motif is generated as an effect of the interchain hydrogen bonding interaction between H(8) atom on C(8) of one molecule with the chlorine atom, Cl(1) of another molecule. Thus the azido ions link the molecules covalently along 'a' axis and numerous such one dimensional chains are supramolecularly extended along 'c' direction [Fig. 3.6]. The hydrogen, H(11c) on one of the methyl carbons has an intramolecular contact with the nitrogen, N(5) of the bridging azide thereby forming a S(5) ring motif [Fig. 3.6, Table 3.5].

Apart from this, the same nitrogen, N(5) also accepts a hydrogen bond from the H(3B) atom of C(3) atom. This actually links the covalently linked azido chains along 'b' direction. In effect, there is a supramolecular three-dimensional extension of the polymeric chains due to the hydrogen bonding interactions.

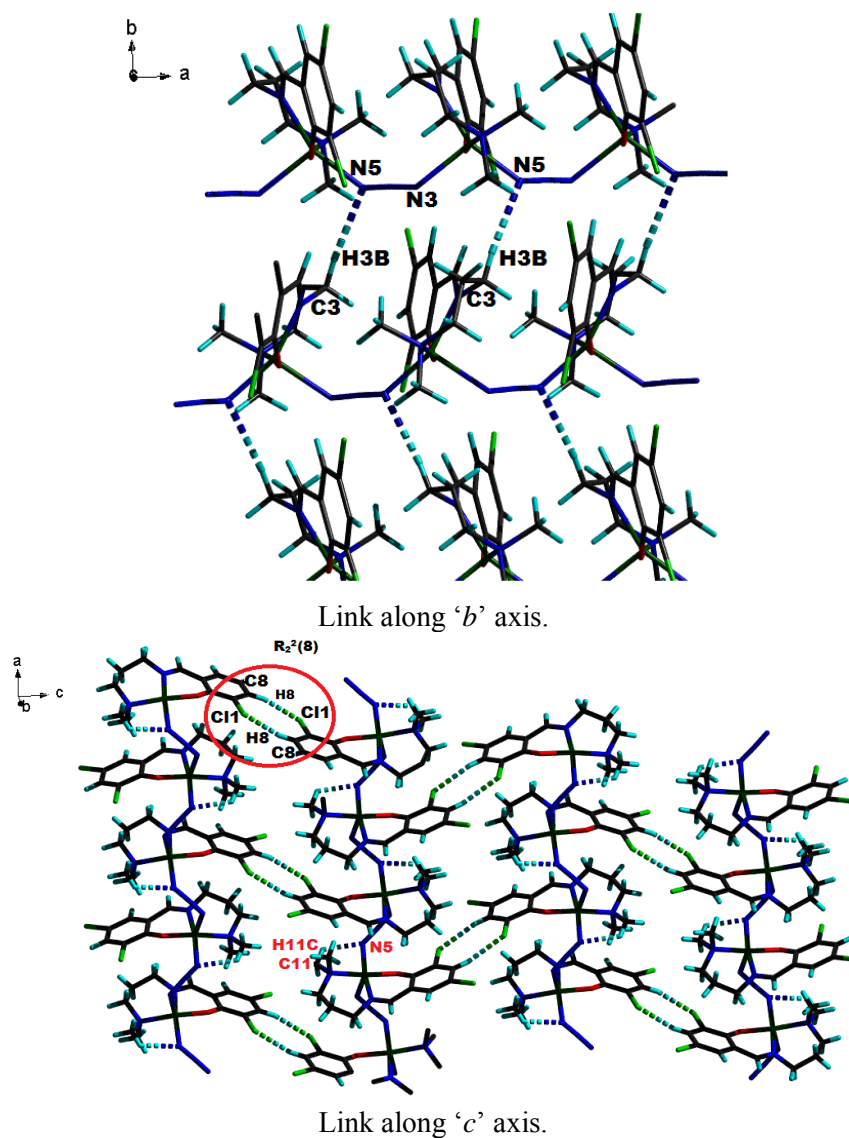


Fig. 3.6. Supramolecular three dimensional extension due to hydrogen bonding interactions.

Table 3.5. Non-conventional hydrogen bonding interactions in complex 4

| D–H···A | D–H (Å) | H···A (Å) | D···A (Å) | D–H···A (°) |
|--|---------|-----------|-----------|-------------|
| Intermolecular hydrogen bonding | | | | |
| C(3)–H(3B)···N(5) ^a | 0.99 | 2.60 | 3.582(3) | 174 |
| C(8)–H(8)···Cl(1) ^b | 0.95 | 2.82 | 3.646(2) | 146 |
| Intramolecular hydrogen bonding | | | | |
| C(11)–H(11C)···N(5) | 0.98 | 2.37 | 2.957(3) | 118 |

Equivalent position codes: a = 3/2 - x, 1/2 + y, z; b = 1 - x, 1 - y, 1 - z

An intrachain intermolecular C–H··· π interaction exists between the H(3A) atom and the halogen bearing ring, Cg(3) [C5 to C10] which might also contribute to the closeness of the monomeric units in the chain [Fig. 3.7, Table 3.6].

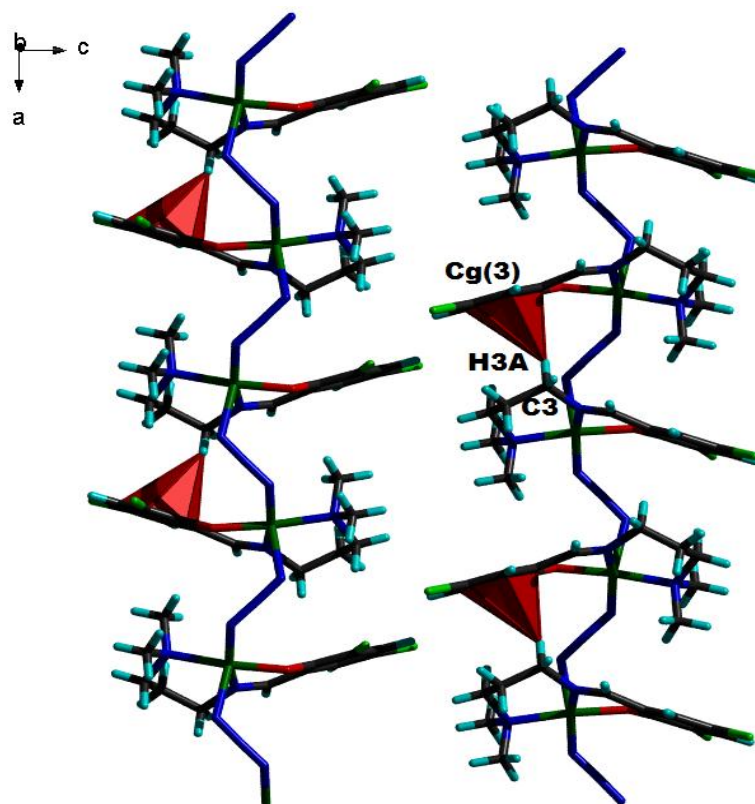
**Fig. 3.7.** Intrachain intermolecular C–H··· π interaction.

Table 3.6. C–H...Cg interaction in complex **4**

| C–H(I)...Cg(J) | H...Cg (Å) | C...Cg (Å) | C–H...Cg (°) |
|---------------------------------|------------|------------|--------------|
| C(3)–H(3A)...Cg(3) ^c | 2.75 | 3.591(2) | 135 |

Equivalent position code: $c = \frac{1}{2} + x, y, \frac{1}{2} - z$

Cg, centroid

Cg(3) = C(5), C(6), C(7), C(8), C(9), C(10)

Cg(J) = Center of gravity of ring J (plane number above)

C–H...Cg = C–H...Cg angle (°)

C...Cg = Distance of C to Cg (Å)

H...Cg = Distance of H to Cg (Å)

3.3.2.2. [Cu(L²)(N(CN)₂)_n]_n (**5**)

The asymmetric unit of the complex is as shown in the ORTEP plot [Fig. 3.8]. The relevant bond dimensions are given in the Table 3.3. The basal plane of the (4 + 1) geometry is furnished by the donor atoms from the Schiff base coordinating in a meridional mode along with the nitrogen atom of equatorially linked dicyanamide. Selected bond lengths (Å) and bond angles (°) for the complex are given in Table 3.7.

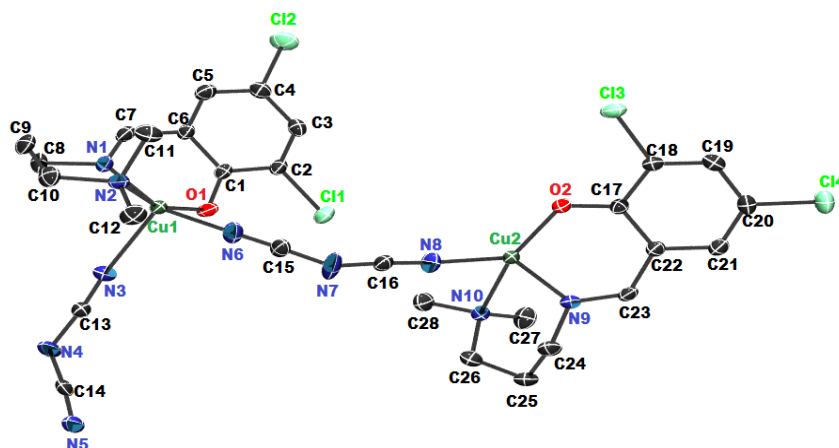


Fig. 3.8. ORTEP diagram showing the atom labelling of the asymmetric unit of the complex **5** (drawn with 30% probability ellipsoid and the hydrogen atoms are omitted for clarity).

Table 3.7. Selected bond lengths (Å) and bond angles (°) for complex **5**

| Bond lengths (Å) | | | |
|-------------------------|------------|------------------|------------|
| Cu(1)–O(1) | | 1.945(2) | |
| Cu(1)–N(1) | | 1.981(2) | |
| Cu(1)–N(2) | | 2.120(3) | |
| Cu(1)–N(3) | | 2.187(3) | |
| Cu(1)–N(6) | | 2.003(3) | |
| N(6)–C(15) | | 1.142(4) | |
| C(15)–N(7) | | 1.294(4) | |
| N(7)–C(16) | | 1.301(5) | |
| C(16)–N(8) | | 1.138(5) | |
| N(5)–C(14) | | 1.137(4) | |
| C(14)–N(4) | | 1.300(4) | |
| N(4)–C(13) | | 1.296(5) | |
| C(13)–N(3) | | 1.142(5) | |
| Cu(2)–N(5b) | | 2.000(3) | |
| Cu(2)–N(8) | | 2.195(3) | |
| Cu(2)–O(2) | | 1.941(2) | |
| Cu(2)–N(9) | | 1.976(2) | |
| Cu(2)–N(10) | | 2.116(2) | |
| Bond angles (°) | | | |
| O(1)–Cu(1)–N(6) | 85.68(11) | O(2)–Cu(2)–N(9) | 87.29(9) |
| N(6)–Cu(1)–N(3) | 97.41(12) | N(9)–Cu(2)–N(10) | 88.49(9) |
| N(3)–Cu(1)–N(2) | 92.93(11) | N(10)–Cu(2)–N(8) | 91.95(10) |
| N(2)–Cu(1)–N(1) | 89.16(10) | N(8)–Cu(2)–N(5b) | 96.48(12) |
| N(1)–Cu(1)–O(1) | 87.04(9) | N(5b)–Cu(2)–O(2) | 85.36(11) |
| O(1)–Cu(1)–N(2) | 160.50(9) | O(2)–Cu(2)–N(8) | 107.03(11) |
| O(1)–Cu(1)–N(3) | 106.58(10) | O(2)–Cu(2)–N(10) | 161.01(9) |
| N(1)–Cu(1)–N(3) | 102.01(10) | N(5b)–Cu(2)–N(9) | 160.33(11) |
| N(1)–Cu(1)–N(6) | 160.50(11) | N(5)–Cu(2)–N(10) | 92.57(11) |
| N(2)–Cu(1)–N(6) | 91.70(12) | N(8)–Cu(2)–N(9) | 160.33(11) |
| C(15)–N(7)–C(16) | 122.5(3) | C(14)–N(4)–C(13) | 122.4(3) |
| Cu(1)–N(3)–C(13) | 172.6(3) | Cu(2)–N(8)–C(16) | 168.8(3) |
| Cu(1)–N(6)–C(15) | 166.9(3) | Cu(2)–N(5)–C(14) | 163.6(3) |

The vertex of the geometry is occupied by the nitrogen atom of the other dicyanamide which is in *cis* mode [$96.48(12)^\circ$ & $97.41(12)^\circ$] to the other. The bent molecule, dicyanamide bridges in *trans* $\mu_{1,5}$ – fashion and sews the molecules into a 1-D chain along ‘*b*’ axis [Fig. 3.9]. Though the *trans* basal angles around the copper centres deviate largely from that expected for a regular square pyramidal topology, they are almost same – N1–Cu1–N6/ $160.50(11)^\circ$, N2–Cu1–O1/ $160.50(9)^\circ$ and N9–Cu2–N5/ $160.33(11)^\circ$, O2–Cu2–N10/ $161.01(9)^\circ$. Therefore the distortion of the coordination polyhedron as computed by trigonality index, τ for both the metal centres [$\tau_1 = 0 / \tau_2 = 0.0113$] indicate an almost perfect square pyramidal geometry. The bridging array Cu–NCNCN–Cu assumes a “V” type conformation with central C–N–C bond angles of $122.4(3)^\circ$ and $122.5(3)^\circ$ respectively [Table 3.7]. The carbon atoms of the pseudohalide have *sp* hybridization with almost linear N–C–N bond angles [N7–C16–N8 = $172.0(4)^\circ$, N7–C15–N6 = $172.2(4)^\circ$, N4–C14–N5 = $173.0(4)^\circ$, N4–C13–N3 = $172.7(4)^\circ$].

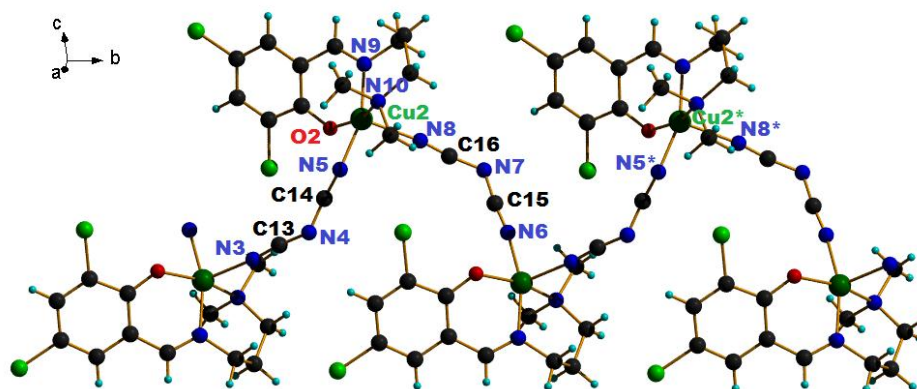


Fig. 3.9. Perspective view of complex 5 along with atom numbering scheme.

The environment of Cu2 is found to be more distorted than Cu1 as assessed from the deviation of metal centres from the least squares plane, the Addison parameter and the summation of bond angles around the metal centres [Cu2 : $0.4572 \text{ \AA} / 0.0113 / 353.71^\circ$; Cu1: $0.2693 \text{ \AA} / 0 / 353.58^\circ$]. The metal-metal separation *via* the non-linear pseudohalide is $7.9041(5) \text{ \AA}$ whilst the

shortest interchain separation is 11.2092(8) Å. The bond strength of the ligating atoms with the metal atom follows the order: Cu–O (phenolate) > Cu–N (azomethine nitrogen) > Cu–N (equatorial nitrogen) > Cu–N (amino nitrogen) > Cu–N (axial nitrogen). Chelation generates stable hexamembered metallocycles Cg(1), Cg(2) and Cg(3), Cg(4) around Cu1 and Cu2 respectively. Both Cg(2) [Cu1/N1/C8/C9/C10/N2] and Cg(4) [Cu2/N9/C24/C25/C26/N10] metallorings adopt a chair conformation with puckering parameters $Q(2) = 0.026(3)$ Å, $\Phi(2) = 67(6)^\circ$, $Q(3) = 0.615(3)$ Å, $Q = 0.615(3)$ Å and $\theta = 2.6(3)^\circ$ for the first ring and $Q(2) = 0.036(3)$ Å, $\Phi(2) = 41(5)^\circ$, $Q(3) = 0.619(3)$ Å, $Q = 0.620(3)$ Å and $\theta = 3.3(3)^\circ$ for the latter. Short-ring interactions exist between aromatic rings, Cg(6) [Table 3.8].

Table 3.8. Short ring interaction for complex 5

| Cg(I)⋯Cg(J) | Cg(I)⋯Cg(J) (Å) | γ (°) |
|--------------------------|-----------------|--------------|
| Cg(6)⋯Cg(6) ^a | 3.7953(19) | 25.1 |

Equivalent position code: a = 2-x, 1-y, -z

Cg, centroid

Cg(6) = C(17), C(18), C(19), C(20), C(21), C(22)

Cg(I) = Center of gravity of ring I

Cg(J) = Center of gravity of ring J (plane number above)

γ = Angle between Cg(I)⋯Cg(J) vector and normal to plane J (°)

Cg(I)⋯Cg(J) = Distance of Cg(I) to Cg(J) (Å)

Two intramolecular hydrogen bonding interactions are established by the hydrogen atoms, H(12a) and H(28a) with the nitrogen atoms N(6) and N(5) of the dca ligand generating a S(5) ring motif [Fig. 3.10, Table 3.9].

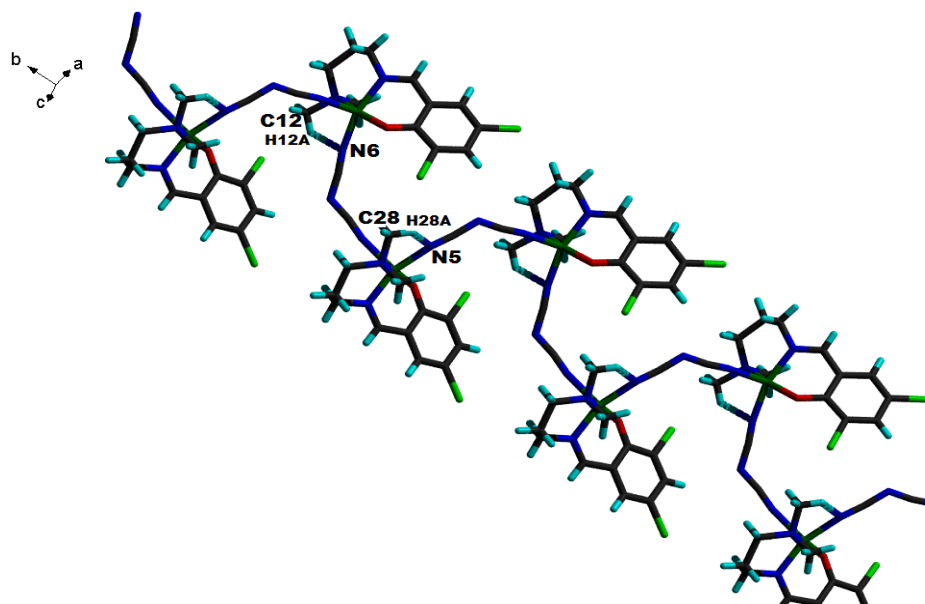

Fig. 3.10. Intramolecular hydrogen bonding ring interactions.

Table 3.9. Hydrogen bonding interactions in the complex **5**

| D–H...A | D–H (Å) | H...A (Å) | D...A (Å) | D–H...A (°) |
|----------------------------------|---------|-----------|-----------|-------------|
| Intramolecular hydrogen bonding | | | | |
| C(12)–H(12A)...N(6) | 0.96 | 2.44 | 2.962(4) | 114 |
| C(28)–H(28A)...N(5) ^b | 0.96 | 2.47 | 2.980(5) | 113 |

 Equivalent position code: $b = x, 1+y, z$

3.3.3. Optical emissive response

The fluorescent spectra of the complexes were recorded in acetonitrile medium at an excitation wavelength of 350 nm. The spectra is shown in Fig. 3.11. and the results are consolidated in Table 3.10. Both the complexes show ligand-centered blue emission at 462 and 458 nm respectively.

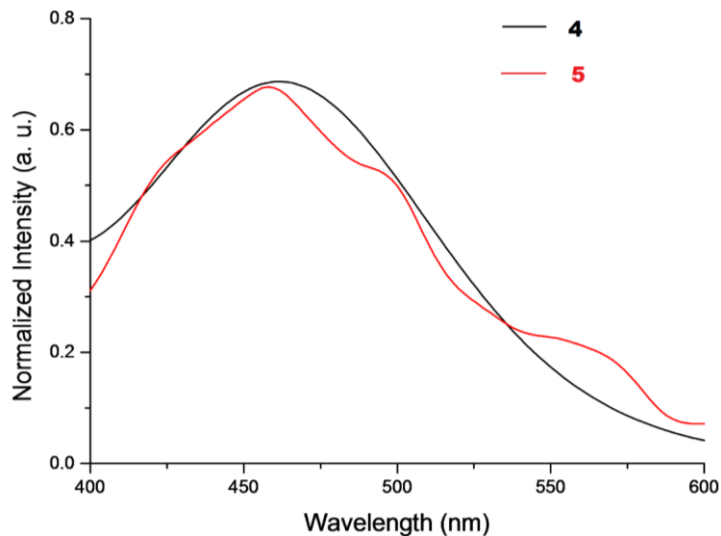


Fig. 3.11. Normalized fluorescent spectrum of complexes **4** and **5**.

Table 3.10. Photophysical data of complexes

| Complexes | Solution state emission (nm) at excitation of 350 nm |
|---|--|
| $[\text{Cu}(\text{L}^2)(\text{N}_3)]_n$ (4) | 462 |
| $[\text{Cu}(\text{L}^2)(\text{N}(\text{CN})_2)]_n$ (5) | 458 |

3.3.4. Thermal studies

The thermal behavior of complexes were characterized in N_2 atmosphere using thermogravimetric analysis (TG), differential thermogravimetric analysis (DTG) and differential scanning calorimetry (DSC). The stability of the complexes can be arrived at on the basis of thermal decomposition profile.

The double stage endothermic decomposition thermogram of azido complex **4** matches with the removal of ammonia (4.14%, calcd. 4.47%) in the 150-200 °C followed by the loss of two nitrogen molecules (15.09%, calcd. 15.43%) in 210-250 °C. A gradual decomposition finally resulting in the

formation of a stable metal oxide is inferred from the TG graph [Fig. 3.12]. For the dicyanamido complex **5**, a weight loss of 3.76% (calcd. 3.46%) is consistent with the endothermic loss of nitrogen in the 230-270 °C. In the heating range of 350-500 °C, a second dip observed in the derivative curve highlights the exothermic loss of three fragments – propyl amine, dicyanamide and chloride species, altogether fitting to 27.31% release (calcd. 27.32%) trailed by a gradual decomposition pattern [Fig. 3.12].

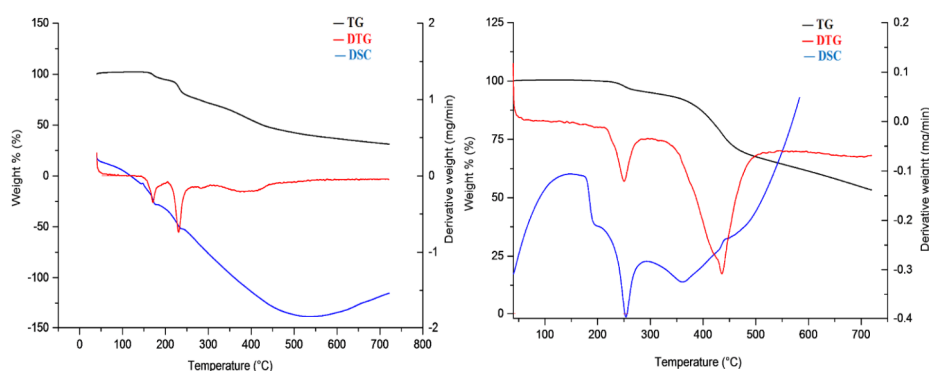


Fig. 3.12. Thermogram of the complexes **4** and **5**.

3.3.5. EPR spectral studies

The EPR spectra of the azido complex **4** in polycrystalline state reveals an axial nature for the spectra with $g_{\parallel} = 2.200$ and $g_{\perp} = 2.056$ with $g_{\parallel} > g_{\perp} > g_e$ (2.0023). The G value of $3.6816 < 4$, indicates the presence of considerable exchange interaction between the metal centres. However the spectra of the sample recorded in frozen DMF at 77 K highlights the presence of four hyperfine splittings [$g_{\parallel} = 2.232$ and $g_{\perp} = 2.085$; $A_{\parallel} = 200 \times 10^{-4} \text{ cm}^{-1}$, $A_{\perp} = 36 \times 10^{-4} \text{ cm}^{-1}$] in the parallel region, characteristic of a typical Cu(II) complex although the perpendicular region doesn't show any such splittings. The hyperfine splitting is due to the interaction of the electron spin with the copper nuclear spin ($I=3/2$) [Fig. 3.13, Table 3.11].

The EPR spectra are simulated using EasySpin package [9] and the experimental (red) and simulated (blue) best fits are included.

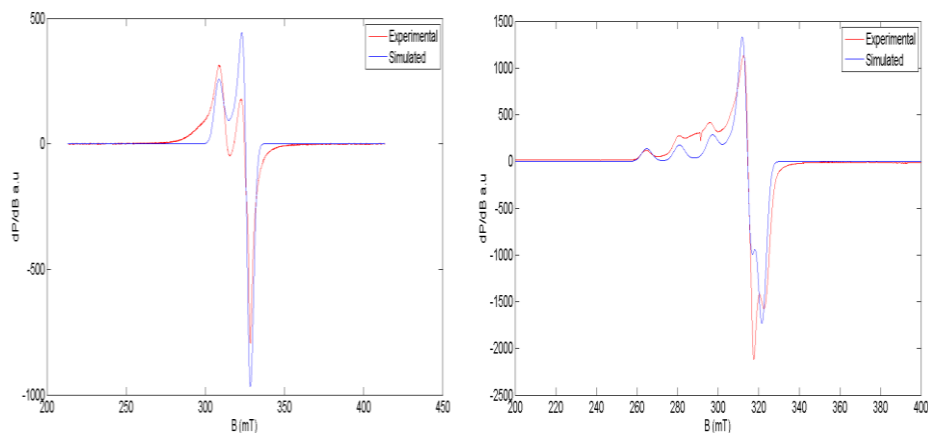


Fig. 3.13. EPR spectra of complex **4** in polycrystalline state and in DMF (77 K).

The dicyanamido complex is also subjected to EPR study and the nature of the spectra was typical of an axial one, both in the polycrystalline state and at low temperature. However the spectra at 77 K was much more resolved with hyperfine splittings evidently seen in the parallel region with the g tensor values, $g_{\parallel} = 2.202$ and $g_{\perp} = 2.120$. The exchange interaction in our polymeric complex is further evidenced by the geometric parameter, G having a value of 3.3397, symptomatic of considerable interaction between the copper(II) centres [Fig. 3.14, Table 3.11].

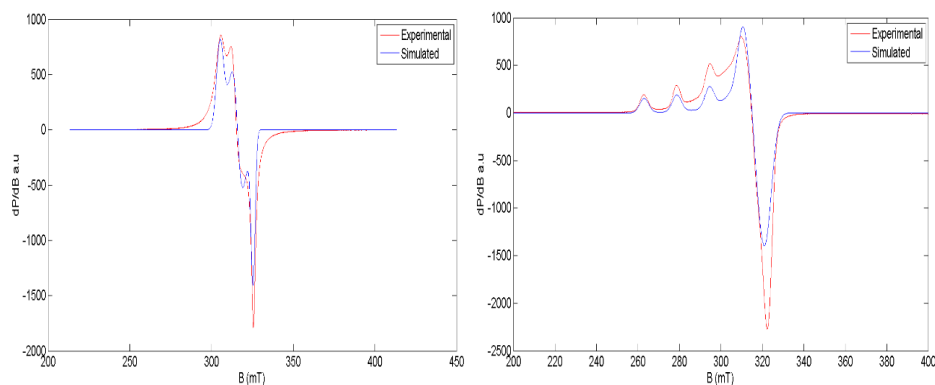


Fig. 3.14. EPR spectra of complex **5** in polycrystalline state and in DMF (77 K).

Table 3.11. Spin Hamiltonian and bonding parameters of copper(II) complexes

| Compounds | Polycrystalline state (298 K) | | | | | | DMF solution (77 K) | | | | | | | | | |
|---|-------------------------------|-----------------|-------------|--------|--------------------|-------------------|---------------------|-----------------|-------------|-----------------|------------|-----------|------------|-----------------|-------------|-------|
| | g_{iso} | g_{\parallel} | g_{\perp} | G | $g_{\parallel}g_3$ | $g_{\perp}g_1g_2$ | g_{av} | A_{\parallel} | A_{\perp} | A_{av} | α^2 | β^2 | γ^2 | K_{\parallel} | K_{\perp} | f |
| $[\text{Cu}(\text{L}_2)(\text{N}_3)]_n$ (4) | -- | 2.200 | 2.056 | 3.6816 | 2.232 | 2.085 | 2.1337 | 200 | 36 | 91 | 0.8602 | 0.8890 | 1.0668 | 0.7647 | 0.9177 | 119.0 |
| $[\text{Cu}(\text{L}_2)(\text{N}(\text{CN})_2)]_n$ (5) | -- | 2.195 | 2.060 | 3.3397 | 2.202 | 2.120 | 2.1471 | 214 | 39 | 97 | 0.8863 | 0.8058 | 1.2373 | 0.7142 | 1.0966 | 120.3 |

In all the complexes, $g_{\parallel} > g_{\perp} > 2.0023$. The fact that g_{\parallel} values are less than 2.3 is an indication of significant covalent character to the M–L bond [10,11]. The α^2 value, a measure of the covalence of the in-plane σ -bonds, calculated for the complexes lie in between 0.5 and 1, implying that the metal-ligand bonds in the complexes under investigation are partially ionic and partially covalent in nature. The bonding parameters, K_{\parallel} and K_{\perp} were evaluated for our complexes and it was found that they hold the relation $K_{\parallel} < K_{\perp}$, i.e. in plane π bonding is significant.

References

- [1] A.Y. Robin, K.M. Fromm, *Coordination Chemistry Reviews* **2006**, 250, 2127.
- [2] S.R. Batten, S.M. Neville, D.R. Turner, *Coordination Polymers: Design, Analysis and Application* Published by Royal Society of Chemistry **2009**.
- [3] P. Bhowmik, H.P. Nayek, M. Corbella, N. Aliaga-Alcalde, S. Chattopadhyay, *Dalton Trans.* **2011**, 40, 7916.
- [4] A. Ray, G.M. Rosair, G. Pilet, B. Dede, C.J. Gómez-García, S. Signorella, S. Bellú, S. Mitra, *Inorg. Chim. Acta* **2011**, 375, 20.
- [5] A. Ray, G. Pilet, C.J. Gómez-García, S. Mitra, *Polyhedron* 2009, 28, 511.
- [6] G. Bhargavi, M.V. Rajasekharan, J.P. Costes and J.P. Tuchagues, *Dalton Trans.* **2013**, 42, 8113.
- [7] T. Renger, B. Grundkotter, M.A. Madjet, F. Muh, *PNAS*, **2008**, 105, 13235.
- [8] M. Homocianu¹, A. Airinei, D.O. Dorohoi, *Journal of Advanced Research in Physics* **2011**, 2.
- [9] S. Stoll, *Spectral Simulations in Solid-State Electron Paramagnetic Resonance*, Ph.D. thesis, ETH, Zurich, **2003**.
- [10] J.R. Wasson, C. Trapp, *J. Phys. Chem.* **1969**, 73, 3763.
- [11] D. Kivelson, R. Neiman, *J. Chem. Soc. Dalton Trans.* **1961**, 49.



Monomers, polymers and a dimer based on *N,N*-dimethylethylenediamine/*N*-methyl 1,3-propanediamine and 3,5-dichloro-2-hydroxyacetophenone

| | |
|-----------------|-----------------------------|
| Contents | 4.1. Introduction |
| | 4.2. Experimental |
| | 4.3. Results and discussion |

Conspectus

*In this chapter, we have used the tridentate Schiff base derived from *N,N*-dimethylethylenediamine/*N*-methyl-1,3-propanediamine and 3,5-dichloro-2-hydroxyacetophenone as the blocking ligand. We got a potpourri of five crystals, with pseudohalides incorporated – Of them, two were monomers, two polymers and the remaining one turned out to be an azido dimer. Negative solvatochromic effect was observed for the charge-transfer bands of the complexes and the influence of the solvents on the geometry of the complexes could be well assessed from the low energy ligand based *d-d* bands. Complex 6 is an azido polymer with a trans helical propagation and the dicyanamido species has a meso-helical nature. Both the complexes develop into supramolecular architectures due to the interplay of covalent & non-covalent forces. The same forces stitch the monomeric cyanato and thiocyanato complexes propagating them as chains. The azido dimer is centrosymmetric with the azide group in end-on bridging mode and the presence of hydrogen bonding interactions enable the formation of a box-like structure. Along with preliminary investigations, the optical emission studies, quantum yield calculations, thermal and EPR studies of the complexes are also carried out.*

4.1. Introduction

We have employed HL system with 3,5-dichloro-2-hydroxyacetophenone as the carbonyl portion. We could isolate five single crystals with the azido bridging enabling the formation of a polymer and a dimer, cyanato and thiocyanato forming monomers and the non-linear dicyanamide forming a polymer. The synthesis, spectral characterization, crystal structures, packing interactions (supramolecular assemblies), photophysical studies and EPR studies are discussed here.

4.2. Experimental

4.2.1. Materials

All chemicals were of reagent grade and purchased from commercial sources. The solvents were purified according to standard procedures. 3,5-Dichloro-2-hydroxyacetophenone (Aldrich), *N,N*-dimethyl-1,2-diaminoethane (Aldrich), *N*-methyl-1,3-propanediamine (Aldrich) $\text{Cu}(\text{OAc})_2 \cdot \text{H}_2\text{O}$, $\text{CuCl}_2 \cdot 2\text{H}_2\text{O}$, $\text{Cu}(\text{NO}_3)_2 \cdot 3\text{H}_2\text{O}$, NaN_3 , KSCN , NaCNO , $\text{Na}[\text{N}(\text{CN})_2]$ (all are BDH, AR quality) were used as received.

The Schiff bases were formed *in situ*.

Caution! Azido compounds are potentially explosive. Although no problems were encountered in the present study, it should be prepared only in small quantities and handled with care.

4.2.2. Synthetic strategy

4.2.2.1. Synthesis of $[\text{Cu}(\text{L}^3)(\text{N}_3)]_n$ (6)

[$\text{HL}^3 = 2,4\text{-dichlorido-6-(1-(2-(dimethylamino)ethylimino)ethyl)phenol}$]

3,5-Dichloro-2-hydroxyacetophenone (0.205 g, 1 mmol) and *N,N*-dimethyl-1,2-diaminoethane (0.088 g, 1 mmol) were dissolved in 10 mL methanol and refluxed for about an hour. A methanolic solution (10 mL) of copper(II) acetate monohydrate (0.199 g, 1 mmol) was added to the hot reaction mixture. To the resulting deep green solution, sodium azide (0.130 g, 2 mmol) in a MeOH/H₂O (1:9) mixture was added dropwise with continuous

stirring and filtered. Suitable single crystals for structure determination by X-ray diffraction were obtained by slow evaporation of the mother liquor in air.

Yield: 0.2653 g (70%). *Anal.* Calc. for $C_{12}H_{15}Cl_2CuN_5O$ (379.73): C, 37.96; H, 3.98; N, 18.44.

Found C, 37.98; H, 4.02; N, 18.42%.

UV-vis, λ_{max}/nm ($\epsilon_{max}/10^3 M^{-1}cm^{-1}$) (acetonitrile): 372 (4.90), 238 (19.74).

IR spectral values : 2049, 1473, 761 cm^{-1} .

4.2.2.2. Synthesis of [Cu(L³)(NCS)] (7)

[HL³ = 2,4-dichlorido-6-(1-(2-(dimethylamino)ethylimino)ethyl)phenol]

Complex **7** was prepared by a method similar to that of complex **6** except for the metal salt used. Here copper(II) chloride dihydrate (0.170 g, 1 mmol) was added to the hot reaction mixture followed by sodium thiocyanate (0.130 g, 2 mmol) in a MeOH/H₂O (1:9) mixture with continuous stirring and filtered. Suitable single crystals for structure determination by X-ray diffraction were obtained by slow evaporation of the mother liquor in air.

Yield: 0.2046 g (51.80%). *Anal.* Calc. for $C_{13}H_{15}Cl_2CuN_3OS$ (395.79): C, 39.45; H, 3.82; N, 10.62. Found C, 39.40; H, 3.78; N, 10.58%.

UV-vis, λ_{max}/nm ($\epsilon_{max}/10^3 M^{-1}cm^{-1}$) (acetonitrile): 378 (4.92), 269 (23.41), 262 (27.08), 238 (28.99)

4.2.2.3. Synthesis of [Cu(L³)(NCO)] (8)

[HL³ = 2,4-dichlorido-6-(1-(2-(dimethylamino)ethylimino)ethyl)phenol]

Similar synthetic strategy was employed with copper(II) nitrate trihydrate (0.241 g, 1 mmol) as the salt and sodium cyanate (0.130 g, 2 mmol) in MeOH/H₂O mixture as the coligand. Diffraction quality single crystals for structure determination were obtained by slow evaporation of this mother liquor in air.

Yield: 0.2634 g (69.50%). *Anal.* Calc. for $C_{13}H_{15}Cl_2CuN_3O_2$ (379.73): C, 41.12; H, 3.98; N, 11.07. Found C, 41.11; H, 3.90; N, 11.02%.

UV-vis, λ_{max}/nm ($\epsilon_{max}/10^3 M^{-1}cm^{-1}$) (acetonitrile): 378 (2.87), 232 (13.44).

4.2.2.4. Synthesis of [Cu(L³)[N(CN)₂]_n (9)**[HL³ = 2,4-dichlorido-6-(1-(2-(dimethylamino)ethylimino)ethyl)phenol]**

Complex **9** was obtained by refluxing Schiff base with copper(II) acetate monohydrate (0.199 g, 1 mmol) for about half an hour followed by the dropwise addition of sodium dicyanamide (0.178 g, 2 mmol) in a MeOH/H₂O mixture. The solution was further stirred for *ca.* 2 h and filtered. Diffraction quality single crystals for structure determination were obtained by slow evaporation of this mother liquor in air.

Yield: 0.2409 g (59.20%). *Anal. Calc.* for C₁₄H₁₉Cl₂CuN₅O (407.78): C, 41.23; H, 4.70; N, 17.17. Found C, 41.19; H, 4.65; N, 17.12%.

UV-vis, λ_{max} /nm (ε_{max}/10³ M⁻¹cm⁻¹) (acetonitrile): 380 (12.96), 237 (71.05).

IR spectral values : 2288, 2231, 2160 cm⁻¹.

4.2.2.5. Synthesis of [Cu(L⁴)(N₃)₂ (10)**[HL⁴ = 2,4-dichlorido-6-((3-(dimethylamino)propylimino)methyl)phenol]**

3,5-Dichloro-2-hydroxyacetophenone (0.191 g, 1 mmol) and *N*-methyl-1,3-propanediamine (0.088 g, 1 mmol) were dissolved in 10 mL methanol and refluxed for about an hour. The synthetic strategy for the preparation of complex **10** was similar to that stated above except that copper(II) chloride dihydrate (0.170 g, 1 mmol) was added to the hot reaction mixture and refluxed for half an hour. To the resulting deep green solution, sodium azide (0.130 g, 2 mmol) in a MeOH/H₂O (1:9) mixture was added dropwise with continuous stirring and filtered. Suitable single crystals were obtained by slow evaporation of the mother liquor in air.

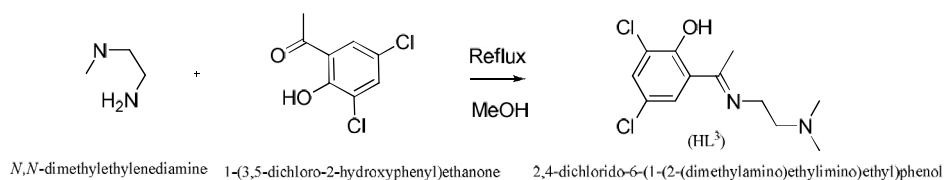
Yield: 0.4250 g (56%). *Anal. Calc.* for C₂₄H₃₀Cl₄Cu₂N₁₀O₂ (759.46): C, 37.96; H, 3.98; N, 18.44. Found C, 37.93; H, 3.96; N, 18.12%.

UV-vis, λ_{max} /nm (ε_{max}/10³ M⁻¹cm⁻¹) (acetonitrile): 372 (5.59), 264 (13.92), 237 (21.52).

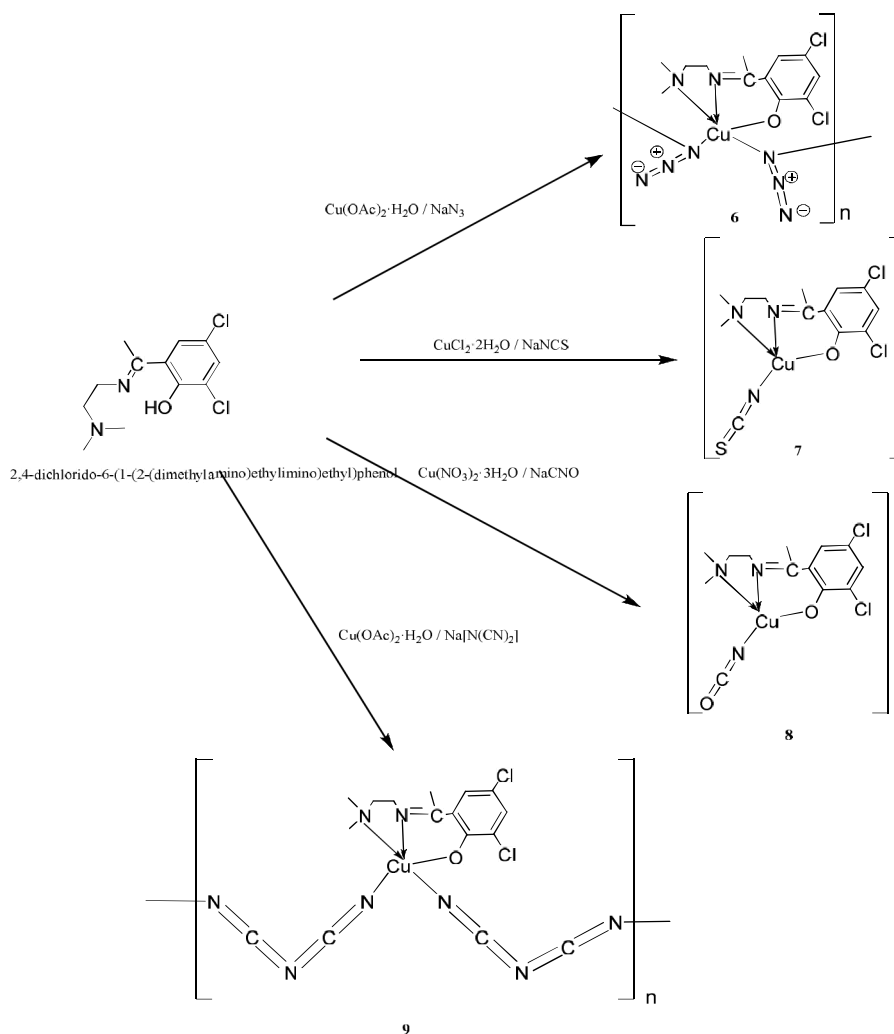
4.3. Results and discussion

The synthetic strategy adopted for the complexes was exactly the same except for the carbonyl compound used, i.e. 3,5-dichloro-2-hydroxyacetophenone instead of the aldehyde [Scheme 4.1]. The tridentate Schiff base system was

generated *in-situ* followed by the addition of metal salts and pseudohalides (1:2) for the preparation of the respective complexes [Scheme 4.2].

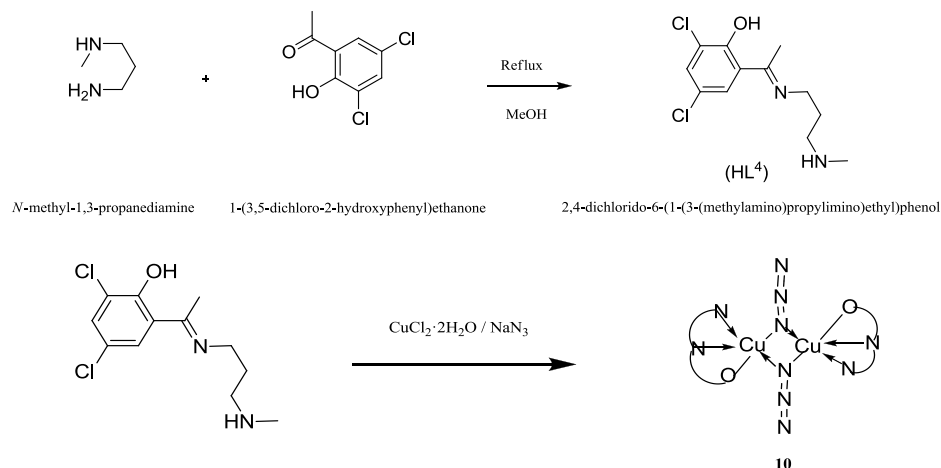


Scheme 4.1. Formation of tridentate Schiff base ligand.



Scheme 4.2. Synthetic route to copper complexes.

A similar procedure was followed for the preparation of the dimeric complex from *N*-methyl-1,3-propanediamine and 3,5-dichloro-2-hydroxyacetophenone as starting materials [Scheme 4.3].



Scheme 4.3. Synthetic route to the dimeric complex from HL⁴.

4.3.1. Spectroscopic signature

4.3.1.1. IR and electronic spectra

Complex **6** shows a characteristic unsplit strong peak at 2049 cm^{-1} attributable to asymmetric bridging nature of the azido ion [1]. The symmetric stretching, $\nu_s(\text{N}_3)$ and bending mode $\delta(\text{N}_3)$ of the azido group is ascertained from the peak positions at 1437 and 761 cm^{-1} respectively [2]. Single strong peak at 2099 cm^{-1} in the spectrum is registered by (-NCS) group present in the complex [Fig. 4.1] [3]. The presence of N-bonded cyanato group in complex **8** is confirmed by a peak at 2200 cm^{-1} [4] [Fig. 4.1]. In the case of dicyanamido complex, the bands at 2288 ($\nu_{\text{as}} + \nu_s(\text{C}=\text{N})$ combination modes), 2231 ($\nu_{\text{as}}(\text{C}=\text{N})$) and 2160 cm^{-1} ($\nu_s(\text{C}=\text{N})$) respectively is indicative of the bridging bidentate dca [5]. Except for the cyanato complex which has a C=N stretching frequency of 1634 cm^{-1} , the other three exhibits stretching at 1590 cm^{-1} . Dinuclear azido complex $[\text{Cu}(\text{L})(\text{N}_3)]_2$ (**10**) has a strong band at

2046 cm^{-1} , a medium band at 776 cm^{-1} and a weak band at 480 cm^{-1} corresponding to $\nu_{as}(\text{N}_3)$, $\nu_s(\text{N}_3)$ and $\delta(\text{N}_3)$ respectively [Fig. 4.1] [6].

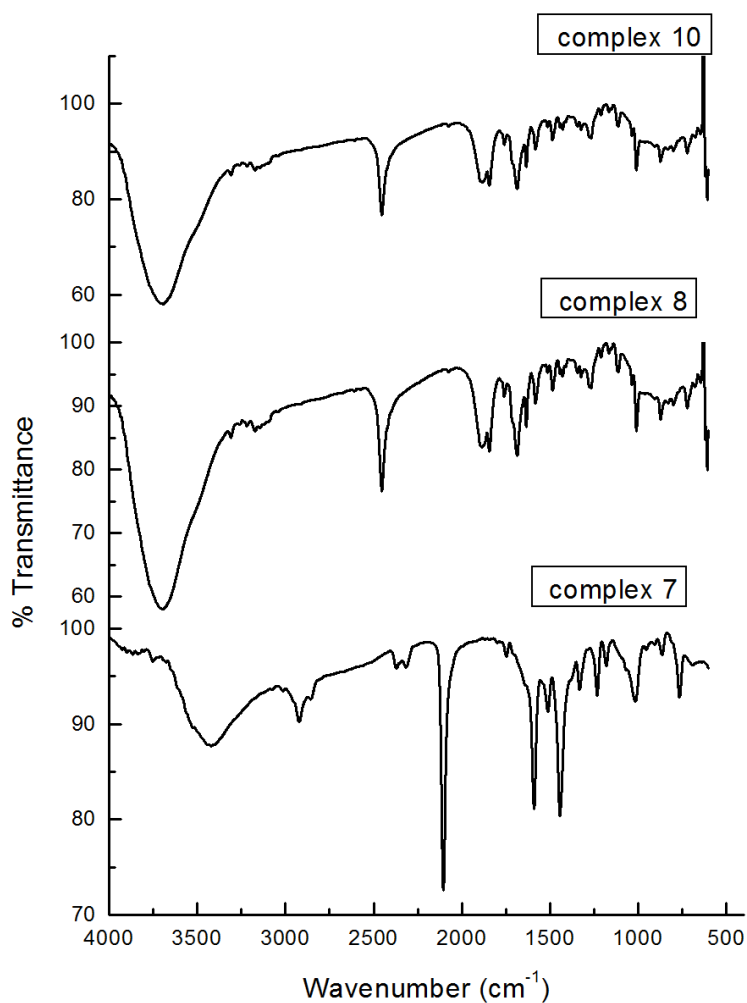


Fig. 4.1. The IR spectra of the complexes 7, 8 and 10.

The electronic spectra of all the five complexes were recorded in acetonitrile in the 200-1000 nm region at room temperature. Broad bands in the high energy 370-390 nm region is consistent with the LMCT transitions from the coordinating atoms of respective pseudohalides to the metal centre

[7,8] apart from O→Cu, N→Cu transitions. The high energy ligand based bands are found at *ca.* 238 nm [9a,b]. The ϵ values for these bands is supportive of the charge transfer and intraligand transitions. The complexes also exhibit a single low energy ligand field band at 573, 598, 601, 540 & 576 nm respectively, typical of a square based environment for Cu(II) [10].

4.3.1.2. Solvatochromic studies

To investigate the solvent effect on the absorption bands (CT and *dd*) of the synthesized complexes, the electronic spectra was recorded in variety of solvents ranging from polar protic (methanol), polar aprotic (tetrahydrofuran, ethyl acetate, acetone and acetonitrile) to non-polar solvents (toluene, chloroform). Solubility of complexes in a wide range of organic solvents make them good solvatochromic probes. Solvents were found to influence both the chromophoric groups as well as the coordination environment of the metal centre.

With increasing solvent polarity, within each classification of solvents (polar protic, polar aprotic and non-polar), the ground state molecule is found to be better stabilized by solvation than the molecule in the excited state, resulting in negative solvatochromism.[11]. This is attributable to a solvent-induced change of the electronic ground-state structure from a less dipolar (in non-polar solvents) to a more dipolar chromophore (in polar solvents) with increasing solvent polarity. The λ_{\max} (nm) along with their ϵ ($M^{-1}cm^{-1}$) values in various solvents are tabulated [Fig. 4.2, Table 4.1].

To ascertain the coordination mode of the complexes in solution phase, especially those of the polymeric ones (**6** and **9**), we carried out the solvatochromic study of the *d-d* bands also.

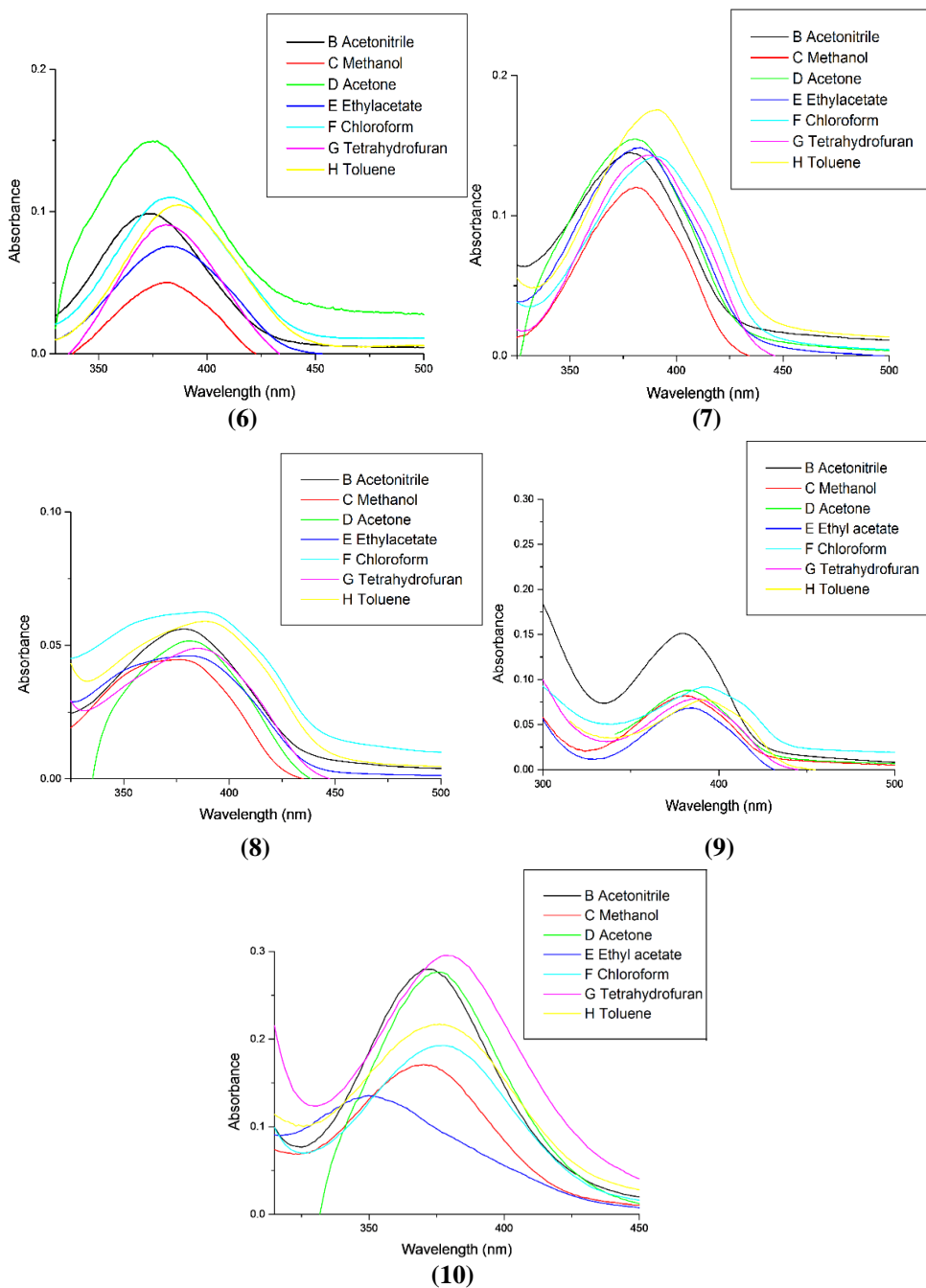


Fig. 4.2. Spectra showing the solvatochromic effect on the charge-transfer transitions of the complexes (con: 1×10^{-3} M).

Table 4.1. The λ_{\max} (nm) values along with their ϵ ($M^{-1}cm^{-1}$) in various solvents

| Polarity Index* | Solvents | Complex 6 | | Complex 7 | | Complex 8 | | Complex 9 | | Complex 10 | |
|-----------------|-----------------|-----------------------|---------------------------------------|-----------------------|---------------------------------------|-----------------------|---------------------------------------|-----------------------|---------------------------------------|-----------------------|---------------------------------------|
| | | λ_{\max} (nm) | $\epsilon * 10^3$ ($M^{-1}cm^{-1}$) | λ_{\max} (nm) | $\epsilon * 10^3$ ($M^{-1}cm^{-1}$) | λ_{\max} (nm) | $\epsilon * 10^3$ ($M^{-1}cm^{-1}$) | λ_{\max} (nm) | $\epsilon * 10^3$ ($M^{-1}cm^{-1}$) | λ_{\max} (nm) | $\epsilon * 10^3$ ($M^{-1}cm^{-1}$) |
| 5.1 | Methanol | 382 | 2.49 | 381 | 4.08 | 378 | 2.28 | 381 | 4.36 | 370 | 3.41 |
| | | 237 | 15.42 | 231 | 26.11 | | | 267 | 10.95 | 234 | 18.95 |
| | | 204 | 17.90 | 205 | 53.65 | | | | | | |
| 5.8 | Acetonitrile | 372 | 4.90 | 378 | 4.92 | 378 | 2.87 | 380 | 12.96 | 372 | 5.59 |
| | | 238 | 19.74 | 269 | 23.41 | 232 | 13.44 | 237 | 71.05 | 264 | 13.92 |
| | | | | 262 | 27.08 | | | | | | 237 |
| | | 238 | 28.99 | | | | | | | | |
| 5.1 | Acetone | 377 | 7.45 | 381 | 5.24 | 379 | 2.65 | 384 | 4.68 | 376 | 5.53 |
| 4.4 | Ethylacetate | 381 | 4.51 | 383 | 5.04 | 381 | 2.36 | 385 | 3.64 | 378 | 5.90 |
| | | | | 253 | 14.98 | | | | | | |
| 4.0 | Tetrahydrofuran | 383 | 3.76 | 387 | 4.85 | 386 | 2.50 | 386 | 4.19 | 380 | 2.70 |
| | | | | 241 | 24.17 | | | 291 | 7.27 | | |
| 4.1 | Chloroform | 382 | 5.47 | 391 | 4.82 | 390 | 3.19 | 393 | 4.88 | 377 | 3.85 |
| | | 247 | 16.54 | 285 | 8.74 | 290 | 14.22 | 284 | 8.89 | 263 | 28.85 |
| 2.4 | Toluene | 387 | 5.21 | 391 | 5.95 | 390 | 3.03 | 393 | 4.13 | 376 | 4.34 |
| | | | | 286 | 8.84 | | | | | | |

*Relative measure of degree of interaction of the solvents with various polar test solutes

Appreciable shift in the *d-d* absorption bands is a compelling evidence for the effect of solvents on the coordination environment of the metal. Of the various parameters known to govern solvent effect, it is the donor power of the solvent that is referred to for comparison. Four solvents of varying donor powers – DMSO, MeOH, CH₃CN and DCM were chosen for the study and it was found that the *d-d* band shifts to red with increasing donor number of the solvent. Observed shift as a function of donor power of chosen solvents showed positive solvatochromic effect.

Visible spectra of the complexes showed a broad band attributable to the promotion of an electron from the low energy orbitals to the hole in $d_{x^2-y^2}$ orbital of the copper(II) ion (d^9). With an increase in the donor number (DN) of the solvents, these bands show a red shift. The solvents approach the metal centre along the *z* axis and with an increase in its donor power, the interaction with the *z* orbitals intensifies, causing them to be at energetically higher position over the others. Eventually as the solvents with higher donor power occupies the axial site, the coordination geometry also changes from square planar to square pyramidal, which is mirrored as bathochromism [Fig. 4.3, Table 4.2]. The electronic response is conclusive for the existence of polymeric complexes as a discrete species [12] with the spacer being replaced by the solvent molecule in the axial position of the coordination sphere [13].

Table 4.2. The λ_{\max} (nm) values along with their ϵ ($M^{-1} cm^{-1}$) of *d-d* bands in various solvents

| Solvents | Donor number of solvents (DN) | Complex 6 | | Complex 7 | | Complex 8 | | Complex 9 | | Complex 10 | |
|----------|-------------------------------|-----------------------|--------------------------------|-----------------------|--------------------------------|-----------------------|--------------------------------|-----------------------|--------------------------------|-----------------------|--------------------------------|
| | | λ_{\max} (nm) | ϵ ($M^{-1}cm^{-1}$) | λ_{\max} (nm) | ϵ ($M^{-1}cm^{-1}$) | λ_{\max} (nm) | ϵ ($M^{-1}cm^{-1}$) | λ_{\max} (nm) | ϵ ($M^{-1}cm^{-1}$) | λ_{\max} (nm) | ϵ ($M^{-1}cm^{-1}$) |
| DMSO | 29.8 | 681 | 41 | 624 | 60 | 620 | 65 | 622 | 149 | 636 | 166 |
| MeOH | 19.0 | 605 | 177 | 620 | 106 | 611 | 79 | 587 | 266 | 607 | 219 |
| AcN | 14.1 | 573 | 79 | 598 | 109 | 601 | 106 | 563 | 223 | 576 | 308 |
| DCM | 0.0 | 543 | 105 | 592 | 119 | 598 | 79 | 540 | 238 | 568 | 328 |

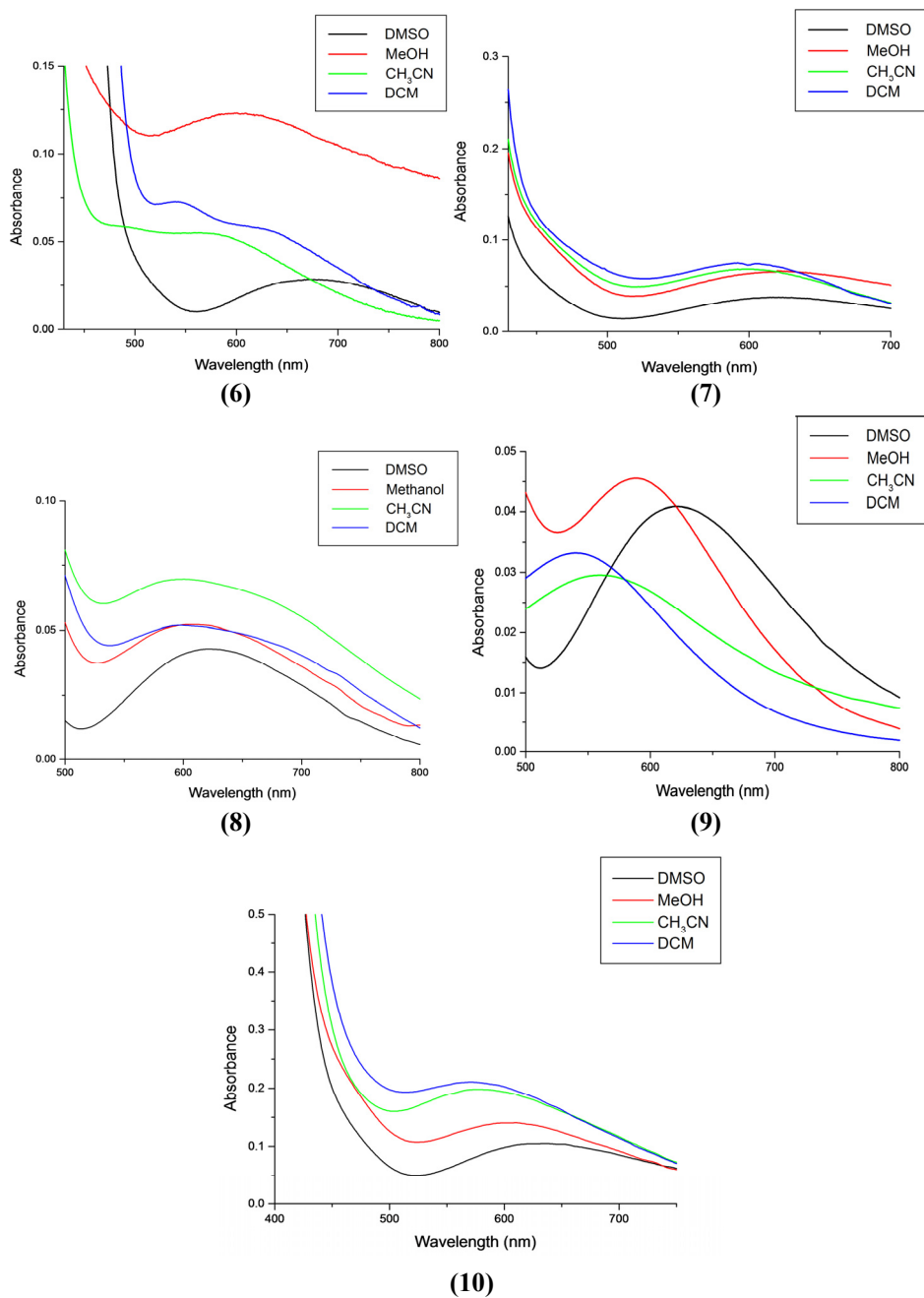


Fig. 4.3. The spectra showing solvatochromic behavior of *d-d* transitions (con: 2×10^{-3} M) of complexes in various solvents.

The solvatochromic effect was found to be profound for the azido complex followed by the dicyanamido complex with a variation in energy of 3732 cm^{-1} and 2441 cm^{-1} respectively as we proceed from DMSO to DCM.

4.3.2. X-ray crystallography and crystal structure description

Single crystals of compounds $[\text{Cu}(\text{L}^3)(\text{N}_3)]_n$ (**6**), $[\text{Cu}(\text{L}^3)(\text{NCS})]$ (**7**), $[\text{Cu}(\text{L}^3)(\text{NCO})]$ (**8**) $[\text{Cu}(\text{L}^3)[\text{N}(\text{CN})_2]]_n$ (**9**) & $[\text{Cu}(\text{L}^4)(\text{N}_3)_2]$ (**10**) suitable for X-ray diffraction studies were grown from their methanol solutions by slow evaporation at room temperature.

In all the complexes, the non-hydrogen atoms were refined anisotropically and all H atoms on C were placed in calculated positions guided by difference maps with C–H bond distances 0.93–0.97 Å. The H atoms were assigned as $U_{\text{iso}}=1.2U_{\text{eq}}$ (1.5 for Me). For the cyanato complex **8**, the atoms C9, C10, C11, C12 and N2 were disordered over two sites with an occupancy of 66.5% and 33.5% respectively. The above atoms which were bound to one another is assumed to move in similar directions with approximately similar amplitudes and therefore they were restrained to have same U^{ij} components by the SIMU command. The similarity restraint SADI restrains the distance between N1–C9 and N1–C9B to be equal within a default standard uncertainty of 0.02 Å. The EADP instruction for the atoms N2, N2B and C9, C9B constrains the atom pairs to have identical anisotropic displacement parameters. The terminal nitrogen atom, N5 of the azido group of the dimeric complex **10** was disordered over two sites with an occupancy of 55% and 45% respectively [14].

4.3.2.1. $[\text{Cu}(\text{L}^3)(\text{N}_3)]_n$ (6**)**

Compound crystallizes in monoclinic $P2_1/c$ space group. A perspective view of the complex with atom labelling scheme is shown in Fig. 4.4. Bond parameters are given in Table 4.3.

Table 4.3. Crystal data and refinement details of complexes **6** and **7**

| Parameters | 6 | 7 |
|-----------------------------------|---|---|
| Empirical formula | C ₁₂ H ₁₅ Cl ₂ CuN ₅ O | C ₁₃ H ₁₅ Cl ₂ CuN ₃ OS |
| Formula weight | 379.74 | 395.79 |
| Temperature | 296(2) K | 296(2) K |
| Wavelength | 0.71073 Å | 0.71073 Å |
| Crystal system | Monoclinic | Orthorhombic |
| Space group | <i>P</i> 2 ₁ / <i>c</i> | <i>P</i> bca |
| Unit cell dimensions | a = 10.4122(6) Å α = 90° b = 7.4498(6) Å β = 100.906(3)° c = 20.0450(14) Å γ = 90° | a = 9.2787(6) Å α = 90° b = 14.5940(7) Å β = 90° c = 23.4347(11) Å γ = 90° |
| Volume | 1526.78(19) Å ³ | 3173.4(3) Å ³ |
| Z | 4 | 8 |
| Density (calculated) | 1.652 Mg m ⁻³ | 1.657 Mg m ⁻³ |
| Absorption coefficient | 1.785 mm ⁻¹ | 1.845 mm ⁻¹ |
| <i>F</i> (000) | 772 | 1608 |
| Crystal size | 0.40 × 0.25 × 0.20 mm ³ | 0.50 × 0.45 × 0.40 mm ³ |
| θ range for data collection | 2.59 to 28.25° | 2.74 to 26.00° |
| Limiting indices | -13 ≤ h ≤ 13, -9 ≤ k ≤ 9, -26 ≤ l ≤ 26 | -11 ≤ h ≤ 8, -17 ≤ k ≤ 18, -28 ≤ l ≤ 28 |
| Reflections collected | 17694 | 15473 |
| Unique reflections | 3761 [R(int) = 0.0420] | 3117 [R(int) = 0.0348] |
| Refinement method | Full-matrix least-squares on F ² | Full-matrix least-squares on F ² |
| Data / restraints / parameters | 3730 / 0 / 190 | 3106 / 0 / 193 |
| Goodness-of-fit on F ² | 1.017 | 1.035 |
| Final R indices [I > 2σ(I)] | R ₁ = 0.0384, wR ₂ = 0.0952 | R ₁ = 0.0307, wR ₂ = 0.0751 |
| R indices (all data) | R ₁ = 0.0668, wR ₂ = 0.1117 | R ₁ = 0.0460, wR ₂ = 0.0848 |
| Largest diff. peak and hole | 0.363 and -0.460 e.Å ⁻³ | 0.392 and -0.367 e.Å ⁻³ |

$$R_1 = \frac{\sum ||F_o| - |F_c||}{\sum |F_o|}$$

$$wR_2 = [\sum w(F_o^2 - F_c^2)^2 / \sum w(F_o^2)^2]^{1/2}$$

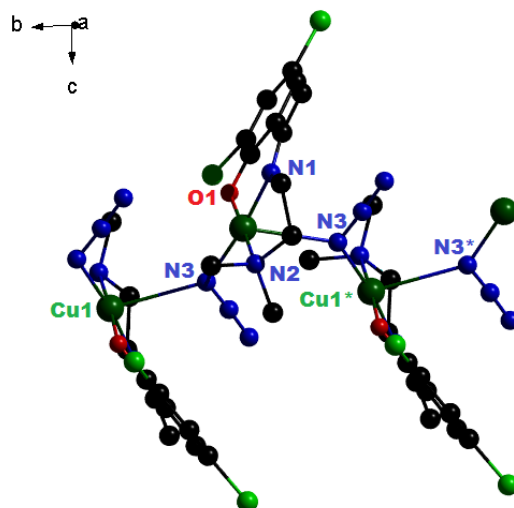


Fig. 4.4. Perspective view of the complex 6.

The ORTEP projects the asymmetric unit of the copper(II) complex as a square planar structure with NNO atoms of the tridentate Schiff base and N of the azido group as the ligating entities [Fig. 4.5] although in the entire polymeric structure, the copper(II) centres are pentacoordinated, with the fifth coordination site being satisfied by the N of the second azido group in apical position [Fig. 4.4].

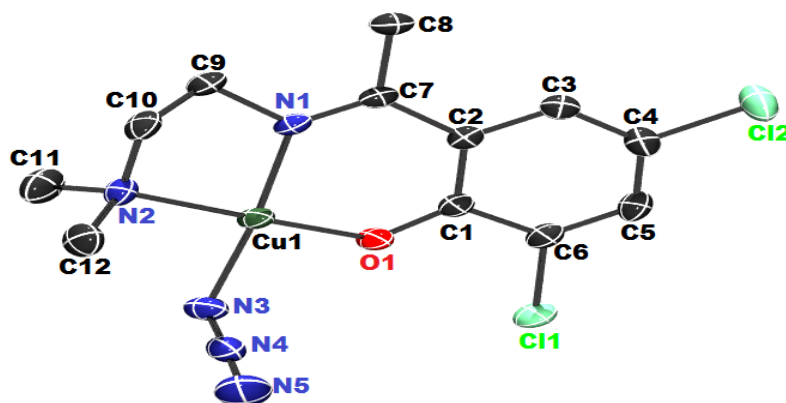


Fig. 4.5. ORTEP diagram projecting the asymmetric unit of the complex 6 (Hydrogen atoms are omitted for clarity, ellipsoid plots drawn with 30% probability).

Thus the azide with its *end-on* coordination acts as a spacer in constructing the chain. The asymmetric bonding mode of azide is evident from Cu–N3 bond lengths of 1.980(3) Å (basal)/2.811(3) Å (apical). Selected bond lengths and angles are given in Table 4.4.

Table 4.4. Selected bond lengths (Å) and bond angles (°) for complex **6**

| Bond lengths (Å) | | Bond angles (°) | |
|------------------|----------|-------------------|------------|
| Cu(1)–O(1) | 1.887(2) | O(1)–Cu(1)–N(1) | 92.16(9) |
| Cu(1)–N(1) | 1.960(2) | O(1)–Cu(1)–N(3) | 89.35(11) |
| Cu(1)–N(3) | 1.980(3) | N(1)–Cu(1)–N(3) | 171.64(11) |
| Cu(1)–N(2) | 2.033(2) | O(1)–Cu(1)–N(2) | 176.85(10) |
| O(1)–C(1) | 1.289(4) | N(1)–Cu(1)–N(2) | 86.44(9) |
| Cl(1)–C(2) | 1.737(3) | N(3)–Cu(1)–N(2) | 91.64(11) |
| Cl(2)–C(4) | 1.745(3) | N(4)–N(3)–Cu(1) | 115.2(2) |
| N(1)–C(7) | 1.290(4) | N(5)–N(4)–N(3) | 177.3(4) |
| N(1)–C(9) | 1.468(4) | C(11)–N(2)–C(12) | 108.7(3) |
| N(3)–N(4) | 1.191(4) | Cu(1)–N(3)–Cu(1)b | 134.6(1) |
| N(4)–N(5) | 1.144(5) | O(1)–Cu(1)–N(3)a | 91.84(9) |
| Cu(1)–N(3)a | 2.811(3) | N(1)–Cu(1)–N(3)a | 82.05(9) |
| | | N(3)–Cu(1)–N(3)a | 106.12(10) |

The geometry of the complex is conveniently measured by Addison parameter, $\tau = (\beta - \alpha)/60$ [15] (α and β are the two largest L–M–L angles of the coordination sphere; for perfect square pyramidal and trigonal bipyramidal geometries the values of τ are zero and unity respectively). The τ value of 0.0868 is indicative of a distorted square pyramidal geometry for the complex. The metal centre is pulled out from the least squares mean plane by a distance of 0.0766 Å towards the apical donor atom. Among the donor atoms, it's the imine nitrogen (0.0660 Å) that deviates the most. The azido group builds the structure into a one dimensional polymer along 'b' axis with the pseudohalide in $\mu_{1,1}$ *trans* bridging mode. In addition to the *trans* mode of bridging, the 2_1 translational element of symmetry gives a helical nature to the chain. The metal centres bridged *via* azido group is at a distance of 4.4310(6) Å from each other whereas the interchain Cu...Cu distance is 10.619(8) Å. Pseudolinearity of the azido group is evident from its bond angle of 177.3(4)°.

We have already reported two examples of helical *trans*- $\mu_{1,1}$ chains with Cu(II) [16] and this compound is structurally similar except for the greater spacing of the alternate teeth (7.4498 Å) in the zipper-like formation [Fig. 4.6].

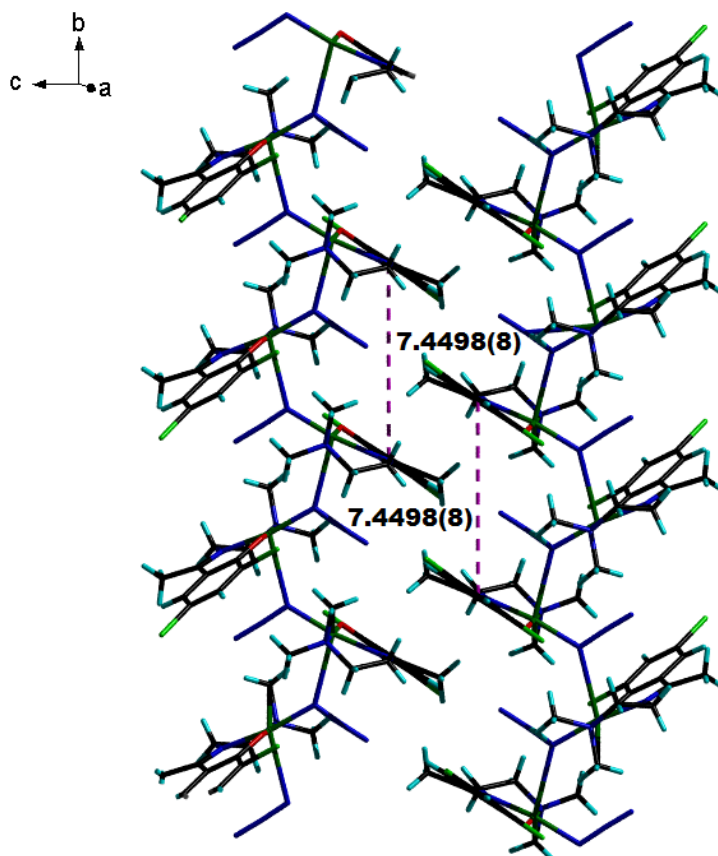


Fig. 4.6. Zipper-like formation seen in complex 6.

The metrical parameters like metal-N-metal bridge angle (Cu1–N3–Cu1) in this metal-azido complex is $134.6(1)^\circ$ and the N3–Cu1–N3 bond angle emerges to $106.12(10)^\circ$. The bond strength follows the order: metal-phenoxo oxygen [1.887(2) Å] > metal-imino nitrogen [1.960(2) Å] > metal-equatorial azido nitrogen [1.980(3) Å] > metal-amino nitrogen [2.033(2) Å] > metal-axial azido nitrogen [2.811(3) Å].

The five membered chelate ring, Cg(1) [Cu(1)–N(1)–C(9)–C(10)–N(2)] with C(10) as the flap atom of the envelope conformation has pseudorotation parameters, $P = 262.0(2)^\circ$ and $\tau = 47.4(2)^\circ$. The envelope conformation was further confirmed in terms of pseudorotation parameters $P = 264.6(3)^\circ$ and $\tau = 47.3(3)^\circ$ for reference bond Cu(1)–N(1) [17]. The six membered metallocycle, Cu(1)–O(1)–C(1)–C(6)–C(7)–N(1) has a screw-boat conformation with puckering amplitude $Q = 0.233(2) \text{ \AA}$, $\theta = 110.9(7)^\circ$ and $\Phi = 209.1(7)^\circ$.

An S(3) ring motif is created as a result of bifurcated hydrogen bonding interaction between the hydrogen, H(12B) borne by the methyl carbon C(12) with the nitrogen atoms N(3) and N(4) of the azido group. The other hydrogen atom, H(12A) of the same methyl group engages in an intermolecular interaction with the phenoxo oxygen, O(1) [Fig. 4.7].

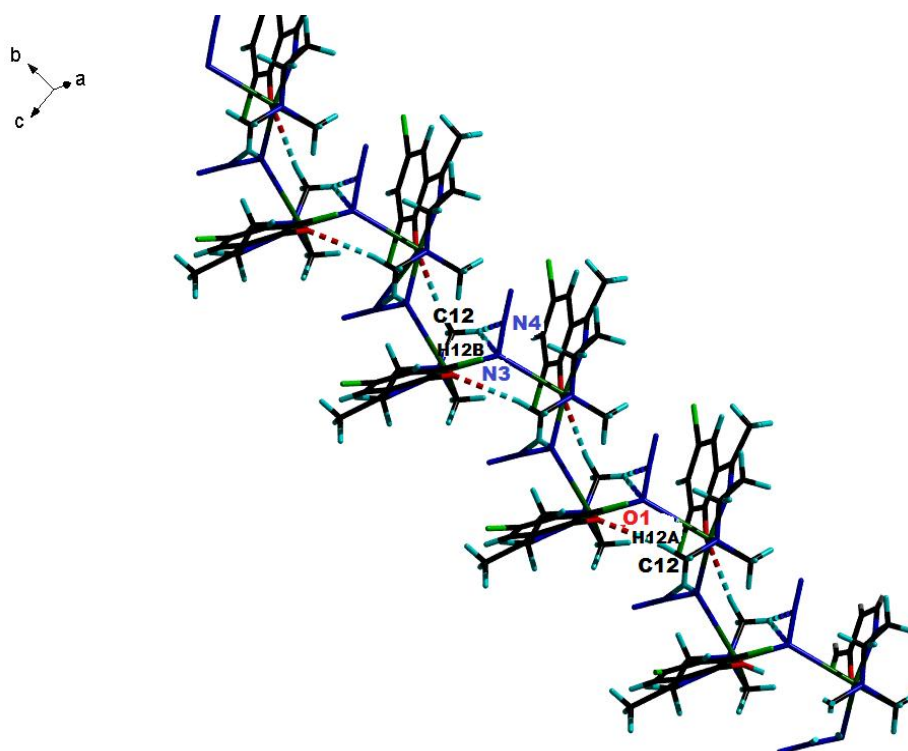


Fig. 4.7. Intrachain hydrogen bonding interaction (intramolecular and intermolecular hydrogen bond interactions).

The H(5) atom associated with the C(5) also indulges in an intermolecular interchain contact with the terminal nitrogen, N(5) of the bridging azido group [Fig. 4.8, Table 4.5]. This intermolecular interaction coupled with the bridging nature of the azido group establishes a two dimensional supramolecular array along 'bc' plane [Fig. 4.8].

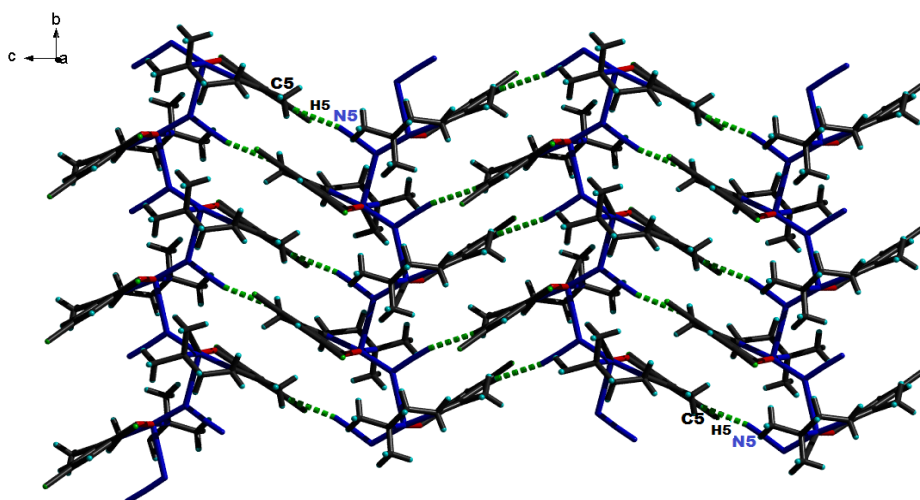


Fig. 4.8. Supramolecular 2-D array along 'bc' plane.

Table 4.5. Non-conventional hydrogen bonding interactions in complex 6

| D-H...A | D-H (Å) | H...A (Å) | D...A (Å) | D-H...A (°) |
|--|---------|-----------|-----------|-------------|
| Intermolecular hydrogen bonding | | | | |
| C(5)-H(5)...N(5) ^a | 0.93 | 2.49 | 3.381(5) | 161 |
| C(12)-H(12A)...O(1) ^b | 0.96 | 2.58 | 3.524(4) | 169 |
| Intramolecular hydrogen bonding | | | | |
| C(12)-H(12B)...N(3) | 0.96 | 2.58 | 3.072(5) | 112 |
| C(12)-H(12B)...N(4) | 0.96 | 2.59 | 3.167(5) | 119 |

Equivalent position codes: a = x, 1/2 - y, -1/2 + z; b = 2 - x, -1/2 + y, 1/2 - z

4.3.2.2. [Cu(L³)(NCS)] (7)

This monomeric complex crystallizes in orthorhombic *Pbca* space group. The asymmetric unit of the complex in ORTEP shows a square planar geometry with the metal being coordinated by the amino nitrogen N2, imino

nitrogen N1, phenoxo oxygen O1 and nitrogen N3 of the thiocyanato group [Fig. 4.9]. The crystallographic details are given in Table 4.3.

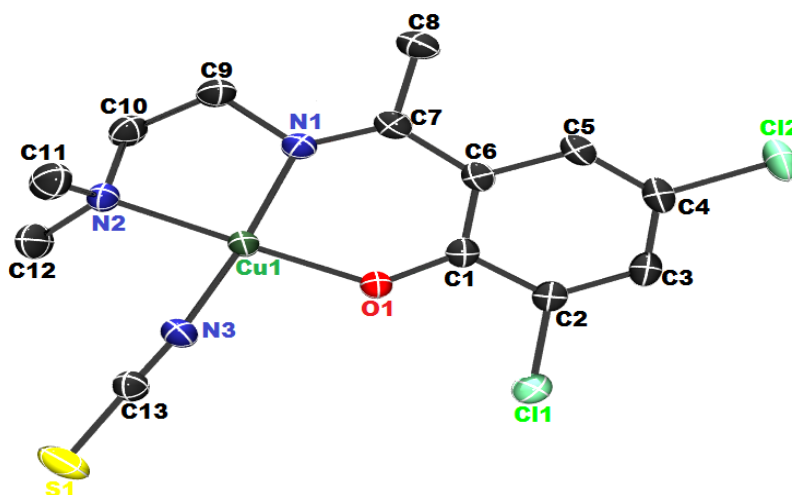


Fig. 4.9. ORTEP diagram showing the asymmetric unit of complex **7** (Hydrogen atoms are omitted for clarity, ellipsoid plots drawn with 30% probability).

Pentagonal and hexagonal metallo-chelate rings are formed with chelate bite angles of $85.92(9)^\circ$ and $92.54(8)^\circ$ respectively as a result of coordination. Selected bond lengths and angles are collated in Table 4.6.

Table 4.6. Selected bond lengths (\AA) and bond angles ($^\circ$) for **7**

| Bond lengths (\AA) | | Bond angles ($^\circ$) | |
|-------------------------------|------------|--------------------------|------------|
| Cu(1)–O(1) | 1.8880(18) | O(1)–Cu(1)–N(1) | 92.54(8) |
| Cu(1)–N(1) | 1.964(2) | O(1)–Cu(1)–N(3) | 90.88(9) |
| Cu(1)–N(2) | 2.047(2) | N(3)–Cu(1)–N(2) | 91.04(9) |
| Cu(1)–N(3) | 1.952(2) | N(1)–Cu(1)–N(2) | 85.92(9) |
| N(3)–C(13) | 1.150(3) | N(1)–Cu(1)–N(3) | 164.20(11) |
| C(2)–Cl(1) | 1.738(3) | O(1)–Cu(1)–N(2) | 177.78(8) |
| C(4)–Cl(2) | 1.746(3) | N(3)–C(13)–S(1) | 178.9(3) |
| C(13)–S(1) | 1.630(3) | | |

The extent of deformation in a tetracoordinated complex is given by the τ_4 index - a measure of the extent of distortion between a perfect tetrahedron ($\tau_4 = 1$) and perfect square planar geometry ($\tau_4 = 0$), given by the formula: $\tau_4 = [360^\circ - (\alpha + \beta)]/141^\circ$, α and β being the two largest angles around the central

metal atom in the complex. The τ_4 value of 0.1278, for this complex confirms a slightly distorted square planar geometry. Moreover, the different angles around the copper metal summate to 362.04° , a value slightly varied from that required for a perfect geometry. The metal centre is pulled out, off the plane by a distance of 0.0088 \AA and among the other coordinating atoms, the nitrogen of thiocyanato group deviates the most. The pseudolinearity of the coligand is evident from the bond angle of $178.9(3)^\circ$. The metal-donor bond strength follows the order Cu1-O1 (phenolate oxygen) > Cu1-N3 (thiocyanato nitrogen) > Cu1-N1 (imino nitrogen) > Cu1-N2 (amino nitrogen).

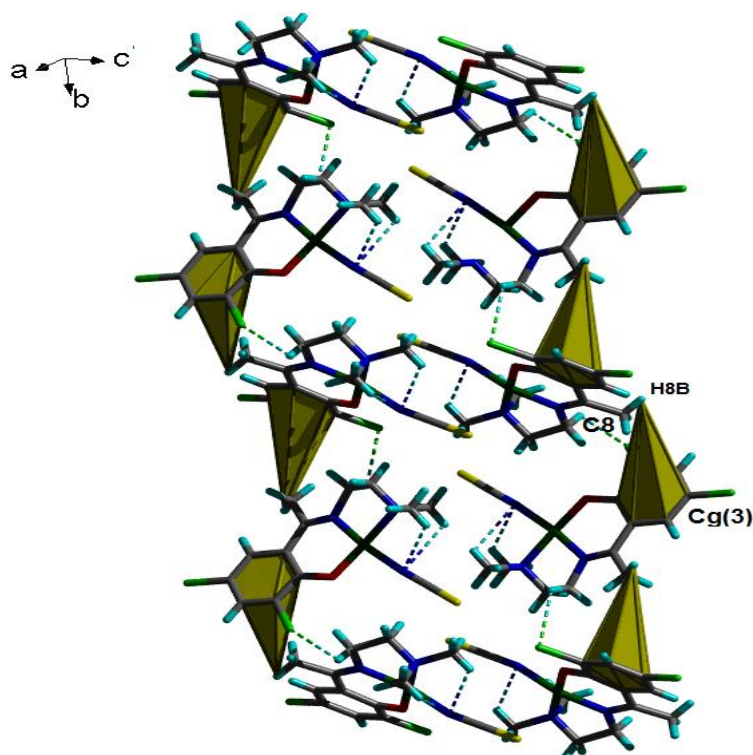


Fig. 4.10. C–H...Cg interaction propagating the monomeric units along b' axis.

Table 4.7. X–H...Cg interactions

| C–H...Cg(J) | H...Cg (Å) | C...Cg (Å) | C–H...Cg (°) |
|---------------------------------|------------|------------|--------------|
| C(8)–H(8B)...Cg(3) ^a | 2.860 | 3.509(3) | 126.0 |

Equivalent position code: $a = -1/2 + x, y, 1/2 - z$

The monomeric units are connected *via* C–H···Cg interaction between H(8B) borne by C(8) atom and Cg(3) ring thus forming a linear chain along ‘*b*’ axis [Fig. 4.10]. Geometric features of C–H··· π interactions are collated in Table 4.7. The Cg(1) [Cu1/N1/C9/C10/N2] assumes an envelope conformation with C(10) as the flap atom and $P = 84.8(2)^\circ$ and $\tau_m = 48.6(2)^\circ$ as the pseudorotation parameters.

4.3.2.3. [Cu(L³)(NCO)] (8)

The monoclinic monomeric complex crystallizes in $P2_1/n$ space group. The ORTEP plot shows the asymmetric unit of the complex with a square planar geometry; the coordination polyhedron being satisfied by phenolate oxygen (O1), azomethine nitrogen (N1), amino nitrogen (N2) and cyanato nitrogen (N3) [Fig. 4.11]. The coordination results in five and six membered chelate rings with bite angles of $92.32(8)^\circ$ and $83.5(3)^\circ$ respectively. Bond parameters are given in Table 4.8.

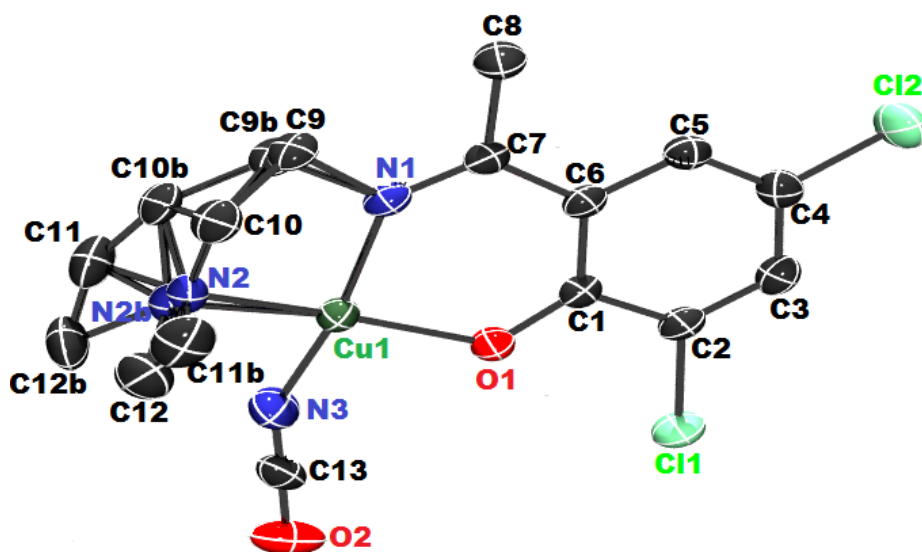


Fig. 4.11. ORTEP diagram showing the asymmetric unit of complex **8** (Hydrogen atoms are omitted for clarity, ellipsoid plots drawn with 30% probability).

Table 4.8. Crystal data and refinement details of complexes **8**, **9** and **10**

| Parameters | 8 | 9 | 10 |
|-----------------------------------|--|---|--|
| Empirical formula | C ₁₃ H ₁₅ Cl ₂ CuN ₃ O ₂ | C ₁₄ H ₁₅ Cl ₂ CuN ₅ O | C ₂₄ H ₂₈ Cl ₄ Cu ₂ N ₁₀ O ₂ |
| Formula weight | 379.72 | 403.76 | 757.46 |
| Temperature | 296(2) K | 296(2) K | 296(2) K |
| Wavelength | 0.71073 Å | 0.71073 Å | 0.71073 Å |
| Crystal system | Monoclinic | Monoclinic | Triclinic |
| Space group | <i>P2</i> ₁ / <i>n</i> | <i>P2</i> ₁ / <i>c</i> | <i>P</i> $\bar{1}$ |
| Unit cell dimensions | a = 10.7176(7) Å α = 90° b = 13.5195(8) Å β = 107.479(3) c = 11.1725(6) Å γ = 90° | a = 7.1981(3) Å α = 90° b = 11.0859(6) Å β = 99.460(2)° c = 20.4001(9) Å γ = 90° | a = 8.3769(5) Å α = 94.528(3)° b = 9.3239(6) Å β = 106.656(2)° c = 10.7678(7) Å γ = 103.156(2)° |
| Volume | 1544.11(16) Å ³ | 1605.74(13) Å ³ | 775.16(9) Å ³ |
| Z | 4 | 4 | 1 |
| Density (calculated) | 1.633 Mg m ⁻³ | 1.670 Mg m ⁻³ | 1.623 Mg m ⁻³ |
| Absorption coefficient | 1.766 mm ⁻¹ | 1.703 mm ⁻¹ | 1.758 mm ⁻¹ |
| <i>F</i> (000) | 772 | 820 | 384 |
| Crystal size | 0.300 × 0.300 × 0.280 mm ³ | 0.415 × 0.315 × 0.255 mm ³ | 0.400 × 0.300 × 0.200 mm ³ |
| θ range for data collection | 2.434 to 28.362° | 2.73 to 28.29° | 2.759 to 28.385° |
| Limiting indices | -9 ≤ h ≤ 14, -18 ≤ k ≤ 18 14 ≤ l ≤ 9 | -6 ≤ h ≤ 9, -11 ≤ k ≤ 14, -27 ≤ l ≤ 27 | -11 ≤ h ≤ 7, -12 ≤ k ≤ 12, -14 ≤ l ≤ 14 |
| Reflections collected | 12241 | 12895 | 7175 |
| Unique reflections | 3764 [R(int) = 0.0240] | 3995 [R(int) = 0.0000] | 3884 [R(int) = 0.0172] |
| Refinement method | Full-matrix least-squares on F ² | Full-matrix least-squares on F ² | Full-matrix least-squares on F ² |
| Data / restraints / parameters | 3764 / 153 / 230 | 3979 / 0 / 211 | 3793 / 0 / 200 |
| Goodness-of-fit on F ² | 1.028 | 0.691 | 0.808 |
| Final R indices [I > 2σ(I)] | R ₁ = 0.0355, wR ₂ = 0.0927 | R ₁ = 0.0282, wR ₂ = 0.0828 | R ₁ = 0.0349, wR ₂ = 0.1049 |
| R indices (all data) | R ₁ = 0.0522, wR ₂ = 0.1046 | R ₁ = 0.0364, wR ₂ = 0.0921 | R ₁ = 0.0450, wR ₂ = 0.1179 |
| Largest diff. peak and hole | 0.453 and -0.500 e.Å ⁻³ | 0.434 and -0.546 e.Å ⁻³ | 0.706 and -0.529 e.Å ⁻³ |

$$R_1 = \frac{\sum ||F_o| - |F_c||}{\sum |F_o|}$$

$$wR_2 = [\frac{\sum w(F_o^2 - F_c^2)^2}{\sum w(F_o^2)^2}]^{1/2}$$

A measure of the extent of distortion between a perfect tetrahedron ($\tau_4 = 1$) and perfect square planar geometry ($\tau_4 = 0$), is given by the formula: $\tau_4 = [360^\circ - (\alpha + \beta)]/141^\circ$, α and β being the two largest angles around the central metal atom in the complex. The extent of deformation in this tetracoordinated complex is given by τ_4 value of 0.1994, confirming a slightly distorted square planar geometry. The deviation of metal centre out of the plane by a distance of 0.0449 Å and the angle summation of 364.11° all are in favor of the distorted geometry. The cyanato coligand is pseudolinear with an angle of 178.8(3)°. Bond strength order follows the same trend as seen for the thiocyanato complex. Selected bond lengths and angles are collated in Table 4.9.

Table 4.9. Selected bond lengths (Å) and bond angles (°) for **8**

| Bond lengths (Å) | | Bond angles (°) | |
|------------------|------------|------------------|------------|
| Cu(1)–O(1) | 1.8806(19) | O(1)–Cu(1)–N(1) | 92.32(8) |
| Cu(1)–N(1) | 1.9481(19) | O(1)–Cu(1)–N(3) | 92.49(10) |
| Cu(1)–N(2) | 2.036(12) | N(3)–Cu(1)–N(2) | 95.8(3) |
| Cu(1)–N(2b) | 2.11(2) | N(3)–Cu(1)–N(2b) | 88.2(5) |
| Cu(1)–N(3) | 1.920(2) | N(1)–Cu(1)–N(2) | 83.5(3) |
| N(3)–C(13) | 1.147(4) | N(1)–Cu(1)–N(2b) | 90.4(5) |
| C(2)–Cl(1) | 1.736(2) | N(1)–Cu(1)–N(3) | 166.28(10) |
| C(4)–Cl(2) | 1.742(2) | O(1)–Cu(1)–N(2) | 161.4(3) |
| C(13)–O(2) | 1.193(3) | O(1)–Cu(1)–N(2b) | 165.6(6) |
| | | N(3)–C(13)–O(2) | 178.8(3) |

The intermolecular hydrogen bonding interaction established with the cyanato oxygen [Fig. 4.12, Table 4.10] connects the monomeric species whilst the hydrogen bonded species are sewn together by Cg...Cg interaction [Fig. 4.13, Table 4.11].

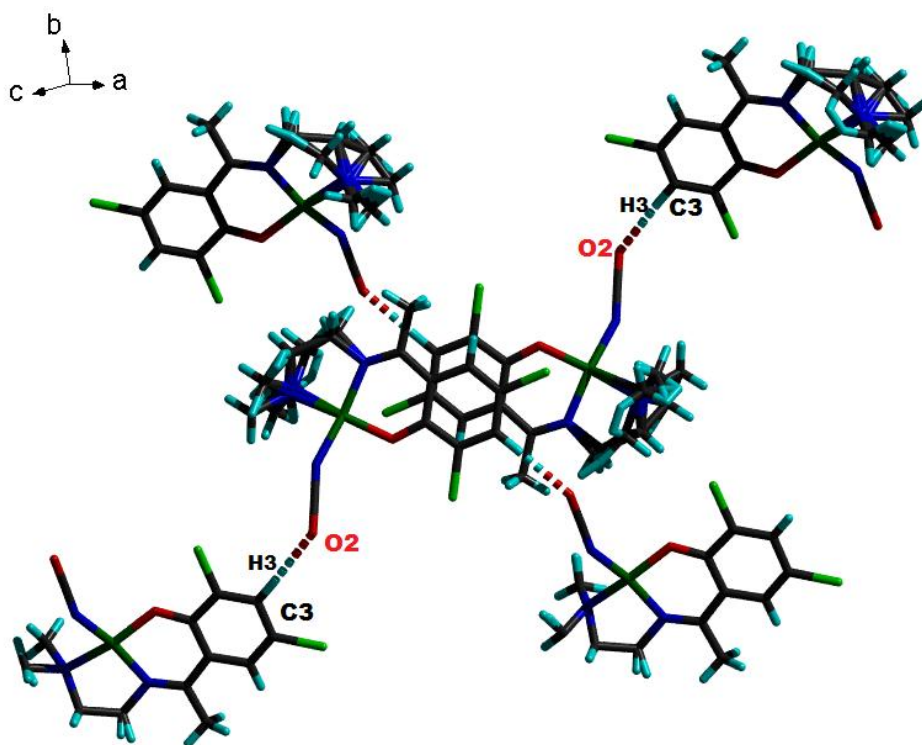


Fig. 4.12. Intermolecular hydrogen bonding interaction sewing the monomeric units.

Table 4.10. Non-conventional hydrogen bonding interactions in the complex **3**

| D–H···A | D–H (Å) | H···A (Å) | D···A (Å) | D–H···A (°) |
|--|---------|-----------|-----------|-------------|
| Intermolecular hydrogen bonding | | | | |
| C(3)–H(3)···O(2) ^a | 0.93 | 2.38 | 3.310(4) | 176 |

Equivalent position code: $a = 1/2 + x, 5/2 - y, -1/2 + z$

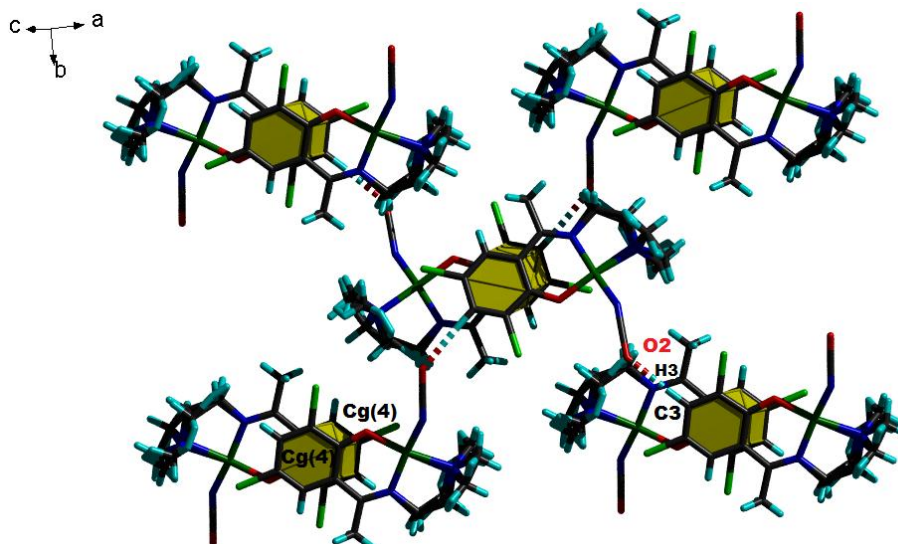


Fig. 4.13. The hydrogen bonded species sewn together by Cg...Cg interaction.

Table 4.11. Cg...Cg (π -ring) interactions

| Cg(I)...Cg(J) | Cg...Cg (Å) | α (°) | β (°) | γ (°) |
|----------------------------|-------------|--------------|-------------|--------------|
| Cg(4)...Cg(4) ^b | 3.650(1) | 0 | 17.1 | 17.1 |

Equivalent position code: $b = 2 - x, 2 - y, -z$

Cg, centroid

Cg(4) = C(1), C(2), C(3), C(4), C(5), C(6)

α = Dihedral angle between planes I and J (°)

β = Angle between Cg...Cg and normal to plane I

γ = Angle between Cg...Cg and normal to plane J

The metallocycle Cg(1) [Cu1,N1,C9,C10,N2] assumes an envelope conformation with C(10) as the flap atom and pseudorotation parameters $P = 261.4(4)^\circ$ and $\tau = 44.6(4)^\circ$. Also, the six membered ring, Cg(3) [Cu1,O1,C1,C6,C7,N1] assumes envelope conformation with $Q = 0.1858(16)$ Å, $\theta = 59.7(6)^\circ$ and $\Phi = 358.7(8)^\circ$.

4.3.2.4. [Cu(L³)[N(CN)₂]_n (9)

A perspective view of the complex along with atom labelling scheme is given in Fig. 4.14. Bond parameters are included in Table 4.8. The

asymmetric unit has two crystallographically different monomeric square planar species with NNO donor atoms from the tridentate Schiff base and the nitrogen of the dicyanamide group satisfying the topological requirement. Selected bond lengths are summarized in Table 4.12.

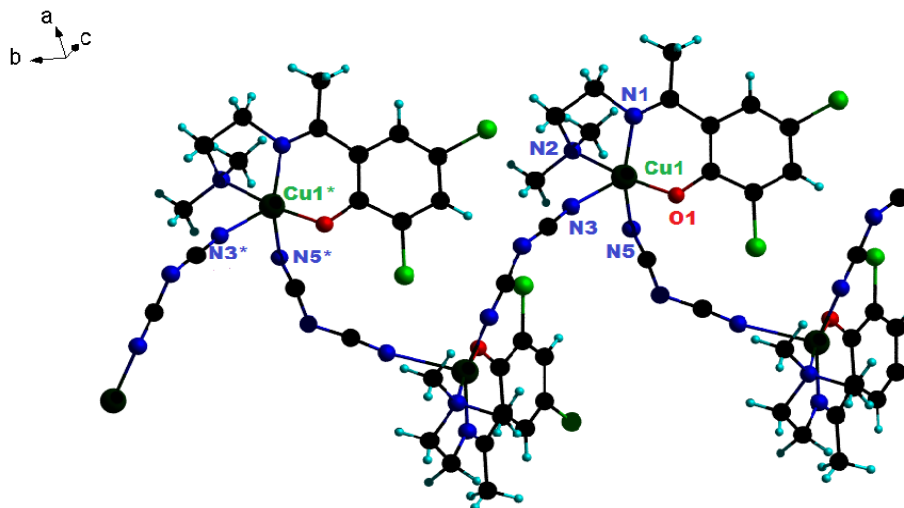


Fig. 4.14. Perspective view of the complex along with atom labelling scheme.

Table 4.12. Selected bond lengths (Å) and bond angles (°) for **9**

| Bond lengths (Å) | | Bond angles (°) | |
|------------------|----------|------------------|-----------|
| Cu(1)–O(1) | 1.890(1) | O(1)–Cu(1)–N(1) | 90.59(6) |
| Cu(1)–N(1) | 1.995(1) | O(1)–Cu(1)–N(2) | 172.41(6) |
| Cu(1)–N(2) | 2.032(1) | O(1)–Cu(1)–N(3) | 94.91(6) |
| Cu(1)–N(3) | 2.368(1) | O(1)–Cu(1)–N(5) | 88.36(6) |
| Cu(1)–N(5) | 2.003(1) | N(1)–Cu(1)–N(2) | 84.10(6) |
| N(5)–C(14) | 1.148(2) | N(1)–Cu(1)–N(3) | 104.45(6) |
| C(14)–N(4) | 1.296(2) | N(1)–Cu(1)–N(5) | 156.95(7) |
| N(4)–C(13) | 1.308(3) | N(2)–Cu(1)–N(3) | 91.67(6) |
| C(13)–N(3) | 1.151(3) | N(2)–Cu(1)–N(5) | 94.40(6) |
| C(4)–Cl(2) | 1.740(2) | N(3)–Cu(1)–N(5) | 98.59(6) |
| C(2)–Cl(1) | 1.729(2) | Cu(1)–N(3)–C(13) | 170.0(1) |
| | | Cu(1)–N(5)–C(14) | 159.1(1) |
| | | C(13)–N(4)–C(14) | 121.6(1) |

The non-linear dicyanamido group stitches the molecules into a one dimensional polymeric chain along 'b' axis of a monoclinic unit cell *via trans* $\mu_{1,5}$ bridging [18]. Each Cu(II) centre is linked to two adjacent centres by two dca groups in *end-to-end* fashion, thus providing a helical nature to the developing polymer [Fig. 4.15].

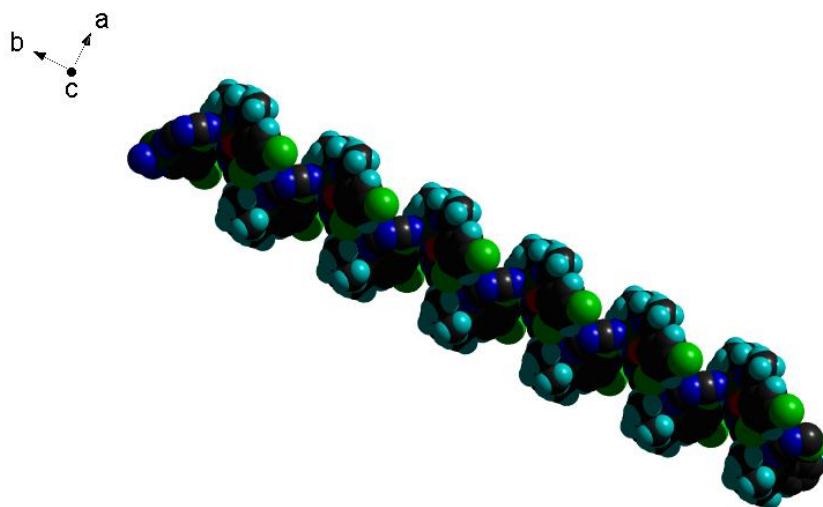


Fig. 4.15. Helical nature of the developing polymer.

The two dca molecules are *cis* to each other with an angle of $98.59(6)^\circ$ with each other. The copper centre assumes an almost square pyramidal geometry with the square basal plane lodged by amino nitrogen, N(2), one imine nitrogen, N(1), phenoxo oxygen, O(1) of the tridentate Schiff base in a meridional mode and the two nitrogen atoms N(5) and N(3) of the two dicyanamido ligands satisfying the remaining basal and apical positions. The coordination generates a pentahedral and hexahedral chelate rings with bite angles of $84.10(6)^\circ$ and $90.59(6)^\circ$ respectively. The distortion in the square pyramidal geometry is quantitatively measured as $\tau = (\beta - \alpha)/60$ and the value for this complex is 0.2576. The bond strength of the coordinating atoms follow the order $\text{Cu1-O1(phenoxo oxygen)} > \text{Cu1-N1(imine nitrogen)} > \text{Cu1-N2(amino nitrogen)} > \text{Cu1-N5(dicyanamido nitrogen)}$. The copper centre protrudes by a distance of 0.2035 \AA from the plane.

The metal-metal distance through the bridging dicyanamide is 7.8840(4) Å whereas the shortest interchain Cu...Cu distance is only 7.3315(4) Å. The bridging array Cu–NCNCN–Cu adopts a “V” conformation with central C–N–C angle of 121.6(1)°. The Cu–N bond lengths of 2.003(1) and 2.368(1) Å make it evident that the dca bridge assumes an asymmetrical basal-apical disposition with the same dca molecule residing on the apical position of one copper but in the basal plane of the other. As found in similar systems, the Cu–N₁_{imine} distance [1.995(1)] is shorter than Cu–N₂_{amino} distance [2.032(1)]. The carbon atoms of the dca ligand are *sp* hybridized and almost linear with N–C–N angles of 173.8(1) and 173.5(2)° respectively whilst the C–N–Cu angles, 170.0(1) and 159.1(1)° deviate from linearity. The five-membered metallocycle, Cg(1) [Cu(1)/N(1)/C(9)/C(10)/N(2)] assumes envelope conformation with N(2) as the flap atom and $Q(2) = 0.4909(18)$ Å, $\Phi(2) = 316.2(2)^\circ$ as the puckering parameters [19]. A similar six membered chelate ring involving the ketonic moiety, Cg(2) [Cu1/O1/C1/C6/C7/N1] adopts an half-chair conformation with $Q(2) = 0.2135(15)$ Å and $\Phi(2) = 205.5(4)^\circ$. The CuN₃O basal planes of the alternate units along a chain are placed parallel to each other. Also, the dca bridged species are disposed at an angle of 60° to each other.

The intrachain hydrogen bonding between the hydrogen atom, H(12B) borne on methyl carbon and the chlorine atom, Cl(1) [Fig. 4.16, Table 4.13] actually brings the complex units more closer as is evident from the smaller metal-metal separation when compared to the metal-metal distance of similar systems [20].

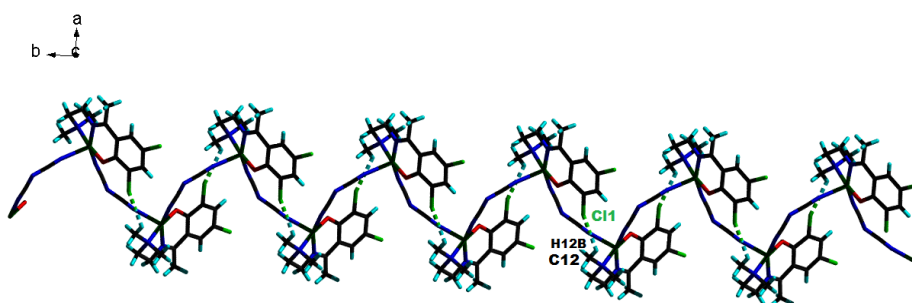


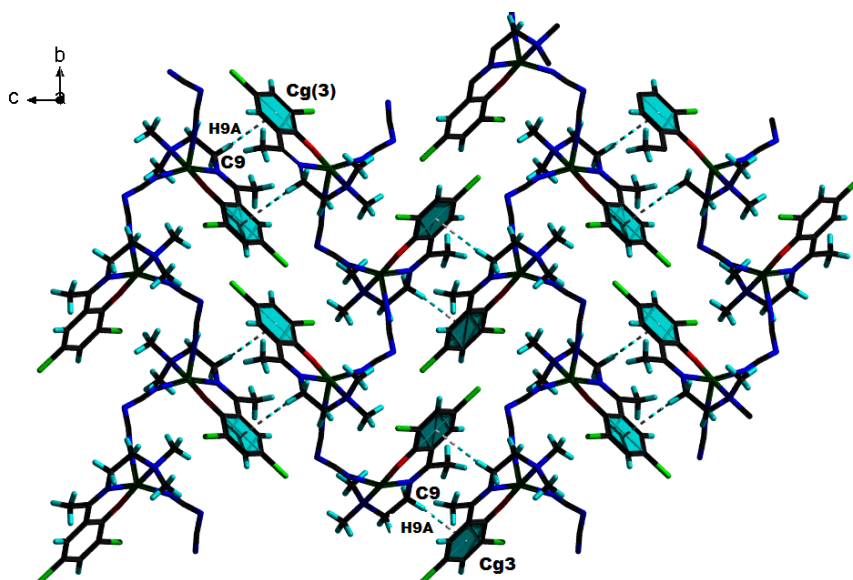
Fig. 4.16. Intrachain hydrogen bonding interaction in complex 9.

Table 4.13. Hydrogen bonding interactions in complex **9**

| D–H···A | D–H (Å) | H···A (Å) | D···A (Å) | D–H···A (°) |
|--|---------|-----------|-----------|-------------|
| Intermolecular hydrogen bonding | | | | |
| C(12)–H(12B)···Cl(1) ^a | 0.96 | 2.77 | 3.294(2) | 115 |

Equivalent position code: a = 2-x, -1/2+y, 3/2-z

Although no classic hydrogen bonds are present in the system, weak forces like C–H··· π interactions enable the process of self-assembly and a supramolecular 2D architecture is built along ‘ac’ plane [Fig. 4.17, Table 4.14].

**Fig. 4.17.** C–H··· π interactions observed in complex **9**.**Table 4.14.** X–H···Cg interactions

| C–H(I)···Cg(J) | H···Cg (Å) | C···Cg (Å) | C–H···Cg (°) |
|---------------------------------|------------|------------|--------------|
| C(9)–H(9A)···Cg(3) ^b | 2.97 | 3.861(2) | 153 |

Equivalent position code: b = 1 - x, -y, 1 - z

Cg, centroid

Cg(3) = C(1), C(2), C(3), C(4), C(5), C(6)

Cg(J) = Center of gravity of ring J (Plane number above)

C–H···Cg = C–H···Cg angle (°)

C···Cg = Distance of C to Cg (Å)

H···Cg = Distance of H to Cg (Å)

The angles around the central metal atom summate to 357.45° . Significant difference in the *trans* basal angles [$172.41(6)/156.95(7)^\circ$] consistent with a greater value of τ , the deviation of metal atom from the basal square plane and the summation value of bite angles around the central metal (357.45°) are all conclusive of the distortion from the regular square pyramidal geometry.

Non-linear pseudohalide makes a longer bridge compared to azide which is evident from the metal-metal separation of $7.8840(4) \text{ \AA}$ [21]. The Cu(II) atoms are linked by $\text{N}(\text{CN})_2^-$ anions leading to infinite *meso* helical chains along '*b*' axis. Similar to helix, several 1D *meso*-helix coordination polymers have been characterized [22]. As shown in Fig. 4.18, a *meso*-helix is a 3D presentation of a lemniscate.

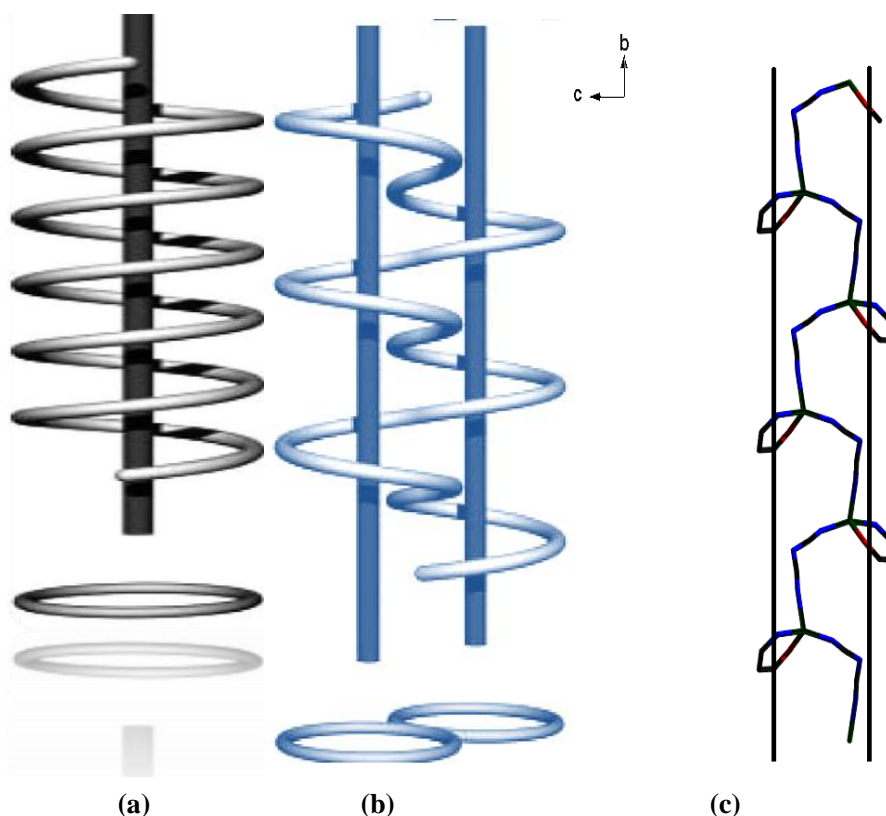


Fig. 4.18. Generation of a) helix b) *meso*-helix c) Infinite *meso* helical chains of complex **9** along '*b*' axis.

4.3.2.5. $[\text{Cu}(\text{L}^4)(\text{N}_3)]_2$ (**10**)

An ORTEP diagram of the compound along with atom numbering scheme is given in Fig. 4.19. Crystallographic details are summarized in Table 4.7. Bond dimensions are collated in Table 4.15. The structural study reveals the compound to be a centrosymmetric dimer in which the copper centres enjoy a pentacoordinated environment, being bonded to NNO tridentate Schiff base and two coordinating azido anions. Each azido ion bridges in an *end-on* fashion and this leads to relatively smaller Cu...Cu distance of 3.198(5) Å. The metalloplane (Cu_2N_2) formed due to di- $\mu_{1,1}$ -azido bridging results in a parallelogram with angle summation of 360° and two different Cu–N edge lengths of 2.302(3) and 2.044(1) Å respectively. The pseudohalide is asymmetric (basal-apical) with respect to its bonding lengths and deviate from linearity with N–N–N angle of $167.9(12)^\circ$.

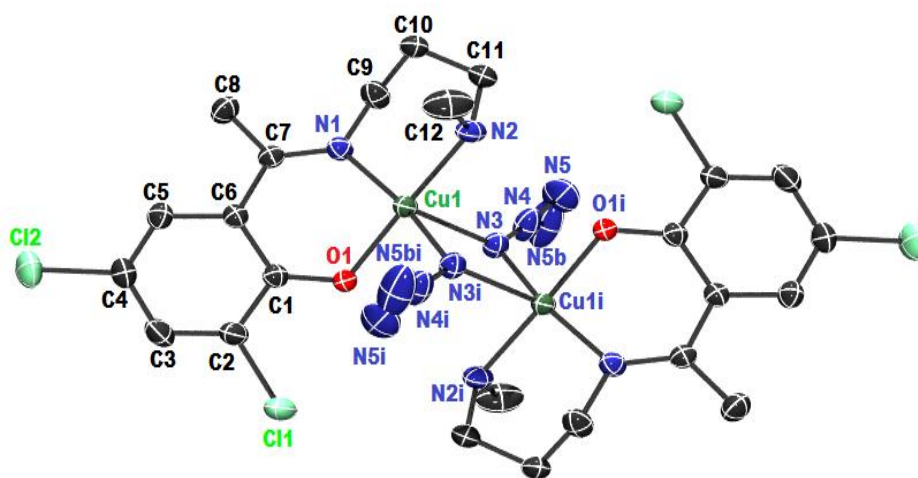


Fig. 4.19. ORTEP diagram along with atom numbering scheme of the dimeric complex **10** (thermal ellipsoid drawn with 30% probability, terminal nitrogen atoms of azido group are disordered).

Table 4.15. Selected bond lengths (Å) and bond angles (°) of complex **10**

| Bond lengths (Å) | | Bond angles (°) | |
|------------------|----------|-------------------|------------|
| Cu(1)–O(1) | 1.917(1) | O(1)–Cu(1)–N(1) | 88.43(8) |
| Cu(1)–N(1) | 1.986(2) | N(1)–Cu(1)–N(2) | 95.94(10) |
| Cu(1)–N(2) | 2.022(2) | N(2)–Cu(1)–N(3) | 90.85(9) |
| Cu(1)–N(3) | 2.302(3) | N(3)–Cu(1)–N(3a) | 85.41(9) |
| Cu(1)–N(3a) | 2.044(1) | N(3)–Cu(1)–O(1) | 91.04(9) |
| C(1)–O(1) | 1.302(3) | O(1)–Cu(1)–N(2) | 174.32(9) |
| N(3)–N(4) | 1.167(4) | N(1)–Cu(1)–N(3) | 110.15(9) |
| N(4)–N(5) | 1.17(2) | N(1)–Cu(1)–N(3a) | 164.17(10) |
| N(4)–N(5b) | 1.19(5) | N(3)–Cu(1)–O(1) | 91.04(9) |
| C(2)–Cl(1) | 1.729(3) | N(3)–N(4)–N(5) | 167.9(12) |
| C(4)–Cl(2) | 1.742(3) | Cu(1)–N(3)–Cu(1a) | 94.59(9) |
| | | N(3)–N(4)–N(5b) | 155(4) |
| | | N(2)–Cu(1)–N(3a) | 86.42(9) |
| | | N(3a)–Cu(1)–O(1) | 88.40(8) |

The geometry around the copper centre can be described as trigonally distorted square pyramid [23] with the basal plane occupied by the tricoordinating entities of the Schiff base and the nitrogen atom of one of the bridging azide whereas the apical position is decked with the nitrogen of the centrosymmetrically related azide ion. Computation of Addison parameter, an index of trigonality has a value 0.17, highlighting the distortion of the coordination polyhedron from square pyramid towards trigonality. The least squares plane calculation reveals that the metal deviates below the plane by a distance of 0.0411 Å towards apical nitrogen atom. Two hexametallo cycles with bite angles of 88.40(8)° [N1–Cu1–O1] and 95.94(10)° [N1–Cu1–N2] are formed as a result of coordination. The chelate bite angles around the central metal in the basal plane summates to a value of 359.19°.

The six membered metallo cycle Cg(2) [Cu1/O1/C1/C6/C7/N1] assumes half-chair conformation with puckering parameters $Q(2) = 0.526(2)$ Å, $\Phi(2) = 15.8(3)^\circ$, $Q(3) = 0.229(2)$ Å, $Q = 0.5737(19)$ Å and $\theta = 66.5(2)^\circ$. Inter-dimeric hydrogen bonding interaction between the hydrogen atom, H(8C) borne on C(8) with the oxygen atom, O(1) of adjacent entity forms a box-like structure with $R_2^2(8)$ motif [Fig. 4.20, Table 4.16].

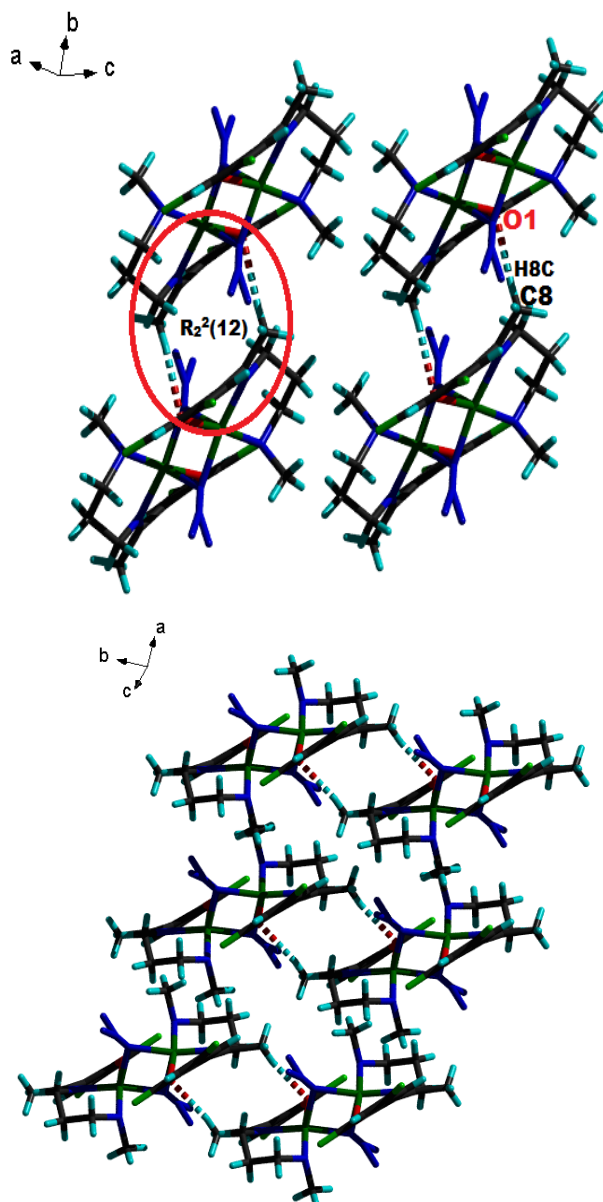


Fig. 4.20. Inter-dimeric hydrogen bonding interaction in complex **10**, formation of box-like structure.

Table 4.16. Hydrogen bonding interactions in the complex **10**

| D–H···A | D–H (Å) | H···A (Å) | D···A (Å) | D–H···A (°) |
|--|---------|-----------|-----------|-------------|
| Intermolecular hydrogen bonding | | | | |
| C(12)–H(8C)···O(1) ^a | 0.96 | 2.42 | 3.346(4) | 163 |

Equivalent position code: a = 1 - x, 1 - y, -z

The planes consisting of the donor atoms of the Schiff base and the copper atom on either side of the dimeric box are parallel to each other whilst the same plane is almost orthogonal [89.74(7)°] to the dimeric plane [N3/Cu1/N3/Cu1a].

4.3.3. Optical emissive response

The photoluminescence behavior of the five complexes which differ only in the coordinated anion were examined in acetonitrile medium. On excitation at 330 nm, the complexes were found to emit in the violet region of the spectrum (431 nm) [Fig. 4.21].

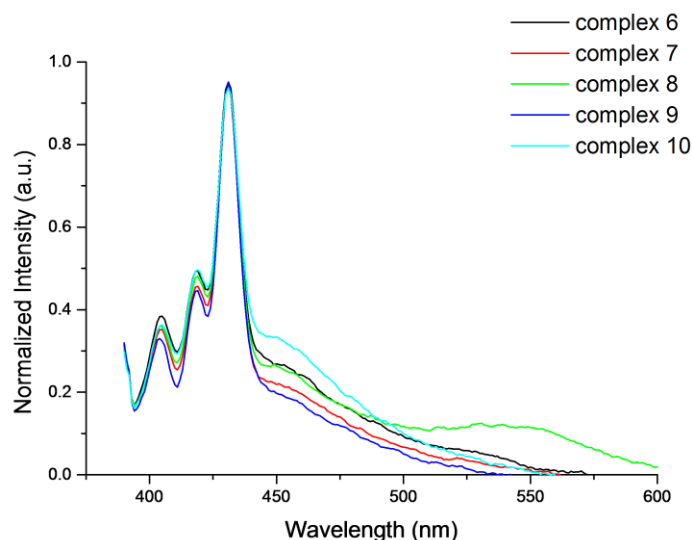


Fig. 4.21. Merged fluorescence spectra of the complexes (acetonitrile, con: 1×10^{-3} M).

The quantum yield values of the complexes were calculated [Table 4.17] and found that all our complexes have low quantum yield with the azido polymer (**6**) having the highest of the lot.

Table 4.17. The quantum yield values of the complexes

| Samples | Quantum yield |
|---|---------------|
| [Cu(L)(N ₃) _n] (6) | 0.0625 |
| [Cu(L)(NCS)] (7) | 0.0081 |
| [Cu(L)(NCO)] (8) | 0.0287 |
| [Cu(L)[N(CN) ₂] _n] (9) | 0.0214 |
| [Cu(L)(N ₃) ₂] (10) | 0.0447 |

4.3.4. Thermal studies

The thermal behaviors of complexes were characterized in N₂ atmosphere using thermogravimetric analysis (TG), differential thermogravimetric analysis (DTG) and differential scanning calorimetry (DSC). The thermal decomposition profile for all the complexes are almost similar. The change in mass, over a range of 214 - 243 °C estimated from the TG curve for the azido complex (31.65%, calcd. 32.65%) corresponds to the loss of amine followed by chloride ion as HCl [Fig. 4.22]. The DSC curve records this as an endothermic process. Beyond this major loss, there is a gradual thermal decomposition. For the monomeric thiocyanato complex, the amine and the pseudohalide is released in the temperature 200-315 °C range, fitting to a mass loss of 37.14% (calcd. 34.018%) and is an endothermic process as seen in DSC. Thereafter, a gradual decomposition leading to the formation of a stable metal oxide is inferred from the TG graph [Fig. 4.22].

For the cyanato complex **8**, the endothermic decomposition profile is consistent with the loss of chloride in the 220-260 °C temperature with a mass loss of 21.4% (calcd. 19.87%). The dicyanamido complex shows a single stage exothermic decomposition pattern (215-335 °C) with the TG curve agreeing to a weight loss of N₂ and chloride ion as HCl (15.62%, calcd. 15.85%). Subsequently, a gradual decomposition pattern is observed. The dimeric azido complex is marked with a single stage loss consistent with the elimination of a chloride molecule and four ammonia molecules in the 190-215 °C range (16.83%, calcd. 18.21%). The DSC curve records this as endothermic phenomenon and the TG plot deduces the generation of a final stable metal oxide species. Thermal plots are given in Fig. 4.22.

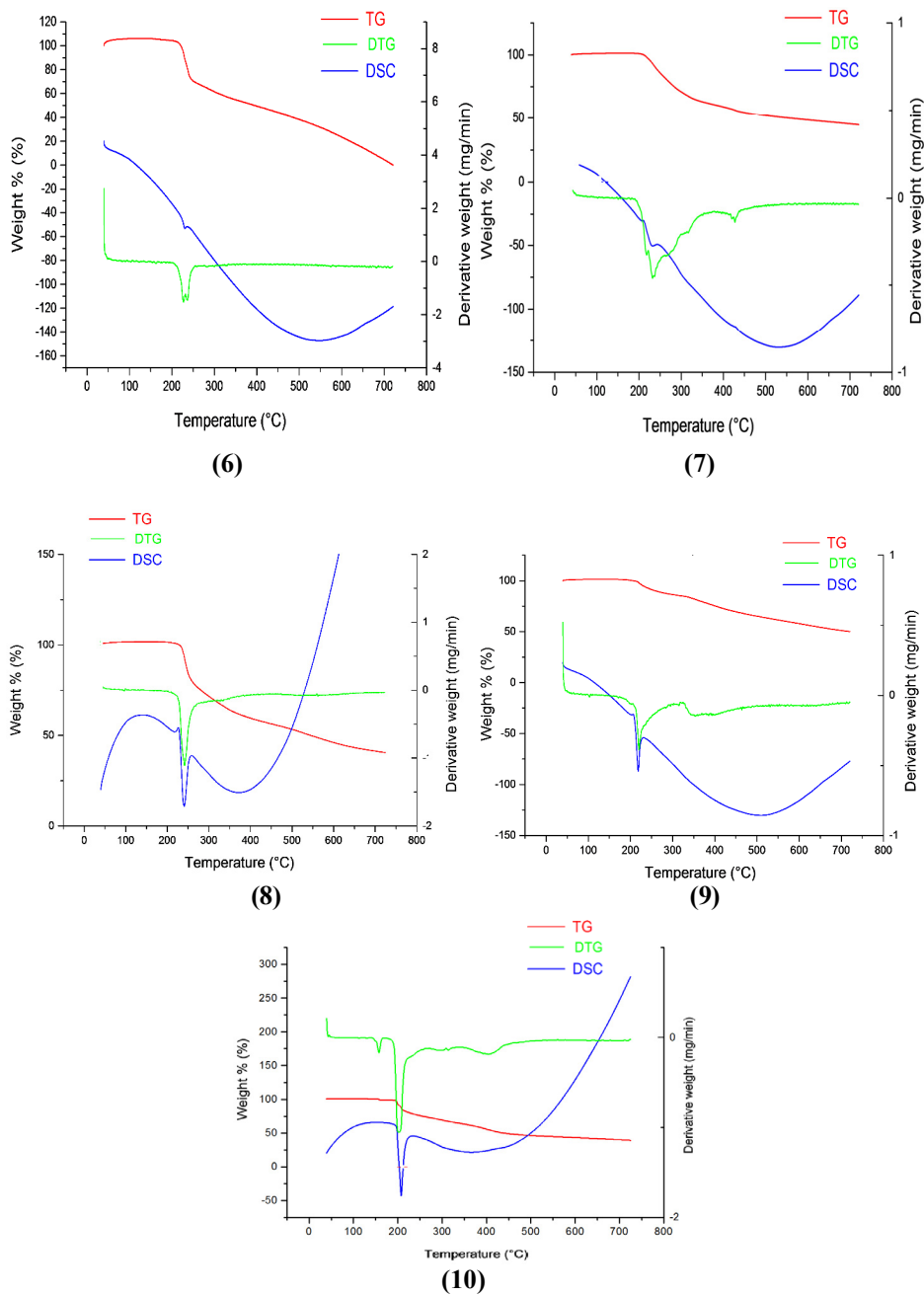


Fig. 4.22. Thermogram of the complexes

4.3.5. EPR studies

The EPR spectra of the polymeric species **6** and **9**, in the polycrystalline phase at 298 K shows typical axial spectra [Fig. 4.23a], characterized by g tensor values holding the relation, $g_{\parallel} > g_{\perp} > g_e$. This powder state spectra reveals a magnetically diluted phase due to the appearance of hyperfine splittings which are not so well resolved. Three of the four hyperfine splittings of Cu(II) ion in complex **9** is seen while the fourth one overlaps with the perpendicular region. The azido complex has splittings only in the parallel region [$A_{\parallel} = 197 \cdot 10^{-4} \text{ cm}^{-1}$], whilst the dicyamido species has them in both the regions [$A_{\parallel} = 197 \cdot 10^{-4} \text{ cm}^{-1}$, $A_{\perp} = 21 \cdot 10^{-4} \text{ cm}^{-1}$].

The g values are correlated to the exchange interaction coupling constant (G) by the expression,

$$G = (g_{\parallel} - 2.0023) / (g_{\perp} - 2.0023) \quad [24]$$

and its value is a measure of the exchange interaction between Cu(II) centers in the solid polycrystalline complexes.

The G values for complexes **6** and **9** are less than 4 indicating the presence of considerable exchange interaction which in turn underscores the covalency in metal-ligand bonding. More insight into the geometry and nature of bonding is gained by recording the spectra in frozen DMF at 77 K.

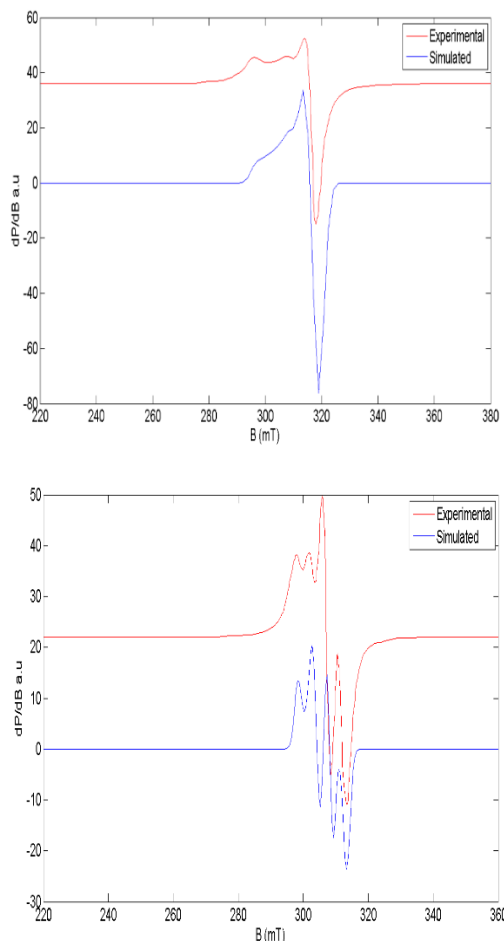


Fig. 4.23a. EPR spectra of complex **6** (top) and **9** (bottom) in polycrystalline state.

Well defined axial spectra [$(g_{\parallel} = 2.217, g_{\perp} = 2.054)$ and $(g_{\parallel} = 2.223, g_{\perp} = 2.046)$] with hyperfine splittings due to the interaction of odd electron with the nuclear spin ($^{63,65}\text{Cu}, I = 3/2$) are seen in parallel and perpendicular regions of complexes **6** and **9** respectively. The g tensor values with $g_{\parallel} > g_{\perp} > g_e$ (2.0023), for the complexes even at frozen state confirms the presence of $d_{x^2-y^2}$ ground state located in a square-based environment. Generally, a square-based CuN_4 chromophore is expected to show a g_{\parallel} value of 2.200 and A_{\parallel} value of $200 \cdot 10^{-4} \text{ cm}^{-1}$ and a distortion from square planar coordination geometry or

axial interaction would increase the g_{\parallel} value and decrease the A_{\parallel} value [25]. Our complexes **6** and **9** have CuN_3O chromophore with g_{\parallel} values (2.217, 2.054) and A_{\parallel} values ($197 \times 10^{-4} \text{ cm}^{-1}$ for both) suggesting a strong axial interaction and a considerable deviation from basal plane [Fig. 4.23b].

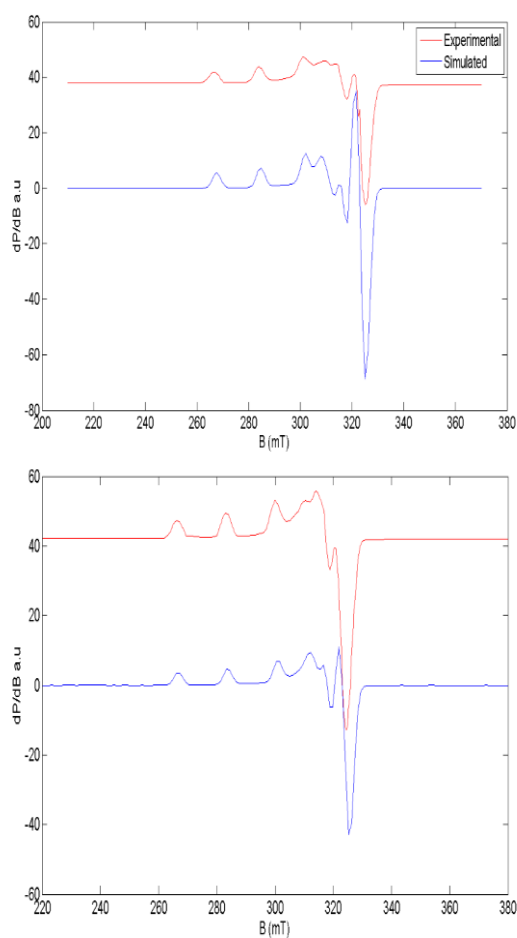


Fig. 4.23b. EPR spectra of complex **6** (top) and **9** (bottom) in DMF at 77 K.

The polycrystalline spectra of complexes **7** and **8** display features corresponding to axial and rhombic type respectively. The axial spectra has $g_{\parallel} = 2.115$ and $g_{\perp} = 2.069$ whereas complex **8** has three g values – $g_x = 2.034$,

$g_y = 2.059$ and $g_z = 2.230$. The G value is abnormally small for thiocyanate complex while it is greater than 4 for cyanato complex indicating the absence of exchange interaction [Fig. 4.23c].

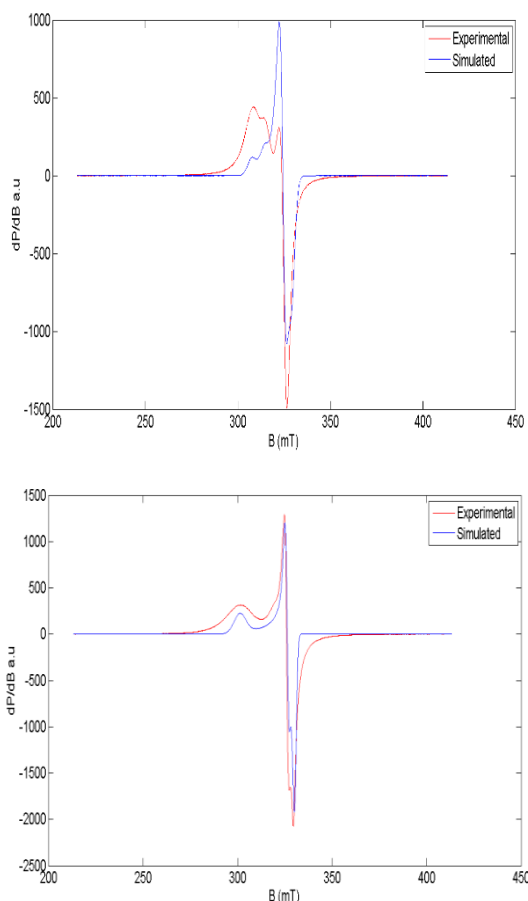


Fig. 4.23c. EPR spectra of complex **7** (top) and **8** (bottom) in polycrystalline state.

The frozen state spectra were recorded for the same complexes at 77 K. Complex **7** maintains its axial nature but with much more resolved hyperfine splittings in the parallel region [$g_{\parallel} = 2.227$, $g_{\perp} = 2.055$, $A_{\parallel} = 209 \cdot 10^{-4} \text{ cm}^{-1}$]. The high intense field region is barely resolved. Similar hyperfine splittings in the parallel region are observed for complex **8** also. The square planar geometry

of both the complexes is confirmed from the g values confirming the presence of $d_{x^2-y^2}$ ground state [Fig. 4.23d].

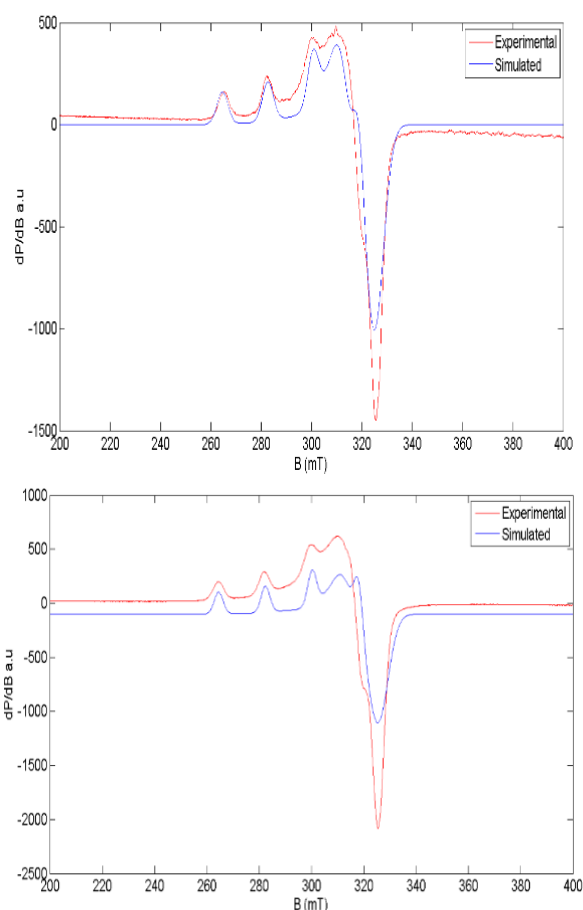


Fig. 4.23d. EPR spectra of complex **7** (top) and **8** (bottom) in DMF at 77 K.

Complex **10** displays axial features in its polycrystalline state with $g_{\parallel} = 2.175$, $g_{\perp} = 2.057$ while the same complex in its frozen state shows well resolved hyperfine splittings in the parallel region with $g_{\parallel} = 2.230$ and $g_{\perp} = 2.054$. The resolution is but not observed in the perpendicular region of the spectrum [Fig. 4.23e].

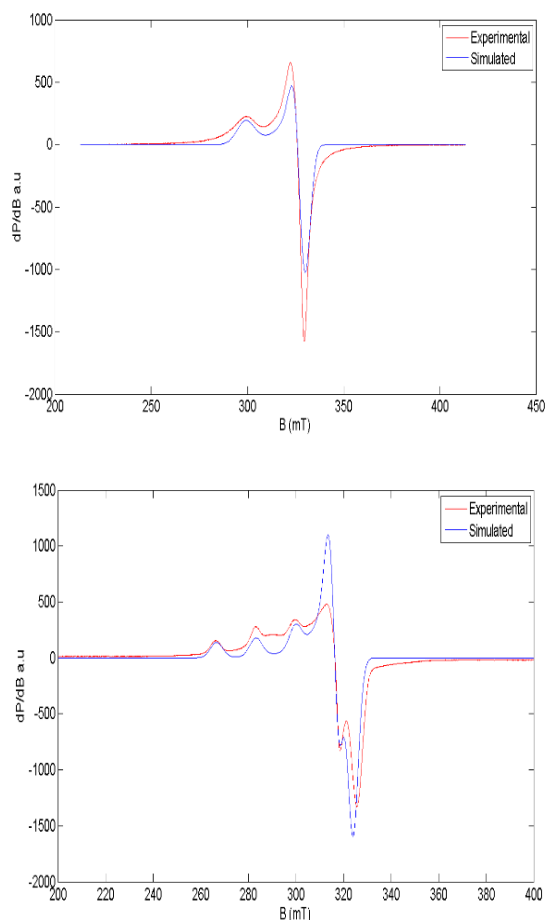


Fig. 4.23e. EPR spectra of complex (10) in polycrystalline state (top) and in DMF at 77 K (bottom).

The EPR parameters like g_{\parallel} and A_{\parallel} varies according to the interaction of the orbitals of the equatorially coordinated atoms with the $d_{x^2-y^2}$ orbital of Cu(II) ion and the axially coordinated ones least affect it [26]. Almost similar values of g_{\parallel} and A_{\parallel} indicates the similar coordinating moiety around the central metal ion. The nature of metal-ligand bond – whether ionic/covalent can be assessed from the g_{\parallel} values [27] [$g_{\parallel} \geq 2.3$ for ionic, $g_{\parallel} < 2.3$ for covalent]. For our complexes, the values are indicative of significant metal-ligand covalency [28]. The index of tetragonal distortion, f is calculated as $f = g_{\parallel}/A_{\parallel}$, whose

value may vary from 105-135 for small to medium distortion and depends on the nature of the coordinated atom [29]. In all complexes distortion is medium and is found to be in the range 105-115 cm [30].

The bonding parameters α^2 , β^2 and γ^2 , considered to be the measure of the covalency of in-plane σ -bonds, in-plane π -bonds and out-of-plane π -bonds respectively and are evaluated using the EPR parameters g_{\parallel} , g_{\perp} , g_{av} , A_{\parallel} (Cu) and A_{\perp} (Cu) along with the energies of $d-d$ transition.

The value of in-plane sigma bonding parameter α^2 was estimated from the expression [31]

$$\alpha^2 = -A_{\parallel} / 0.036 + (g_{\parallel} - 2.0023) + 3/7 (g_{\perp} - 2.0023) + 0.04$$

The following simplified expressions were used to calculate the bonding parameters

$$K_{\parallel}^2 = (g_{\parallel} - 2.0023) E_{d-d} / 8\lambda_0$$

$$K_{\perp}^2 = (g_{\perp} - 2.0023) E_{d-d} / 2\lambda_0$$

$$K_{\parallel}^2 = \alpha^2 \beta^2$$

$$K_{\perp}^2 = \alpha^2 \gamma^2$$

Where K_{\parallel} and K_{\perp} are orbital reduction factors and λ_0 represents the one electron spin orbit coupling constant which equals -828 cm^{-1} .

Hathaway [32] has pointed out that for pure sigma bonding $K_{\parallel} \approx K_{\perp} \approx 0.77$, for in plane π -bonding $K_{\parallel} < K_{\perp}$ and for out-of-plane π -bonding, $K_{\perp} < K_{\parallel}$. For all the complexes, it is observed that $K_{\parallel} > K_{\perp}$ which indicates the presence of significant out-of-plane π -bonding. The nature of metal-ligand bond is further evaluated by comparing the value of in-plane sigma bonding parameter α^2 [$\alpha^2 = 1$, for purely ionic, $\alpha^2 = 0.5$, for covalent] [33]. Here α^2 values calculated for all the complexes lie in between 0.5 and 1, implying partially ionic and partially covalent nature of M-L bonds under study.

Table 4.18. Spin Hamiltonian and bonding parameters of copper(II) complexes

| Compounds | Polycrystalline state (298 K) | | | | | | | DMF solution (77 K) | | | | | | | |
|-----------|-------------------------------|-------------|--------|--------------------|---------------------|----------|-----------------|---------------------|----------|------------|-----------|------------|-----------------|-------------|-----|
| | g_{\parallel} | g_{\perp} | G | $g_{\parallel}g_3$ | $g_{\perp}g_1, g_2$ | g_{av} | A_{\parallel} | A_{\perp} | A_{av} | α^2 | β^2 | γ^2 | K_{\parallel} | K_{\perp} | f |
| 6 | 2.150 | 2.048 | 3.2319 | 2.217 | 2.054 | 2.108 | 197 | -- | -- | 0.8226 | 0.9143 | 0.9008 | 0.7521 | 0.7410 | 113 |
| 7 | 2.115 | 2.069 | 1.6897 | 2.227 | 2.055 | 2.112 | 209 | -- | -- | 0.8671 | 0.8686 | 0.8413 | 0.7532 | 0.7295 | 107 |
| 8 | 2.034, 2.059 | 2.230 | 5.1342 | 2.229 | 2.047 | 2.107 | 208 | -- | -- | 0.8619 | 0.8755 | 0.7776 | 0.7546 | 0.6702 | 107 |
| 9 | 2.126 | 2.119 | 1.0600 | 2.223 | 2.046 | 2.105 | 197 | 21 | 80 | 0.8265 | 0.9308 | 0.8283 | 0.7693 | 0.6846 | 113 |
| 10 | 2.175 | 2.057 | 3.1572 | 2.230 | 2.054 | 2.112 | 192 | -- | -- | 0.8213 | 0.8952 | 0.8550 | 0.7352 | 0.7006 | 116 |

A values in 10^{-4} cm^{-1}

References

- [1] M. Das, S. Chattopadhyay, *Transit. Met. Chem.* **2013**, 38, 191.
- [2] S. Sasi, M. Sithambaresan, M.R.P. Kurup, H-K. Fun, *Polyhedron* **2010**, 29, 2643.
- [3] X. Lin, Y. Sang, W. Xiao, *J. Chem. Crystallogr.* **2012**, 42, 578.
- [4] P. Bhowmik, A. Bhattacharyya, K. Harms, S. Sproules, S. Chattopadhyay, *Polyhedron* **2015**, 85, 221.
- [5] A. Ray, G. Pilet, C.J. Gomez-Garcia, S. Mitra, *Polyhedron* **2009**, 28, 511.
- [6] A.B.P. Lever, E. Mantovani, B.S. Ramaswami, *Can. J. Chem.* **1971**, 49, 1957.
- [7] T.A. Reena, E.B. Seenaa, M.R.P. Kurup, *Polyhedron* **2008**, 27, 1825.
- [8] B. Shaabani, A.A. Khandar, M. Dusek, M. Pojarova, F. Mahmoudi, *Inorg. Chim. Acta* **2013**, 394, 563.
- [9] a) S. Biswas, A. Ghosh, *Polyhedron* **2013**, 65, 322.
b) R. Gup, B. Kirkan, *Spectrochim. Acta A* **2005**, 62, 1188.
- [10] S. Naiya, C. Biswas, M.G.B. Drew, C.J. Gomez-García, J.M. Clemente-Juan, A. Ghosh, *Inorg. Chem.* **2010**, 49, 6616.
- [11] C. Reichardt, *Chem. Rev.* **1994**, 94, 2319.
- [12] M. Jiang, Y. Li, Z. Wu, Z. Yin, *J. Coord. Chem.* **2009**, 62, 380.
- [13] K. Sone, Y. Fukuda, *Inorganic Thermochemistry in Inorganic Chemistry Concepts* Vol. 10, Springer-Verlag, Berlin, **1987**, 72.
- [14] P. Muller, R. Herbst-Irmer, A.L. Spek, T.R. Schneider, M.R. Sawaya, *Crystal Structure Refinement*, Oxford Science Publications, **2012**.
- [15] A.W. Addison, T.N. Rao, J. Reedijk, J. Van Rijn, G.C. Verschoor, *J. Chem. Soc., Dalton Trans.* **1984**, 1349.
- [16] N. Aiswarya, M. Sithambaresan, S.S. Sreejith, S.W. Ng, M.R.P. Kurup, *Inorg. Chim. Acta* **2016**, 443, 251.

- [17] S.T. Rao, E. Westhof, M. Sundaralingam, *Acta Crystallogr., Sect. A: Struct. Rep. Online* **1981**, 37, 421.
- [18] P.K. Bhaumik, K. Harms, S. Chattopadhyay, *Inorg. Chim. Acta* **2013**, 405, 400.
- [19] D. Cremer, J.A. Pople, *J. Am. Chem. Soc.* **1975**, 97, 1354.
- [20] S.S. Massoud, M.M. Lemieux, Lucie Le Quan, Ramon Vicente, J.H. Albering, F.A. Mautner, *Inorg. Chim. Acta* **2012**, 388, 71.
- [21] Y.M. Chow, *Inorg. Chem.* **1971**, 10, 1938.
- [22] (a) L. Plasseraud, H. Maid, F. Hample, R.W. Saalfrank, *Chem. Eur. J.* **2001**, 7, 4007.
(b) G. Becker, B. Eschbach, O. Mundt, N. Seidler, *Z. Anorg. Allg. Chem.* **1994**, 620, 1381. (c) R.A. Bartlett, M.M. Olmstead, P.P. Power, *Inorg. Chem.* **1986**, 25, 1243.
- [23] M.S. Ray, A. Ghosh, R. Bhattacharya, G. Mukhopadhyay, M.G.B. Drew, J. Ribas, *Dalton Trans.* **2004**, 252.
- [24] S. Stoll, *Spectral Simulations in Solid-State Electron Paramagnetic Resonance*, Ph.D. thesis, ETH, Zurich, **2003**.
- [25] I.M. Procter, B.J. Hathaway, P. Nicholis, *J. Chem. Soc. A* **1968**, 1678.
- [26] M. Palaniandavar, I. Somasundaram, M. Lakshminarayanan, H. Manohar, *Dalton Trans.* **1996**, 1333.
- [27] J. Peisach, W.E. Blumberg, *Arch. Biochem. Biophys.* **1974**, 165, 691.
- [28] T.D. Smith, J. Pilbrow, *Coord. Chem. Rev.* **1974**, 13, 173.
- [29] D. Kivelson, R. Neiman, *J. Chem. Phys.* **1961**, 35, 149.
- [30] L. Latheef, M.R.P Kurup, *Spectrochim. Acta A* **2008**, 70, 86.
- [31] R.P. John, A. Sreekanth, V. Rajakannan, T.A. Ajith, M.R.P. Kurup, *Polyhedron* **2004**, 23, 2549.

- [32] B.N. Figgis, *Introduction to Ligand fields*, Interscience, New York, **1996**, 295.
- [33] B.J. Hathaway, in: G. Wilkinson, R.D. Gillard, J.A. McCleverty (Eds.), *Comprehensive Coordination Chemistry*, Vol. 5, Pergamon, Oxford, **1987**, p. 533.

.....✂.....

Chapter 5

Complexes derived from *N,N*-dimethylethylenediamine and mono halosubstituted carbonyl compounds

| | |
|--------------------------------------|-----------------------------|
| C o n t e n t s | 5.1. Introduction |
| | Section A |
| | 5.2. Experimental |
| | 5.3. Results and discussion |
| | Section B |
| | 5.4. Experimental |
| | 5.5. Results and discussion |
| | Section C |
| | 5.6. Experimental |
| | 5.7. Results and discussion |

Conspectus

*Unlike the previous chapters, here we have employed Schiff bases derived from monohalo (chloro, bromo and fluoro) substituted carbonyl compounds and *N,N*-dimethylethylenediamine as blocking ligands. We have isolated a total of seven crystals from this system. We witness the development of monomers into supramolecular structures due to the presence of non-covalent forces. The halogen atoms satisfy their electrophilicity by getting involved in various weak interactions. Also, the ambidenticity of pseudohalides like azide and thiocyanate is unveiled. Three monomers and four polymers are obtained. All preliminary characterization studies along with spectroscopic and solvatochromic studies are carried out.*

5.1. Introduction

The chapter is divided into three sections on the basis of the halosubstituted carbonyl compounds that we have used for the synthesis of the Schiff base system.

In section A, we have discussed three complexes derived from 5-chlorosalicylaldehyde and *N,N*-dimethylethylenediamine. Two monomers and a single polymer are isolated. Although monomers in their asymmetric unit, presence of weak but stabilizing interactions sew the monomers into chains while the azido complex is a one dimensional coordination polymer. The studies associated are also dealt in detail.

Section B portrays the structural aspects and the studies of the single monomeric thiocyanato complex having 5-bromosalicylaldehyde in its skeletal ligand backbone.

The crystal structures and other spectroscopic studies of the complexes derived from fluoro substituted system are discussed in Section C. Here, two coordination polymers with the coligands in *end-to-end* bridging mode are isolated. Apart from this, an unusual stair-like polymer is also obtained.

Section A

5.2. Experimental

5.2.1. Materials

All chemicals used for synthesis were of Analar grade and used without further purification. The Schiff bases were formed *in situ*.

5.2.2. Synthetic protocol

5.2.2.1. Synthesis of [Cu(L⁵)(NCO)] (11) / [Cu(L⁵)(NCS)] (12)

[HL⁵ = 4-chloro-2-((2-(dimethylamino)ethylimino)methyl)phenol]

5-Chlorosalicylaldehyde (0.156 g, 1 mmol) and *N,N*-dimethylethylenediamine (0.088 g, 1 mmol) were dissolved in 10 mL methanol and refluxed for about an

hour. A methanolic solution (10 mL) of copper(II) nitrate trihydrate (0.241 g, 1 mmol) was added to this hot methanolic solution (10 mL) and stirred for 30 minutes. To the resulting deep green solution, sodium cyanate (0.130 g, 2 mmol) in a MeOH/H₂O (1:9) mixture was added dropwise and further stirred for *ca.* 2 h and filtered. Diffraction quality single crystals for structure determination were obtained by slow evaporation of this mother liquor in air. The thiocyanato complex was prepared by the aforesaid method except for the addition of potassium thiocyanate (0.194 g, 2 mmol).

Yield: 0.1655 g (50%). *Anal.* Calc. for C₁₂H₁₄ClCuN₃O₂: C, 43.51; H, 4.26; N, 12.69. Found C, 43.48; H, 4.24; N, 12.70 %.

Yield: 0.1908 g (55%). *Anal.* Calc. for C₁₂H₁₄ClCuN₃OS: C, 41.50; H, 4.06; N, 12.10. Found C, 41.49; H, 4.07; N, 12.11 %.

5.2.2.2. Synthesis of [Cu(L⁶)(N₃)]_n (13)

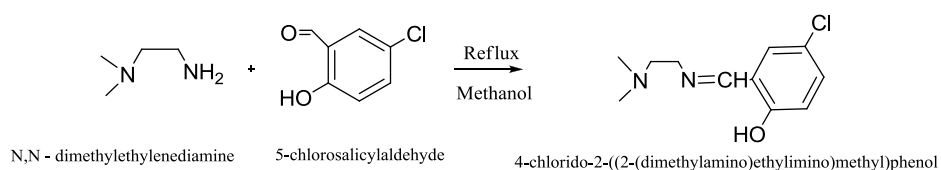
[HL⁶ = 4-chloro-2-(1-(2-(dimethylamino)ethylimino)ethyl)phenol]

A methanolic solution (10 mL) of copper(II) chloride dihydrate (0.170 g, 1 mmol) was added to the hot methanolic solution (10 mL) of the reaction mixture obtained by refluxing 5-chloro-2-hydroxyacetophenone (0.170 g, 1 mmol) and *N,N*-dimethylethylenediamine (0.088 g, 1 mmol). This solution was then stirred for 30 minutes. To the resulting deep green solution, sodium azide (0.130 g, 2 mmol) in a MeOH/H₂O (1:9) mixture was added dropwise and further stirred for *ca.* 2 h and filtered. Diffraction quality single crystals for structure determination were obtained by slow evaporation of this mother liquor in air.

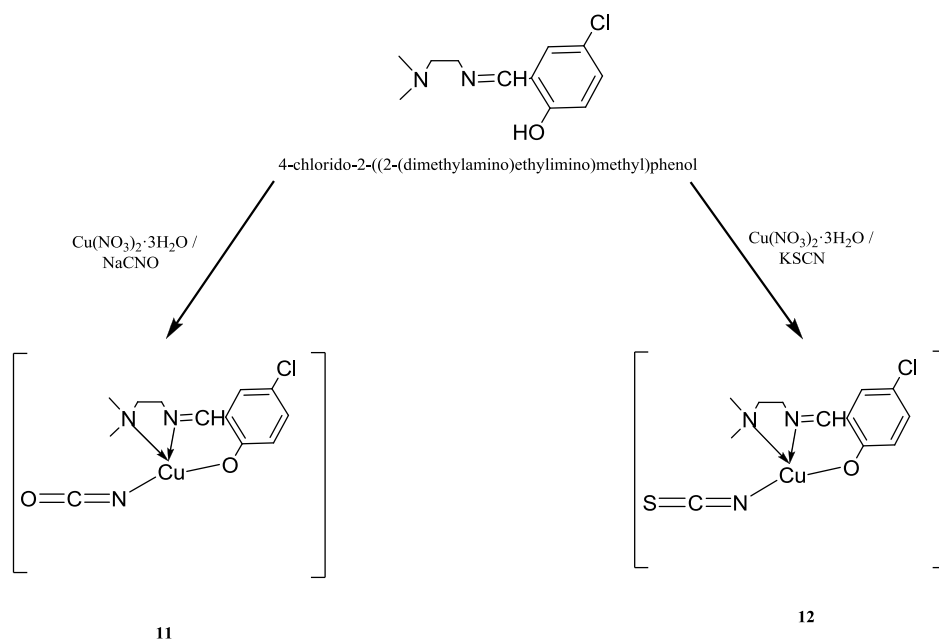
Yield: 0.2018 g (58.5%). *Anal.* Calc. for C₁₂H₁₆ClCuN₅O: C, 41.74; H, 4.67; N, 20.28. Found C, 41.72; H, 4.65; N, 20.25 %.

5.3. Results and discussion

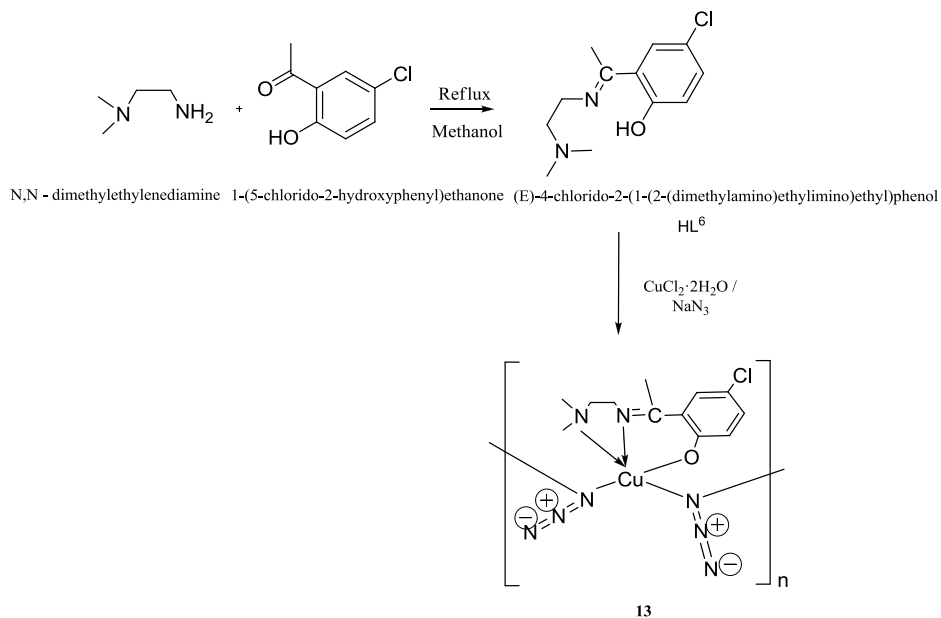
Schemes 5.1, 5.2 and 5.3 portrays the synthetic route to complexes using the template method for synthesis.

HL⁵

Scheme 5.1. Formation of the tridentate Schiff base system



Scheme 5.2. Synthetic route to complexes



Scheme 5.3. Synthetic route to complex **13**.

5.3.1. Spectroscopic features

5.3.1.1. IR and electronic spectroscopy

The sharp peaks in the range $1600 - 1635 \text{ cm}^{-1}$ assignable to azomethine C=N bond is customarily noticed for all the three complexes. Peaks at 2230 , 2010 and 2055 cm^{-1} are consistent with the presence of N coordinated cyanato, N coordinated thiocyanato and monodentate azido group respectively [1-3]. The bands in the $1300\text{-}1600 \text{ cm}^{-1}$ are not clearly attributable due to the appearance of several absorption bands from Schiff base ligands. The IR spectra of the complexes are shown in Fig. 5.1.

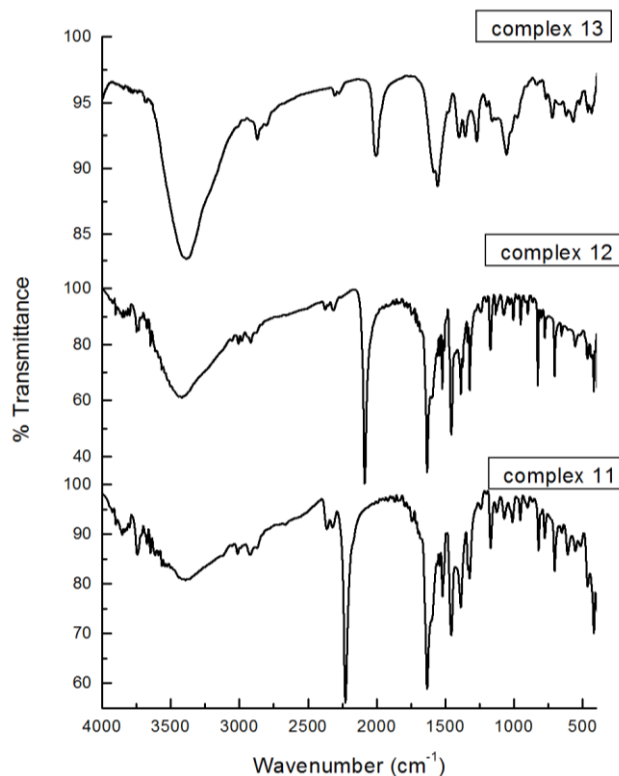


Fig. 5.1. IR spectra of the complexes **11**, **12** and **13**.

The electronic spectra of the complexes were recorded in acetonitrile medium in the range 200-900 nm. The charge transfer bands from Schiff base ligands to the metal ion is noticed at 383, 379 and 370 nm respectively. Also intraligand transitions at the high energy region are found in 220-230 nm. Well defined square planar geometry of the complexes **11** and **12** is additionally supported by the $d-d$ transition *ca.* 610-630 nm, corresponding to the transitions *viz.*, $d_{x^2-y^2} \rightarrow d_{xy}$, $d_{x^2-y^2} \rightarrow d_{z^2}$ and $d_{x^2-y^2} \rightarrow d_{xz}$, d_{yz} (${}^2B_{2g} \leftarrow {}^2B_{1g}$, ${}^2A_{1g} \leftarrow {}^2B_{1g}$ and ${}^2E_g \leftarrow {}^2B_{1g}$) [4]. Since the four d orbitals lie very close together, each transition cannot be distinguished by its energy and hence it is very difficult to resolve the three bands into separate components. The azido complex has a band around 590 nm, characteristic of a pentacoordinated square based geometry ($d_{x^2-y^2} \rightarrow d_{xz}$, d_{yz} , $d_{x^2-y^2} \rightarrow d_{z^2}$) [5,6].

5.3.1.2. Solvatochromic studies

With the aim to explore the dependency of electronic response on the solvents, we carried out solvatochromic studies of the complexes in seven chosen solvents which varied in their polarity. For charge-transfer transitions, a negative solvatochromic effect is seen within each classification of solvents which is an effect of greater stabilization of ground electronic state than the excited one. The λ_{max} (nm) along with their ϵ ($\text{M}^{-1}\text{cm}^{-1}$) values in various solvents are tabulated [Fig. 5.2, Table 5.1].

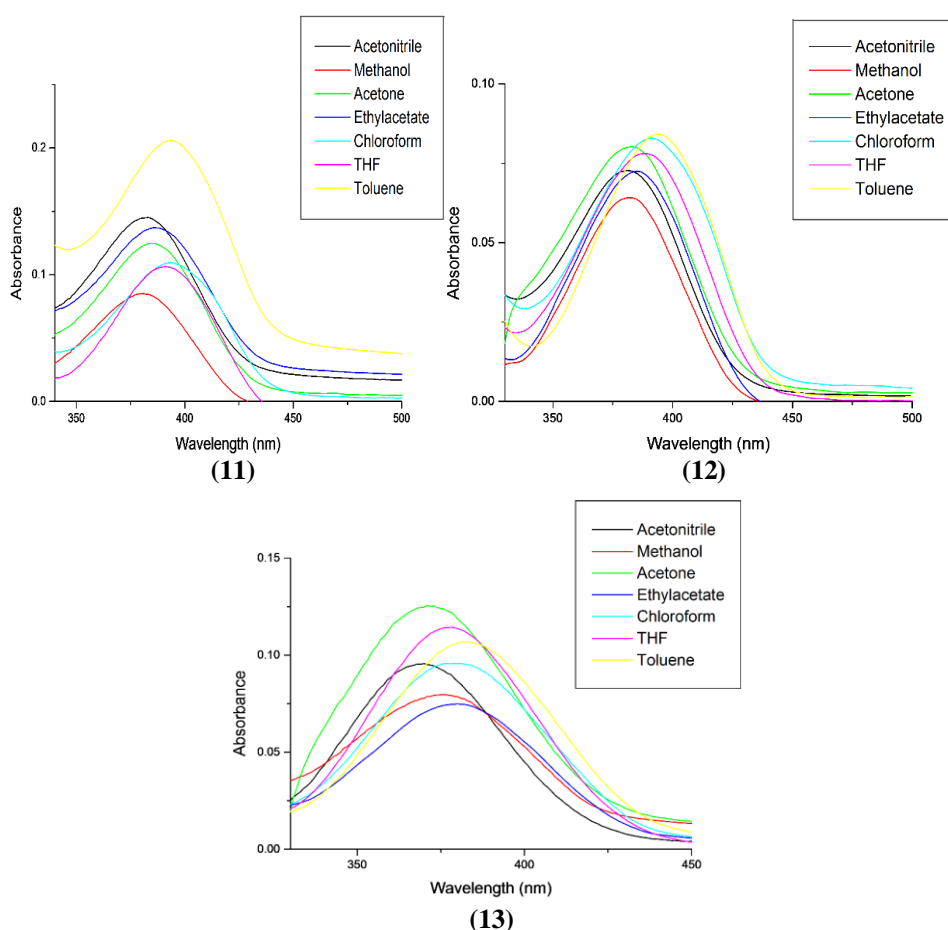


Fig. 5.2. Spectra showing the solvatochromic effect on the charge-transfer transitions of the complexes, con: $1 \cdot 10^{-3}$ M).

Table 5.1. The λ_{\max} (nm) values along with their ϵ ($M^{-1}cm^{-1}$) in various solvents

| Polarity Index* | Solvents | Complex 11 | | Complex 12 | | Complex 13 | |
|-----------------|-----------------|-----------------------|---------------------------------------|-----------------------|---------------------------------------|-----------------------|---------------------------------------|
| | | λ_{\max} (nm) | $\epsilon * 10^3$ ($M^{-1}cm^{-1}$) | λ_{\max} (nm) | $\epsilon * 10^3$ ($M^{-1}cm^{-1}$) | λ_{\max} (nm) | $\epsilon * 10^3$ ($M^{-1}cm^{-1}$) |
| 5.1 | Methanol | 381 | 4.27 | 384 | 4.96 | 376 | 3.730 |
| | | 227 | 29.36 | | | 234 | 21.23 |
| 5.8 | Acetonitrile | 383 | 7.28 | 379 | 5.68 | 370 | 4.48 |
| | | 229 | 39.01 | | | 236 | 18.95 |
| 5.1 | Acetone | 385 | 6.26 | 383 | 6.32 | 371 | 5.88 |
| 4.4 | Ethylacetate | 388 | 6.87 | 387 | 5.63 | 378 | 5.90 |
| 4.0 | Tetrahydrofuran | 391 | 5.34 | 389 | 6.04 | 378 | 5.35 |
| 4.1 | Chloroform | 394 | 5.48 | 390 | 6.49 | 380 | 4.48 |
| 2.4 | Toluene | 394 | 10.33 | 394 | 6.55 | 383 | 5.01 |

*Relative measure of degree of interaction of the solvents with various polar test solutes

Solvents apart from influencing the high intense CT and intraligand bands, also has its profound effect on the environment of the metal centre, which is mirrored as a change in the coordination polyhedra of the metal centre. Solvents like DMSO, MeOH, CH_3CN and DCM were chosen for the study based on the donor number variation. The $d-d$ bands showed significant shift as a function of donor power of solvents [Fig. 5.3, Table 5.2]. A red shift— an increase in λ_{\max} (nm) value with increase in donor power of solvent was observed.

A plausible explanation for the effect is explained below. In the case of square planar complexes, **11** and **12**, the axial positions are vacant in their solid structures. In solution, these positions are occupied by the solvent molecules, which solvate the chelate from above and below the plane [7]. Here, the equatorial ligand field strength of both the complexes remain the same and the axial field strength varies with solvents. The repulsion between the electron pair in d_{z^2} orbital and the axial ligands (solvents) impart instability to the energy state and hence the energy required to excite the electron to hole in $d_{x^2-y^2}$ decreases, leading to red shift. The aforementioned effect increases with the coordinating ability/donor power of the coexisting solvent species.

This implies that DCM has the least axial field strength and DMSO, the highest and therefore the resultant red shift. So, in effect the topology changes from square planar to a series of structures with various degrees of elongation from a regular octahedron, depending on the solvent species [7].

Similar explanation holds good for the azido linked polymeric species also. Here, the intervention of solvent species disrupts the polymeric chain into discrete species. The linear π conjugation present in the azido group makes them easily solvated and therefore are weaker ligands in solution. Hence we expect the solvent molecules to occupy the axial site by the replacement of the existing pseudohalide.

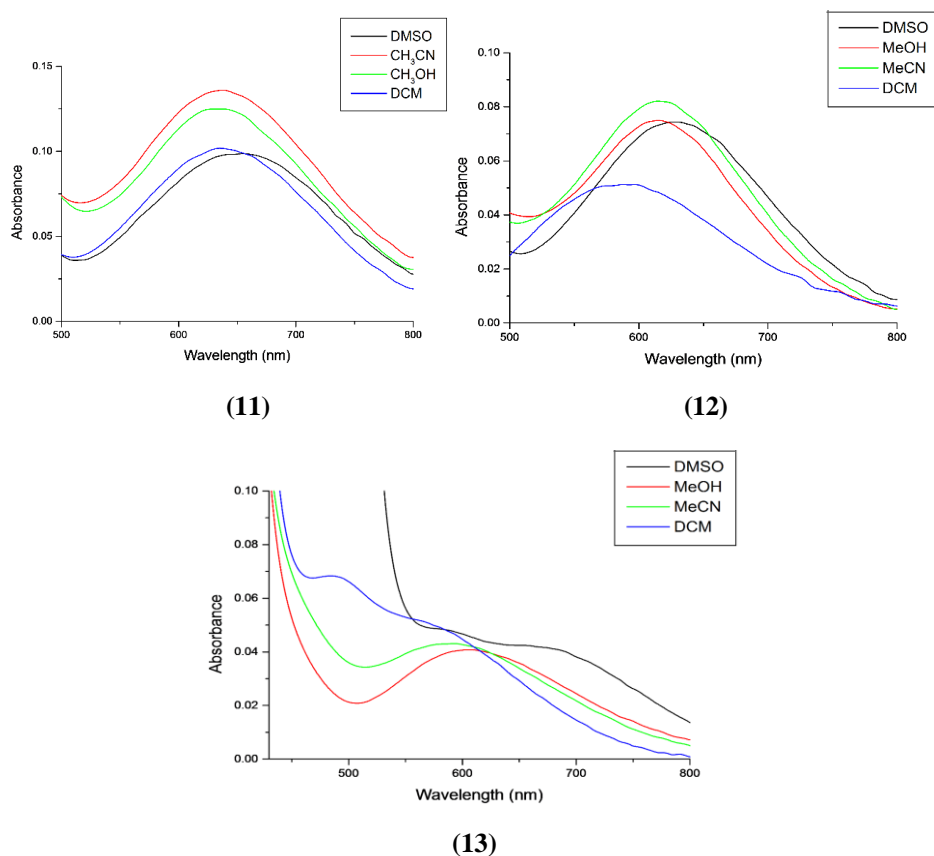


Fig. 5.3. The spectra showing solvatochromic behavior of *d-d* transitions (con: 2×10^{-3} M) of complexes in various solvents.

Table 5.2. The λ_{\max} (nm) values along with their ε ($M^{-1}cm^{-1}$) of *d-d* bands in various solvents

| Solvents | Donor number of solvents (DN) | Complex 11 | | Complex 12 | | Complex 13 | |
|--------------|-------------------------------|-----------------------|-----------------------------------|-----------------------|-----------------------------------|-----------------------|-----------------------------------|
| | | λ_{\max} (nm) | ε ($M^{-1}cm^{-1}$) | λ_{\max} (nm) | ε ($M^{-1}cm^{-1}$) | λ_{\max} (nm) | ε ($M^{-1}cm^{-1}$) |
| DMSO | 29.8 | 657 | 151 | 623 | 193 | 638 | 190 |
| Methanol | 19.0 | 640 | 211 | 616 | 283 | 607 | 174 |
| Acetonitrile | 14.1 | 638 | 190 | 614 | 254 | 595 | 220 |
| DCM | 0.0 | 634 | 156 | 584 | 144 | 487 | 364 |

5.3.2. X-ray crystallography and description of the structures

Single crystals of compounds [Cu(L⁵)(NCO)] (**11**), [Cu(L⁵)(NCS)] (**12**) and [Cu(L⁶(N₃)]_n (**13**) suitable for X-ray diffraction studies were grown from their methanol solutions by slow evaporation at room temperature.

All non-hydrogen atoms were refined anisotropically and all H atoms on C were placed in calculated positions guided by difference maps with C–H bond distances 0.93–0.97 Å. The H atoms were assigned as $U_{iso}=1.2U_{eq}$ (1.5 for Me). In the cyanato complex **11**, the atoms C1 and C2 were disordered about special position. The above atoms which were bound to one another was assumed to move in similar directions with approximately similar amplitudes and therefore they were restrained to have same U^{ij} components by the SIMU command. The similarity restraint SADI restrains the distance between N1–C1, N1–C2 and C1–C2 to be equal within a default standard uncertainty of 0.02 Å. Complex **12** possess a crystallographic mirror symmetry with all the atoms lying on a mirror plane and hence enjoys an occupancy factor of 0.50 (special position constraint). The atom C9 was disordered about special position and the sulfur atom was disordered over two sites with an occupancy of 36% and 64% respectively [8].

5.3.2.1. [Cu(L⁵)(NCO)] (11)

Complex **11** crystallizes in orthorhombic *Pnma* space group. The asymmetric unit is a monomeric square planar copper(II) complex as shown in the ORTEP diagram [Fig. 5.4].

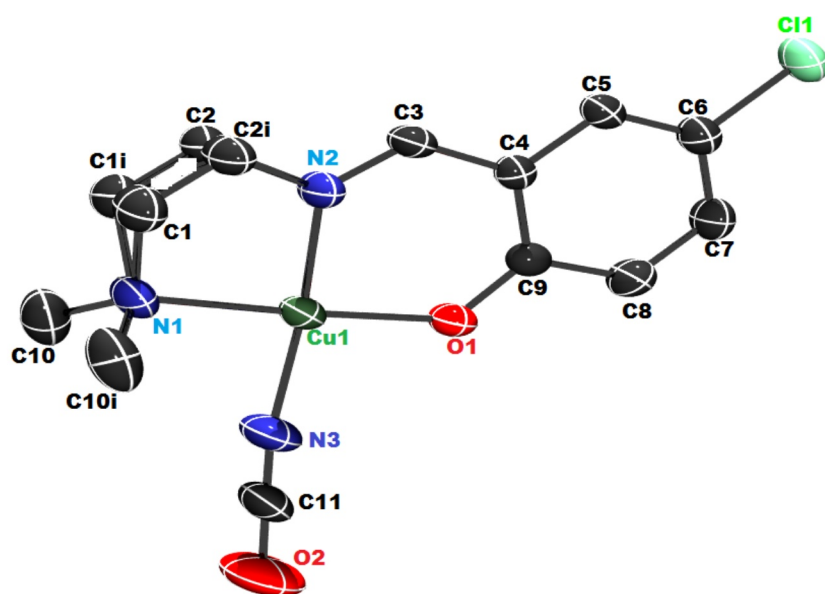


Fig. 5.4. ORTEP diagram showing the atom labelling of the asymmetric unit of the complex **11** (drawn with 30% ellipsoid probability and the hydrogen atoms are omitted for clarity).

Refinement details and selected bond dimensions are collated in Tables 5.3 and 5.4 respectively. The Cu(II) centre is tetracoordinated with the three coordination sites satisfied by the imine nitrogen (N2), amino nitrogen (N1) and phenoxy oxygen (O1) atom and fourth site occupied by the cyanato nitrogen (N3).

Table 5.3. Crystal data and refinement details of complex **11**

| Parameters | Complex 11 |
|-----------------------------------|--|
| Empirical formula | C ₁₂ H ₁₄ ClCuN ₃ O ₂ |
| Formula weight | 331.26 |
| Temperature | 293(2) K |
| Wavelength | 0.71073 Å |
| Crystal system | Orthorhombic |
| Space group | <i>Pnma</i> |
| Unit cell dimensions | a = 18.3355(9) Å α = 90° b = 6.8834(3) Å β = 90° c = 10.9105(6) Å γ = 90° |
| Volume | 1377.02(12) Å ³ |
| Z | 4 |
| Density (calculated) | 1.598 Mg m ⁻³ |
| Absorption coefficient | 1.780 mm ⁻¹ |
| <i>F</i> (000) | 676 |
| Crystal size | 0.35 × 0.25 × 0.20 mm ³ |
| θ range for data collection | 2.90 to 24.99° |
| Limiting indices | -21 ≤ h ≤ 21, -8 ≤ k ≤ 7, -12 ≤ l ≤ 12 |
| Reflections collected | 8875 |
| Unique reflections | 1322 [R(int) = 0.0242] |
| Refinement method | Full-matrix least-squares on F ² |
| Data / restraints / parameters | 1320 / 0 / 119 |
| Goodness-of-fit on F ² | 1.113 |
| Final R indices [I > 2σ(I)] | R ₁ = 0.0331, wR ₂ = 0.0829 |
| R indices (all data) | R ₁ = 0.0413, wR ₂ = 0.0933 |
| Largest diff. peak and hole | 0.392 and -0.348 e.Å ⁻³ |

$R_1 = \frac{\sum ||F_o| - |F_c||}{\sum |F_o|}$
 $wR_2 = [\sum w(F_o^2 - F_c^2)^2 / \sum w(F_o^2)^2]^{1/2}$

Table 5.4. Selected bond lengths (Å) and bond angles (°) for **11**

| Bond lengths (Å) | | Bond angles (°) | |
|------------------|----------|-----------------|------------|
| Cu(1)–O(1) | 1.898(2) | O(1)–Cu(1)–N(2) | 92.79(13) |
| Cu(1)–N(1) | 2.062(3) | O(1)–Cu(1)–N(3) | 92.20(15) |
| Cu(1)–N(2) | 1.912(3) | O(1)–Cu(1)–N(1) | 176.85(13) |
| Cu(1)–N(3) | 1.909(4) | N(1)–Cu(1)–N(2) | 84.05(14) |
| N(2)–C(3) | 1.285(5) | N(1)–Cu(1)–N(3) | 90.95(17) |
| N(3)–C(11) | 1.110(7) | N(2)–Cu(1)–N(3) | 175.01(17) |
| O(2)–C(11) | 1.182(7) | N(3)–C(11)–O(2) | 179.10(6) |

The two largest angles, α and β have values 176.85(13) and 175.01(17)° respectively, thus giving a value of 0.0577 for the τ₄ index [9]. The bond

angles subtended by the various donor atoms at the metal centre summate to 359.999° and all those atoms are surprisingly coplanar with a null deviation from the least square plane. The value of τ_4 , angular summation at Cu(II) centre and measure of least squares plane altogether sketches a perfect geometry for the complex. Bond strength follows the order Cu–O1 (phenoxo oxygen) > Cu–N3 (cyanao nitrogen) > Cu–N2 (amino nitrogen) > Cu1–N1 (imino nitrogen). Cyanato ligand is pseudolinear with a bond angle of $179.10(6)^\circ$. Coordination imposes a penta and hexa metalocycle with chelate bite angles of $84.05(14)^\circ$ (N2–Cu1–N1) and $92.79(13)^\circ$ (N2–Cu1–O1) respectively.

The saturated five membered ring Cu1–N1–C1–C2–N2 is twisted on C(1)–C(2) with puckering parameters $Q(2) = 0.522(6) \text{ \AA}$ and $\phi(2) = 88.5(4)^\circ$ and it possess a twist-boat conformation. The C1 and C2 atoms of the ring are disordered and the five membered ring with these disordered constituents also has a twist-boat conformation with $Q(2) = 0.522(6) \text{ \AA}$ and $\phi(2) = 268.5(4)^\circ$. The six membered ring constituted by N1–C1–C2–N2–C2a–C1a has a boat form with puckering parameters $Q(2) = 1.471(5) \text{ \AA}$, $Q(3) = -0.023(6) \text{ \AA}$, $\phi(2) = 360.0(3)^\circ$.

Packing interactions

The monomeric cyanato units *via* intermolecular hydrogen bonding interaction between H(2A) and oxygen atom, O(2) generates a one dimensional chain down ‘a’ axis, which is related to each other by C_2 symmetry [Fig. 5.5, Table 5.5]. A S(5) ring motif is also present in the monomeric unit due to intramolecular H interaction with N(3) as the acceptor atom [Fig. 5.5].

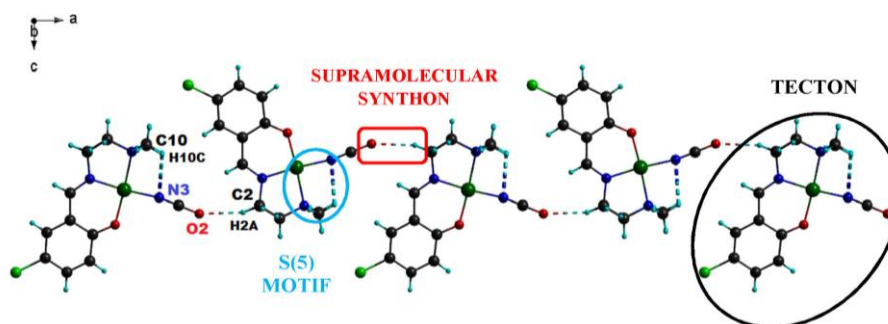


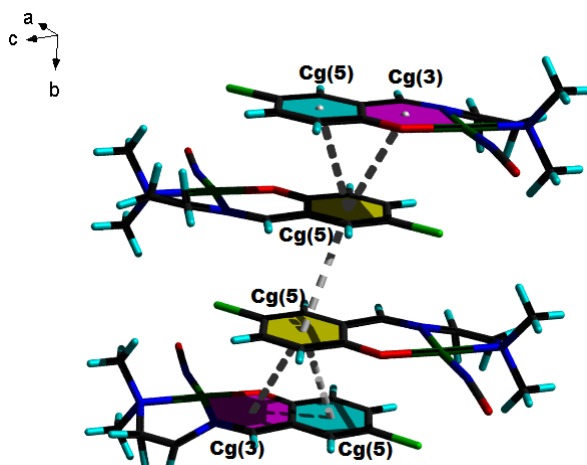
Fig. 5.5. Intermolecular hydrogen bond generates a one dimensional chain down ‘a’ axis.

Table 5.5. Non-conventional hydrogen bonding interactions in the complex

| D–H···A | D–H (Å) | H···A (Å) | D···A (Å) | D–H···A (°) |
|--|---------|-----------|-----------|-------------|
| Intermolecular hydrogen bonding | | | | |
| C(2)–H(2A)···O(2) ^a | 0.97 | 2.34 | 3.262(7) | 159 |
| Intramolecular hydrogen bonding | | | | |
| C(10)–H(10C)···N(3) | 0.96 | 2.62 | 3.120(5) | 113 |

Equivalent position code: a = $-1/2 + x$, $1/2 - y$, $3/2 - z$

Face to face π interactions exist between the metallocycle Cg(3) and Cg(5) and also between rings involving carbon atoms [Cg(5)/Cg(5)] with slippage of 1.989 and 1.803 Å respectively [Fig. 5.6, Table 5.6].

**Fig. 5.6.** Cg···Cg interactions along 'b' axis.**Table 5.6.** Short ring interactions

| Cg(I)···Cg(J) | Cg(I)···Cg(J) (Å) | γ (°) |
|----------------------------|-------------------|--------------|
| Cg(3)···Cg(5) ^b | 3.9749(11) | 30 |
| Cg(3)···Cg(5) ^c | 3.8853(11) | 27.6 |

Equivalent position code: b = $-x$, $-y$, $2 - z$, c = $-x$, $-1/2 + y$, $2 - z$

Cg, centroid

Cg(3) = Cu(1), O(1), C(3), C(4), C(9), N(2)

Cg(5) = C(4), C(5), C(6), C(7), C(8), C(9)

Cg(I) = Center of gravity of ring I

Cg(J) = Center of gravity of ring J

γ = Angle between Cg(I)···Cg(J) vector and normal to plane J (°)

Cg(I)···Cg(J) = Distance of Cg(I) to Cg(J) (Å)

Apart from the aforesaid non-covalent stacking interactions, the complex also has C–Cl \cdots π force between the Cl(1) atom and the Cg(3) ring, adding to the additional crystal stability [Fig. 5.7, Table. 5.7].

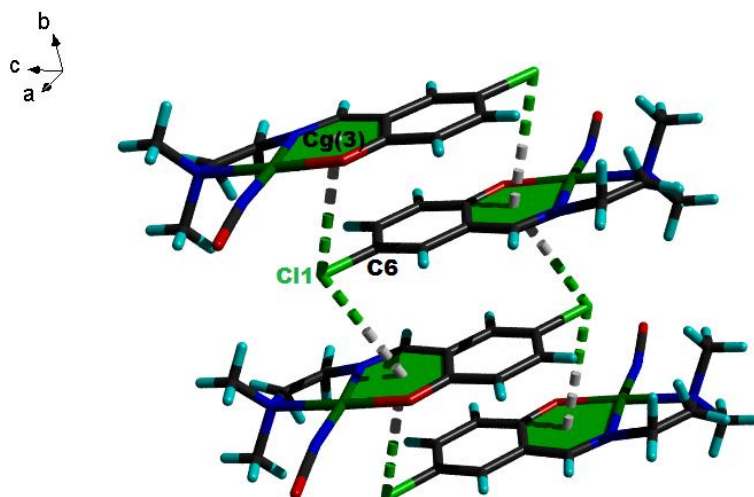


Fig. 5.7. C–Cl \cdots π forces stitching the units.

Table 5.7. C–X \cdots Cg interactions

| C–X(I) \cdots Cg(J) | X \cdots Cg (Å) | C \cdots Cg (Å) | C–X \cdots Cg (°) |
|--|-------------------|-------------------|---------------------|
| C(6)–Cl(1) \cdots Cg(3) ^{b,c,d,e} | 3.6834(7) | 3.5206(9) | 70.85(3) |

Equivalent position codes: b = -x, -1/2 + y, 2 - z, c = -x, 1/2 + y, 2 - z, d = -x, -y, 2 - z, e = -x, 1 - y, 2 - z

The entire packing of the complex witnesses a two dimensional supramolecular sheet propagation along ‘ab’ plane with the hydrogen bonds directing the monomeric units along ‘a’ axis and the weaker aromatic-aromatic interaction along with the X \cdots π forces stretching them in ‘b’ direction [Fig. 5.8].

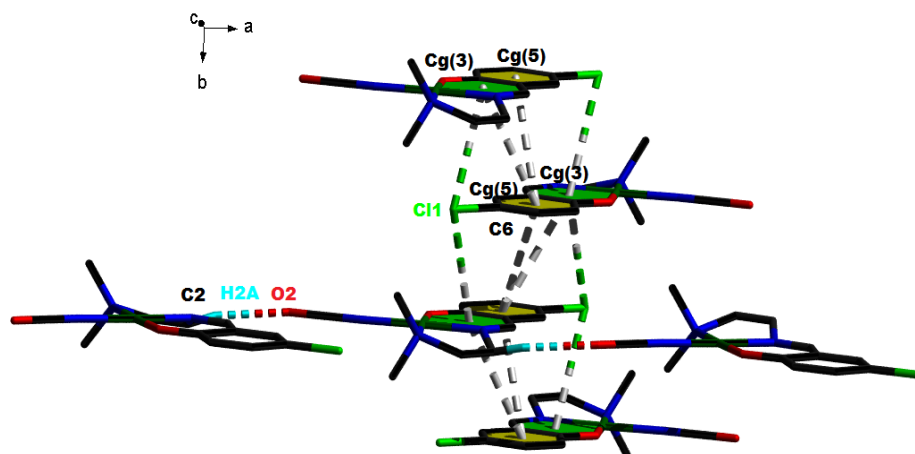


Fig. 5.8. Supramolecular sheet propagation.

5.3.2.2. $[\text{Cu}(\text{L}^5)(\text{NCS})]$ (**12**)

The monomeric thiocyanato complex crystallizes in orthorhombic $Pnma$ space group and the asymmetric unit as shown in ORTEP diagram [Fig. 5.9] describes the geometry to be a simple square planar. The crystallographic details are given in Table. 5.8. The crystal structure alone has been already reported by You *et al.* [10]. So we reproduced the complex for further comparative studies.

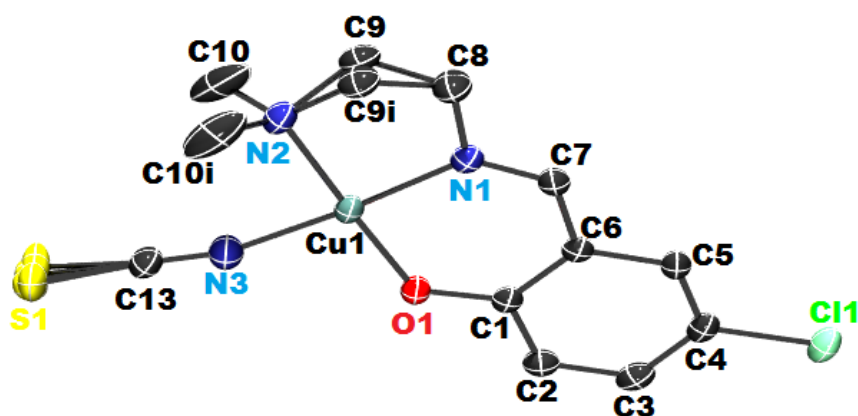


Fig. 5.9. ORTEP diagram showing the atom labelling of the asymmetric unit of the complex **12** (drawn with 30% ellipsoid probability and the hydrogen atoms are omitted for clarity).

Table 5.8. Crystal data and refinement details of complex **12**

| Parameters | Complex 12 |
|-----------------------------------|--|
| Empirical formula | C ₁₂ H ₁₃ ClCuN ₃ OS |
| Formula weight | 346.32 |
| Temperature | 296(2) K |
| Wavelength | 0.71073 Å |
| Crystal system | Orthorhombic |
| Space group | <i>Pnma</i> |
| Unit cell dimensions | a = 19.1549(13) Å α = 90° b = 6.7627(4) Å β = 90° c = 11.3247(7) Å γ = 90°. |
| Volume | 1466.99(16) Å ³ |
| Z | 4 |
| Density (calculated) | 1.568 Mg m ⁻³ |
| Absorption coefficient | 1.807 mm ⁻¹ |
| F(000) | 704 |
| Crystal size | 0.35 × 0.25 × 0.20 mm ³ |
| θ range for data collection | 2.79 to 28.25° |
| Limiting indices | -25 ≤ h ≤ 23, -8 ≤ k ≤ 4, -13 ≤ l ≤ 14 |
| Reflections collected | 6919 |
| Unique reflections | 1957 [R(int) = 0.0237] |
| Refinement method | Full-matrix least-squares on F ² |
| Data / restraints / parameters | 1950 / 0 / 130 |
| Goodness-of-fit on F ² | 1.051 |
| Final R indices [I > 2σ(I)] | R ₁ = 0.0325, wR ₂ = 0.0892 |
| R indices (all data) | R ₁ = 0.0469, wR ₂ = 0.0988 |
| Largest diff. peak and hole | 0.337 and -0.277 e.Å ⁻³ |

$$R_1 = \frac{\sum ||F_o| - |F_c||}{\sum |F_o|}$$

$$wR_2 = \left[\frac{\sum w(F_o^2 - F_c^2)^2}{\sum w(F_o^2)^2} \right]^{1/2}$$

Selected bond lengths (Å) and bond angles (°) are given in Table 5.9. The geometrical requirement is satisfied by the amino nitrogen (N2), imino nitrogen (N1), phenoxo oxygen (O1) and thiocyanato nitrogen (N3). The summation of the chelate angles subtended at the central metal by the donor atoms [360°] and the least squares plane calculation of atoms in the basal plane [Cu1/N3/O1/N1/N2] [no deviation found] are symptomatic of a perfect topology

although a negligibly small value of 0.0476 appears for τ_4 index [9] [A measure of the extent of distortion between a perfect tetrahedron ($\tau_4 = 1$) and perfect square planar geometry ($\tau_4 = 0$), given by the formula: $\tau_4 = [360^\circ - (\alpha + \beta)]/141^\circ$, α and β being the two largest angles around the central metal atom in the complex]. The thiocyanato ligand deviates largely from linearity with an angle of $173.0(3)^\circ$ [N3–C13–S1A].

Table 5.9. Selected bond lengths (Å) and bond angles ($^\circ$) for complex **12**

| Bond lengths (Å) | | Bond angles ($^\circ$) | |
|------------------|----------|--------------------------|------------|
| Cu(1)–O(1) | 1.905(2) | O(1)–Cu(1)–N(1) | 93.04(9) |
| Cu(1)–N(1) | 1.922(2) | O(1)–Cu(1)–N(3) | 91.63(12) |
| Cu(1)–N(3) | 1.929(3) | N(3)–Cu(1)–N(2) | 90.42(13) |
| Cu(1)–N(2) | 2.067(3) | N(1)–Cu(1)–N(2) | 84.91(11) |
| N(1)–C(7) | 1.285(4) | N(1)–Cu(1)–N(3) | 175.33(12) |
| N(3)–C(13) | 1.142(4) | O(1)–Cu(1)–N(2) | 177.95(10) |
| C(13)–S(1A) | 1.66(2) | N(3)–C(13)–S(1A) | 173.0(3) |
| C(13)–S(1B) | 1.62(2) | N(3)–C(13)–S(1B) | 169.0(3) |

A comparative bond length analysis of the two different monomeric complexes is given below [Table 5.10] from which we can conclude that cyanato nitrogen is bonded strongly than the nitrogen of thiocyanato ligand. Also cyanato ligand is almost linear whereas the thiocyanato one deviates significantly from linearity.

Table 5.10. A comparative bond length analysis of monomeric complexes

| Bonds | Distance in Å (–NCO) | Distance in Å (–NCS) |
|-------------------------------------|----------------------|----------------------|
| Cu1–O1 (phenoxo) | 1.898(2) | 1.905(2) |
| Cu1–N1 (imino) | 2.062(3) | 1.922(2) |
| Cu1–N2 (amino) | 1.912(3) | 2.067(3) |
| Cu1–N3 (cyanato) / (thiocyanato) | 1.909(4) | 1.929(3) |

The metalloring Cg(4) [Cu(1)/N(1)/C(8)/C(9)/N(2)] assumes an envelope conformation at C(9) with $Q(2) = 0.389(4) \text{ \AA}$, $\Phi(2) = 295.4(4)^\circ$ and pseudorotation parameters, $P = 83.2(2)^\circ$ and $\tau_m = 43.0(2)^\circ$. Corresponding metalloring Cg(5), involving the disordered atom, C(9a) also adopts envelope form. Though no hydrogen bonding is seen, stacking interactions self-assemble the monomers to a one dimensional chain down the 'b' axis [Fig. 5.10, Tables 5.11 and 5.12].

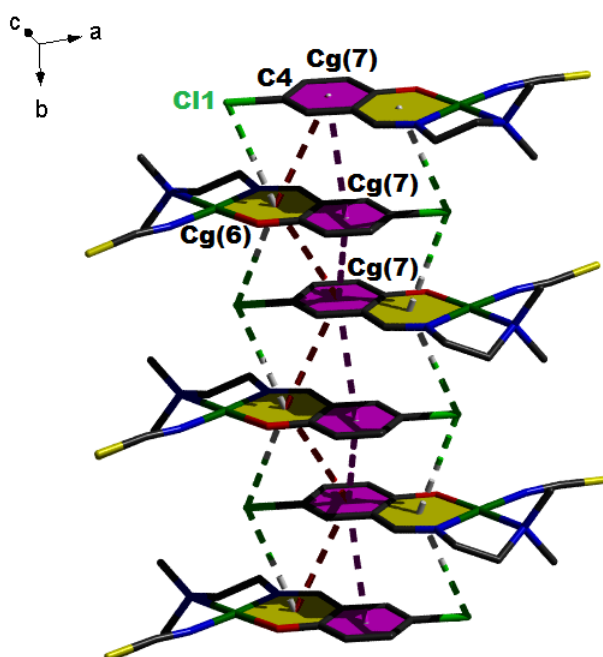


Fig. 5.10. Self-assembly of the monomers to a one dimensional chain down the 'b' axis.

Table 5.11. C–X...Cg interactions

| C–X...Cg | X...Cg (Å) | C...Cg (Å) | C–X...Cg (°) |
|---------------------------------|------------|------------|--------------|
| C(4)–Cl(1)...Cg(6) ^a | 3.6518(5) | 3.4309(6) | 68.78(2) |

Equivalent position code: $a = 1 - x, -1/2 + y, 1 - z$

Table 5.12. Short ring interactions

| Cg(I)⋯Cg(J) | Cg(I)⋯Cg(J) (Å) | γ(°) |
|--------------------------|-----------------|------|
| Cg(6)⋯Cg(7) ^b | 3.8569(8) | 28.8 |
| Cg(7)⋯Cg(6) ^b | 3.8570(8) | 28.8 |
| Cg(7)⋯Cg(7) ^b | 3.7867(9) | 26.8 |

Equivalent position code: b = 1 - x, -1/2 + y, 1 - z

Cg, centroid

Cg(6) = Cu(1), O(1), C(1), C(6), C(7), N(1)

Cg(7) = C(1), C(2), C(3), C(4), C(5), C(6)

Cg(I) = Center of gravity of ring I

Cg(J) = Center of gravity of ring J

γ = Angle Cg(I)⋯Cg(J) vector and normal to plane J (°)

Cg(I)⋯Cg(J) = Distance of Cg(I) to Cg(J) (Å)

5.3.2.3. [Cu(L⁶)(N₃)_n] (13)

The azido complex crystallizes in orthorhombic *Pbca* space group. Although the asymmetric unit shows a square planar topology [Fig. 5.11], the actual structure is square pyramidal with the additional coordination site being occupied by azido coligand which drags the molecular unit to a one-dimensional polymer along [0 1 0] direction [Fig. 5.12].

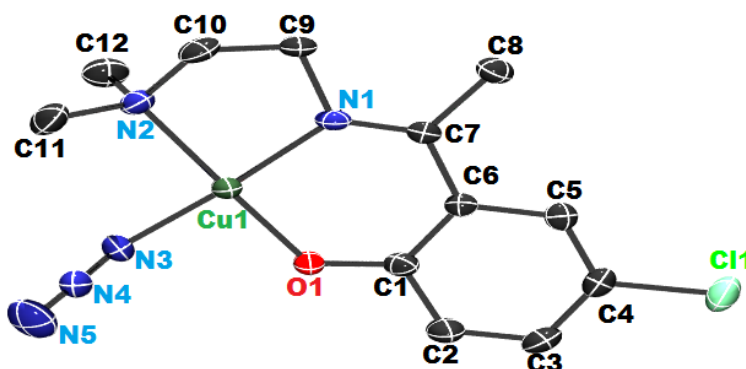


Fig. 5.11. ORTEP diagram showing the atom labelling of the asymmetric unit of the complex **13** (drawn with 30% ellipsoid probability and the hydrogen atoms are omitted for clarity).

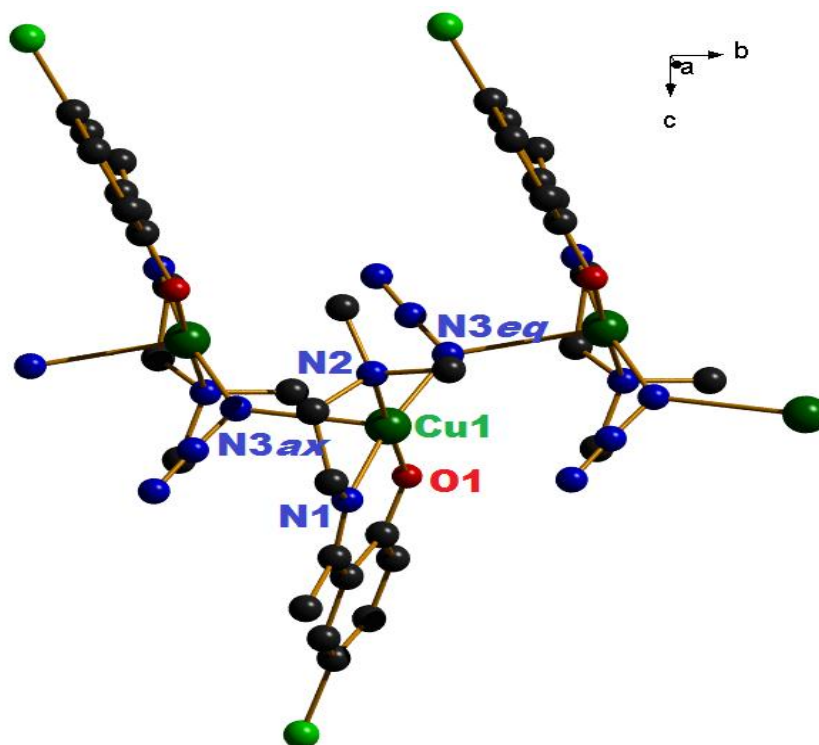


Fig. 5.12. Perspective view of the complex 13.

All the essential crystallographic details, geometrical parameters etc. are given in Table 5.13. The central Cu(II) atom is coordinated to NNO tridentate Schiff base along with the nitrogen of one of the azido nitrogens in the square basal plane whilst the nitrogen of the other azido group occupies the axial position. The iteration of pendant-like azido group in *trans* $\mu_{1,1}$ -*end-on* fashion builds the entire coordination polymer. The asymmetric bonding nature of the pseudohalide is evident from the two different Cu–N distances of 1.988(3) (equatorial) and 2.669(3) Å (axial) respectively [Table 5.14].

Table 5.13. Crystal data and refinement details of complex **13**

| Parameters | Complex 13 |
|---|--|
| Empirical formula | C ₁₂ H ₁₆ ClCuN ₅ O |
| Formula weight | 345.30 |
| Temperature | 296(2) K |
| Wavelength | 0.71073 Å |
| Crystal system | Orthorhombic |
| Space group | Pbca |
| Unit cell dimensions | a = 19.575(2) Å α = 90° b = 7.0313(7) Å β = 90° c = 21.2368(19) Å γ = 90° |
| Volume | 2923.0(5) Å ³ |
| Z | 8 |
| Density (calculated) | 1.569 Mg m ⁻³ |
| Absorption coefficient | 1.680 mm ⁻¹ |
| F(000) | 1416 |
| Crystal size | 0.60 × 0.40 × 0.20 mm ³ |
| θ range for data collection | 2.830 to 28.262° |
| Limiting indices | -25 ≤ h ≤ 24, -9 ≤ k ≤ 9, -20 ≤ l ≤ 27 |
| Reflections collected | 14589 |
| Unique reflections | 3577 [R(int) = 0.0537] |
| Refinement method | Full-matrix least-squares on F ² |
| Data / restraints / parameters | 3626 / 0 / 184 |
| Goodness-of-fit on F ² | 0.901 |
| Final R indices [I > 2σ(I)] | R ₁ = 0.0404, wR ₂ = 0.0976 |
| R indices (all data) | R ₁ = 0.0836, wR ₂ = 0.1210 |
| Largest diff. peak and hole | 0.327 and -0.393 e.Å ⁻³ |
| $R_1 = \frac{\sum F_o - F_c }{\sum F_o }$ $wR_2 = \left[\frac{\sum w(F_o^2 - F_c^2)^2}{\sum w(F_o^2)^2} \right]^{1/2}$ | |

Table 5.14. Selected bond lengths (Å) and bond angles (°) for complex **13**

| Bond lengths (Å) | | Bond angles (°) | |
|------------------|----------|-------------------|------------|
| Cu(1)–O(1) | 1.887(2) | N(3)–Cu(1)–O(1) | 88.82(10) |
| Cu(1)–N(1) | 1.967(2) | N(2)–Cu(1)–N(3) | 91.64(11) |
| Cu(1)–N(2) | 2.055(2) | N(1)–Cu(1)–N(2) | 86.37(10) |
| Cu(1)–N(3) | 1.988(3) | O(1)–Cu(1)–N(1) | 92.68(10) |
| Cu(1)–N(3a) | 2.669(3) | N(1)–Cu(1)–N(3) | 169.67(10) |
| N(3)–N(4) | 1.204(4) | O(1)–Cu(1)–N(2) | 177.13(10) |
| N(4)–N(5) | 1.147(5) | N(3)–N(4)–N(5) | 177.7(4) |
| C(4)–Cl(1) | 1.748(3) | Cu(1)–N(3)–Cu(1b) | 130.15(13) |
| | | N(3)–Cu(1)–N(3a) | 104.57(10) |
| | | N(4)–N(3)–Cu(1b) | 111.6(2) |
| | | Cu(1)–N(3)–N(4) | 118.2(2) |
| | | N(3a)–Cu(1)–O(1) | 90.24(9) |
| | | N(3a)–Cu(1)–N(2) | 92.39(10) |
| | | N(3a)–Cu(1)–N(1) | 85.65(9) |
| | | N(3a)–Cu(1)–N(3) | 104.57(10) |

The least squares plane calculation brings out the deviation of the metal atom to be the largest, 0.0893 Å below the basal plane. Also, the value of τ - the angular structural parameter, an index of degree of trigonality is 0.12, given by the equation $\tau = (\beta - \alpha)/60$ [11] (for perfect square pyramidal and trigonal bipyramidal geometries the values of τ are zero and unity respectively) is symptomatic of a largely distorted square pyramidal geometry. This large value of Addison parameter throws light on the wide variation in the transoid angles. The bond angles subtended by the various ligating atoms at the pivotal metal centre computes to a total value of 359.51°. The packing index calculated using PLATON is 67.6% [12]. The Cu...Cu non-bonded distance between two adjacent symmetrically related units is 4.2326(7) Å. The metrical parameters, Cu–N–Cu = 130.15(13)° and N–Cu–N bond angle is around 104.57(10)°. The azido ligand is pseudolinear with a bond angle of 177.7(4)°.

The interchain Cu...Cu distance is a little larger compared to similar systems [27] – 10.9393(11) Å. The five membered chelate ring incorporating the copper atom i.e. Cg(1) [Cu1,N5,C4,C5,N6] adopts an envelope conformation with C(10) as the flap atom of the envelope, with a puckering amplitude of

$Q = 0.416(3) \text{ \AA}$ and $\phi = 110.0(3)^\circ$ [13]. The puckering of the metallocycle is also calculated in terms of pseudorotation parameters P and τ_m [14] and the envelope conformation was confirmed with $P = 265.7(2)^\circ$ and $\tau = 46.6(2)^\circ$ for reference bond $\text{Cu}(1)\text{--N}(1)$. The six membered metallocycle, $\text{Cg}(2)$ [$\text{Cu}1, \text{N}5, \text{N}4, \text{C}3, \text{C}2, \text{C}1$] assumes a screw-boat conformation with puckering amplitude, $Q = 0.131(2) \text{ \AA}$ and $\phi = 210.8(12)^\circ$.

Packing forces

Two intrachain intermolecular hydrogen bonding is established with the same acceptor atom, $\text{O}(1)$. This three centre hydrogen bonded interaction accepts the hydrogen atoms, $\text{H}(11\text{B})$ and $\text{H}(12\text{A})$ from the carbons, $\text{C}(11)$ and $\text{C}(12)$ respectively. The $\text{N}(5)$ atom of the terminal azido group along a chain readily accepts the hydrogen of $\text{C}(5)$ atom in the immediate neighbouring chain thereby forming the rungs of the stair-like structure [Fig. 5.13, Table 5.15].

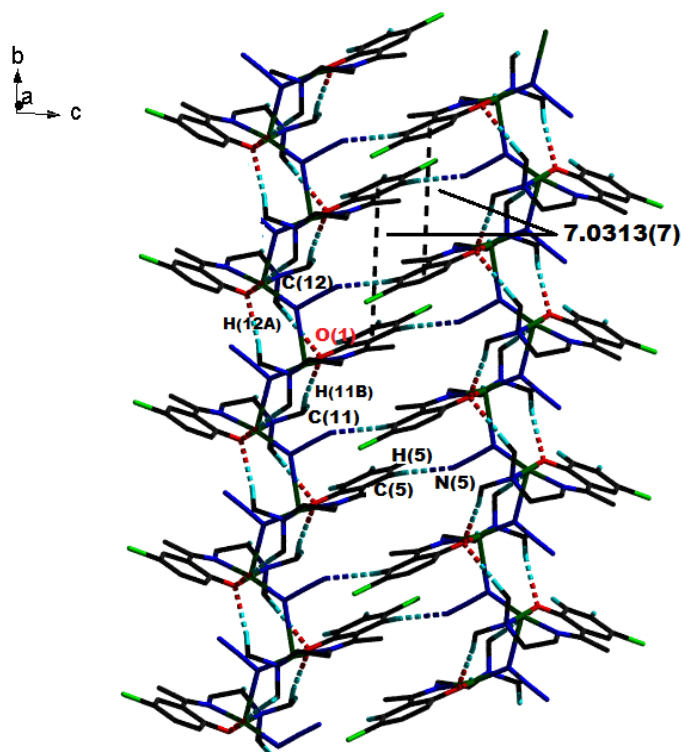


Fig. 5.13. Intrachain intermolecular interactions in complex 13.

Table 5.15. Non-conventional hydrogen bonding interactions in complex **13**

| D–H⋯A | D–H (Å) | H⋯A (Å) | D⋯A (Å) | D–H⋯A (°) |
|--|---------|---------|----------|-----------|
| Intermolecular hydrogen bonding | | | | |
| C(5)–H(5)⋯N(5) ^d | 0.93 | 2.57 | 3.477(5) | 164 |
| C(11)–H(11B)⋯O(1) ^e | 0.96 | 2.41 | 3.354(5) | 168 |
| C(12)–H(12A)⋯O(1) ^f | 0.96 | 2.58 | 3.539(4) | 178 |

Equivalent position codes: d = x, 1/2 - y, -1/2 + z, e = -x, -1/2 + y, 1/2 - z, f = -x, 1/2 + y, 1/2 - z

Apart from the azido ligand acting as a linker and propagating the chain in one dimension down ‘*b*’ axis, there are two more intrachain ring interactions along the same direction – N(4)–N(5)⋯Cg(2) with N(5)⋯ π distances of 3.771(4) and 3.618(4) Å units [Fig. 5.14, Table 5.16].

In addition, the H(8A) atom of C(8) in one chain establishes a ring interaction with the Cg(3) ring of adjacent chain with a H⋯ π distance of 2.95 Å units and thus spreads the coordination polymer into a two dimensional sheet in ‘*bc*’ plane [Fig. 5.14, Table 5.17].

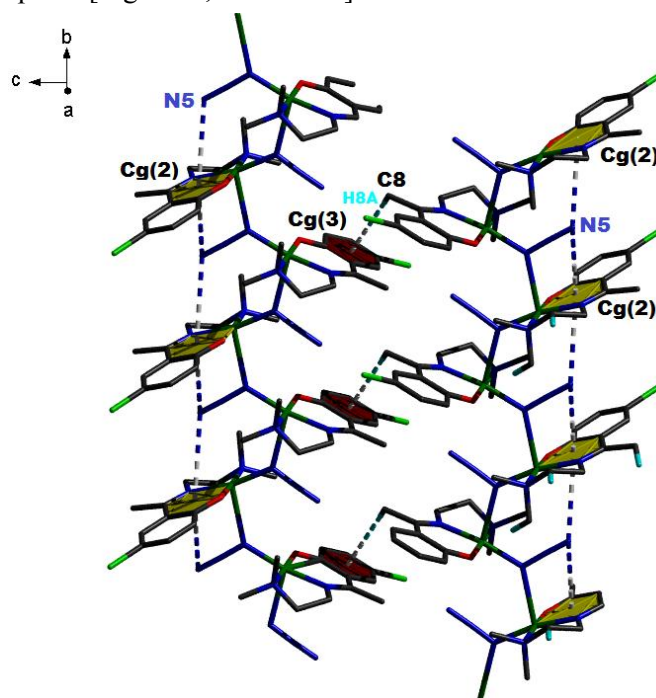


Fig. 5.14. N–N⋯Cg(2) and C–H⋯Cg(3) interactions.

Table 5.16. Y–X...Cg interactions in complex **13**

| Y–X...Cg | Y...Cg (Å) | X...Cg (Å) | Y–X...Cg (°) |
|--------------------------------|------------|------------|--------------|
| N(4)–N(5)...Cg(2) ^b | 4.457(3) | 3.771(4) | 120.0 |
| N(4)–N(5)...Cg(2) ^c | 3.183(3) | 3.618(4) | 59.0 |

Equivalent position codes: b = - x, -1/2 + y, 1/2 - z, c = - x, 1/2 + y, 1/2 - z
Cg(2) = Cu1, N5, N4, C3, C2, C1

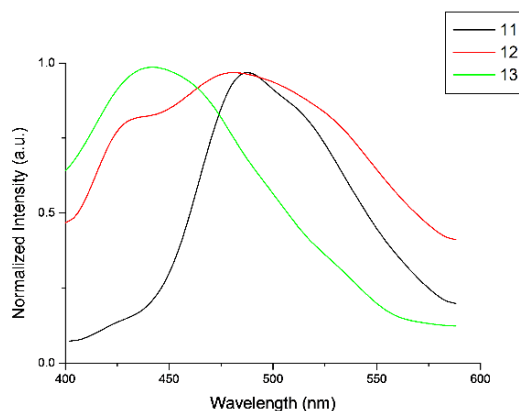
Table 5.17. C–H...Cg interactions

| C–H...Cg | H...Cg (Å) | C...Cg (Å) | C–H...Cg (°) |
|---------------------------------|------------|------------|--------------|
| C(8)–H(8a)...Cg(3) ^a | 2.95 | 3.747(3) | 142 |

Equivalent position codes: a = - x, 1-y, - z
Cg(3) = C2, C3, C9, C10, C11, C12

5.3.3. Photoluminescence study

The fluorescent spectra of the three complexes were examined in acetonitrile medium at an excitation wavelength of 350 nm. The cyanato and thiocyanato complexes emit in the blue region of the spectrum while the polymeric azido complex fluoresces in the violet region [Fig. 5.15, Table 5.18].

**Fig. 5.15.** Normalized fluorescence spectra of the complexes (acetonitrile, con: 1×10^{-3} M).**Table 5.18.** Photophysical data of complexes

| Complexes | Solution state emission (nm) at excitation of 350 nm |
|--|--|
| [Cu(L)(NCO)] (11) | 486 |
| [Cu(L)(NCS)] (12) | 482 |
| [Cu(L ₂)(N ₃) _n] (13) | 432 |

5.3.4. Thermal studies

The thermal profiles of the chloro complexes were recorded up to 700 °C so as to assess their stability. The cyanato species when heated, loses the amine portion in the temperature range 224-255 °C. This exothermic process corresponds to a weight loss of 27.55% (calcd. 26.5%). There is an ultimate formation of a stable metal oxide, as inferred from TG graph. The thiocyanato species also has a similar exothermic decomposition pattern with the loss of amine (22.98%, calcd. 25.36%) in the temperature range of 206-217 °C followed by the formation of a stable metal oxide species. The polymeric azido complex shows an endothermic weight loss (30.98%, calcd. 33.62%) corresponding to the removal of the amino portion and nitrogen in the temperature range of 220-245 °C followed by a region showing not much variation. The calculated and theoretical weight losses are comparable in all the cases [Fig. 5.16].

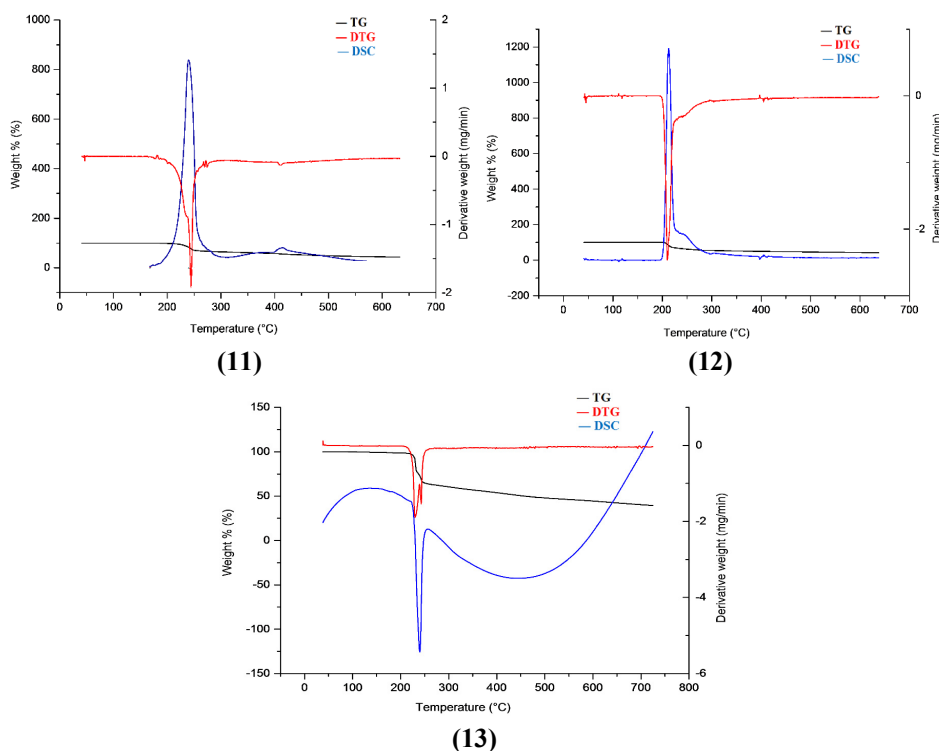


Fig. 5.16. Thermogram of the complexes 11, 12 and 13.

5.3.5. EPR spectral studies

Some of the EPR spectra are simulated using EasySpin package [15] and the experimental (red) and simulated (blue) best fits are included.

The EPR spectra of the cyanato complex, **11** recorded in the polycrystalline state at 298 K gave a spectrum with axial nature having $g_{\parallel} = 2.144$ and $g_{\perp} = 2.058$. The EPR of the same sample was taken in frozen DMF so as to gain more perception on the spectral features from which a confirmation of the coordination geometry can be arrived at. The spectrum displays four hyperfine splittings in the parallel region with a nuclear hyperfine splitting constant, $A_{\parallel} = 209 * 10^{-4} \text{ cm}^{-1}$ between the split lines while the high intense region shows an A_{\perp} value of $15 * 10^{-4} \text{ cm}^{-1}$ although the splitting is not evidently seen [Fig. 5.17a].

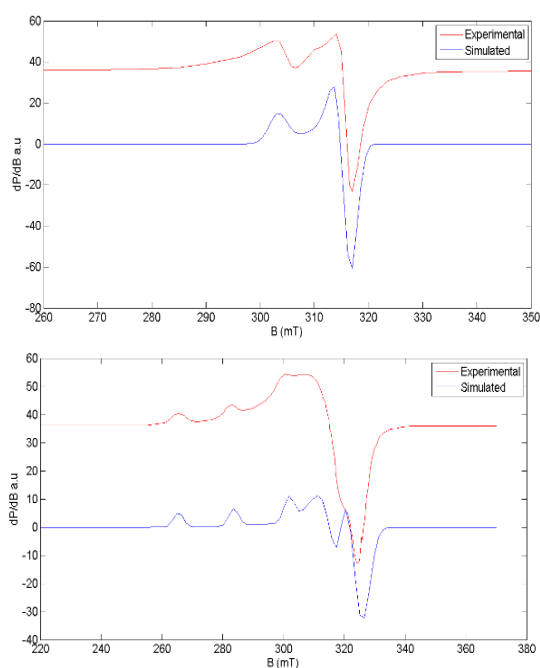


Fig. 5.17a. EPR spectra of complex **11** in polycrystalline state (top) and in DMF at 77 K (bottom).

The interaction between the orbitals of the central ion Cu(II), and those of the equatorially coordinating atoms are reflected in some ESR parameters [16] and therefore CW-EPR spectroscopy is a technique sensitive to the

identity and the number of the equatorially coordinating atoms. Since all our complexes have the same coordinating entities in the equatorial positions (CuN_3O), not much of a difference could be observed in the corresponding EPR spectra.

The thiocyanato complex **12** revealed an axial nature for the spectra in the polycrystalline state and the nature of the spectra is sustained in frozen DMF except for the resolved hyperfine splittings in the parallel region ($A_{\parallel} = 209 \cdot 10^{-4} \text{ cm}^{-1}$). The perpendicular region shows a trend for splitting although it is not well-defined as in the parallel region ($A_{\perp} = 20 \cdot 10^{-4} \text{ cm}^{-1}$) [Fig. 5.17b].

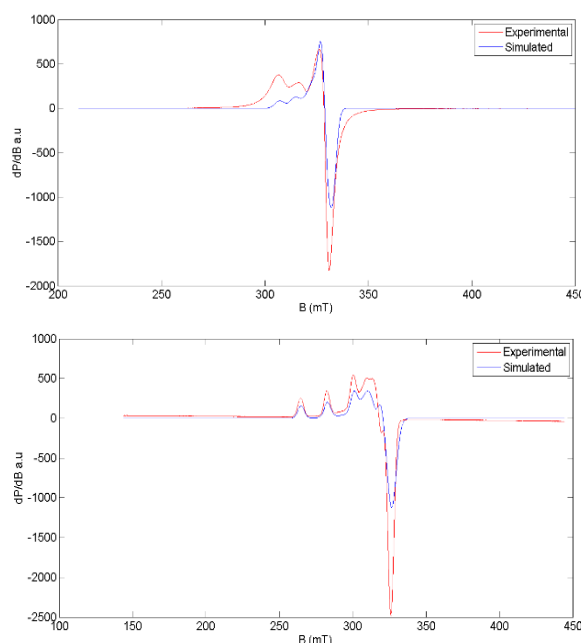


Fig. 5.17b. EPR spectra of complex **12** in polycrystalline state (top) and in DMF at 77 K (bottom).

Similar to those explained above, the room temperature EPR spectrum of the azido complex **13** gives an axial spectrum with $g_{\parallel} = 2.165$ and $g_{\perp} = 2.075$. Whilst at low temperature, we observe four resolved hyperfine splittings in the parallel region with a spacing given by nuclear hyperfine splitting constant,

$A_{\parallel} = 216 * 10^{-4} \text{ cm}^{-1}$. The perpendicular region also shows up a splitting with A_{\perp} value of $35 * 10^{-4} \text{ cm}^{-1}$ although only three signals are observed [Fig. 5.17c].

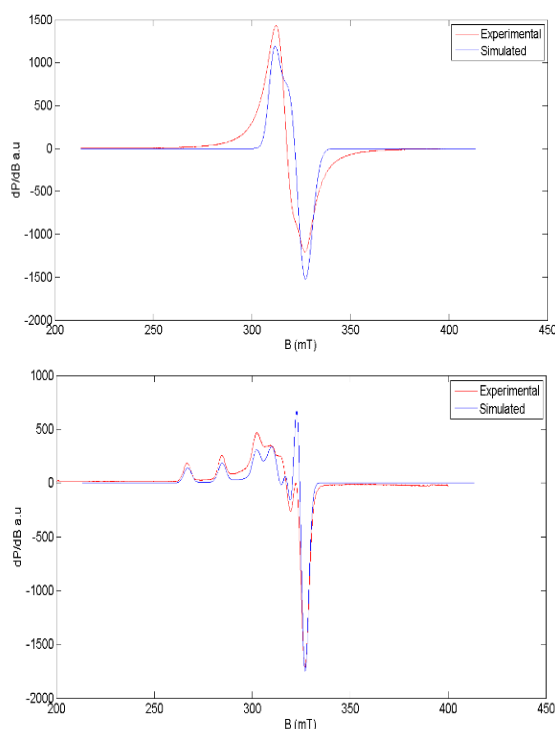


Fig. 5.17c. EPR spectra of complex **13** in polycrystalline state (top) and in DMF at 77 K (bottom).

In all the cases, the g_{av} and A_{av} values are calculated from the equations, $g_{av} = 1/3 (g_{\parallel} + 2g_{\perp})$ and $A_{av} = 1/3 (A_{\parallel} + 2A_{\perp})$ respectively [Table 5.19].

The geometric parameter G for the complexes **11**, **12** and **13** are 2.544, 2.416 and 2.238 respectively, indicating the presence of magnetically equivalent sites in the unit cell of the compound. The trend in g tensor values can be used to assess the geometry and the nature of the M–L bonding in complexes. In our complexes, $g_{\parallel} > g_{\perp} > 2.0023$ and G values are within the range 2-4 which confirms the square based geometry with $d_{x^2-y^2}$ as the ground state [17-21] and negates the possibility of trigonal bipyramidal structure.

Table 5.19. Spin Hamiltonian and bonding parameters of copper(II) complexes

| Compounds | Polycrystalline state (298 K) | | | | | | DMF solution (77 K) | | | | | | | | |
|---|----------------------------------|-------------|-------|--------------------|---------------------|----------|---------------------|-------------|----------|------------|-----------|------------|-----------------|-------------|-----|
| | g_{\parallel} | g_{\perp} | G | $g_{\parallel}g_3$ | $g_{\perp}g_1, g_2$ | g_{av} | A_{\parallel} | A_{\perp} | A_{av} | α^2 | β^2 | γ^2 | K_{\parallel} | K_{\perp} | f |
| [Cu(L)(NCO)] (11) | 2.144 | 2.058 | 2.544 | 2.220 | 2.053 | 2.108 | 209 | 15 | 79 | 0.8603 | 0.8222 | 0.7934 | 0.7073 | 0.6826 | 106 |
| [Cu(L)(NCS)] (12) | 2.120 | 2.051 | 2.416 | 2.227 | 2.047 | 2.107 | 209 | 22 | 84 | 0.8637 | 0.8543 | 0.7621 | 0.7379 | 0.6582 | 107 |
| [Cu(L ₂)(N ₃)] _n (13) | 2.165 | 2.075 | 2.238 | 2.299 | 2.120 | 2.179 | 216 | 35 | 95 | 0.9858 | 0.8500 | 1.0707 | 0.8379 | 1.0555 | 106 |

A values in 10⁻⁴ cm⁻¹

The g_{\parallel} values are less than 2.3, implying that Cu–L bond has considerable covalent nature [22]. Apart from this, the calculated values of the bonding parameters - α^2 , β^2 and γ^2 for the complexes lie between 0.5 and 1, supportive of the mixed ionic-covalent nature of M–L bonding. The value of γ^2 for complex **13** is slightly higher than 1 which is unexpected. In addition, we have the orbital reduction factors, K_{\parallel} and K_{\perp} the values of which will help us to deduce about the in-plane and out-of-plane π bonding [23]. For complexes **11** and **12**, we find $K_{\parallel} > K_{\perp}$ indicating out-of-plane bonding and the azido complex has $K_{\parallel} < K_{\perp}$ highlighting in-plane bonding. The empirical factor, f for our complexes are indicative of slight distortion from planarity [24,25].

Section B

5.4. Experimental

5.4.1. Synthesis of [Cu(L⁷)(NCS)] (14)

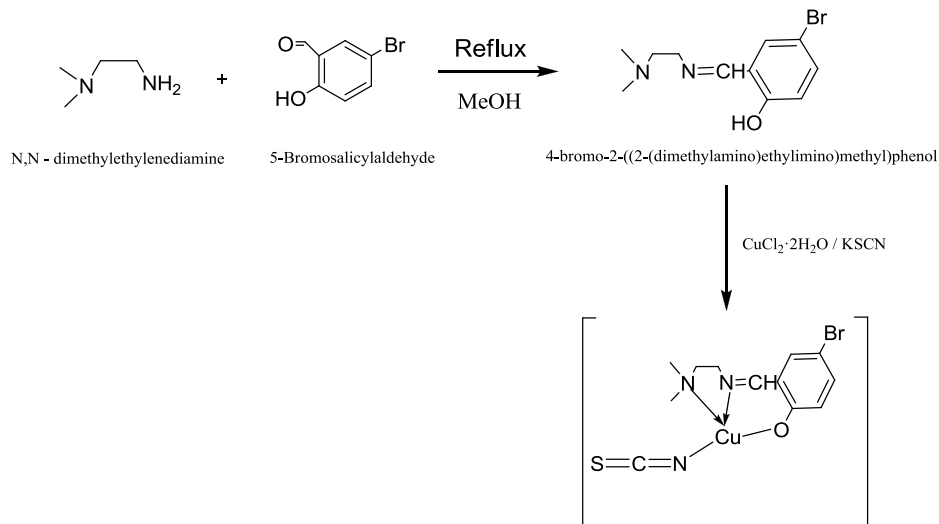
[HL⁷ = 4-bromo-2-((2-(dimethylamino)ethylimino)methyl)phenol]

N,N-Dimethylethylenediamine was refluxed with 5-bromosalicylaldehyde (1:1) for about 2 h. A methanolic solution (10 mL) of copper(II) chloride dihydrate (0.170 g, 1 mmol) was added to this hot methanolic solution (10 mL) and stirred for 30 minutes. To the resulting deep green solution, potassium thiocyanate (0.194 g, 2 mmol) in a MeOH/H₂O (1:9) mixture was added dropwise and further stirred for *ca.* 2 h and filtered. Diffraction quality single crystals for structure determination were obtained by slow evaporation of this mother liquor in air.

Yield: 0.2346 g (60%). *Anal.* Calc. for C₁₂H₁₄BrCuN₃OS: C, 36.79; H, 3.60; N, 10.73. Found C, 36.81; H, 3.65; N, 10.75%.

5.5. Results and discussion

The schematic representation for the synthesis of the complex is shown below [Scheme 5.4].



Scheme 5.4. Synthetic route to the formation of complex **14**.

5.5.1. Spectral features

The N-coordinated thiocyanato group present in this monomeric complex is evidenced by a peak at 2086 cm^{-1} [26]. Also the peak at 1630 cm^{-1} is assignable to C=N (azomethine) stretching frequency [Fig. 5.18].

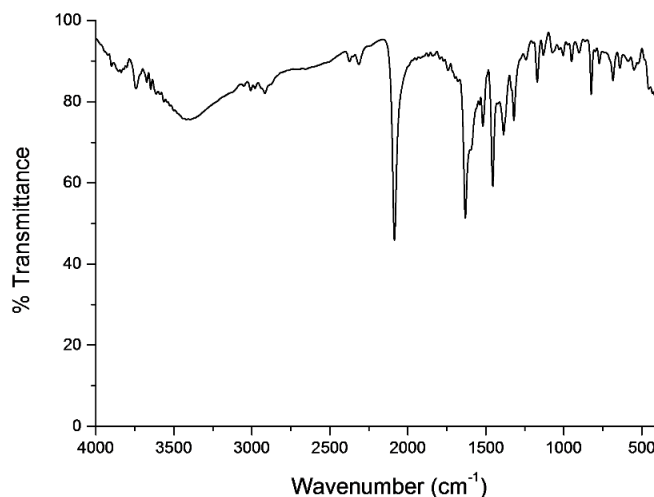


Fig. 5.18. IR spectrum of $[\text{Cu}(\text{L}^7)(\text{NCS})]$.

The effect of solvents on the spectral properties of the complex was investigated by choosing the same set of solvents (on the basis of polarity) as described earlier in Sec. 5.3.2.2. The trend was almost similar as seen for earlier cases with a general hypsochromic effect, with rise in solvent polarity [Fig. 5.19, Table 5.20].

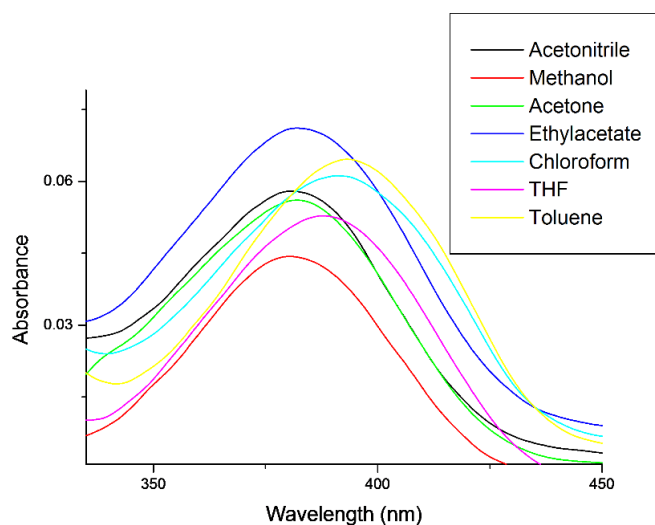


Fig. 5.19. Spectra showing the solvatochromic effect on the charge-transfer transitions of the complexes, con: 1×10^{-3} M).

Table 5.20. The λ_{\max} (nm) values along with their ϵ ($M^{-1}cm^{-1}$) in various solvents

| Polarity Index* | Solvents | Complex 14 | |
|-----------------|-----------------|-----------------------|--|
| | | λ_{\max} (nm) | $\epsilon \times 10^3$ ($M^{-1}cm^{-1}$) |
| 5.1 | Methanol | 382 | 3.60 |
| | | 209 | 62.62 |
| 5.8 | Acetonitrile | 379 | 4.71 |
| | | 229 | 39.01 |
| 5.1 | Acetone | 382 | 4.57 |
| 4.4 | Ethylacetate | 381 | 5.73 |
| 4.0 | Tetrahydrofuran | 388 | 4.22 |
| 4.1 | Chloroform | 393 | 4.95 |
| 2.4 | Toluene | 388 | 5.21 |

*Relative measure of degree of interaction of the solvents with various polar test solutes

The solvent effect is also studied for the *d-d* bands of the complexes and unlike the case of CT bands, here a red shift is observed with rise in donor number of the solvents. The shift is considerable and it reflects the change in the coordination geometry of the complex species due to axial solvation. The strength of solvation in turn depends on the donor number of the solvent [Fig. 5.20, Table 5.21].

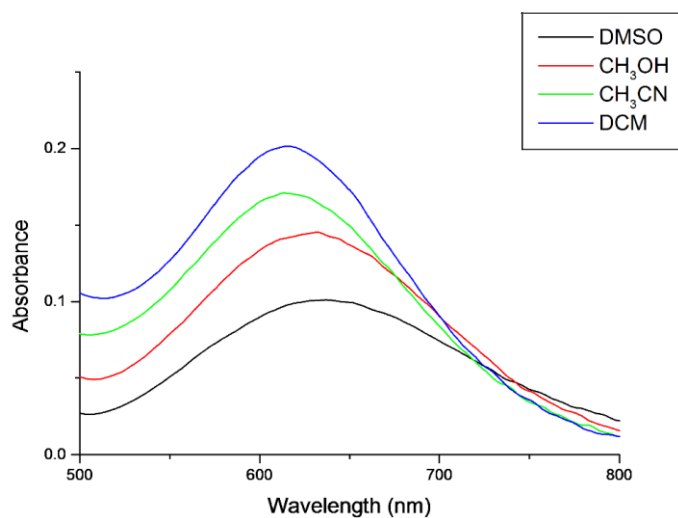


Fig. 5.20. Spectra showing the solvatochromic effect on the *d-d* transitions of the complexes, con: $2 \cdot 10^{-3}$ M).

Table 5.21. The λ_{\max} (nm) values along with their ϵ ($M^{-1}cm^{-1}$) of *d-d* bands in various solvents

| Solvents | Donor number of solvents (DN) | Complex 14 | |
|--------------|-------------------------------|-----------------------|--------------------------------|
| | | λ_{\max} (nm) | ϵ ($M^{-1}cm^{-1}$) |
| DMSO | 29.8 | 636 | 163 |
| Methanol | 19.0 | 632 | 231 |
| Acetonitrile | 14.1 | 618 | 275 |
| DCM | 0.0 | 615 | 320 |

5.5.2. Description of the crystal structure

The non-hydrogen atoms of the complex were refined anisotropically and all H atoms on C were placed in calculated positions guided by difference maps with C–H bond distances 0.93-0.97 Å. The H atoms were assigned as $U_{\text{iso}}=1.2U_{\text{eq}}$ (1.5 for Me). Complex **14** possess a crystallographic mirror symmetry with all the atoms lying on a mirror plane and hence enjoys an occupancy factor of 0.50 (special position constraint). The C9 atom was disordered about a special position [8].

The monomeric thiocyanato complex crystallizes in orthorhombic crystal system with $Pnma$ space group. Asymmetric unit shows a square planar geometry for the crystal structure, satisfied by the NNO tridentate Schiff base along with the N of the thiocyanato group [Fig. 5.21]. Refinement details are given in Table 5.22. Chosen dimensions are enlisted in Table 5.23.

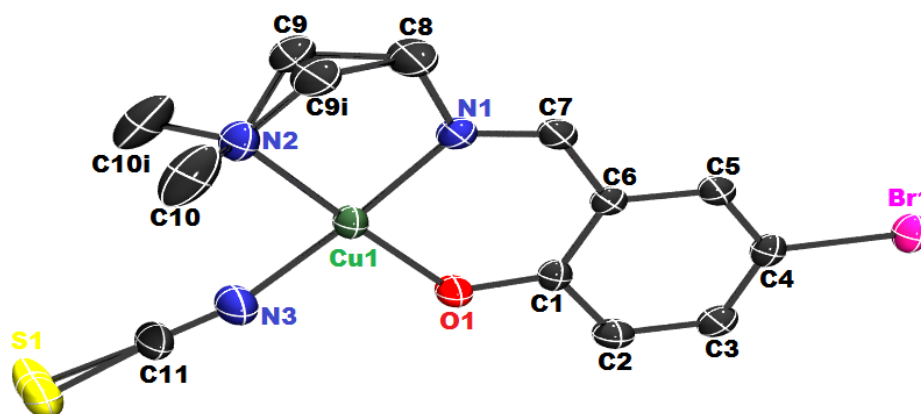


Fig. 5.21. ORTEP diagram showing the atom labelling of the asymmetric unit of the complex **14** (drawn with 30% ellipsoid probability and the hydrogen atoms are omitted for clarity).

Table 5.22. Crystal data and refinement details of complex **14**

| Parameters | Complex 14 |
|-----------------------------------|--|
| Empirical formula | C ₁₂ H ₁₃ BrCuN ₃ OS |
| Formula weight | 390.77 |
| Temperature | 293(2) K |
| Wavelength | 0.71073 Å |
| Crystal system | Orthorhombic |
| Space group | <i>Pnma</i> |
| Unit cell dimensions | a = 19.2249(13) Å α = 90° b = 6.8307(4) Å β = 90° c = 11.3255(8) Å γ = 90° |
| Volume | 1487.26(17) Å ³ |
| Z | 2 |
| Density (calculated) | 1.745 Mg m ⁻³ |
| Absorption coefficient | 4.290 mm ⁻¹ |
| <i>F</i> (000) | 776 |
| Crystal size | 0.30 × 0.20 × 0.15 mm ³ |
| θ range for data collection | 2.78 to 28.25° |
| Limiting indices | -25 ≤ h ≤ 22, -8 ≤ k ≤ 8, -13 ≤ l ≤ 15 |
| Reflections collected | 10921 |
| Unique reflections | 1985 [R(int) = 0.0366] |
| Refinement method | Full-matrix least-squares on F ² |
| Data / restraints / parameters | 1962 / 0 / 119 |
| Goodness-of-fit on F ² | 1.050 |
| Final R indices [I > 2σ(I)] | R ₁ = 0.0343, wR ₂ = 0.0773 |
| R indices (all data) | R ₁ = 0.0581, wR ₂ = 0.0865 |
| Largest diff. peak and hole | 0.407 and -0.690 e.Å ⁻³ |

$$R_1 = \frac{\sum ||F_o| - |F_c||}{\sum |F_o|}$$

$$wR_2 = [\sum w(F_o^2 - F_c^2)^2 / \sum w(F_o^2)^2]^{1/2}$$

Table 5.23. Selected bond lengths (Å) and bond angles (°) for complex **14**

| Bond lengths (Å) | | Bond angles (°) | |
|------------------|----------|-----------------|------------|
| Cu(1)–O(1) | 1.903(2) | O(1)–Cu(1)–N(1) | 93.01(13) |
| Cu(1)–N(1) | 1.918(3) | O(1)–Cu(1)–N(3) | 91.34(13) |
| Cu(1)–N(3) | 1.926(4) | N(3)–Cu(1)–N(2) | 90.82(15) |
| Cu(1)–N(2) | 2.059(3) | N(1)–Cu(1)–N(2) | 84.83(14) |
| N(1)–C(7) | 1.278(5) | N(1)–Cu(1)–N(3) | 175.65(15) |
| N(3)–C(11) | 1.138(5) | O(1)–Cu(1)–N(2) | 177.84(13) |
| C(11)–S(1) | 1.622(5) | N(3)–C(11)–S(1) | 172.2(5) |

The least squares plane calculation produces surprising result with no deviation for the chelating atoms. The *trans* angles also doesn't aberrate much from their ideality, as mirrored in the τ_4 value of 0.0461 [8]. The *cisoid* bite angles subtended at the central atom by the donor atoms add up to a total of 359.99° substantiating the not so distorted geometry of the complex. The coligand, with N–C–S bond angle of $172.2(5)^\circ$ underscores the deviation from linearity. Bond strength follows the same order as that seen for a similar monomeric thiocyanato system and is compared in the Table 5.24. Juxtaposing both, we have the metal-donor bond lengths to be a bit smaller for the complex with bromo substituent.

Table 5.24. Comparative analysis of the monomeric thiocyanato complexes **12** and **14**

| Bonds | Distance in Å (Complex 12) | Distance in Å (Complex 14) |
|--------------------------------|-------------------------------|-------------------------------|
| Cu1–O1 (phenoxo) | 1.905(2) | 1.903(2) |
| Cu1–N1 (imino) | 1.922(2) | 1.918(3) |
| Cu1–N3 (cyanato)/(thiocyanato) | 1.929(3) | 1.926(4) |
| Cu1–N2 (amino) | 2.067(3) | 2.059(3) |

The coordination imposes a five membered and six membered metallocycles, Cg(2) and Cg(4) – of which the Cg(2) ring [Cu1/N1/C8/C9/N2] assumes an

envelope conformation with C9 as the flap atom and puckering amplitudes, $Q = 0.382(5)$ and $\Phi = 295.4(5)^\circ$. The disordered counterpart of the above ring, Cg(3) also adopts envelope conformation with $Q = 0.382(5)$ and $\Phi = 115.4(5)^\circ$.

5.5.2.1. Structural adhesives

Unlike the complex with chloro substituent, this complex has a hydrogen bonding interaction, C(10)–H(10B)⋯Br1 which actually creates a supramolecular chain along ‘*b*’ axis [Fig. 5.22, Table 5.25].

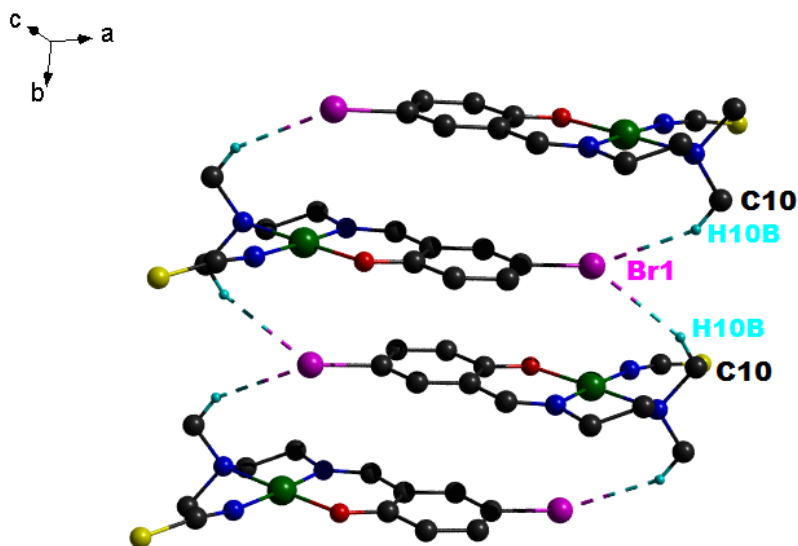


Fig. 5.22. Hydrogen bonding interaction creating a supramolecular chain along ‘*b*’ axis.

Table 5.25. Non-conventional hydrogen bonding interactions in the complex **14**

| D–H⋯A | D–H (Å) | H⋯A (Å) | D⋯A (Å) | D–H⋯A (°) |
|--|---------|---------|----------|-----------|
| Intermolecular hydrogen bonding | | | | |
| C(10)–H(10B)⋯Br(1) ^a | 0.96 | 2.90 | 3.742(4) | 147 |

Equivalent position code: $a = 1 - x, -1/2 + y, 1 - z$

The bromine atom is also involved in a ring interaction, bringing out its electrophilic nature [Fig. 5.23, Table 5.26].

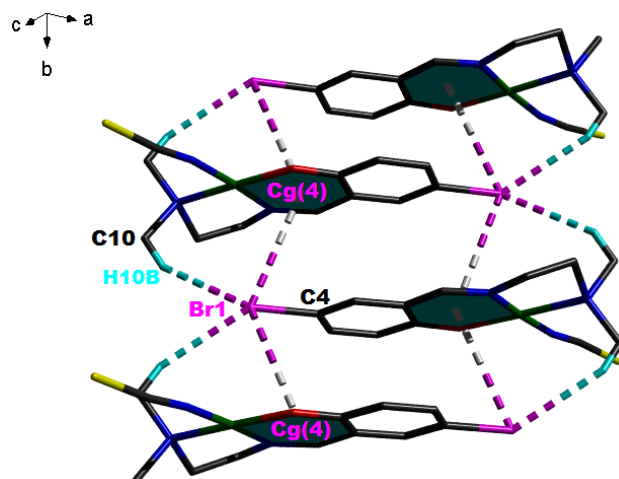


Fig. 5.23. Bromine atom involved in ring interaction.

Table 5.26. C–X...Cg interactions

| C–X...Cg | X...Cg (Å) | C...Cg (Å) | C–X...Cg (°) |
|---------------------------------|------------|------------|--------------|
| C(4)–Br(1)...Cg(4) ^b | 3.6837(6) | 3.4851(8) | 68.91(2) |

Equivalent position codes: b = 1 - x, -1/2 + y, 1 - z

Aromatic ring interactions also enhances the packing stability [Fig. 5.24, Table 5.27].

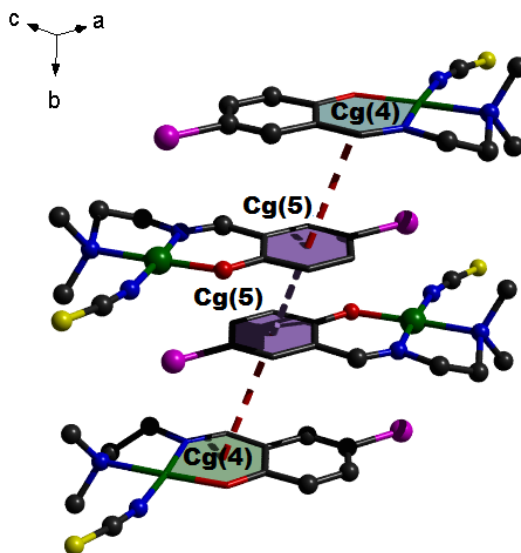


Fig. 5.24. Cg...Cg ring interactions.

Table 5.27. Short ring interactions

| Cg(I)⋯Cg(J) | Cg(I)⋯Cg(J) (Å) | γ(°) |
|--------------------------|------------------------|-------------|
| Cg(4)⋯Cg(5) ^c | 3.9531(10) | 30.2 |
| Cg(5)⋯Cg(4) ^c | 3.9530(10) | 30.2 |
| Cg(5)⋯Cg(5) ^c | 3.8025(9) | 26.1 |

Equivalent position code: $c = 1 - x, -1/2 + y, 1 - z$

Cg, centroid

Cg(4) = Cu(1), O(1), C(1), C(6), C(7), N(1)

Cg(5) = C(1), C(2), C(3), C(4), C(5), C(6)

Cg(I) = Center of gravity of ring I

Cg(J) = Center of gravity of ring J (Plane number above)

γ = Angle Cg(I)⋯Cg(J) vector and normal to plane J (°)

Cg(I)⋯Cg(J) = Distance of Cg(I) to Cg(J) (Å)

5.5.3. Photoluminescence study

The complex showed an emission at 428 nm (violet region) when excited at 378 nm [Fig. 5.25].

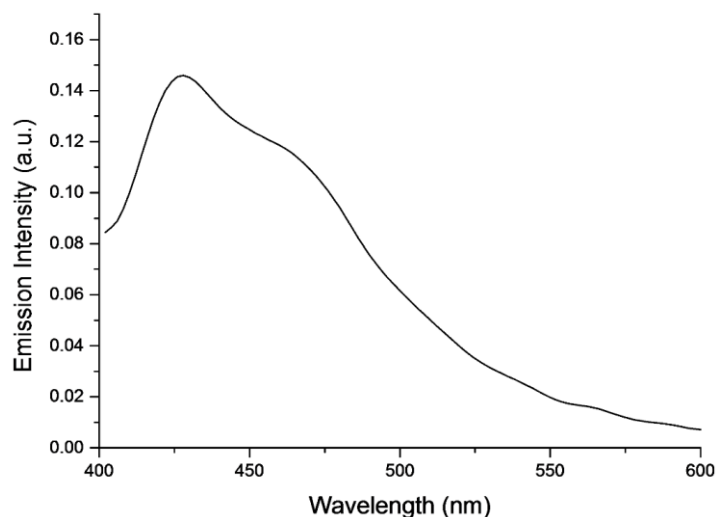


Fig. 5.25. Fluorescence spectra of complex **14** (acetonitrile, con: 1×10^{-3} M).

5.5.4. Thermal study

The thiocyanato species loses a molecule of nitrogen (6.70%, calcd. 7.16%) in the temperature range 234- 242 °C after which a gradual thermal decomposition pattern is witnessed [Fig. 5.26]. The observed single stage degradation process is endothermic. This complex is found to be more stable when compared with similar complex having chloride as the substituent.

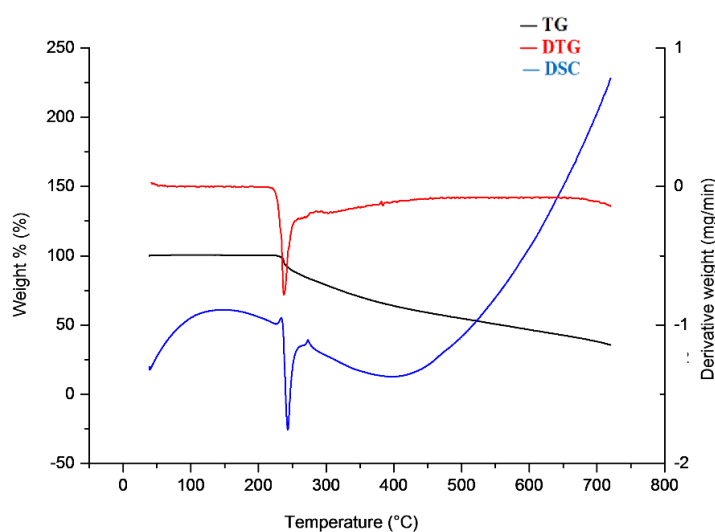


Fig. 5.26. Thermogram of complex 14.

5.5.5. EPR spectral study

The polycrystalline state revealed an axial spectra with $g_{\parallel} = 2.200$ and $g_{\perp} = 2.051$. The value of G is slightly higher than 4 ruling out the possibility of an exchange interaction. In frozen DMF, we witness only three resolved hyperfine splittings with the fourth one being merged with the high intense perpendicular region. The peaks in the parallel region are split with a hyperfine splitting constant of $210 \times 10^{-4} \text{ cm}^{-1}$ whilst no such splittings are observed in the perpendicular region [Fig. 5.27].

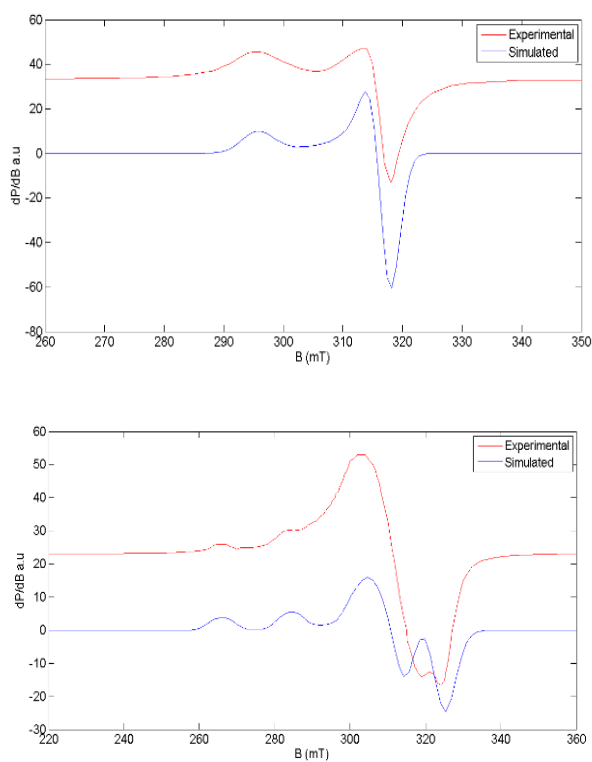


Fig. 5.27. EPR spectra of complex **14** in polycrystalline state (top) and in DMF at 77 K (bottom).

The values of the bonding parameters and the orbital reduction factors are supportive for the covalent nature of the M–L bond [Table 5.28].

Table 5.28. Spin Hamiltonian and bonding parameters of copper(II) complexes

| Compounds | Polycrystalline state (298 K) | | | | | | DMF solution (77 K) | | | | | | | |
|---------------------------------|-------------------------------|-------------|--------|--------------------|---------------------|----------|---------------------|-------------|------------|-----------|------------|-----------------|-------------|-----|
| | g_{\parallel} | g_{\perp} | G | $g_{\parallel}g_3$ | $g_{\perp}g_1, g_2$ | g_{av} | A_{\parallel} | A_{\perp} | α^2 | β^2 | γ^2 | K_{\parallel} | K_{\perp} | f |
| [Cu(L ₆)(NCS)] (14) | 2.200 | 2.051 | 4.0595 | 2.215 | 2.079 | 2.124 | 210 | -- | 0.8680 | 0.8185 | 0.9832 | 0.7105 | 0.8534 | 106 |

A values in 10^{-4} cm^{-1}

Section C

5.6. Experimental

5.6.1. Synthesis of $[\text{Cu}(\text{L}^8)(\text{N}_3)]_n$ (**15**)/ $[\text{Cu}(\text{L}^8)(\text{NCS})]_n$ (**16**)

$[\text{HL}^8 = 2\text{-}((2\text{-}(\text{dimethylamino})\text{ethylimino})\text{methyl})\text{-6-fluorophenol}]$

To the reaction mixture prepared *in situ* by refluxing *N,N*-dimethylethylenediamine and 3-fluorosalicylaldehyde for 2 h (1:1), copper(II) nitrate trihydrate (0.241 g, 1 mmol) was added and refluxed for half an hour. To the resulting solution, aq. solution of sodium azide in methanol (0.130 g, 2 mmol) was added and heated for about 2 h. The crystalline precipitate obtained was recrystallized from DMSO solution to isolate green block crystals of complex **15**.

The procedure was replicated exactly for the preparation of complex **16** except for the addition of ammonium thiocyanate (0.152 g, 2 mmol). Here also, we could isolate quality single crystals by recrystallization from DMSO.

Complex **15**:

Yield: 0.1951 g (62%). *Anal.* Calc. for $\text{C}_{11}\text{H}_{14}\text{CuFN}_5\text{O}$: C, 41.97; H, 4.48; N, 22.25. Found: C, 41.95; H, 4.47; N, 22.27.

Complex **16**:

Yield: 0.2242 g (65%). *Anal.* Calc. for $\text{C}_{12}\text{H}_{14}\text{CuFN}_3\text{OS}$: C, 45.27; H, 4.68; N, 12.18. Found: C, 45.30; H, 4.65; N, 12.17.

5.6.2. Synthesis of $[\text{Cu}(\text{L}^9)(\text{N}_3)]_n$ (**17**)

$[\text{HL}^9 = \text{N}'\text{-}((3\text{-fluoropyridin-2-yl})\text{methylene})\text{carbamo}(\text{hydrazonic acid})]$

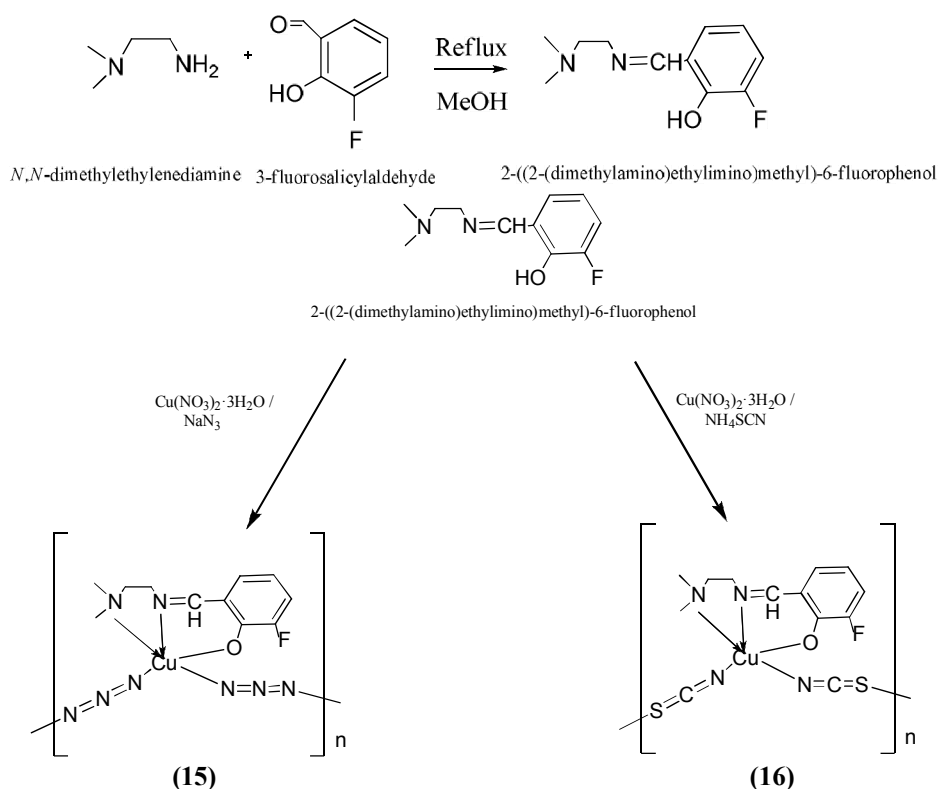
Methanolic solution of 3-fluoropyridine-2-carbaldehyde (0.125 g, 1 mmol) was refluxed with semicarbazide hydrochloride (0.120 g, 1 mmol) for about 2 h. To this solution, a copper(II) chloride dihydrate dissolved in methanolic

solution was added and refluxed for 30 minutes. Then methanol-water (10:1) solution of sodium azide (0.130 g, 2 mmol) was added and refluxed for another 2 h. The green solution thus obtained was kept aside at room temperature. After few days, single crystals suitable for X-ray diffraction were obtained on slow evaporation of the mother liquor.

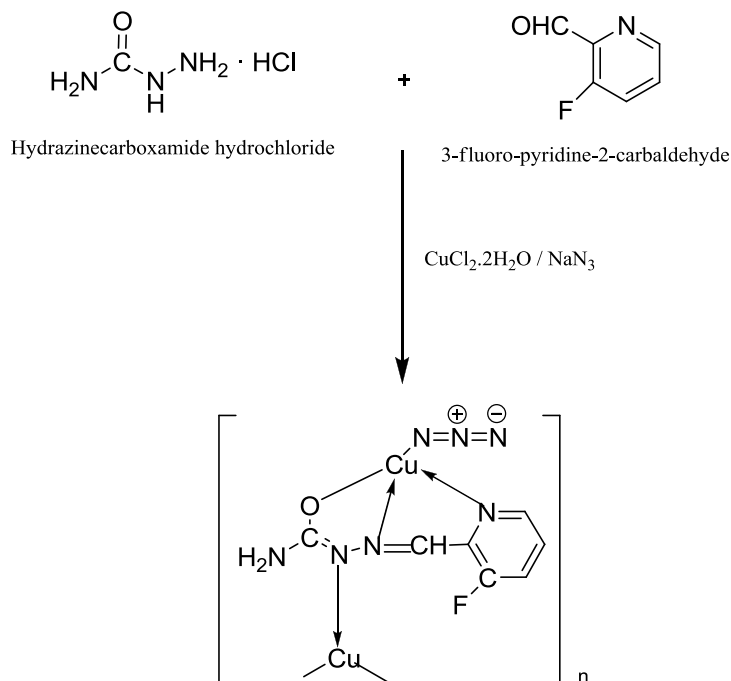
Yield: 0.1497 g (52%). *Anal.* Calc. for $C_7H_7CuFN_7O$: C, 29.12; H, 2.79; N, 33.96. Found: C, 29.15; H, 2.74, N 33.98.

5.7. Results and discussion

The schematic representation for the synthesis of the complexes are as shown below [Scheme 5.5 and 5.6].



Scheme 5.5. Synthetic route to complexes 15 and 16.



Scheme 5.6. Synthetic route to complex **17**.

5.7.1. Spectral features

5.7.1.1. IR and linear optical response

The peaks at 1620, 1542 and 1591 cm^{-1} respectively stands for the azomethine bond formation in complexes **15**, **16** and **17** [27]. The *end-to-end* azide functional group in complex **15** is evidenced by the peak at 2039 cm^{-1} [28] and the $\mu_{1,3}$ thiocyanate is featured by a sharp intense peak at 2093 cm^{-1} . The complex **17** shows a peak at 2054 cm^{-1} consistent with the presence of terminally coordinated azido group. It is additionally characterized by the presence of keto group at 1637 cm^{-1} , free amino group at 3491 and 3376 cm^{-1} [29]. IR spectra of the complexes are given in Fig. 5.28.

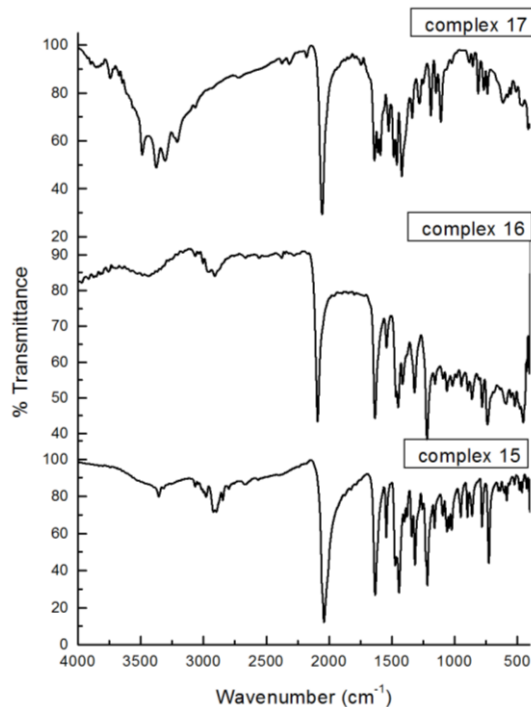


Fig. 5.28. IR spectra of the complexes **15**, **16** and **17**.

The linear electronic response was recorded in acetonitrile medium in the range 200-1000 nm. Both high energy CT bands as well as metal-based low energy transitions were found in the spectra. The high intense bands with ϵ values > 3000 was found in the wavelength, $\lambda < 400$ nm consistent with ligand to metal charge transfer transitions. Still higher ϵ values were found for ligand based transitions. The metal based transitions, being forbidden transitions have lower extinction coefficients and correspond to a square-based environment for complexes **15** and **16** ($d_{x^2-y^2} \rightarrow d_{xz}$, d_{yz} , $d_{x^2-y^2} \rightarrow d_{z^2}$). However, we could not locate $d-d$ bands in acetonitrile and DCM for complex **17** and this may be due to masking by high energy CT bands [30,31].

5.7.1.2. Solvatochromic studies

The compounds were all readily soluble in organic solvents which made their solvatochromic study pretty easy. Solvents of different polarity were

chosen so as to deduce their effect on the chelate complexes. Solvents do affect the topology of the complexes and that is observed as negative solvatochromic effect for high energy transitions and as positive effect for the metal based transitions.

All the three complexes under investigation are polymeric in nature. As discussed earlier, they lose their polymeric identity when dissolved and exist as monomeric species. The complexes (in general) showed up a decrease in λ_{max} value with rise in polarity which is due to the solvent induced stabilization of ground state when compared to that of the excited state. The λ_{max} (nm) along with their ϵ ($\text{M}^{-1}\text{cm}^{-1}$) values in various solvents are tabulated [Fig. 5.29, Table 5.29].

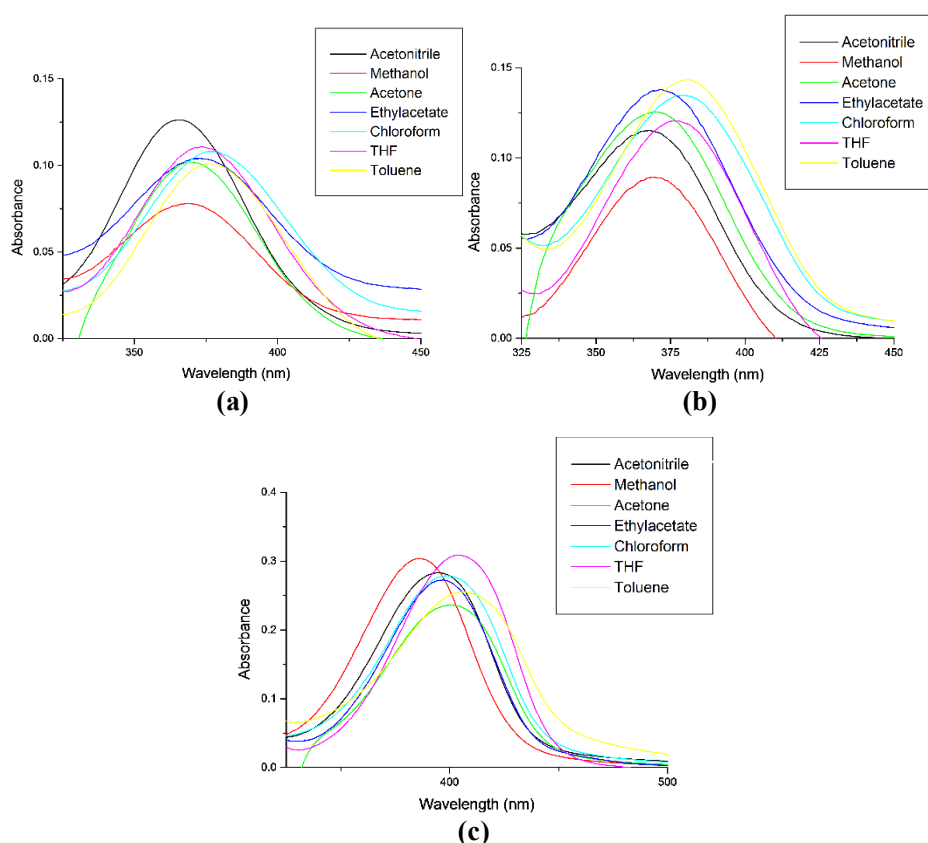


Fig. 5.29. The spectra showing solvatochromic behavior of CT transitions (con: 1×10^{-3} M) of complexes in various solvents.

Table 5.29. The λ_{\max} (nm) along with their ε ($M^{-1}cm^{-1}$) values of complexes in various solvents

| Polarity Index* | Solvents | Complex 15 | | Complex 16 | | Complex 17 | |
|-----------------|-----------------|-----------------------|----------------------|-----------------------|----------------------|-----------------------|----------------------|
| | | λ_{\max} (nm) | $\varepsilon * 10^3$ | λ_{\max} (nm) | $\varepsilon * 10^3$ | λ_{\max} (nm) | $\varepsilon * 10^3$ |
| | | $(M^{-1}cm^{-1})$ | | $(M^{-1}cm^{-1})$ | | $(M^{-1}cm^{-1})$ | |
| 5.1 | Methanol | 369 | 4.08 | 369 | 2.71 | 386 | 8.73 |
| | | 269 | 16.48 | 269 | 16.39 | 249 | 7.49 |
| | | 219 | 24.28 | | | 207 | 26.62 |
| 5.8 | Acetonitrile | 365 | 13.08 | 368 | 3.49 | 395 | 8.13 |
| | | 267 | 33.88 | 234 | 18.40 | 251 | 6.66 |
| | | 228 | 58.79 | | | | |
| 5.1 | Acetone | 369 | 5.32 | 370 | 3.80 | 400 | 6.78 |
| 4.4 | Ethylacetate | 373 | 5.44 | 372 | 4.18 | 397 | 7.82 |
| | | 270 | 17.88 | 269 | 16.84 | 269 | 16.84 |
| 4.0 | Tetrahydrofuran | 373 | 5.80 | 376 | 3.65 | 403 | 8.80 |
| | | 241 | 15.58 | 267 | 11.48 | 261 | 33.42 |
| 4.1 | Chloroform | 378 | 5.65 | 379 | 4.08 | 399 | 8.00 |
| | | 283 | 10.20 | 284 | 11.62 | 256 | 8.66 |
| 2.4 | Toluene | 376 | 5.29 | 381 | 4.34 | 406 | 7.32 |
| | | 273 | 16.13 | | | | |

*Relative measure of degree of interaction of the solvents with various polar test solutes

Similar to all other complexes, the solvents do affect the ligand-field spectra and it was appreciable when compared to CT spectra. The net stabilization/destabilization of the energy levels as a result of the solute-solvent interaction appears as the small shift in the intramolecular/CT transitions. On the contrary, the solvents take up the role of a protagonist in influencing the $d-d$ spectra. Solvents position themselves in such a fashion that it becomes a part of the chelate complex and contributes to the splitting of the d levels of the metal ion [Fig. 5.30, Table 5.30].

Four solvents of varying donor powers – DMSO, Methanol, acetonitrile and DCM are chosen for our study. With increase in donor power of solvents, a rise in λ_{\max} (nm) values are seen and as expected the molar extinction values are less than 400, indicative of the forbidden transitions.

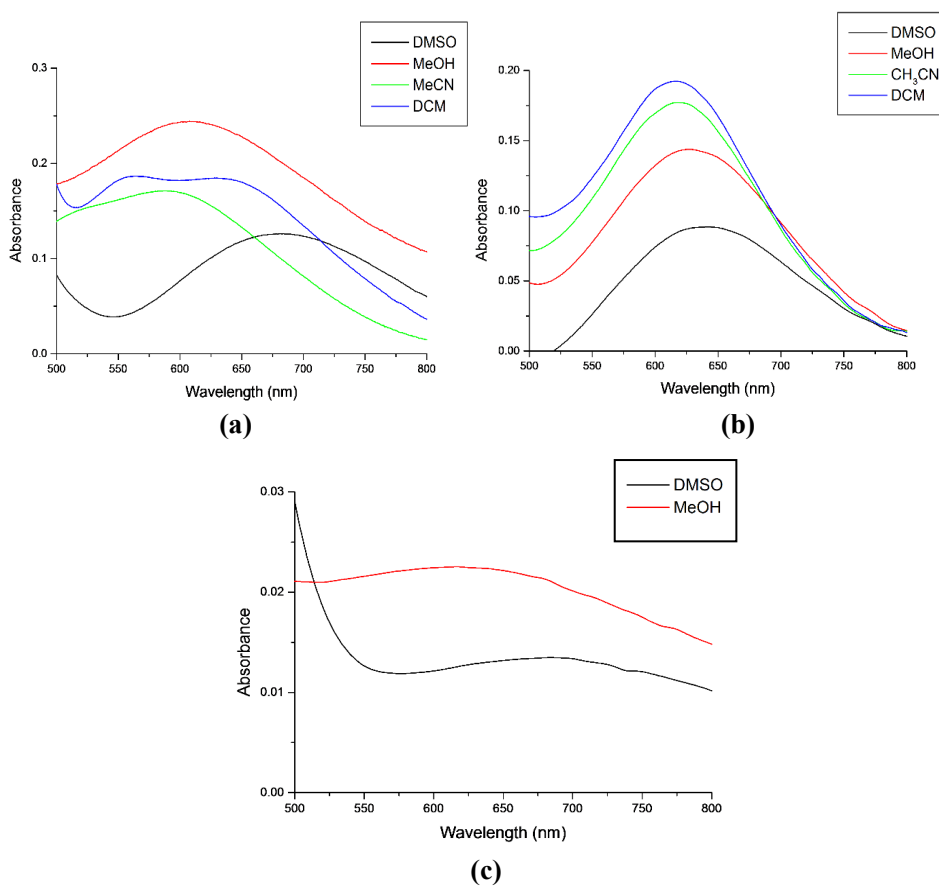


Fig. 5.30. The spectra showing solvatochromic behavior of CT transitions (con: 1×10^{-3} M) of complexes in various solvents.

Table 5.30. The λ_{\max} (nm) values along with their ϵ ($M^{-1}cm^{-1}$) of *d-d* bands in various solvents

| Solvents | Donor number of solvents (DN) | Complex 15 | | Complex 16 | | Complex 17 | |
|--------------|-------------------------------|-----------------------|--------------------------------|-----------------------|--------------------------------|-----------------------|--------------------------------|
| | | λ_{\max} (nm) | ϵ ($M^{-1}cm^{-1}$) | λ_{\max} (nm) | ϵ ($M^{-1}cm^{-1}$) | λ_{\max} (nm) | ϵ ($M^{-1}cm^{-1}$) |
| DMSO | 29.8 | 684 | 186 | 635 | 66 | 684 | 48 |
| Methanol | 19.0 | 608 | 359 | 631 | 84 | 617 | 131 |
| Acetonitrile | 14.1 | 593 | 251 | 622 | 104 | | |
| DCM | 0.0 | 563 | 275 | 630 | 272 | | |

5.7.2. Description of crystal structures

5.7.2.1. $[Cu(L_8)(N_3)]_n$ (15)

The asymmetric unit of the complex contains two crystallographically independent molecules with both of them having square planar geometry [Fig. 5.31]. Crystallographic refinement details and geometrical parameters are enlisted in Table 5.31.

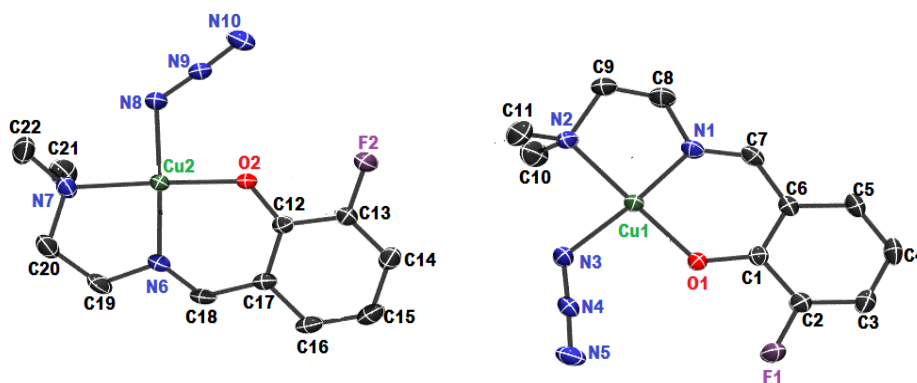


Fig. 5.31. ORTEP diagram showing the atom labelling of the asymmetric unit of the complex **15** (drawn with 30% ellipsoid probability and the hydrogen atoms are omitted for clarity).

Table 5.31. Crystal data and refinement details of complex **15**

| Parameters | Complex 15 |
|-----------------------------------|--|
| Empirical formula | C ₂₂ H ₂₈ N ₁₀ O ₂ F ₂ Cu ₂ |
| Formula weight | 629.64 |
| Temperature | 293(2) K |
| Wavelength | 0.71073 Å |
| Crystal system | Monoclinic |
| Space group | <i>P</i> 2 ₁ / <i>c</i> |
| Unit cell dimensions | a = 21.2989(14) Å α = 90° b = 6.8191(3) Å β = 117.180(2)° c = 19.6523(9) Å γ = 90° |
| Volume | 2539.1(2) Å ³ |
| Z | 4 |
| Density (calculated) | 1.647 Mg m ⁻³ |
| Absorption coefficient | 1.732 mm ⁻¹ |
| <i>F</i> (000) | 1288 |
| Crystal size | 0.35 × 0.30 × 0.25 mm ³ |
| θ range for data collection | 1.07 to 28.30° |
| Limiting indices | -26 ≤ h ≤ 28, -9 ≤ k ≤ 9, -25 ≤ l ≤ 26 |
| Reflections collected | 19226 |
| Unique reflections | 6309 [R(int) = 0.0385] |
| Refinement method | Full-matrix least-squares on F ² |
| Data / restraints / parameters | 6298 / 0 / 347 |
| Goodness-of-fit on F ² | 0.976 |
| Final R indices [I > 2σ(I)] | R ₁ = 0.0358, wR ₂ = 0.0799 |
| R indices (all data) | R ₁ = 0.0631, wR ₂ = 0.0910 |
| Largest diff. peak and hole | 0.346 and -0.476 e.Å ⁻³ |

$$R_1 = \frac{\sum ||F_o| - |F_c||}{\sum |F_o|}$$

$$wR_2 = \left[\frac{\sum w(F_o^2 - F_c^2)^2}{\sum w(F_o^2)^2} \right]^{1/2}$$

The ambidenticity of the azido ligand is evident from the flexible coordination modes adopted by it – one end of the azido ligand occupies the equatorial plane while the other end in the axial position, thereby a $\mu_{1,3}$ *end-on* bridging is observed [Fig. 5.32]. In effect, a coordination polymer is formed with totally asymmetric environment, with four different Cu–N bond lengths [Cu1–N3 = 1.972(2) Å, Cu1–N10 = 2.805(3) Å & Cu2–N8 = 1.968(3) Å, Cu2–N5 = 2.748(2) Å] and each metal centre disposing in a square pyramidal geometry [Table 5.32].

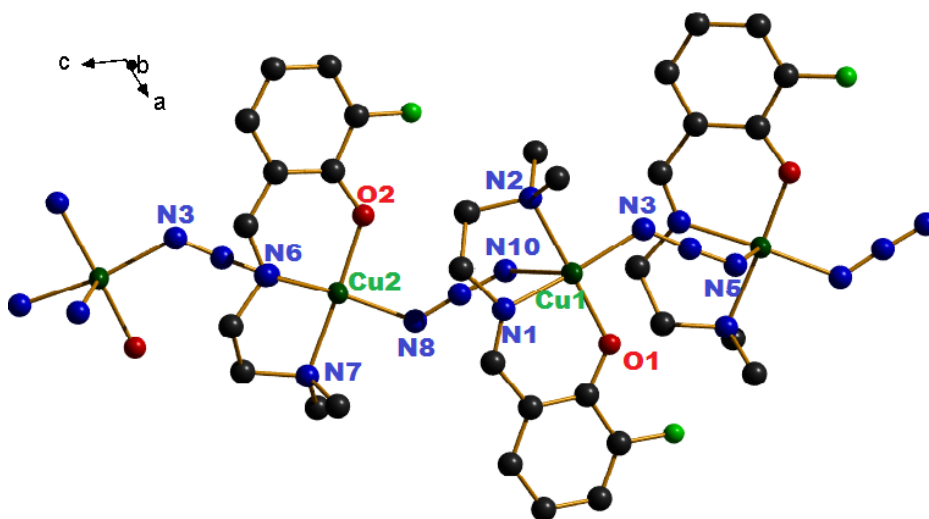


Fig. 5.32. Perspective view of the complex 15.

The Addison parameter, τ computed for Cu1 and Cu2 are, $\tau_1 = 0.15$ and $\tau_2 = 0.18$ respectively reflecting the slightly higher deviations in the *transoid* angles around Cu2 centre. The *cisoid* bond angles subtended at the metal centre by the donor atoms in the basal plane totals to a value of 359.4° around Cu1 and 360.0° around Cu2. The least squares plane calculation reveals the Cu1 centre to have a deviation of 0.0077 below the plane while the Cu2 centre deviates only by 0.0062 Å. Except for the trigonality index value, the other parameters like bond angle summation and the least square plane calculations are supportive of the greater perturbation around Cu1.

Table 5.32. Selected bond lengths (Å) and bond angles (°) for **15**

| Bond angles (°) | | | |
|-------------------------|------------|------------------|------------|
| O(1)–Cu(1)–N(1) | 93.51(9) | N(6)–Cu(2)–O(2) | 93.19(9) |
| O(1)–Cu(1)–N(3) | 92.30(18) | O(2)–Cu(2)–N(8) | 92.36(9) |
| N(1)–Cu(1)–N(2) | 84.21(10) | N(8)–Cu(2)–N(7) | 89.86(10) |
| N(2)–Cu(1)–N(3) | 89.38(10) | N(7)–Cu(2)–N(6) | 84.59(10) |
| N(1)–Cu(1)–N(10) | 86.62(8) | N(5c)–Cu(2)–N(6) | 83.58(8) |
| N(10)–Cu(1)–N(2) | 86.97(9) | N(5c)–Cu(2)–O(2) | 91.42(7) |
| N(1)–Cu(1)–N(3) | 167.24(10) | N(5c)–Cu(2)–N(8) | 108.25(10) |
| O(1)–Cu(1)–N(2) | 176.35(7) | N(5)–Cu(2)–N(7) | 88.15(8) |
| N(10)–Cu(1)–N(3) | 104.09(9) | N(6)–Cu(2)–N(8) | 166.81(10) |
| N(10)–Cu(1)–O(1) | 95.76(9) | N(7)–Cu(2)–O(2) | 177.77(9) |
| N(10)–N(9)–N(8) | 176.9(4) | N(5)–N(4)–N(3) | 177.0(3) |
| Cu(1)–N(3)–N(4) | 126.1(2) | Cu(2)–N(8)–N(9) | 125.9(2) |
| Cu(1b)–N(10)–N(9) | 116.68(19) | Cu(2c)–N(5)–N(4) | 114.03(17) |
| N(3)–Cu(1)–N(10a) | 104.09(9) | N(8)–Cu(2)–N(5c) | 108.25(10) |
| Bond lengths (Å) | | | |
| Cu(1)–O(1) | 1.898(2) | Cu(2)–O(2) | 1.8993(18) |
| Cu(1)–N(1) | 1.949(2) | Cu(2)–N(7) | 2.052(2) |
| Cu(1)–N(2) | 2.052(3) | Cu(2)–N(6) | 1.949(2) |
| Cu(1)–N(3) | 1.972(2) | Cu(2)–N(5c) | 2.748(2) |
| Cu(1)–N(10a) | 2.805(3) | Cu(2)–N(8) | 1.968(3) |
| F(1)–C(2) | 1.365(3) | F(2)–C(13) | 1.365(3) |
| N(1)–C(8) | 1.459(5) | N(6)–C(18) | 1.267(4) |
| N(1)–C(7) | 1.270(3) | N(6)–C(19) | 1.467(3) |
| N(3)–N(4) | 1.186(4) | N(8)–N(9) | 1.183(3) |
| N(4)–N(5) | 1.151(4) | N(9)–N(10) | 1.152(3) |

The packing index value is 70.1% [12]. The five membered metallocycles, Cg(1) and Cg(2) [Cg(1) – Cu1/N1/C8/C9/N2 & Cg(2) – Cu2/N6/C19/C20/N7] assumes envelope conformation with C(9) and C(20) as flap atoms. The conformation has puckering amplitudes of $Q = 0.4(3)$ Å, $\phi = 109.0(3)^\circ$ and $Q = 0.399(3)$ Å, $\phi = 287.3(3)^\circ$ respectively. About the metal atoms Cu1 and Cu2, the bond strength order is the same with metal–phenoxo > metal–imino nitrogen > metal–azido nitrogen (basal) > metal–amino nitrogen > metal–azido

nitrogen (axial). The *end-to-end* azido coligand maintains its pseudolinearity with bond angles of $176.9(4)^\circ$ and $177.0(3)^\circ$ respectively.

Interplay of non-covalent forces

The nitrogen atoms, N(3) and N(8) of the azido group acts as hydrogen bond acceptors of the C(11) and C(22) thereby forming intramolecular S(5) ring motif. There are two interchain intermolecular interactions; one between H(9A) atom borne by C(9) and the phenolate oxygen, O(2) with H \cdots O distance of 2.48 Å and the other between H(19A) and one of the azido nitrogens, N(10) with a distance of 2.57 Å units. All these interactions run along the same direction as that of the pseudohalide, thereby reinforcing the packing [Fig. 5.33, Table 5.33]. The ring-ring interactions present in the complex are given in Table 5.34.

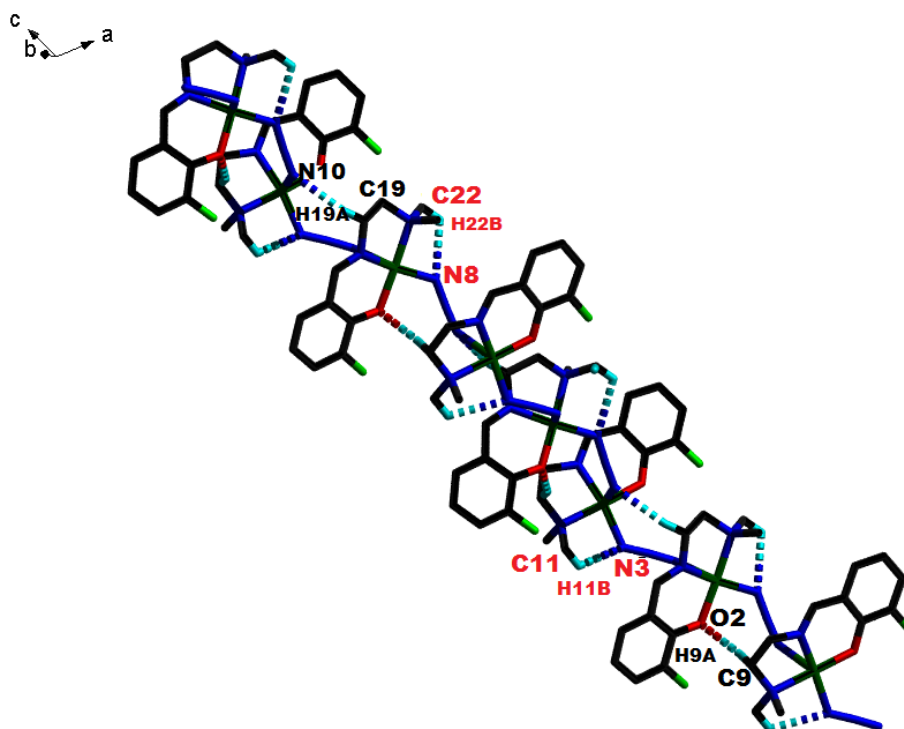


Fig. 5.33. Hydrogen bonding interactions in complex 15.

Table 5.33. Non-conventional hydrogen bonding interactions in complex **15**

| D–H⋯A | D–H (Å) | H⋯A (Å) | D⋯A (Å) | D–H⋯A (°) |
|--|---------|---------|----------|-----------|
| Intermolecular hydrogen bonding | | | | |
| C(9)–H(9A)⋯O(2) ^a | 0.97 | 2.48 | 3.388(3) | 156 |
| C(19)–H(19A)⋯N(10) ^b | 0.97 | 2.57 | 3.514(4) | 164 |
| Intramolecular hydrogen bonding | | | | |
| C(11)–H(11B)⋯N(3) | 0.96 | 2.53 | 3.039(4) | 113 |
| C(22)–H(22B)⋯N(8) | 0.96 | 2.56 | 3.067(4) | 113 |

Equivalent position codes: a = -x, -1/2 + y, 1/2 - z, b = x, 3/2 - y, -1/2 + z

Table 5.34. Cg⋯Cg (π -ring) interactions

| Cg(I)⋯Cg(J) | Cg⋯Cg (Å) | α (°) | β (°) | γ (°) |
|--|-----------|--------------|-------------|--------------|
| Intermolecular hydrogen bonding | | | | |
| Cg(5)⋯Cg(5) ^c | 3.645(1) | 0 | 23.8 | 23.8 |
| Cg(5)⋯Cg(5) ^d | 3.956(1) | 0 | 32.9 | 32.9 |
| Cg(6)⋯Cg(6) ^e | 3.759(1) | 0 | 28.9 | 28.9 |
| Cg(6)⋯Cg(6) ^f | 3.782(1) | 0 | 28.1 | 28.1 |

Equivalent position codes: c = 1 - x, 1 - y, 1 - z, d = 1 - x, 2 - y, 1 - z, e = -x, 1 - y, -z, f = -x, 2 - y, -z

Cg(5) = C(1), C(2), C(3), C(4), C(5), C(6)

Cg(6) = C(12), C(13), C(14), C(15), C(16), C(17)

α = Dihedral angle between planes I and J (°)

β = Angle between Cg⋯Cg and normal to plane I

γ = Angle between Cg⋯Cg and normal to plane J

5.7.2.2. [Cu(L⁸)(NCS)]_n (**16**)

The ORTEP representation of the compound shows the asymmetric unit of the complex having square planar topology with NNO tridentate Schiff base ligand and the nitrogen of the thiocyanate ligand occupying the basal plane [Fig. 5.34].

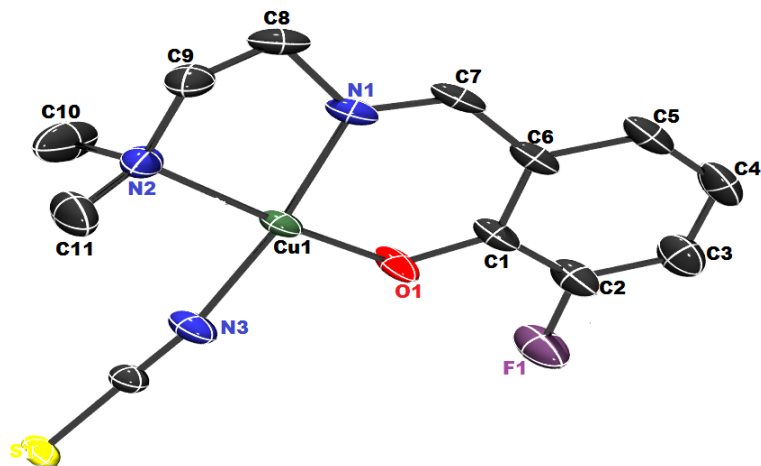


Fig. 5.34. ORTEP diagram showing the atom labelling of the asymmetric unit of the complex **16** (drawn with 30% ellipsoid probability and the hydrogen atoms are omitted for clarity).

The complex actually develops to a coordination polymer along ‘*c*’ direction with the sulfur atom of the other thiocyanate housing the axial position of a pentacoordinated geometry, thereby establishing a $\mu_{1,3}$ *end-to-end* bridging mode of the pseudohalide [Fig. 5.35]. The ambidenticity of the coligand is unveiled here. Refinement details and skeletal details of the structure are given in Table 5.35.

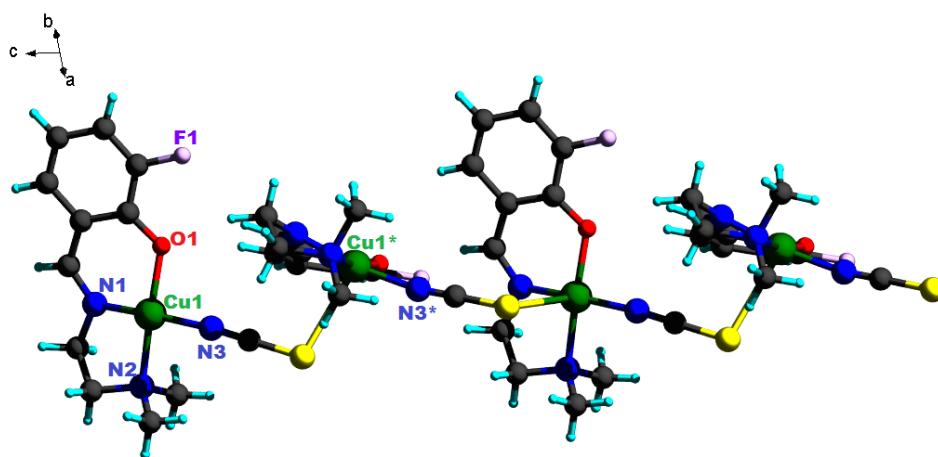


Fig. 5.35. Perspective view of complex **16**.

Table 5.35. Crystal data and refinement details of complex **16**

| Parameters | Complex 16 |
|-----------------------------------|--|
| Empirical formula | C ₁₂ H ₁₄ CuFN ₃ OS |
| Formula weight | 330.87 |
| Temperature | 296(2) K |
| Wavelength | 0.71073 Å |
| Crystal system | Monoclinic |
| Space group | <i>P</i> 2 ₁ / <i>c</i> |
| Unit cell dimensions | a = 15.7317(9) Å α = 90° b = 7.5557 (4) Å β = 102.396(2)° c = 11.8385(5) Å γ = 90° |
| Volume | 1374.37(12) Å ³ |
| Z | 4 |
| Density (calculated) | 1.599 Mg m ⁻³ |
| Absorption coefficient | 1.747 mm ⁻¹ |
| <i>F</i> (000) | 676 |
| Crystal size | 0.50 × 0.40 × 0.40 mm ³ |
| θ range for data collection | 2.651 to 28.427° |
| Limiting indices | -20 ≤ h ≤ 21, -10 ≤ k ≤ 10, -15 ≤ l ≤ 13 |
| Reflections collected | 10688 |
| Unique reflections | 3455 [R(int) = 0.0237] |
| Refinement method | Full-matrix least-squares on F ² |
| Data / restraints / parameters | 3423 / 0 / 175 |
| Goodness-of-fit on F ² | 0.863 |
| Final R indices [I > 2σ(I)] | R ₁ = 0.0279, wR ₂ = 0.0780 |
| R indices (all data) | R ₁ = 0.0390, wR ₂ = 0.0878 |
| Largest diff. peak and hole | 0.268 and -0.412 e.Å ⁻³ |

$$R_1 = \frac{\sum ||F_o| - |F_c||}{\sum |F_o|}$$

$$wR_2 = [\sum w(F_o^2 - F_c^2)^2 / \sum w(F_o^2)^2]^{1/2}$$

The thiocyanate ligand threads the molecules in a such a manner that the adjacent units are tilted by an angle of 78.00(3)° whereas the alternate units are stacked one over the other. The axial elongation of the square pyramidal geometry, an immediate consequence of Jahn-Teller distortion is reflected in the bond lengths made by copper centre: Cu–S = 2.894(7) and Cu–N = 1.950(2) Å [Table 5.36]. The coligand is almost linear with a bond angle of 179.06(1)°.

PLATON software calculates the packing index to be 68% [12]. The bond strength order is the same as seen for other systems with Cu–S bond being weakest.

Table 5.36. Selected bond lengths (Å) and bond angles (°) for **16**

| Bond lengths (Å) | | Bond angles (°) | |
|------------------|-----------|------------------|-----------|
| Cu(1)–O(1) | 1.915(15) | N(3)–Cu(1)–O(1) | 91.10(7) |
| Cu(1)–N(1) | 1.937(16) | N(2)–Cu(1)–N(3) | 91.71(8) |
| Cu(1)–N(2) | 2.067(16) | N(1)–Cu(1)–N(2) | 84.10(8) |
| Cu(1)–N(3) | 1.950(2) | O(1)–Cu(1)–N(1) | 91.69(7) |
| C(12)–N(3) | 1.149(3) | N(1)–Cu(1)–N(3) | 171.26(9) |
| S(1)–C(12) | 1.625(2) | O(1)–Cu(1)–N(2) | 169.36(7) |
| C(2)–F(1) | 1.361(3) | N(3)–Cu(1)–S(1) | 100.86(6) |
| Cu(1)–S(1) | 2.894(7) | N(3)–C(12)–S(1) | 179.06(1) |
| | | Cu(1)–S(1)–C(12) | 103.45(7) |
| | | Cu(1)–N(3)–C(12) | 169.0(1) |

The extent of distortion of the geometry given by Addison parameter, τ has a value of 0.031 indicating not so perfect square pyramidal structure. The bond angle values around the pivotal metal centre summate to 359.4° and the least squares plane calculation indicates a high deviation for the copper centre by a value of 0.1238 Å above the basal plane. The aforementioned parameters underscores the distortions present.

The five membered metallocycles, Cg(1) and Cg(2) [Cu1/N1/C8/C9/N2 and Cu1/O1/C6/C7/N1] assumes envelope conformation with puckering parameters, $Q = 0.394(2)$ Å, $\Phi = 109.5(3)^\circ$ and $Q = 0.296(17)$ Å, $\Phi = 180.1(4)^\circ$ respectively.

The Cu–N–C–S–Cu units are aligned in such a fashion that they alone form the steps of the ladder with a width of $4.7073(7)$ Å units and the connector that links the steps are formed by Cu–S bonds with a height of $2.8944(6)$ Å. Every adjacent connectors [Cu–S] in the staircase structure are having a dihedral angle of $73.13(2)^\circ$ with each other [Fig. 5.36].

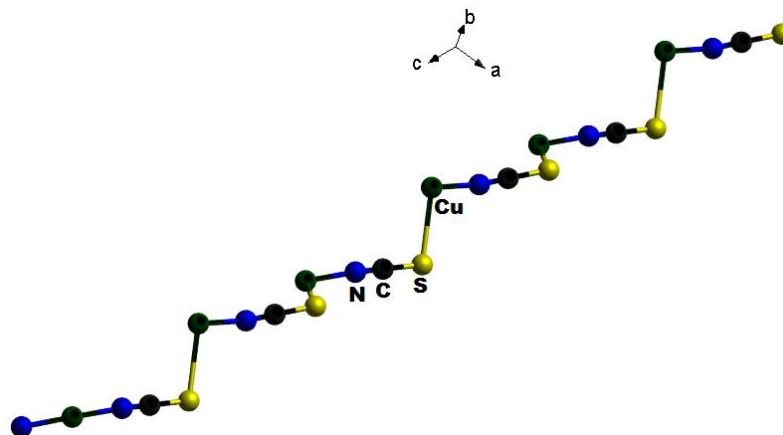


Fig. 5.36. Stair-like structure of complex **16**.

In addition to the covalent linkage by the thiocyanate ligand along the 'c' axis, the intermolecular interchain hydrogen bonding of H(7) with the oxygen atom, O(1) also runs in the same direction [Fig. 5.37, Table 5.37]. The Cu...Cu non-bonded distance along the chain is 6.1329(4) Å units.

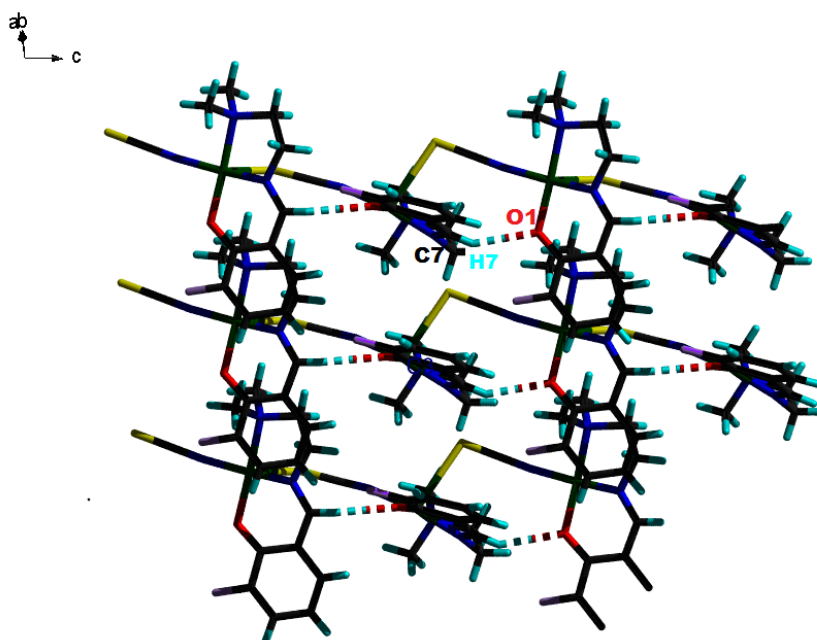


Fig. 5.37. Intermolecular interchain hydrogen bonding interaction.

Table 5.37. Non-conventional hydrogen bonding interaction in complex **16**

| D–H···A | D–H (Å) | H···A (Å) | D···A (Å) | D–H···A (°) |
|--|---------|-----------|-----------|-------------|
| Intermolecular hydrogen bonding | | | | |
| C(7)–H(7)···O(1) ^b | 0.93 | 2.38 | 3.202(2) | 147 |

Equivalent position code: $b = x, 3/2 - y, -1/2 + z$

5.7.2.3. $[\text{Cu}(\text{L}^9)(\text{N}_3)]_n$ (**17**)

The complex crystallizes in monoclinic space group $P2_1/c$. The asymmetric unit of the complex consists of copper atom in a square planar geometry with the donor atoms of the tridentate deprotonated semicarbazone and the nitrogen of azido group satisfying the coordination [Fig. 5.38]. Refinement details and chosen bond angles and bond lengths are given in Tables 5.38 and 5.39 respectively.

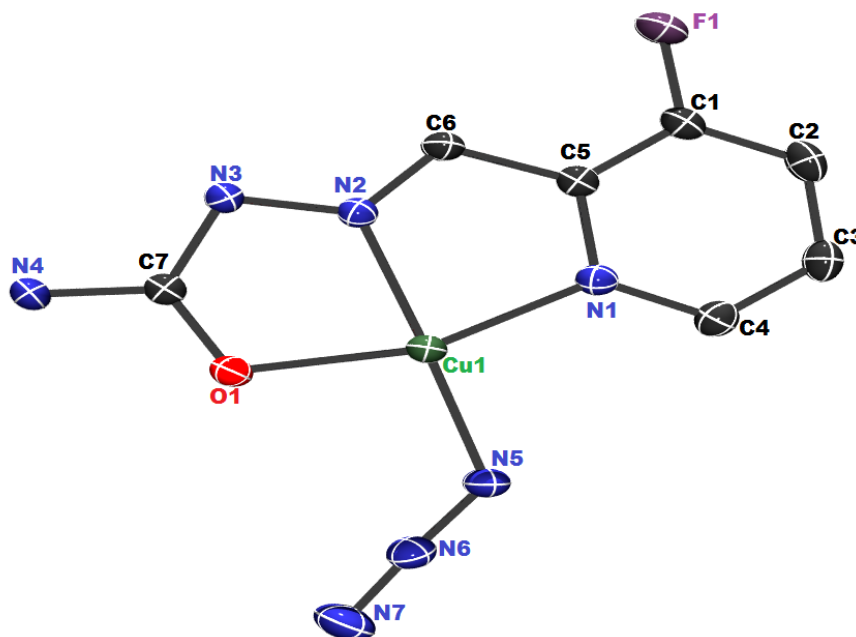


Fig. 5.38. ORTEP diagram showing the atom labelling of the asymmetric unit of the complex **17** (drawn with 30% ellipsoid probability and the hydrogen atoms are omitted for clarity).

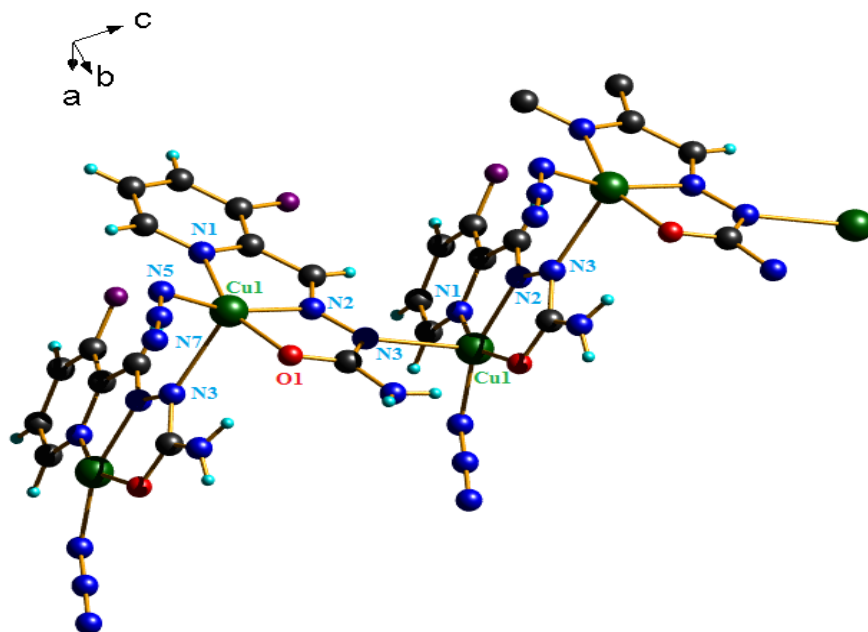
Table 5.38. Crystal data and refinement details of complex **17**

| Parameters | Complex 17 |
|---|---|
| Empirical formula | C ₇ H ₆ CuFN ₇ O |
| Formula weight | 286.74 |
| Temperature | 293(2) K |
| Wavelength | 0.71073 Å |
| Crystal system | Monoclinic |
| Space group | <i>P</i> 2 ₁ / <i>c</i> |
| Unit cell dimensions | <i>a</i> = 10.6451(6) Å α = 90° <i>b</i> = 11.3330(5) Å β = 101.382(2)° <i>c</i> = 8.1660(4) Å γ = 90°. |
| Volume | 965.78(8) Å ³ |
| Z | 4 |
| Density (calculated) | 1.972 Mg m ⁻³ |
| Absorption coefficient | 2.272 mm ⁻¹ |
| F(000) | 572 |
| Crystal size | 0.40 × 0.35 × 0.30 mm ³ |
| θ range for data collection | 3.12 to 27.00° |
| Limiting indices | -13 ≤ <i>h</i> ≤ 13, -12 ≤ <i>k</i> ≤ 14, -7 ≤ <i>l</i> ≤ 10 |
| Reflections collected | 6931 |
| Unique reflections | 2115 [R(int) = 0.0206] |
| Refinement method | Full-matrix least-squares on F ² |
| Data / restraints / parameters | 2105 / 3 / 162 |
| Goodness-of-fit on F ² | 1.094 |
| Final R indices [I > 2σ(I)] | R ₁ = 0.0266, wR ₂ = 0.0688 |
| R indices (all data) | R ₁ = 0.0306, wR ₂ = 0.0706 |
| Largest diff. peak and hole | 0.518 and -0.327 e.Å ⁻³ |
| $R_1 = \frac{\sum F_o - F_c }{\sum F_o }$ $wR_2 = \left[\frac{\sum w(F_o^2 - F_c^2)^2}{\sum w(F_o^2)^2} \right]^{1/2}$ | |

Table 5.39. Selected bond lengths (Å) and bond angles (°) for the complex **17**

| Bond lengths (Å) | | Bond angles (°) | |
|------------------|----------|------------------|-----------|
| Cu1–O1 | 1.965(1) | O(1)–Cu(1)–N(1) | 157.02(7) |
| Cu1–N1 | 2.022(2) | N(2)–Cu(1)–N(1) | 81.08(8) |
| Cu1–N2 | 1.965(1) | N(3)a–Cu(1)–N(1) | 102.38(7) |
| Cu1–N3a | 2.446(2) | O(1)–Cu(1)–N(2) | 78.28(7) |
| Cu1–N5 | 1.947(2) | N(3)–Cu(1)–N(2) | 103.23(7) |
| N5–N6 | 1.204(3) | N(5)–Cu(1)–N(2) | 160.75(9) |
| N6–N7 | 1.142(4) | N(5)–Cu(1)–N(3) | 95.99(8) |
| | | N(1)–Cu(1)–N(3) | 102.38(7) |
| | | O(1)–Cu(1)–N(5) | 100.06(8) |
| | | N(7)–N(6)–N(5) | 176.7(3) |

In the molecular structure [Fig. 5.39], the copper(II) is pentacoordinated with the square basal plane of the polyhedron constituted by the azomethine nitrogen N2, pyridine nitrogen N1, oxygen atom O1 of the deprotonated semicarbazone and the azido nitrogen N5 whereas the N(3) from the symmetry related molecule occupies the apical position.

**Fig. 5.39.** Perspective view of complex **17**.

The geometry of the complex is confirmed to be a distorted square pyramid, as measured by the Addison parameter [9], which is calculated to be 0.0621 in this case [$\tau = (\beta - \alpha)/60$ (for perfect square pyramidal and trigonal bipyramidal geometries the values of τ are zero and unity respectively)]. It is the coordination with the apical nitrogen atom, N(3) that generates a stair-like polymer.

The ladders and the rungs of the stair are uniformly spaced by a distance of 5.2688(5) Å [Fig. 5.40].

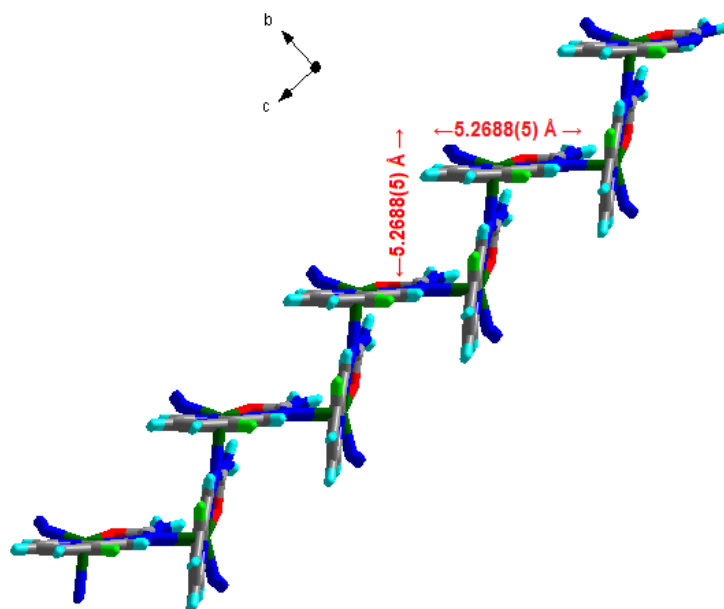


Fig. 5.40. Stair-like polymer formation in complex 17.

The C(7)–N(3) and C(7)–N(4) bond lengths (1.364(3) and 1.338(2) Å) are almost similar to the carbon-nitrogen single bond length for these type of systems. Also, the C(7)–O(1) bond length (1.280(3) Å) indicates partial carbon-oxygen double bond character. These are symptomatic of deprotonated form of semicarbazone system. The semicarbazone maintains its keto form even on complexation but deprotonation from the N3 nitrogen occurs resulting in the polymeric stair architecture.

The torsion angle of Cu1–N2–N3–Cu1 is 177.36(9)° and the Cu...Cu distance in this complex is 5.2688(5) Å, which is greater than that reported for a similar complex. The metal atom deviates by 0.0090 Å from the least squares plane towards the apical donor atom, as is usually seen in case of a square pyramidal geometry. Among the other donor atoms in the basal plane, it is the pyridyl nitrogen, N1 that deviates the most. In the complex, two penta metallocycles [Cg(1) and Cg(2)] are generated due to the coordination of metal atom with the Schiff base system with chelate bite angles of 78.28(7)° and 81.08(8)° respectively. These two rings make an angle of 8.894(5)° with each other thus deviating from the exactly planar configuration.

5.7.2.3.1. Supramolecular features

The hydrogen atom, H4a of the NH₂ group of one semicarbazone establishes a hydrogen bond with the deprotonated oxygen, O1 atom of the adjacent unit along the same chain thereby forming a $R_1^1(6)$ motif. Similarly, the hydrogen of azomethine carbon, C(6) interacts with the pyridyl nitrogen, N(1) along the chain, generating $R_1^1(6)$ motif. The above interactions are intrachain intermolecular interactions and the motifs involve the metal atom. Two other hydrogen bonds participate in packing the adjacent chains together. The hydrogen bonding interaction of terminal nitrogen, N7 of the azido group with the hydrogen of the C2 atom of the pyridine ring, together with the stair like propagation *via* covalent connectivity of the metal atom with the N3 atom extends the whole structure along 'ac' plane [Fig. 5.41a, Table 5.40].

The association of the hydrogen atom of amino nitrogen, H(4) of a semicarbazone entity with the terminal azido nitrogen, N(7) as the acceptor, stitches the two neighbouring staircase structures. This interaction produces an interesting loop, conveniently representable as $R_2^2(14)$ motif as according to Graph-set notation [Fig. 5.41c].

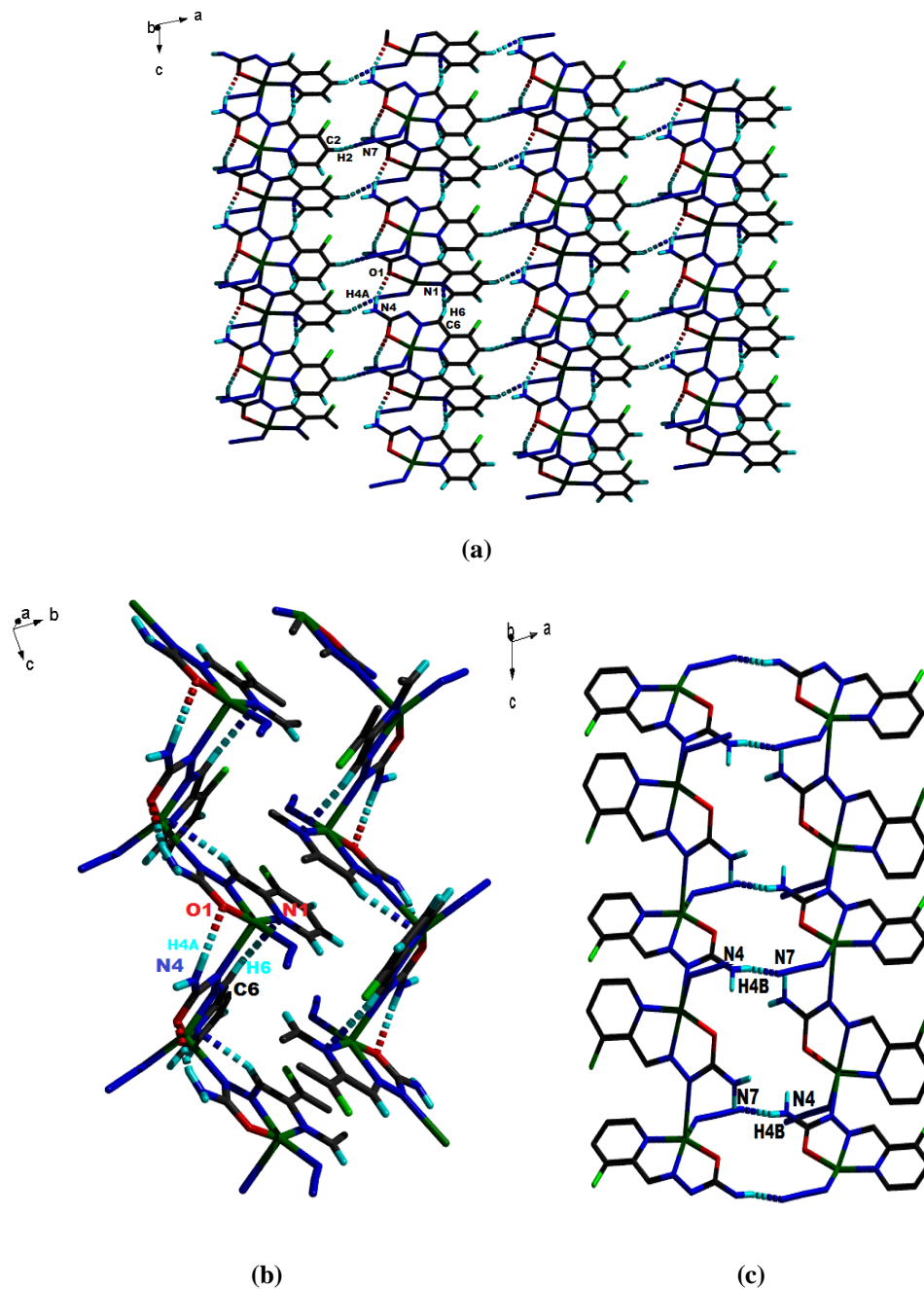


Fig. 5.41. Different views of the hydrogen bonding interactions present in complex 17.

Table 5.40. Hydrogen bonding interactions in the complex **17**

| D–H···A | D–H (Å) | H···A (Å) | D···A (Å) | D–H···A (°) |
|--|----------------|------------------|------------------|--------------------|
| Intermolecular hydrogen bonding | | | | |
| N(4)–H(4A)···O(1) ^a | 0.86(1) | 2.06(1) | 2.879(3) | 155.0(2) |
| N(4)–H(4B)···N(7) ^b | 0.85(1) | 2.27(2) | 3.096(4) | 160.0(1) |
| C(2)–H(2)···N(7) ^c | 0.93 | 2.59 | 3.362(4) | 141 |
| C(6)–H(6)···N(1) ^a | 0.93 | 2.55 | 3.376(3) | 149 |

Equivalent position codes: a = x, ½ - y, ½ + z, b = 1 - x, -y, 1 - z, c = -1 + x, y, z

Diving into the supramolecular forces, we witness C–F···Cg(3) [Fig. 5.42a], Cu···Cg(2)/Cg(3) [Fig. 5.42b], π ··· π [Fig. 5.42c] and C–H··· π [Fig. 5.42d] interactions reinforcing the crystal packing. Thus, an interplay of hydrogen bonding interactions and supramolecular forces like cation··· π , C–H··· π , π ··· π and C–F··· π play vital role in the construction of this self-assembled polymeric stair architecture.

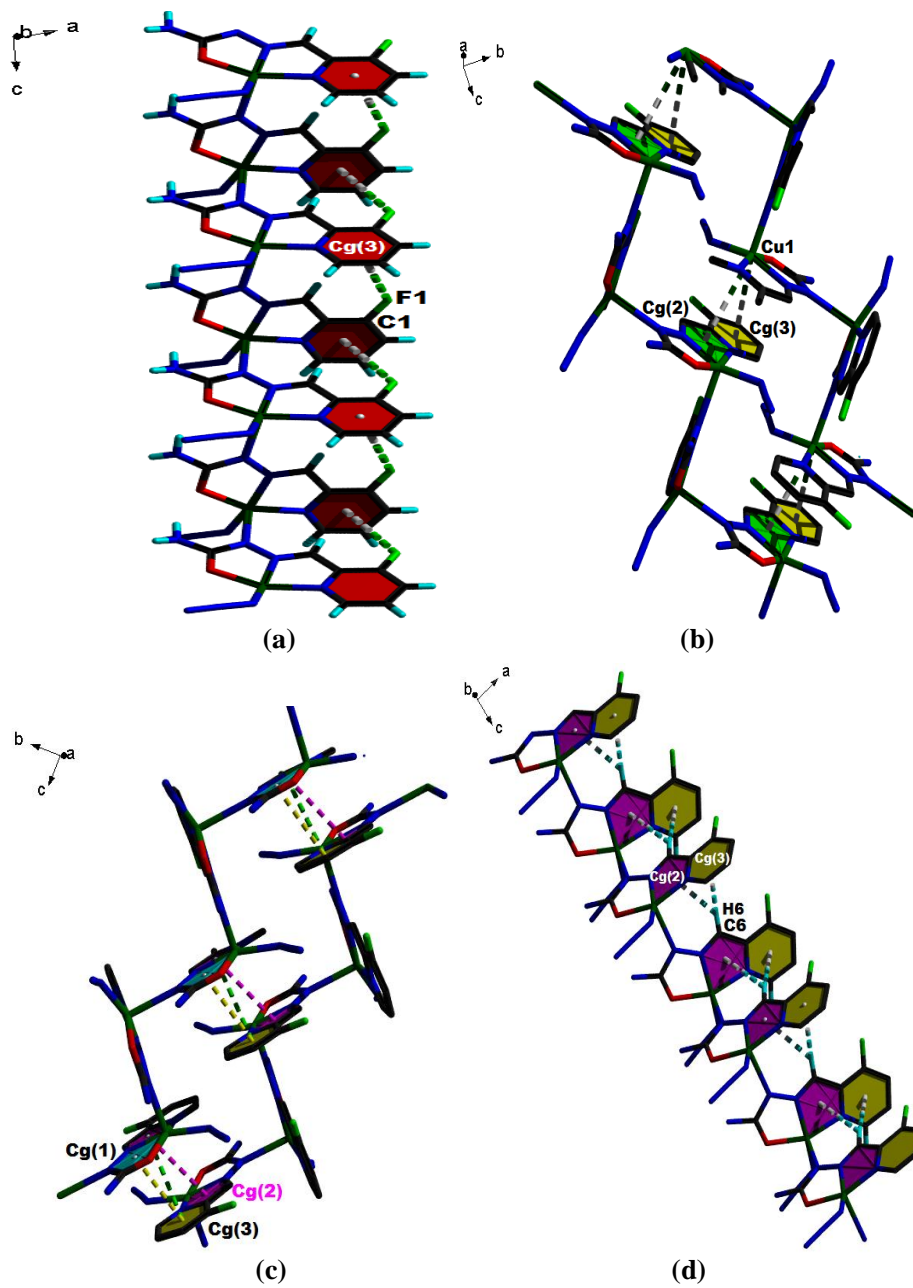


Fig. 5.42. (a) C–F \cdots Cg(3), (b) Cu \cdots Cg(2)/Cg(3), (c) $\pi\cdots\pi$ and (d) C–H $\cdots\pi$ interactions in complex 17.

Geometric features of the supramolecular forces are collated in Tables 5.41, 5.42, 5.43 & 5.44. Also, these non-covalent forces interconnect the chains thereby spreading the polymer in two dimension.

Table 5.41. Short ring interactions

| Cg(I)⋯Cg(J) | Cg⋯Cg | α (°) | β (°) | γ (°) |
|---------------------------|--------------|--------------|--------------|--------------|
| Cg(1)⋯ Cg(3) ^d | 3.3977(12) | 6.96(10) | 7.9 | 10.3 |
| Cg(2)⋯ Cg(2) ^d | 3.6335(12) | 0 | 16.6 | 16.6 |
| Cg(2)⋯ Cg(3) ^d | 3.9606(13) | 2.68(10) | 28.0 | 29.9 |

Equivalent position code: d = -x, -y, 1-z

Cg(1) = Cu(1), O(1), C(7), N(3), N(2)

Cg(2) = Cu(1), N(1), C(5), C(6), N(2)

Cg(3) = N(1), C(1), C(2), C(3), C(4), C(5)

α = Dihedral angle between planes I and J (°)

β = Angle between Cg⋯Cg and normal to plane I

γ = Angle between Cg⋯Cg and normal to plane J

Table 5.42. C–X⋯Cg interactions

| C–X(I)⋯Cg(J) | X⋯Cg (Å) | C⋯Cg (Å) | C–X⋯Cg (°) |
|------------------------------|-----------------|-----------------|-------------------|
| C(1)–F(1)⋯Cg(3) ^e | 3.7537(19) | 4.719(3) | 129.24(13) |

Equivalent position code: e = x, ½ - y, ½ + z

Table 5.43. C–H⋯Cg interactions

| C–H⋯Cg(J) | C⋯Cg (Å) | H⋯Cg (Å) | C–H⋯Cg (°) |
|------------------------------|-----------------|-----------------|-------------------|
| C(6)–H(6)⋯Cg(2) ^f | 3.587(3) | 2.84 | 138 |
| C(6)–H(6)⋯Cg(3) ^f | 3.749(2) | 2.83 | 169 |

Equivalent position code: f = x, ½ - y, ½ + z

Table 5.44. Ring-metal interactions

| Cg(I)⋯ M(J) | Cg(I)–M(J) (Å) |
|--------------------------|-----------------------|
| Cg(2)⋯Cu(1) ^g | 3.818 |
| Cg(3)⋯Cu(1) ^g | 3.703 |

Equivalent position code: g = -x, -y, 1 - z

M = Metal atom.

5.7.3. Photoluminescence studies

The optical emission of the complexes dissolved in acetonitrile was recorded and all the complexes emit in the violet-blue region of the spectrum when excited at 350 nm [Fig. 5.43, Table 5.45].

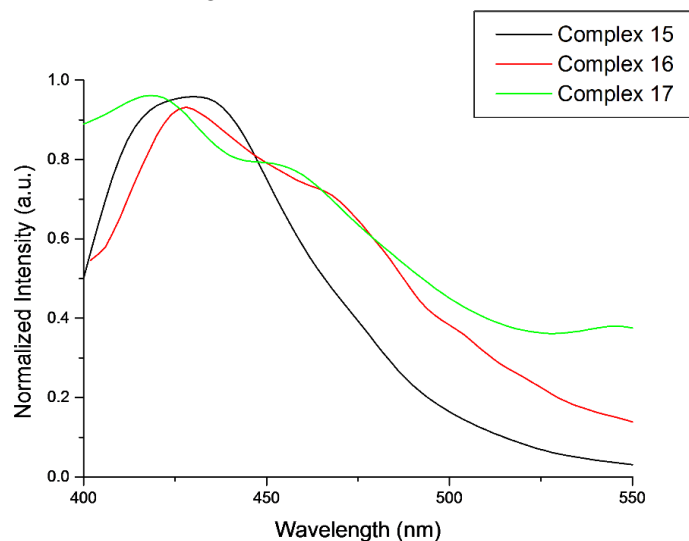


Fig. 5.43. Merged fluorescence spectra of complexes **15**, **16** and **17** (acetonitrile, con: 1×10^{-3} M).

Table 5.45. Photophysical data of complexes

| Complexes | Solution state emission (nm) at excitation of 350 nm |
|---|--|
| $[\text{Cu}(\text{L}^7)(\text{N}_3)]_n$ (15) | 436 |
| $[\text{Cu}(\text{L}^7)(\text{NCS})]_n$ (16) | 426 |
| $[\text{Cu}(\text{L}^8)(\text{N}_3)]_n$ (17) | 424 |

5.7.4. Thermal studies

The *end-to-end* azido complex **15** shows a single stage endothermic decomposition profile consistent with a mass loss of amine and HF (37.37%, calcd. 34.39%) in the temperature range 235 – 265 °C, followed by the formation of stable metal oxide. The complex **16** exhibits a TG curve

corresponding to the removal of thiocyanate (17.37%, calcd. 17.87%) at a temperature of 228 °C. The endothermic process completes at 254 °C. Unlike the azido complex, here a gradual thermal decomposition is observed. In the case of complex **17**, the thermogram shows the removal of both semicarbazide skeleton as well as the azido portion followed by a gradual decomposition pattern [Fig. 5.44].

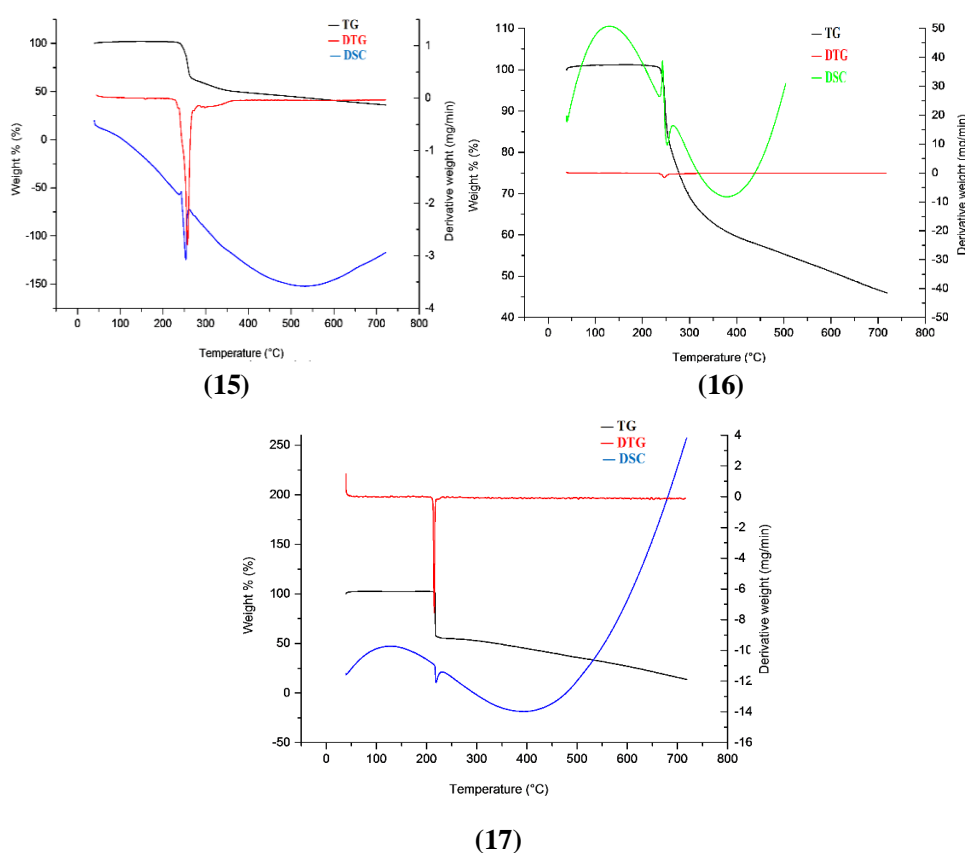


Fig. 5.44. Thermogram of the complexes **15**, **16** and **17**.

5.7.5. EPR spectral studies

The EPR spectrum of the complex **15** recorded in polycrystalline state gave three different g values – g_1 , g_2 and g_3 which is in agreement with rhombic distortion ($g_1 = 2.040$, $g_2 = 2.120$, $g_3 = 2.210$) in the geometry. The spectra

recorded in frozen DMF also displayed rhombic distortion with $g_1 = 2.035$, $g_2 = 2.136$ and $g_3 = 2.227$. The higher g value region witnesses hyperfine splittings with $A_3 = 190 * 10^{-4}$ and $A_2 = 45 * 10^{-4} \text{ cm}^{-1}$ respectively [Fig. 5.45a]. Here, $g_{\parallel} = g_3 = 2.227$ and $g_{\perp} = (g_1 + g_2)/2 = 2.085$.

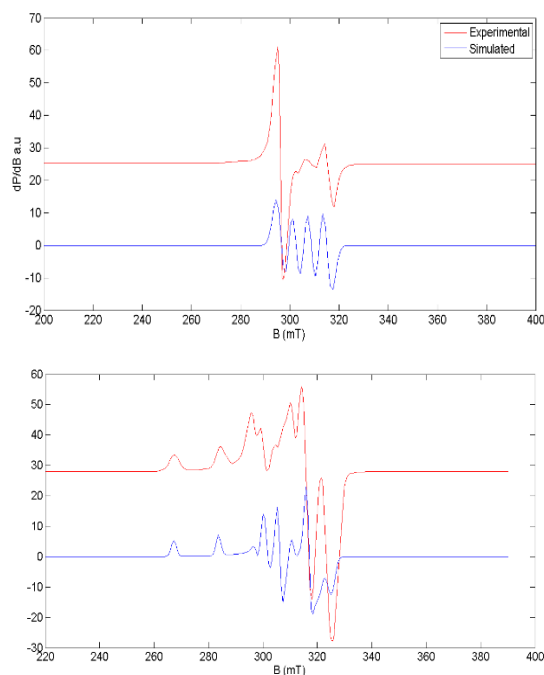


Fig. 5.45a. EPR spectra of complex **15** in polycrystalline state (top) and in DMF at 77 K (bottom).

In polycrystalline state at 298 K, complex **16** revealed an isotropic spectrum with g_{iso} value of 2.190. Such an isotropic spectrum with only one broad signal and hence only one g value arises from extensive exchange coupling through misalignment of the local molecular axes between different molecules in the unit cell (dipolar broadening) and enhanced spin lattice relaxation. This kind of spectra unfortunately give not much information on the electronic ground state of copper(II) ion present in the complex. So the EPR of the same sample was recorded in frozen DMF at 77 K which showed an axial nature for the spectra with $g_{\parallel} = 2.314$ and $g_{\perp} = 2.123$. The hyperfine

splittings are separated by hyperfine splitting constant having a value of $217 \cdot 10^4 \text{ cm}^{-1}$ [Fig. 5.45b].

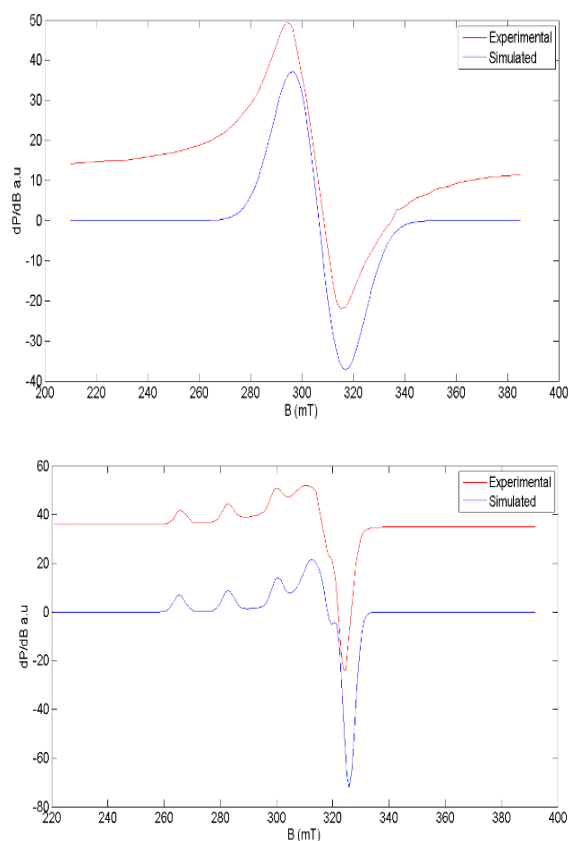


Fig. 5.45b. EPR spectra of complex **16** in polycrystalline state (top) and in DMF at 77 K (bottom).

For the azido complex **17**, polycrystalline state gave an axial spectrum with the g tensor values holding the relation, $g_{\parallel} > g_{\perp} > g_e$ [Table 5.46] reasserting the presence of a square based environment in the complex. The spectra recorded in DMF solution also doesn't gave much information except for the presence of a splitting in the high intense region with a hyperfine

splitting value of $48 \times 10^{-4} \text{ cm}^{-1}$ [Fig. 5.45c]. This may be due to poor glass formation.

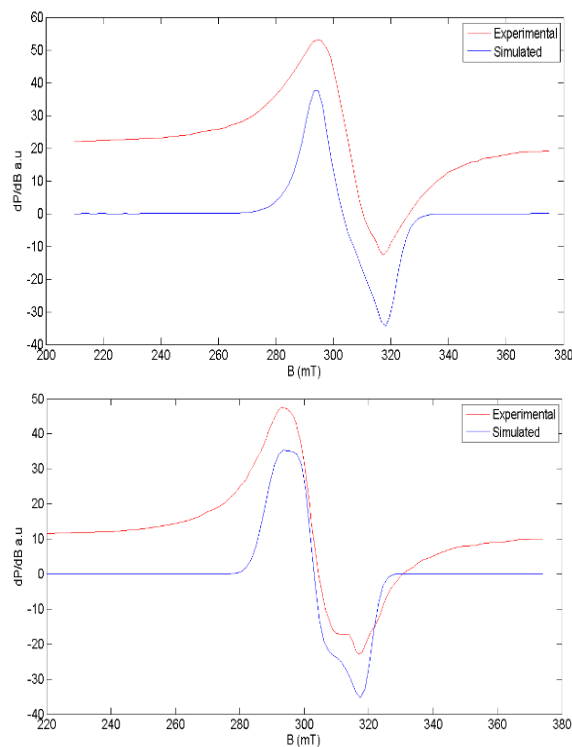


Fig. 5.45c. EPR spectra of complex **17** in polycrystalline state (top) and in DMF at 77 K (bottom).

The value of G , the empirical parameter calculated for all the complexes ($G < 4$) is consistent with the significant exchange interaction present in them. The values for the bonding parameters are expected to be less than 1 if the M–L bond is partially ionic and partially covalent. But contrary to our expectations, value of γ^2 in case of complex **15** and the values of α^2 and γ^2 for complex **16** are observed to be above 1. Significant in-plane π bonding is observed for all the complexes, as deduced from the values of K_{\parallel} and K_{\perp} . They hold the relation $K_{\parallel} < K_{\perp}$. The value of the empirical parameter, f falls in the 105–117 cm range corresponding to small to medium distortion from planarity [24,25] [Table 5.46].

Table 5.46. Spin Hamiltonian and bonding parameters of copper(II) complexes

| Compounds | Polycrystalline state (298 K) | | | | | | | | | | DMF solution (77 K) | | | | | |
|--|-------------------------------|--------------------|-------------------|-------|--------------------|-------------------|-----------------|-----------------|-------------|-----------------|---------------------|-----------|------------|-----------------|-------------|-----|
| | g_{iso} | $g_{\parallel}g_3$ | $g_{\perp}g_1g_2$ | G | $g_{\parallel}g_3$ | $g_{\perp}g_1g_2$ | g_{av} | A_{\parallel} | A_{\perp} | A_{av} | α^2 | β^2 | γ^2 | K_{\parallel} | K_{\perp} | f |
| $[\text{Cu}(\text{L}_8)(\text{N}_3)]_n$ (15) | -- | 2.210 | 2.120, 2.673 | 2.227 | 2.035, | 2.102 | 2.102 | 190 | 45.0 | -- | 0.782 | 0.3432 | 1.388 | 0.2686 | 1.0864 | 117 |
| | | | 2.040 | | 2.136 | | | | | | | | | | | |
| $[\text{Cu}(\text{L}_8)(\text{NCS})]_n$ (16) | 2.190 | -- | -- | --- | 2.314 | 2.123 | 2.186 | 217 | 20.8 | 86.2 | 1.006 | 0.8557 | 1.065 | 0.8608 | 1.0714 | 107 |
| $[\text{Cu}(\text{L}_7)(\text{N}_3)]_n$ (17) | -- | 2.170 | 2.120 | 1.425 | 2.225 | 2.096 | 2.139 | -- | 48.0 | -- | -- | -- | -- | 0.7011 | 0.9095 | -- |

A values in 10^{-4} cm^{-1}

References

- [1] P. Bhowmik, A. Bhattacharyya, K. Harms, S. Sproules, S. Chattopadhyay, *Polyhedron* **2015**, 85, 221.
- [2] X. Lin, Y. Sang, W. Xiao, *J. Chem. Crystallography* **2012**, 42, 578.
- [3] M. Das, S. Chattopadhyay, *Transit. Met. Chem.* **2013**, 38, 191.
- [4] B.J. Hathaway, in: G. Wilkinson, R.D. Gillard, J.A. McCleverty (Eds.), *Comprehensive Coordination Chemistry*, Vol. 5, Pergamon, Oxford, **1987**, 533.
- [5] S.-Q. Bai, E.-Q. Gao, Z. He, C.-J. Fang and C.-H. Yan, *New J. Chem.* **2005**, 29, 935.
- [6] P. Mukherjee, O. Sengupta, M.G.B. Drew, A. Ghosh, *Inorg. Chim. Acta* **2009**, 362, 3285.
- [7] K. Sone, Y. Fukuda, *Inorganic Thermochemistry in Inorganic Chemistry Concepts* Vol. 10, Springer-Verlag, Berlin, **1987**, 72.
- [8] P. Muller, R. Herbst-Irmer, A.L. Spek, T.R. Schneider, M.R. Sawaya, *Crystal Structure Refinement*, Oxford Science Publications, **2012**.
- [9] L. Yang, D.R. Powell, R.P. Houser, *Dalton Trans.* **2007**, 955.
- [10] Zhong-Lu You, *Acta Crystallogr. Sect. E* **2006**, 62, m47.
- [11] A.W. Addison, T.N. Rao, J. Reedijk, J. Van Rijn, G.C. Verschoor, *J. Chem. Soc., Dalton Trans.* **1984**, 1349.
- [12] A.L. Spek, *Acta Cryst. C* **2015**, 71, 9.
- [13] D. Cremer, J.A. Pople, *J. Am. Chem. Soc.* **1975**, 97, 1354.
- [14] S.T. Rao, E. Westhof, M. Sundaralingam, *Acta Crystallogr., Sect. A: Struct. Rep. Online* **1981**, 37, 421.
- [15] S. Stoll, *Spectral Simulations in Solid-State Electron Paramagnetic Resonance*, Ph.D. thesis, ETH, Zurich, **2003**.
- [16] J. Peisach, W.E. Blumberg, *Arch. Biochem. Biophys.* **1974**, 165, 691.

- [17] M.J. Bew, B.J. Hathaway, R.R. Faraday, *J. Chem. Soc., Dalton Trans.* **1972**, 1229.
- [18] E. Garribba, G. Micera, *J. Chem. Educ.* **2006**, 83, 1229.
- [19] D.E. Nickless, M.J. Power, F.L. Vrbach, *Inorg. Chem.* **1983**, 22, 3210.
- [20] E. Manoj, M.R.P. Kurup, A. Punnoose, *Spectrochim. Acta* **2009**, 72, 474.
- [21] B.J. Hathaway, D.E. Billing, *Coord. Chem. Rev.* **1970**, 5, 143.
- [22] D. Kivelson, R. Neiman, *J. Chem. Phys.* **1961**, 35, 149.
- [23] B.J. Hathaway, in: G. Wilkinson, R.D. Gillard, J.A. McCleverty (Eds.), *Comprehensive Coordination Chemistry*, Pergamon, Oxford, **1987**, 5, 533.
- [24] S.I. Findone, K.W.H. Stevens, *Proc. Phys. Soc.* **1959**, 73, 116.
- [25] A. Diaz, R. Pogni, R. Cao, R. Basosi, *Inorg. Chim. Acta* **1998**, 275, 552.
- [26] R.J. Kunnath, M. Sithambaresan, A.A. Aravindakshan, A. Natarajan, M.R.P. Kurup, *Polyhedron* **2016**, 113, 73.
- [27] N. Aiswarya, M. Sithambaresan, S.S. Sreejith, S.W. Ng, M.R.P. Kurup, *Inorg. Chim. Acta* **2016**, 443, 251.
- [28] S. Naiya, C. Biswas, M.G.B. Drews, C.J. Gómez-García, J.M. Clemente-Juan, A. Ghosh, *Inorg. Chem.* **2010**, 49, 6616.
- [29] M. Das, B.N. Ghosh, K. Rissanen, S. Chattopadhyay, *Polyhedron* **2014**, 77, 103.
- [30] B. Jain, M. Verma, S. Malik, *Int. J. Pharm. Res. Sci.* **2014**, 02, 155.
- [31] M.K. Prasanna, K. Pradeepkumar, *Int. J. Pharm. Biomed. Sci.* **2013**, 04, 24.



Complexes derived from 1-aminopyrrolidin-2-one and 5-chloro/5-bromosalicylaldehyde

- 6.1. *Introduction*
- 6.2. *Experimental*
- 6.3. *Results and discussion*

Conspectus

In this chapter, we have discussed about the proligands and the complexes prepared from 1-aminopyrrolidin-2-one hydrochloride and monohalosubstituted aldehydes. Various packing forces are also discussed. The characterization studies along with photoluminescence, thermogravimetric and EPR studies are also dealt with.

6.1. Introduction

The ligand system employed in this chapter is a NOO tridentate system. Single crystals of two proligands and two complexes are isolated. The proligands have 5-bromo/5-chloro salicylaldehyde as the aldehydic portion and the corresponding copper complexes have chloride as the charge satisfying group. The hydrogen bonding interactions and other weak aromatic ring interactions develop the proligands to two dimensional spread. Though the complexes have no hydrogen bonding interactions present in them, the stacking forces chain the monomeric molecules.

6.2. Experimental

6.2.1. Materials

All chemicals used for synthesis were of Analar grade and used without further purification. Single crystals of the proligands were isolated.

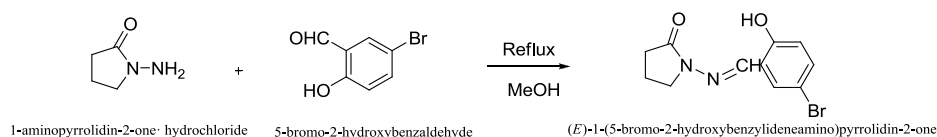
6.2.2. Synthetic protocol

6.2.2.1. Synthesis of proligands

The proligands were prepared by a general method of direct condensation of 1-aminopyrrolidin-2-one-hydrochloride with the respective aldehyde. Both of them were of HL type.

6.2.2.1.1. Preparation of (5-bromo-2-hydroxybenzylideneamino)pyrrolidin-2-one (HL¹⁰)

(5-bromo-2-hydroxybenzylideneamino)pyrrolidin-2-one was synthesized by refluxing a mixture of 5-bromosalicylaldehyde (0.201 g, 1 mmol) and 1-aminopyrrolidin-2-one hydrochloride (0.136 g, 1 mmol) in methanol for 2 h and few drops of dimethylformamide was also added to it. Colorless, needle shaped crystals were obtained by the slow evaporation of the mother liquor [Scheme 6.1].



Scheme 6.1. Formation of HL¹⁰.

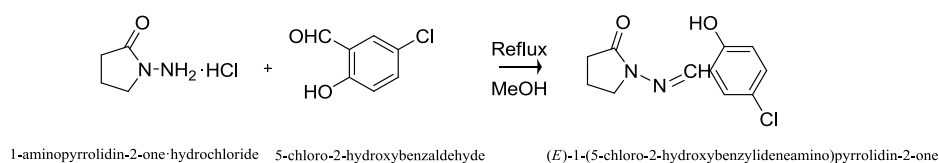
HL¹⁰

Yield: 0.2122 g (75%). *Anal.* Calc. for C₁₁H₁₁N₂O₂Br (283.12): C, 46.66; H, 3.92; N, 9.89 Found C, 46.69; H, 3.89; N, 9.90%.

UV-vis, λ_{max} /nm ($\epsilon_{\text{max}}/10^3 \text{ M}^{-1}\text{cm}^{-1}$) (acetonitrile): 222 (18.58)

6.2.2.1.2. Preparation of (5-chloro-2-hydroxybenzylideneamino)pyrrolidin-2-one (HL¹¹)

The procedure for the synthesis was same as above except that 5-chlorosalicylaldehyde (0.156 g, 1 mmol) was used instead of 5-bromosalicylaldehyde. Single crystals suitable for XRD analysis was isolated from the mother liquor [Scheme 6.2].



Scheme 6.2. Formation of HL¹¹.

HL¹¹

Yield: 0.1720 g (72%). *Anal.* Calc. for C₁₁H₁₁N₂O₂Cl (238.67): C, 55.36; H, 4.65; N, 11.74 Found C, 55.39; H, 4.67; N, 11.75%.

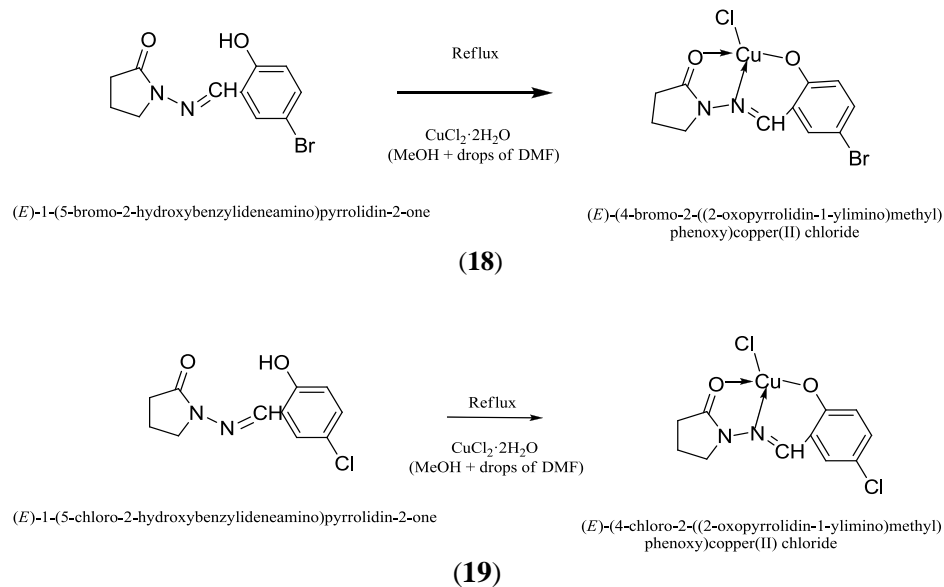
UV-vis, λ_{\max} /nm ($\epsilon_{\max}/10^3 \text{ M}^{-1}\text{cm}^{-1}$) (acetonitrile): 232 (18.58).

6.2.2.2. Synthesis of copper complexes

6.2.2.2.1. Synthesis of [Cu(L¹⁰)Cl] (18)/[Cu(L¹¹)Cl] (19)

(5-Bromo-2-hydroxybenzylideneamino)pyrrolidin-2-one was synthesized *in situ* by heating a mixture of 5-bromosalicylaldehyde (0.201 g, 1 mmol) and 1-aminopyrrolidin-2-one (0.136 g, 1 mmol) in DMF for 2 h. Copper(II) chloride dihydrate (0.170 g, 1 mmol) was dissolved in methanol and few drops of DMF was added to it, and the mixture was heated for 5 h. The resulting pale green solid was collected and recrystallized from DMF to get quality single crystals.

The procedure was repeated by using 5-chlorosalicylaldehyde as the starting material for the synthesis of complex **19**. Single crystals of the complex was obtained by recrystallization from DMF [Scheme 6.3].



Scheme 6.3. Route to the formation of complexes **18** and **19**.

Complex 18:

Yield: 0.2400 g (63%). *Anal.* Calc. for C₁₁H₁₀BrClCuN₂O₂ (381.11): C, 34.67; H, 2.64; N, 7.35 Found C, 34.69; H, 2.66; N, 7.38%.

UV-vis, λ_{\max} /nm ($\epsilon_{\max}/10^3 \text{ M}^{-1}\text{cm}^{-1}$) (acetonitrile): 405 (5.14), 329 (2.79), 284 (14.79), 239 (17.57).

Complex 19:

Yield: 0.2016 g (60%). *Anal.* Calc. for C₁₁H₁₀Cl₂CuN₂O₂ (336.66): C, 39.24; H, 2.99; N, 8.32 Found C, 39.28; H, 3.04; N, 8.37%.

UV-vis, λ_{\max} /nm ($\epsilon_{\max}/10^3 \text{ M}^{-1}\text{cm}^{-1}$) (acetonitrile): 406 (8.82), 286 (21.50), 241 (29.76).

6.3. Results and discussion

6.3.1. Spectroscopic features

6.3.1.1. IR and electronic spectroscopy

The IR spectra of the compounds were recorded in the 4000-400 cm^{-1} range using KBr pellet and the spectral analysis confirmed the presence of characteristic groups in the compound [Fig. 6.1].

The presence of phenolic $-\text{OH}$ is confirmed by a broad signal at 3407 and 3413 cm^{-1} consistent with $\nu(\text{O}-\text{H})$ stretching vibration, for the ligands HL^{10} and HL^{11} respectively. The keto form of both ligands in the solid state records its signature at 1715 cm^{-1} corresponding to $\nu(\text{C}=\text{O})$ stretching frequency. The strong peaks at 1615 and 1613 cm^{-1} is attributable to the $\nu(\text{C}=\text{N})$ stretching mode of the azomethine group of the ligands, HL^{10} and HL^{11} respectively.

In the case of complex **18**, the presence of lattice water is confirmed by a signal at 3495 cm^{-1} and the stretching band at 1598 cm^{-1} indicates the azomethine nitrogen coordination to the copper metal. In complex **19** also, the shift of $\nu(\text{C}=\text{N})$ band to 1603 cm^{-1} is indicative of complex formation.

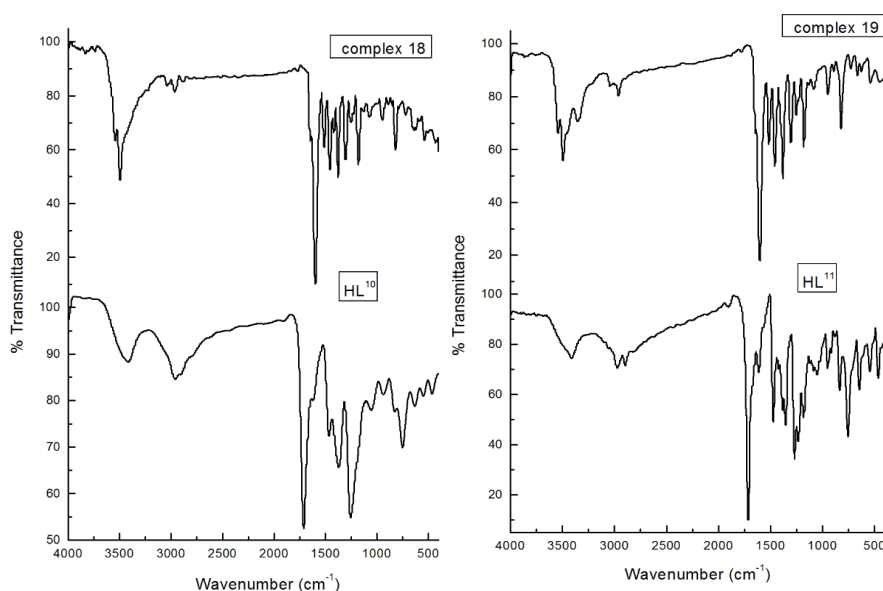


Fig. 6.1. IR spectra of the proligands and the complexes.

The electronic spectra of the ligands as well as the complexes were recorded in acetonitrile medium in the range 200-900 nm. The ligands registered both $\pi \rightarrow \pi^*$ and $n \rightarrow \pi^*$ transitions. The band at 330 nm can be attributed to the normally forbidden $n \rightarrow \pi^*$ transitions of the azomethine chromophore in both the ligands. The rest of the low wavelength signals in the 200 nm region can be assigned to $\pi \rightarrow \pi^*$ transitions arising due to transitions in the azomethine group and the phenyl ring of the ligands. In the case of HL¹⁰, the allowed $\pi \rightarrow \pi^*$ transitions exhibit higher intensity over the forbidden $n \rightarrow \pi^*$ transitions whilst for HL¹¹, the $n \rightarrow \pi^*$ transitions are having a slightly higher intensity when compared with $\pi \rightarrow \pi^*$ transition [1] [Fig. 6.2, Table 6.1].

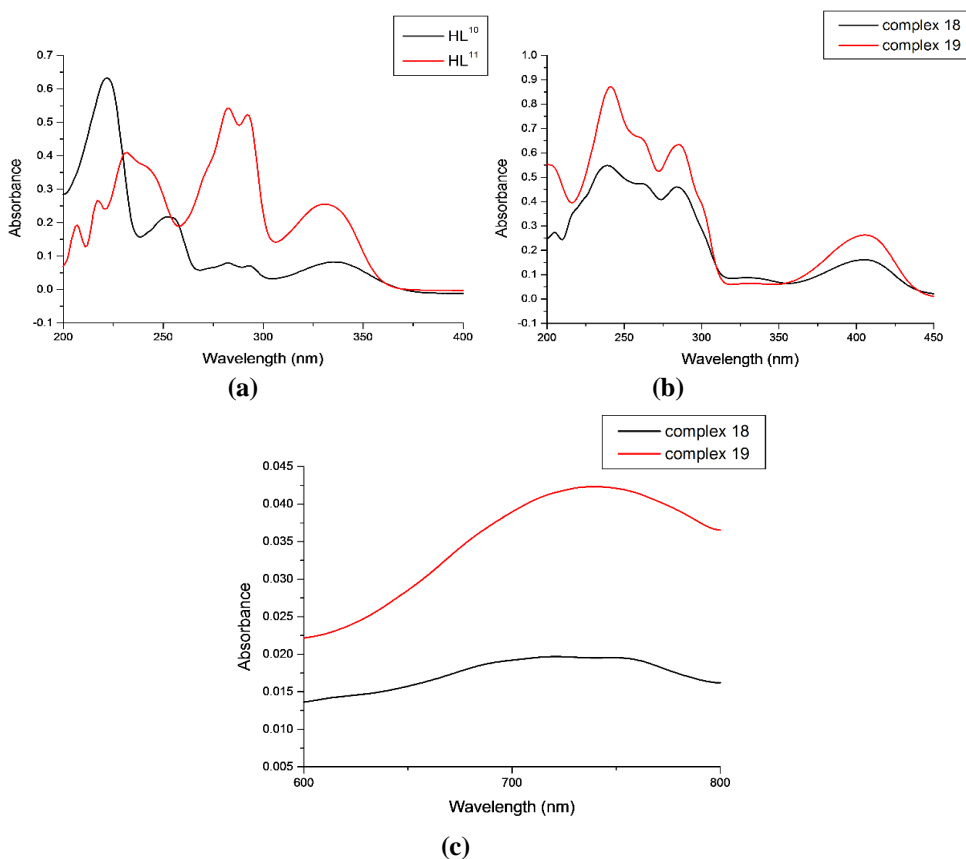


Fig. 6.2. The spectra showing a) intraligand transitions of the ligands b) CT and intraligand transitions of the complexes and c) *d-d* bands of complexes in acetonitrile medium.

In the case of complex **18**, we witness the presence of ligand to metal charge transfer transition at 406 nm apart from the usual $\pi \rightarrow \pi^*$ and $n \rightarrow \pi^*$ transitions. But for complex **19**, only a single signal is registered at 406 nm in addition to the $\pi \rightarrow \pi^*$ transitions in the 250 nm region. Here, we expect the $n \rightarrow \pi^*$ transition to have merged with the LMCT transition resulting in a single band. The complexes **18** and **19** show $d-d$ bands at 722 and 738 nm respectively characteristic of a square based environment [Fig. 6.2, Table 6.1].

Table 6.1. Electronic spectral data of the compounds

| Compounds | $d-d$ bands | | CT | | $n \rightarrow \pi^*$ | | $\pi \rightarrow \pi^*$ | |
|--|-----------------------|--------------------------------|-----------------------|---------------------------------------|-----------------------|---------------------------------------|-------------------------|---------------------------------------|
| | λ_{\max} (nm) | ϵ ($M^{-1}cm^{-1}$) | λ_{\max} (nm) | $\epsilon * 10^3$ ($M^{-1}cm^{-1}$) | λ_{\max} (nm) | $\epsilon * 10^3$ ($M^{-1}cm^{-1}$) | λ_{\max} (nm) | $\epsilon * 10^3$ ($M^{-1}cm^{-1}$) |
| HL ¹⁰ | --- | --- | --- | --- | 335 | 2.41 | 282 | 2.33 |
| | | | | | | | 252 | 6.35 |
| | | | | | | | 222 | 18.58 |
| HL ¹¹ | --- | --- | --- | --- | 329 | 2.41 | 293 | 2.33 |
| | | | | | | | 282 | 6.35 |
| | | | | | | | 232 | 18.58 |
| [Cu(L ¹⁰)Cl] (18) | 723 | 107 | 405 | 5.14 | 329 | 2.79 | 284 | 14.79 |
| | | | | | | | 239 | 17.57 |
| [Cu(L ¹¹)Cl] (19) | 738 | 71 | 406 | 8.82 | --- | --- | 286 | 21.50 |
| | | | | | | | 241 | 29.76 |

6.3.2. X-ray crystallography and crystal structure description

In all the proligands and complexes, the non-hydrogen atoms were refined anisotropically and all H atoms on C were placed in calculated positions guided by difference maps with C–H bond distances 0.93-0.97 Å. In the case of HL¹¹, the O–H hydrogen atoms [O(1)–H(1), O(3)–H(3) and O(5)–H(5) hydrogen atoms], were located from difference maps and their

distances were restrained to 0.84 Å using DFIX instructions. In complex **18**, O(1S)–H(1B) and O(1S)–H(1A) hydrogen atoms were located from difference maps and the O–H distances were restrained to 0.86 Å with a standard deviation of 0.01 Å using DFIX and the distances between the atoms, H1A and H1B which were both bonded to the same O(1S) atom was restrained to 1.36 Å with a standard deviation of 0.02 Å using DANG instruction.

6.3.2.1. 1-(*E*)-[(5-bromo-2-hydroxybenzylideneamino)pyrrolidin-2-one (HL¹⁰)

The molecule crystallizes in monoclinic, $P2_1/c$ space group. The asymmetric unit of the proligand has a single molecule and is shown in Fig. 6.3. The refinement details and bond dimensions are collated in Table 6.2. The C6 and N2 atoms are in *E* configuration with respect to C7=N1 with a torsion angle of 176.7(2)°.

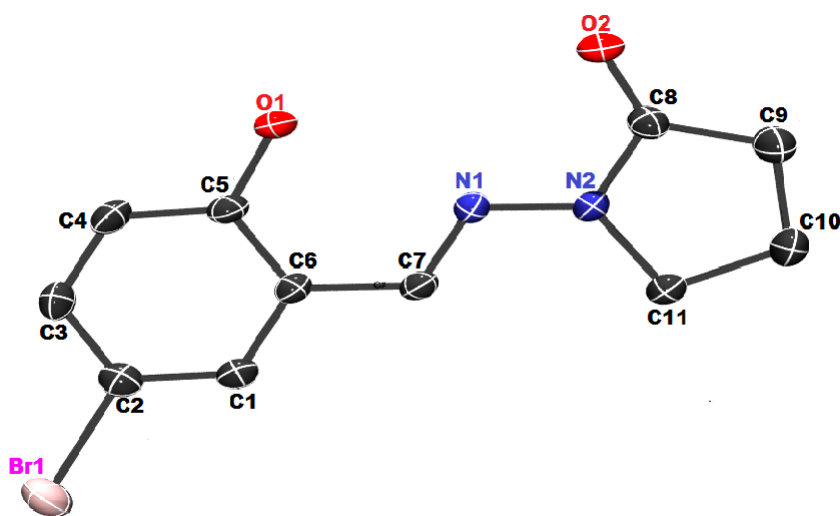


Fig. 6.3. ORTEP diagram showing the atom labelling of the asymmetric unit of the proligand, HL¹⁰ (drawn with 30% thermal ellipsoid and the hydrogen atoms are omitted for clarity).

Table 6.2. Crystal data and refinement details of proligands, HL¹⁰ & HL¹¹

| Parameters | HL ¹⁰ | HL ¹¹ |
|-----------------------------------|---|---|
| Empirical formula | C ₁₁ H ₁₁ BrN ₂ O ₂ | C ₃₃ H ₂₉ Cl ₃ N ₆ O ₆ |
| Formula weight | 283.12 | 711.97 |
| Temperature | 296(2) K | 296(2) K |
| Wavelength | 0.71073 Å | 0.71073 Å |
| Crystal system | Monoclinic | Monoclinic |
| Space group | <i>P</i> 2 ₁ / <i>c</i> | <i>P</i> 2 ₁ / <i>c</i> |
| Unit cell dimensions | a = 12.4812(13) Å α = 90° b = 7.5298(7) Å β = 106.188° c = 12.1722(12) Å γ = 90° | a = 12.2051(14) Å α = 90° b = 22.437(2) Å β = 105.57° c = 12.1279(11) Å γ = 90° |
| Volume | 1098.60(19) Å ³ | 3199.3(6) Å ³ |
| Z | 4 | 4 |
| Density (calculated) | 1.712 Mg m ⁻³ | 1.478 |
| Absorption coefficient | 3.727 mm ⁻¹ | 0.343 |
| <i>F</i> (000) | 568 | 1472.0 |
| Crystal size | 0.35 × 0.25 × 0.20 mm ³ | 0.45 × 0.20 × 0.20 |
| θ range for data collection | 3.19 to 26.98° | 1.82 to 25.10 |
| Limiting indices | -15 ≤ h ≤ 15, -6 ≤ k ≤ 9, -15 ≤ l ≤ 14 | -14 ≤ h ≤ 11, -25 ≤ k ≤ 26, -13 ≤ l ≤ 14 |
| Reflections collected | 6025 | 20167 |
| Unique reflections | 2391 [R(int) = 0.0341] | 5718 [R(int) = 0.0350] |
| Refinement method | Full-matrix least-squares on F ² | Full-matrix least-squares on F ² |
| Data / restraints / parameters | 2374 / 1 / 149 | 5713 / 0 / 423 |
| Goodness-of-fit on F ² | 0.998 | 0.992 |
| Final R indices [I > 2σ(I)] | R ₁ = 0.0372, wR ₂ = 0.0849 | R ₁ = 0.0499, wR ₂ = 0.1477 |
| R indices (all data) | R ₁ = 0.0655, wR ₂ = 0.0966 | R ₁ = 0.1525, wR ₂ = 0.2259 |
| Largest diff. peak and hole | 0.297 and -0.498 e.Å ⁻³ | 0.488 and -0.224 e.Å ⁻³ |

$$R_1 = \frac{\sum ||F_o| - |F_c||}{\sum |F_o|}$$

$$wR_2 = [\sum w(F_o^2 - F_c^2)^2 / \sum w(F_o^2)^2]^{1/2}$$

The molecule is almost planar with a classical intramolecular hydrogen bonding interaction between the proton, H' of the hydroxyl group and the azomethine nitrogen, N1 generating S(6) ring motif. The simple organic molecules are interconnected *via* intermolecular hydrogen bonding interaction between the hydrogen borne on azomethine carbon, C(7) of one unit with the hydroxyl oxygen, O(1) of the adjacent unit thus forming a chain along 'c' axis [Fig. 6.4, Table 6.3].

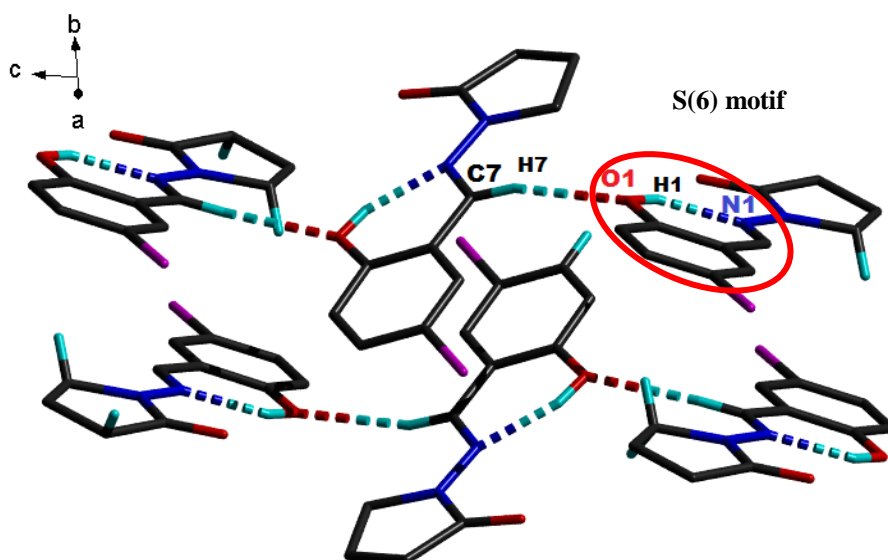


Fig. 6.4. Intermolecular hydrogen bonding interaction forming a chain along 'c' axis.

Table 6.3. Hydrogen bonding interactions in the complex

| D-H...A | D-H (Å) | H...A (Å) | D...A (Å) | D-H...A (°) |
|--|---------|-----------|-----------|-------------|
| Intramolecular hydrogen bonding | | | | |
| O(1)-H(1')...N(1) | 0.84(2) | 1.88(2) | 2.623(3) | 147(2) |
| Intermolecular hydrogen bonding | | | | |
| C(7)-H(7)...O(1) ^a | 0.93 | 2.51 | 3.405(3) | 161 |

Equivalent position code: a = x, 1/2 - y, 1/2 + z

The five membered pyrrolidine ring, Cg(1) [N2,C8,C9,C10,C11] adopts a twisted conformation with the puckering amplitudes, Q = 0.099(4) Å and

$\Phi = 269.2(18)^\circ$. Apart from classical and non-classical hydrogen bonding forces, weaker but significant non-covalent forces like C–H $\cdots\pi$ and C–Br $\cdots\pi$ interactions also contribute to good crystal packing of the complex [Fig. 6.5, Tables 6.4 and 6.5].

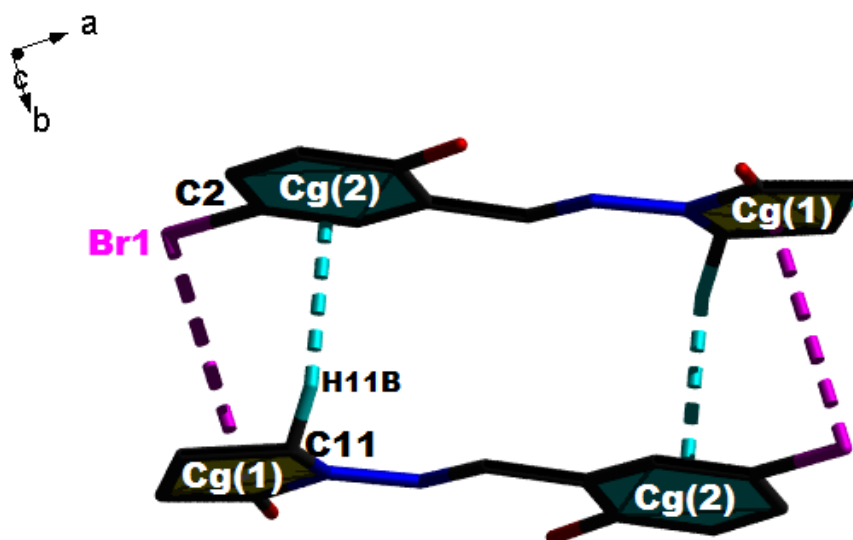


Fig. 6.5. C–H $\cdots\pi$ and C–Br $\cdots\pi$ interactions present in the ligand system.

Table 6.4. C–X \cdots Cg interactions

| C–X(I) \cdots Cg(J) | X \cdots Cg (Å) | C \cdots Cg (Å) | C–X \cdots Cg (°) |
|--|-------------------|-------------------|---------------------|
| C(2)–Br(1) \cdots Cg(1) ^b | 3.935(1) | 3.729(3) | 69.70(7) |

Equivalent position code: b = 1 - x, 1 - y, - z

Table 6.5. C–H \cdots Cg interactions

| X–H \cdots Cg | H \cdots Cg (Å) | X \cdots Cg (Å) | X–H \cdots Cg (°) |
|--|-------------------|-------------------|---------------------|
| C(11)–H(11B) \cdots Cg(2) ^c | 2.89 | 3.723(3) | 144 |

Equivalent position code: c = 1 - x, 1 - y, - z

While the hydrogen bonds connect the molecules along ‘c’ axis, the ring interactions build them along ‘b’ direction and in total develop a two dimensional spread along ‘bc’ plane [Fig. 6.6].

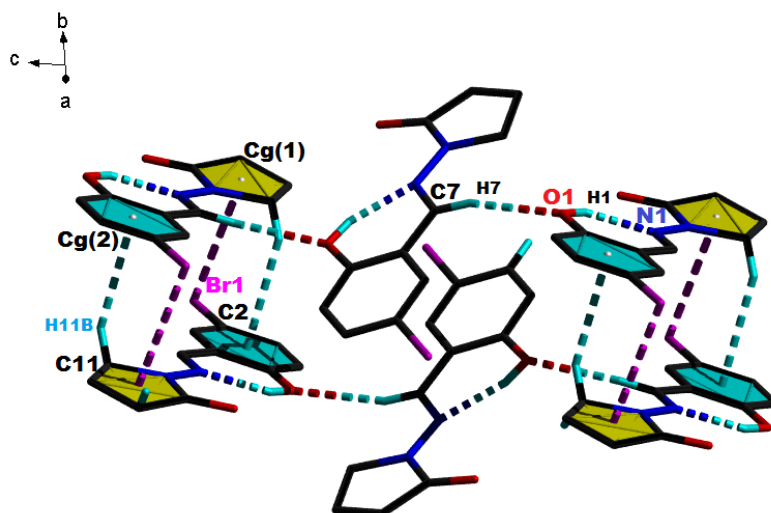


Fig. 6.6. Two dimensional spread along 'bc' plane.

6.3.2.2. 1-(*E*)-[5-chloro-2-oxidobenzylidene]pyrrolidin-2-one (HL¹¹)

The organic molecule crystallizes in monoclinic, $P2_1/c$ space group. The asymmetric unit consists of three crystallographically different entities with slight variations in bond dimensions [Fig. 6.7].

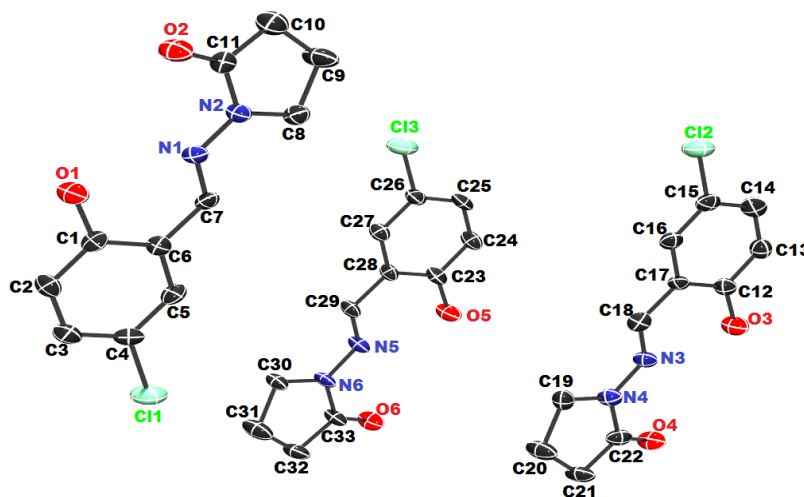


Fig. 6.7. ORTEP diagram showing the atom labelling of the asymmetric unit of the proligand, HL¹¹ (drawn with 30% thermal ellipsoid and the hydrogen atoms are omitted for clarity).

The refinement details and bond dimensions are given in Table 6.2. The carbon atom of benzene ring and pyrrolidine nitrogen atom in all the three entities are in *E* configuration with respect to azomethine double bond with torsion angles of 177.1(3)°, 176.7(3)° and 176.1(3)° respectively.

The intramolecular hydrogen bonding interaction between hydroxyl proton and azomethine nitrogen generates a *S*(6) ring motif [Fig. 6.8, Table 6.6].

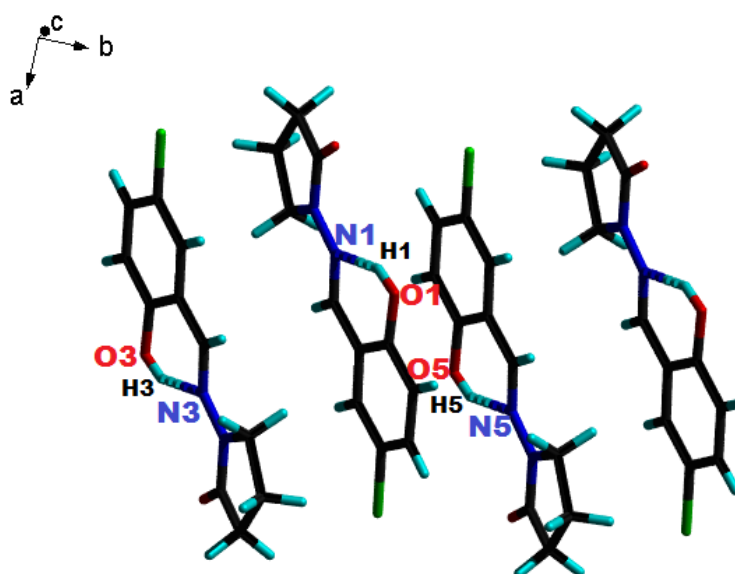


Fig. 6.8. Intramolecular hydrogen bonding interaction.

The ketonic oxygens, O(2) and O(6) are engaged in intermolecular hydrogen interactions with the protons borne by C(8) and C(19) atoms respectively. The hydrogens of the azomethine carbon atoms also involve in hydrogen bonds with the hydroxyl oxygen of the aldehydic moiety. These interactions cement the molecules along 'c' axis. The process of supramolecular self-assembly spreads the structure in 'bc' plane [Fig. 6.9, Table 6.6].

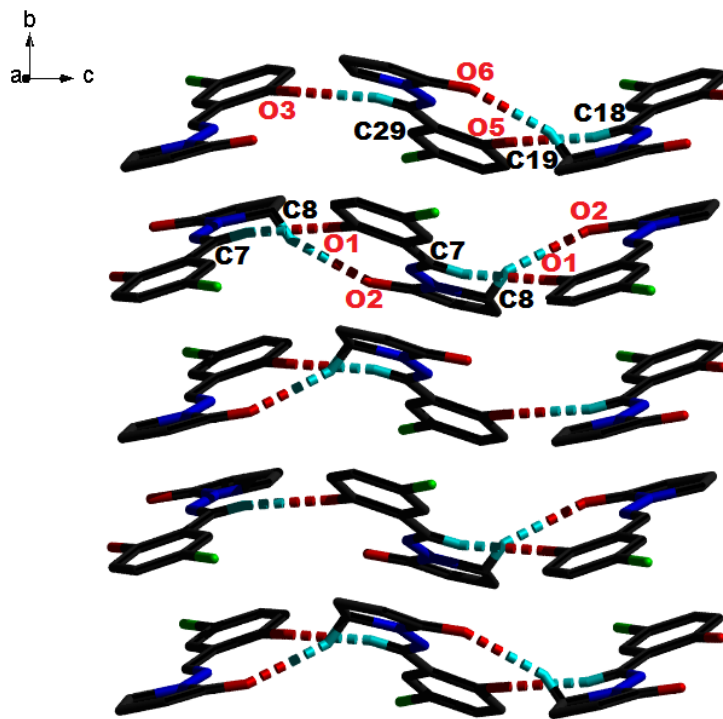


Fig. 6.9. Intermolecular hydrogen bonding interaction.

Table 6.6. Hydrogen bonding interactions in HL¹¹

| D–H···A | D–H (Å) | H···A (Å) | D···A (Å) | D–H···A (°) |
|--|---------|-----------|-----------|-------------|
| Intramolecular hydrogen bonding | | | | |
| O(1)–H(1)···N(1) | 0.82 | 1.92 | 2.639(4) | 146 |
| O(3)–H(3')···N(3) | 0.82 | 1.86 | 2.580(1) | 146 |
| O(5)–H(5')···N(5) | 0.82 | 1.86 | 2.583(1) | 146 |
| Intermolecular hydrogen bonding | | | | |
| C(7)–H(7)···O(1) ^a | 0.93 | 2.48 | 3.377(7) | 163 |
| C(8)–H(8A)···O(2) ^a | 0.97 | 2.58 | 3.365(7) | 138 |
| C(18)–H(18)···O(5) ^b | 0.93 | 2.49 | 3.394(6) | 163 |
| C(19)–H(19B)···O(6) ^b | 0.97 | 2.58 | 3.368(6) | 138 |
| C(29)–H(29)···O(3) ^b | 0.93 | 2.48 | 3.380(6) | 163 |

Equivalent position codes: a = x, 3/2 - y, 1/2 + z, b = x, 3/2 - y, -1/2 + z

Diving deep into those forces responsible for self-assembly, we observe aromatic ring interactions between the halogen atoms and the pyrrolidine rings [Fig. 6.10, Table 6.7] and also C–H··· π interactions with the six membered benzene rings chaining them along ‘*b*’ direction [Fig. 6.10, Table 6.8].

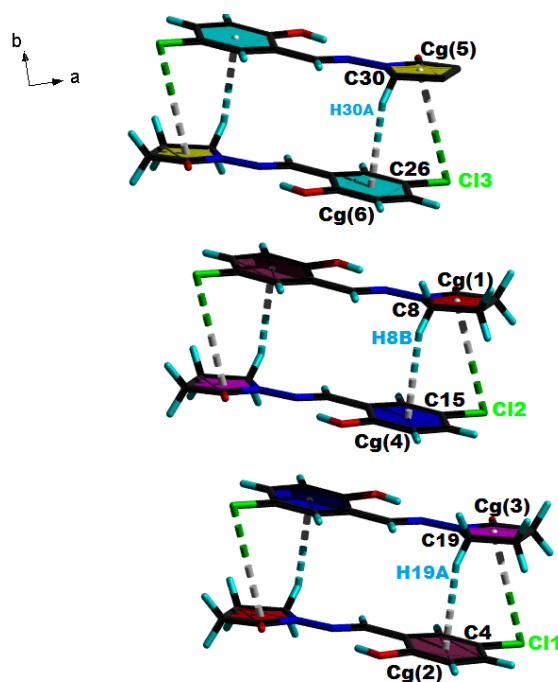


Fig. 6.10. C–Cl··· π and C–H··· π interactions in the proligand HL¹¹.

Table 6.7. C–X···Cg interactions

| C–X(I)···Cg(J) | X···Cg (Å) | C···Cg (Å) | C–X···Cg (°) |
|----------------------------------|------------|------------|--------------|
| C(4)–Cl(1)···Cg(3) ^c | 3.953(3) | 3.691(7) | 68.6(2) |
| C(15)–Cl(2)···Cg(1) ^d | 3.950(3) | 3.693(5) | 68.7(1) |
| C(26)–Cl(3)···Cg(5) ^e | 3.949(3) | 3.686(7) | 68.5(2) |

Equivalent position codes: c = x, y, -1 + z, d = x, y, 1 + z, e = 1 - x, 1 - y, 2 - z

Table 6.8. C–H···Cg interactions

| C–H···Cg | H···Cg (Å) | C···Cg (Å) | C–H···Cg (°) |
|-----------------------------------|------------|------------|--------------|
| C(8)–H(8B)···Cg(4) ^c | 2.88 | 3.682(7) | 140 |
| C(19)–H(19A)···Cg(2) ^d | 2.86 | 3.668(7) | 141 |
| C(30)–H(30A)···Cg(6) ^e | 2.85 | 3.671(7) | 143 |

Equivalent position codes: c = x, y, -1 + z, d = x, y, 1 + z, e = 1 - x, 1 - y, 2 - z

6.3.2.3. [Cu(L¹⁰)Cl] (**18**)

The complex crystallizes in monoclinic, Cc space group. The asymmetric unit of the complex is shown in Fig. 6.11. Crystallographic details are given in Table 6.9. The square planar topology of the complex is satisfied by the NOO tridentate ligand system and the chlorido ligand.

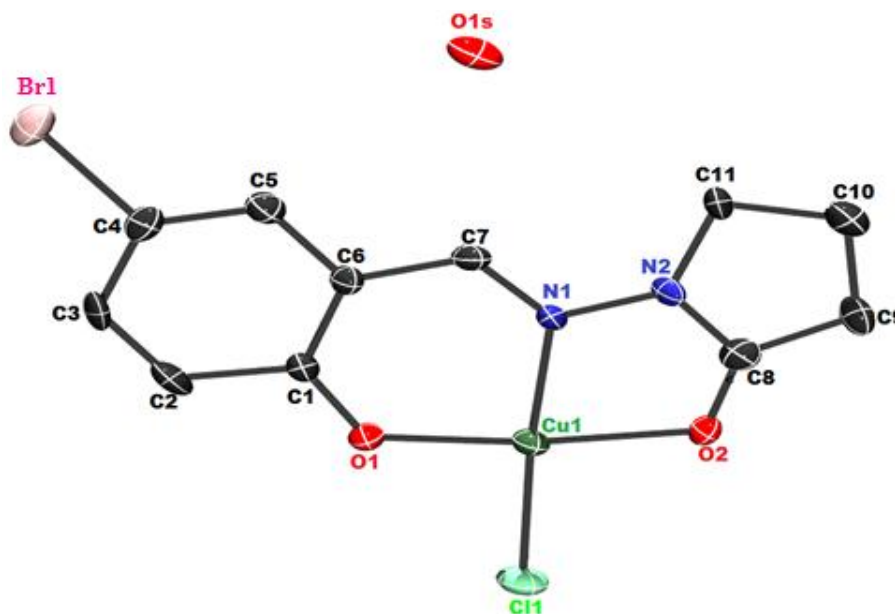


Fig. 6.11. ORTEP diagram showing the atom labelling of the asymmetric unit of the complex **18** (drawn with 30% thermal ellipsoid and the hydrogen atoms are omitted for clarity).

Table 6.9. Crystal data and refinement details of complexes, **18** and **19**

| Parameters | 18 | 19 |
|-----------------------------------|--|---|
| Empirical formula | C ₁₁ H ₁₀ BrClCuN ₂ O ₃ | C ₁₁ H ₁₀ Cl ₂ CuN ₂ O ₂ |
| Formula weight | 397.11 | 336.66 |
| Temperature | 296(2) K | 296(2) K |
| Wavelength | 0.71073 Å | 0.71073 Å |
| Crystal system | Monoclinic | Monoclinic |
| Space group | Cc | P2 ₁ /c |
| Unit cell dimensions | a = 8.8324(11) Å α = 90° b = 23.300(3) Å β = 111.927(6)° c = 6.8995(8) Å γ = 90° | a = 9.1780(14) Å α = 90° b = 14.547(2) Å β = 113.476° c = 9.7057(13) Å γ = 90° |
| Volume | 1317.2(3) Å ³ | 1188.6(3) Å ³ |
| Z | 4 | 4 |
| Density (calculated) | 2.003 Mg m ⁻³ | 1.881 Mg m ⁻³ |
| Absorption coefficient | 4.897 mm ⁻¹ | 2.279 mm ⁻¹ |
| F(000) | 780 | 676 |
| Crystal size | 0.35 × 0.25 × 0.20 mm ³ | 0.40 × 0.25 × 0.25 mm ³ |
| θ range for data collection | 1.75 to 27.00° | 2.68 to 26.70 |
| Limiting indices | -15 ≤ h ≤ 15, -6 ≤ k ≤ 9, -15 ≤ l ≤ 14 | -11 ≤ h ≤ 10, -16 ≤ k ≤ 18, -12 ≤ l ≤ 12 |
| Reflections collected | 4459 | 8098 |
| Unique reflections | 2872 [R(int) = 0.0762] | 2514 [R(int) = 0.0387] |
| Refinement method | Full-matrix least-squares on F ² | Full-matrix least- squares on F ² |
| Data / restraints / parameters | 1437 / 2 / 172 | 2505 / 0 / 163 |
| Goodness-of-fit on F ² | 1.067 | 0.968 |
| Final R indices [I > 2σ(I)] | R ₁ = 0.0597, wR ₂ = 0.1527 | R ₁ = 0.0334, wR ₂ = 0.0860 |
| R indices (all data) | R ₁ = 0.0661, wR ₂ = 0.1643 | R ₁ = 0.0526, wR ₂ = 0.0986 |
| Largest diff. peak and hole | 0.943 and -1.277 e.Å ⁻³ | 0.605 and -0.487 e.Å ⁻³ |

$$R_1 = \frac{\sum ||F_o| - |F_c||}{\sum |F_o|}$$

$$wR_2 = [\sum w(F_o^2 - F_c^2)^2 / \sum w(F_o^2)^2]^{1/2}$$

The distortion from the square planar topology is given by $\tau_4 = [360^\circ - (\alpha + \beta)]/141^\circ$, α and β being the two largest angles around the central metal atom in the complex and the value of 0.0858 shows the extent of deviation from the perfect model. Selected bond lengths and bond angle values are given in Table 6.10. The least squares plane calculation highlights copper atom to have the least deviation and the hydroxyl oxygen to have the highest among all others. The summation of the all angles subtended at the central metal atom by the donor atoms comes to a total value of 360° . Two metallorings - five membered and six membered [Cg(1) – Cu1,O2,C8,N2,N1 and Cg(3) – Cu1,O1, C1,C6,C7,N1] are formed due to coordination.

Table 6.10. Selected bond lengths and bond angles

| Bond lengths (Å) | | Bond angles (°) | |
|------------------|-----------|------------------|----------|
| Cu(1)–O(1) | 1.889(10) | O(2)–Cu(1)–Cl(1) | 94.30(3) |
| Cu(1)–N(1) | 1.945(9) | O(2)–Cu(1)–N(1) | 81.10(4) |
| Cu(1)–O(2) | 2.044(10) | O(1)–Cu(1)–N(1) | 91.6(4) |
| Cu(1)–Cl(1) | 2.197(4) | O(1)–Cu(1)–Cl(1) | 93.0(3) |
| C(4)–Br(2) | 1.886(12) | Cl(1)–Cu(1)–N(1) | 175.4(3) |

No hydrogen bonds are present in the complex. Three types of non-covalent forces enhance the crystal stability of the system – aromatic ring to ring interaction [Fig. 6.12, Table 6.11], metal-ring interaction [Fig. 6.13, Table 6.12] and C–Br $\cdots\pi$ interaction [Fig. 6.14, Table 6.13]. These supramolecular threads are used to sew the monomeric complex units to a one-dimensional chain heading in 'c' direction.

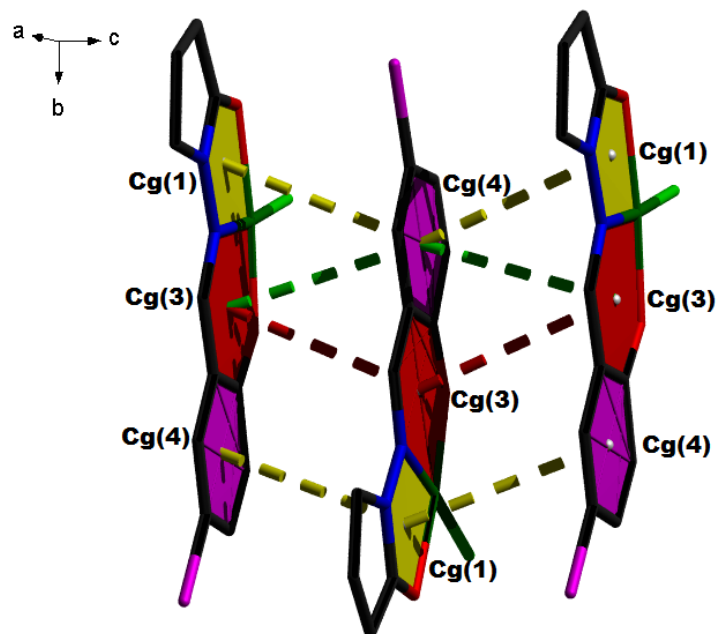


Fig. 6.12. Aromatic ring to ring interaction in complex 18.

Table 6.11. Short ring interactions

| Cg(I)⋯Cg(J) | Cg(I)⋯Cg(J) (Å) | γ (°) |
|--------------------------|-----------------|--------------|
| Cg(1)⋯Cg(4) ^a | 3.696(7) | 23.5 |
| Cg(3)⋯Cg(3) ^a | 3.749(5) | 23.9 |
| Cg(3)⋯Cg(4) ^a | 3.566(7) | 16.0 |

Equivalent position code: $a = x, 1 - y, 1/2 + z$

Cg, centroid

Cg(1) = Cu(1), O(2), C(8), N(2), N(1)

Cg(3) = Cu(1), O(1), C(1), C(6), C(7), N(1)

Cg(4) = C(1), C(2), C(3), C(4), C(5), C(6)

Cg(I) = Center of gravity of ring I

Cg(J) = Center of gravity of ring J

γ = Angle Cg(I)⋯Cg(J) vector and normal to plane J (°)

Cg(I)⋯Cg(J) = Distance of Cg(I) to Cg(J) (Å)

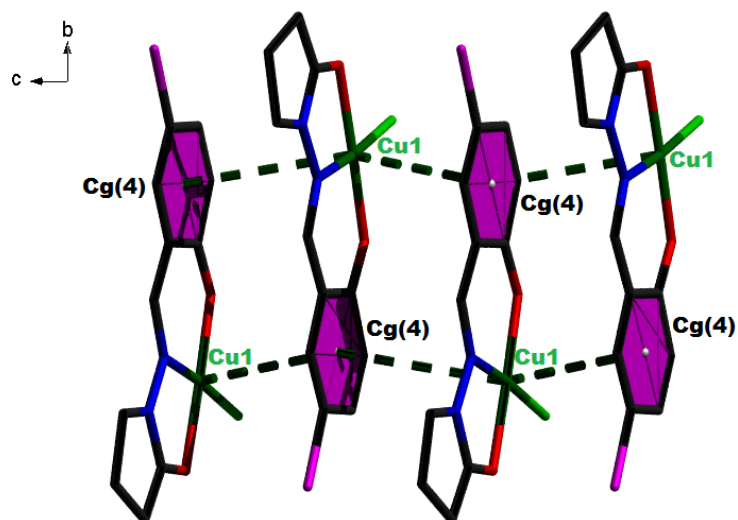


Fig. 6.13. Metal-ring interactions in complex 18.

Table 6.12. Ring-metal interactions

| Cg(I)··· M(J) | Cg(I)-M(J) (Å) |
|----------------------------|----------------|
| Cg(4)···Cu(1) ^b | 3.603 |
| Cg(3)···Cu(1) ^c | 3.667 |

Equivalent position code: $b = x, 1 - y, -1/2 + z$, $c = x, 1 - y, 1/2 + z$

M = Metal atom

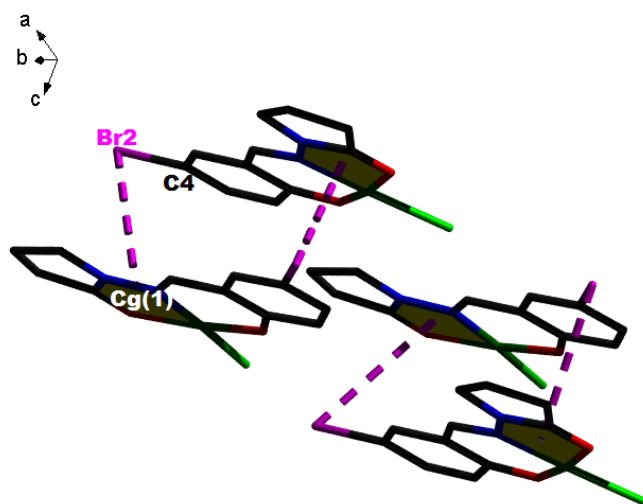
Fig. 6.14. C-Br··· π interaction in complex 18.

Table 6.13. C–Br⋯Cg interactions

| Y–X(I)⋯Cg(J) | X⋯Cg (Å) | Y⋯Cg (Å) | Y–X⋯Cg (°) |
|-------------------------------|----------|-----------|------------|
| C(4)–Br(2)⋯Cg(1) ^b | 3.853(4) | 3.413(12) | 62.3(3) |
| C(4)–Br(2)⋯Cg(1) ^c | 3.970(4) | 3.508(12) | 62.1(4) |

Equivalent position codes: b = x, 1 - y, -1/2 + z, c = x, 1 - y, 1/2 + z

6.3.2.4. [Cu(L¹¹)Cl] (19)

The copper complex crystallizes in monoclinic, $P2_1/c$ space group. The asymmetric unit is a monomeric square planar complex, with the basal plane of the complex being occupied by the NOO tridentate system along with the chlorido group [Fig. 6.15]. Refinement details and selected bond dimensions are collated in Table 6.9. Selected bond angles and bond lengths are given in Table 6.14.

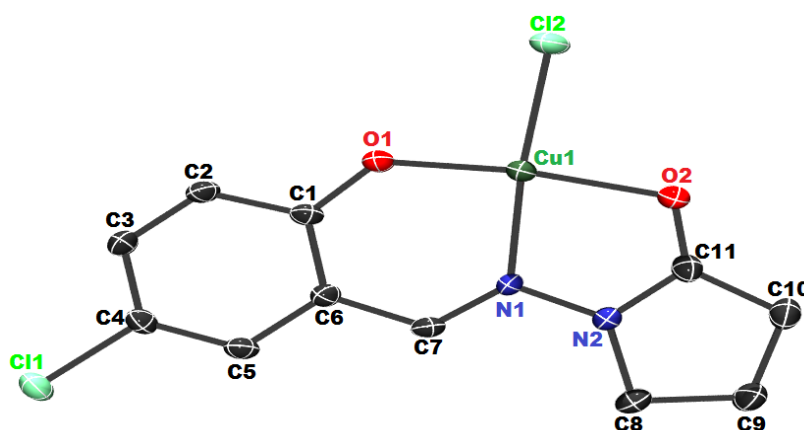


Fig. 6.15. ORTEP diagram showing the atom labelling of the asymmetric unit of the complex **19** (drawn with 30% thermal ellipsoid and the hydrogen atoms are omitted for clarity).

Table 6.14. Selected bond lengths and bond angles

| Bond lengths (Å) | | Bond angles (°) | |
|------------------|-----------|------------------|-----------|
| Cu(1)–O(1) | 1.879(3) | O(1)–Cu(1)–Cl(2) | 92.79(13) |
| Cu(1)–N(1) | 1.941(2) | O(2)–Cu(1)–Cl(2) | 92.20(15) |
| Cu(1)–O(2) | 1.997(3) | O(2)–Cu(1)–N(1) | 81.49(11) |
| Cu(1)–Cl(2) | 2.1930(9) | N(1)–Cu(1)–O(1) | 90.90(11) |
| C(4)–Cl(1) | 1.738(4) | O(1)–Cu(1)–O(2) | 167.97(8) |
| | | N(1)–Cu(1)–Cl(2) | 172.19(8) |

The trigonality index value, τ_4 - a measure of the extent of distortion between a perfect tetrahedron ($\tau_4 = 1$) and perfect square planar geometry ($\tau_4 = 0$) is given by the formula: $\tau_4 = [360^\circ - (\alpha + \beta)]/141^\circ$, α and β being the two largest angles around the central metal atom in the complex. A value of 0.1407 indicates the distortion from perfect square planar topology. The least squares plane calculation of the chelating atoms along with central copper atom shows that the copper atom deviates the least and the azomethine nitrogen, N1 the most. Coordination imposes a five and a six membered metalocycle, Cg(1) [Cu1,O2,C8,N2,N1] and Cg(3) [Cu1,O1,C1,C6,C7,N1] respectively. Bond strength follows the order: Cu1–O1 (phenoxy oxygen) > Cu1–N1 (azomethine N) > Cu1–O2 (ketonic oxygen) > Cu1–Cl2 (chloride). The five membered pyrrolidine ring, Cg(2) [N2,N8,C9,C10,C11] has an envelope conformation with C(9) as the flap atom and puckering amplitudes, $Q = 0.124(4)$ Å and $\Phi = 75.1(16)^\circ$.

Although no H bonding interactions exist for the complex, the presence of stacking forces like $\pi \cdots \pi$, metal $\cdots \pi$ and C–Cl $\cdots \pi$ interactions chain the monomeric molecules [Fig. 6.16, Tables 6.15 - 6.17].

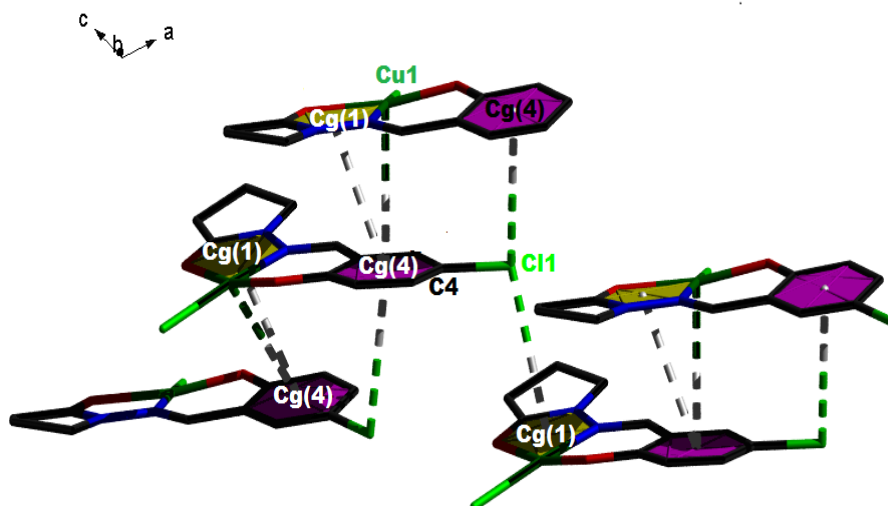


Fig. 6.16. Stacking forces in complex 19.

Table 6.15. Short ring interactions

| Cg(I)⋯Cg(J) | Cg(I)⋯Cg(J) (Å) | γ(°) |
|--------------------------|------------------------|-------------|
| Cg(1)⋯Cg(4) ^a | 3.493(1) | 22.0 |

Equivalent position code: a = x, 1/2 - y, 1/2 + z

Cg, centroid

Cg(1) = Cu(1), O(2), C(11), N(2), N(1)

Cg(4) = C(1), C(2), C(3), C(4), C(5), C(6)

Cg(I) = Center of gravity of ring I

Cg(J) = Center of gravity of ring J

Gamma = Angle Cg(I)⋯Cg(J) vector and normal to plane J (°)

Cg(I)⋯Cg(J) = Distance of Cg(I) to Cg(J) (Å)

Table 6.16. Ring-metal interactions

| Cg(I)⋯M(J) | Cg(I)-M(J) (Å) |
|--------------------------|-----------------------|
| Cg(4)⋯Cu(1) ^b | 3.636 |

Equivalent position code: b = x, 1/2 - y, -1/2 + z

M = Metal atom

Table 6.17. C-X⋯Cg interactions

| C-X(I)⋯Cg(J) | X⋯Cg (Å) | C⋯Cg (Å) | C-X⋯Cg (°) |
|-------------------------------|-----------------|-----------------|-------------------|
| C(4)-Cl(1)⋯Cg(1) ^c | 3.644(1) | 4.356(4) | 102.14(10) |
| C(4)-Cl(1)⋯Cg(2) ^c | 3.468(1) | 4.240(4) | 104.04(10) |
| C(4)-Cl(1)⋯Cg(4) ^d | 3.629(1) | 4.145(3) | 94.49(10) |

Equivalent position codes: c = 1 + x, y, z, d = x, 1/2 - y, -1/2 + z

Cg(1) = Cu(1), O(2), C(11), N(2), N(1)

Cg(2) = N(2), N(8), C(9), C(10), C(11)

Cg(4) = C(1), C(2), C(3), C(4), C(5), C(6)

6.3.2.5. Comparison of ligand and its complex

a) HL¹⁰ and complex 18

The configuration about the azomethine double bond is maintained *i.e.* 'E' with a slight change in the angle – 176.7(2)° to 179.3(9)° in the complex. Also, as the copper metal is incorporated into the system, the benzene and pyrrolidine rings approach planarity as can be seen from the decrease in dihedral angle from 9.405(9)° to 2.144(4)°. The newly formed chelate rings in the complex are almost planar with a slight angular deviation of 1.699(3)°.

b) HL¹¹ and complex 19

The 'E' configuration about the azomethine bond is sustained in the ligand and its complex. Unlike the previous case, here the incorporation of copper atom actually increases the deviation of the benzene and pyrrolidine rings from planarity *i.e.* an increase in the dihedral angle from 9.31(1)° to 14.5(1)°. The metallocycles are slightly deviated from the plane by an angle of 7.52(6)°.

Centrosymmetric copper complex derived from 1-aminopyrrolidin-2-one hydrochloride has already been reported from our group [2].

6.3.3. Photoluminescence studies

The optical emission of the ligands as well as the complexes were recorded in acetonitrile medium by exciting the samples at 350 nm. The emission intensity of the Schiff bases (HL¹⁰ & HL¹¹) decreased dramatically on complexation and this is attributed to the reduction in electron density on Schiff bases with the formation of metal complexes [3] [Fig. 6.17]. Also, complexation results in the blue shift of the emissive wavelength of the Schiff bases. The inability of the metal centre to participate in low-energy metal-centered transitions results in the excited states being ligand-centered and therefore the blue shift of the bands [4] [Table 6.18].

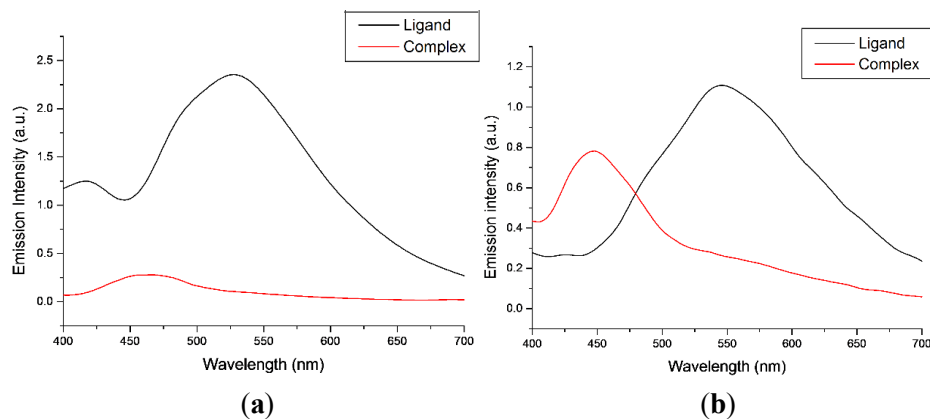


Fig. 6.17. a) Fluorescent emission spectra of HL¹⁰ and complex **18** b) Fluorescent emission spectra of HL¹¹ and complex **19** (acetonitrile, con: 1*10⁻³ M).

Table 6.18. Photophysical data of complexes

| Compounds | Solution state emission (nm) at excitation of 350 nm |
|--|--|
| HL ¹⁰ | 524 |
| [Cu(L ¹⁰)Cl] (18) | 468 |
| HL ¹¹ | 552 |
| [Cu(L ¹¹)Cl] (19) | 446 |

6.3.4. Thermal studies

The stability of the solid complexes were assessed by thermal heating of the samples up to a temperature of 700 °C. The proligand, HL¹⁰ is found to show an endothermic loss of bromine as HBr with calculated and observed weight loss almost close to each other (27.12% calcd. 28.60%). Ultimate formation of a stable species is observed. A two stage endothermic decomposition pattern is seen for the corresponding complex **18**. The initial stage corresponds to the loss of lattice water molecule in the temperature range of 120-155 °C followed by the loss of pyrrolidin-2-one system in 220-320 °C (26.08% calcd. 26.10%). The thermal profile indicates that a stable product is not formed even at a temperature of 700 °C [Fig. 6.18a].

The proligand HL¹¹, shows a two stage decomposition with the initial weight loss corresponding to the removal of chlorophenol (52.90% calcd.

53.84%) succeeded by the the removal of propyl chain. Loss of both the species are exothermic as inferred from their DSC plots. The ligand shows the formation of a stable species thereafter. The corresponding complex **19** shows a single stage exothermic loss of HCl in the range 240-310 °C followed by a gradual decomposition pattern [Fig. 6.18b].

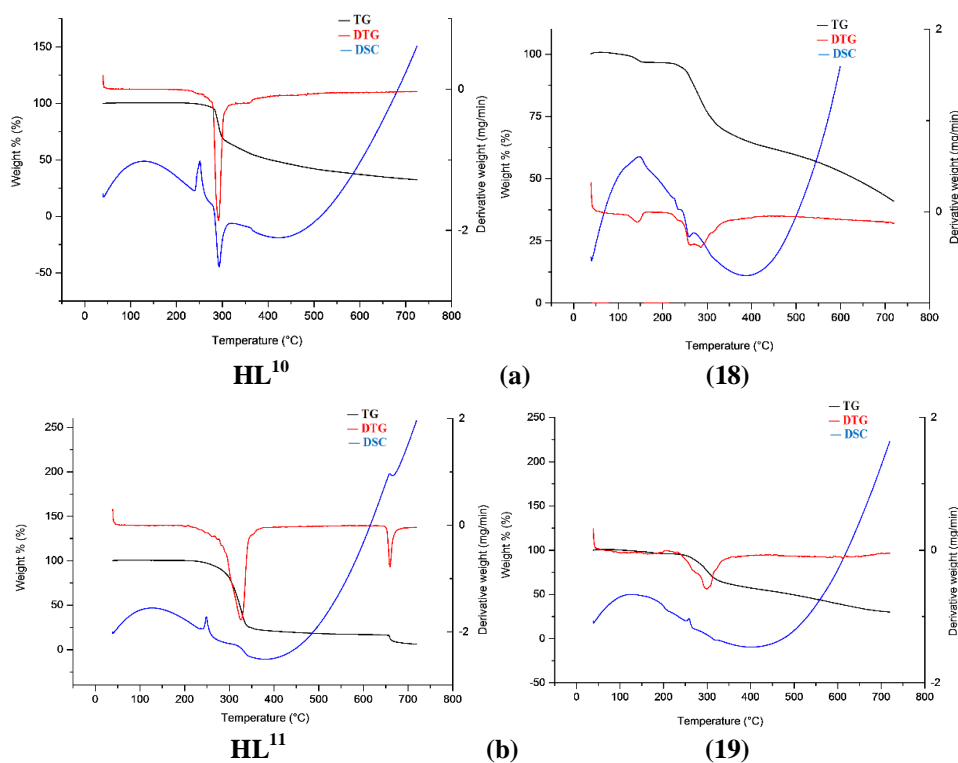


Fig. 6.18. Thermogram of proligands and complexes.

6.3.5. EPR spectral studies

The EPR spectra of the complex, **18** was recorded at room temperature as well as in solution state at 77 K. The complex showed an axial spectra with $g_{\parallel} = 2.190$ and $g_{\perp} = 2.075$ in its powder form. Whereas the same in solution state at 77 K showed four well resolved hyperfine splittings in the parallel region with A_{\parallel} value of $175 \times 10^{-4} \text{ cm}^{-1}$. The splittings in the high intense region are not well-defined. The $g_{\parallel} > g_{\perp} > 2.0023$ suggests a $d_{x^2-y^2}$ ground state and a square planar geometry around Cu(II).

The G value of 2.581 is indicative of significant exchange interactions. The bonding parameters, α^2 , β^2 and γ^2 all lie in between 0.5 – 1, symptomatic of partial ionic and partial covalent bonding nature of M–L bond. Also the $K_{\parallel} < K_{\perp}$, showing significant in-plane π bonding. The parameter $f (g_{\parallel}/A_{\parallel})$ is an index to express the range of tetrahedral distortion from planarity and this value lying in between 105 and 150 cm is supportive of a square planar geometry [5]. The complex has a f value of 131 substantiating the above statement [Fig. 6.19, Table 6.19].

Unfortunately, we didn't get a quality spectrum for the complex **19** and hence not discussed here.

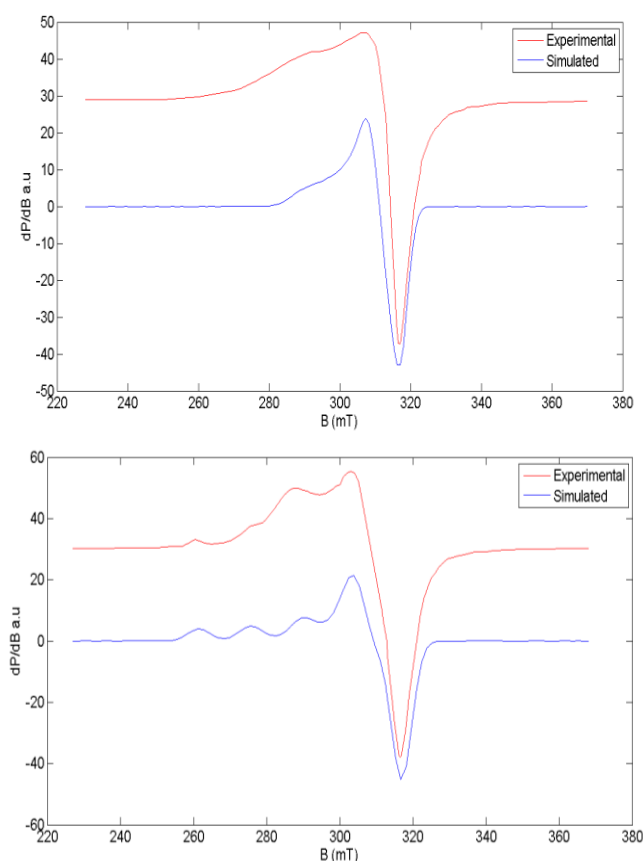


Fig. 6.19. EPR spectra of complex **18** in polycrystalline state (top) and in DMF at 77 K (bottom).

Table 6.19. Spin Hamiltonian and bonding parameters of copper(II) complex

| Compound | Polycrystalline state (298 K) | | | DMF solution (77 K) | | | | | | | | | | | |
|-------------------------------|----------------------------------|-------------|-------|---------------------|---------------------|----------|-----------------|-------------|----------|------------|-----------|------------|-----------------|-------------|-----|
| | g_{\parallel} | g_{\perp} | G | $g_{\parallel}g_3$ | $g_{\perp}g_1, g_2$ | g_{av} | A_{\parallel} | A_{\perp} | A_{av} | α^2 | β^2 | γ^2 | K_{\parallel} | K_{\perp} | f |
| [Cu(L ¹⁰)Cl] (18) | 2.190 | 2.075 | 2.581 | 2.300 | 2.094 | 2.162 | 175 | 27.0 | 76.0 | 0.8625 | 0.8801 | 0.9769 | 0.7591 | 0.8426 | 131 |

A values in 10^{-4} cm^{-1}

References

- [1] R.M. Silverstein, G.C. Bassler, T.C. Morrill, Spectrometric Identification of Organic Compounds 4th Ed., Wiley, New York **1981**.
- [2] R.J. Kunnath, M.R.P. Kurup, S.W. Ng, *Acta Crystallogr., Sect. E: Struct. Rep. Online* **2012**, 68, m1180.
- [3] S. Konar, A. Jana, K. Das, S. Ray, S. Chatterjee, S.K. Kar, *Inorg. Chim. Acta* **2013**, 395, 1.
- [4] P. Kundu, P. Chakraborty, J. Adhikary, T. Chattopadhyay R.C. Fischer, F.A. Mautner, D. Das, *Polyhedron* **2015**, 85, 320.
- [5] U. Sakaguchi, A.W. Addison, *J. Chem. Soc., Dalton Trans.* **1970**, 600.

.....✂.....

Pharmacological, non-linear optical and catecholase activity studies

| | |
|-----------------|---|
| <i>Contents</i> | 7.1. Introduction |
| | 7.2. Pharmacological studies |
| | 7.3. Non-linear Optical Studies |
| | 7.4. Catecholase activity of copper complex |

Conspectus

The present chapter deliberates some of the application studies carried out on the selected compounds. The first session discourses the pharmacological studies with a focus on DNA interaction and the third order NLO activity studies of five of our synthesized compounds and the last portion portrays the catecholase like biomimetic activity shown by a dimeric complex.

7.1. Introduction

The interesting coordination chemistry with respect to geometry, flexible redox property and oxidation state along with the presence of structurally significant azomethine group has made copper Schiff base complexes versatile, from its application perspective. In the ensuing session, we discuss about the complex-DNA interaction studies, mainly the binding and chemical nuclease activity followed by their application in optical field, focusing on third order NLO response. The last session is centered around the copper dimeric complex showing catecholase activity thereby highlighting the ability of a copper complex to behave as a biomimetic model. The biological

studies were carried out at the Dept. of Biotechnology, CUSAT and the NLO studies at the International School of Photonics, CUSAT.

Four complexes derived from *N,N*-dimethylethylenediamine and 3,5-dichloro-2-hydroxyacetophenone and a single complex from *N*-methyl-1,3-propanediamine and 3,5-dichloro-2-hydroxyacetophenone are employed for carrying out the aforementioned studies.

7.2. Pharmacological studies

7.2.1. DNA interaction studies

Pharmacological studies pertaining to chemotherapy revolves round DNA, the genetic carrier. Therefore, any studies towards the development of metallonucleases focus primarily on the interaction of nucleic acids with molecules. Among the so far known drugs, *cis*-platin and its derivatives are the most widely used metal based drugs for cancer therapy. However their use is restricted because of its serious side effects, general toxicity and acquired drug resistance [1,2]. These are the challenges that drive the inorganic chemists to design more effective, economically viable, less toxic and site specific anticancer drugs [3].

Apart from the preparative accessibility and structural variety, the presence of azomethine linkage and the exceptional chelating ability [4,5] are also responsible for the cardinal position of Schiff base complexes in medicinal inorganic field. Biological activity largely is a structure-activity relationship and hence the transition metal complexes which offer a multitude of coordination geometries [6] are, no doubt the best candidates for bio research.

The drug-DNA interaction are of two types – i) DNA binding and ii) DNA cleavage

7.2.1.1. DNA binding

The drug-DNA binding modes can be either covalent or non-covalent. The covalent binding occurs *via* replacement of the labile ligands by binding to nitrogen base of the DNA. It is irreversible and invariably leads to complete

inhibition of DNA processes and subsequent cell death. The chemotherapeutic efficiency of *cis*-platin can be attributed to the covalent binding ability leading to apoptosis.

The non-covalent binding mode can be mainly classified as intercalative binding and groove binding. It is reversible and are considered to be less toxic when compared with covalent binders [7]. It can change DNA conformation, change DNA torsional strain and potentially lead to DNA strand breaks. All these can have its effect on gene expression [8].

The coordinative binding (sometimes termed ‘covalent’) implies inner-sphere coordination of metal ions to DNA (direct binding of metal centers to nucleic acids or the phosphate ester backbone) and the outer-sphere coordination involves interaction between the metal centres and DNA mediated through coordinated ligands. Here, our discussion is centred on the outer-sphere coordination of complexes with DNA.

a) Intercalative binding

Intercalative binding occurs in complexes having planar aromatic portion which favour their insertion between the base pairs of the DNA [Fig. 7.1]. DNA-intercalator complex is stabilized by $\pi \cdots \pi$ stacking interactions. Intercalation stabilizes, lengthens, stiffens, and unwinds the DNA double helix [9]. In order for an intercalator to fit between base pairs, the DNA must dynamically open a space between its base pairs by unwinding. Intercalators are potent mutagens, due to this ability to induce structural and therefore functional changes in the duplex DNA (including inhibition of transcription, replication, and DNA repair processes) [10].

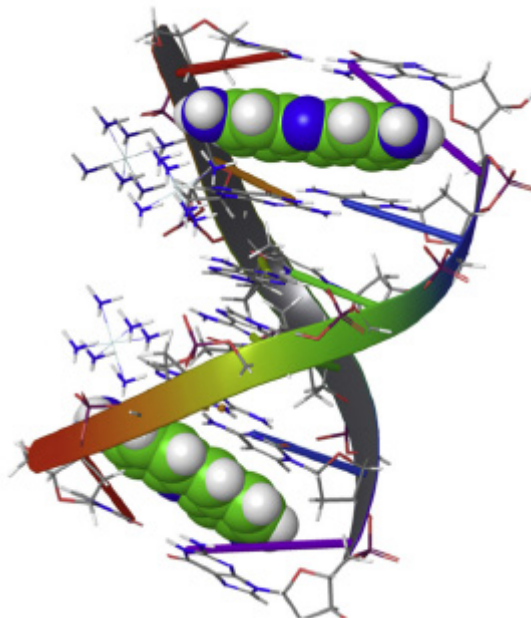


Fig. 7.1. Intercalation of a planar ligand of the complex in the DNA base pairs stack.

b) Groove binding

Groove binders interact with the edges of base pairs in either of the major (G-C) or minor (A-T) grooves of nucleic acids and it does not induce large conformational changes in DNA. It involves the association of the whole or a part of the metal complex with either or both of the grooves of the polynucleotide [Fig. 7.2]. Groove binding is driven by a combination of electrostatics, van der Waals contacts, hydrophobic interactions and hydrogen bonding. The suitability of a particular substrate for a given groove depends on the conformation of the polynucleotide as changes in sequence and structure can influence the dimensions and functionality of both the major and minor grooves [11]. Usually metal complexes bind in minor groove. A/T-rich sequences are generally preferred to G/C-rich sites due to the greater electronegative potential and narrower but more flexible structure at A–T steps in the minor groove. Unlike to intercalators, groove-binding drugs induce little

or no structural rearrangement of the DNA helix. Groove binding molecules contain unfused aromatic ring systems connected by bonds with torsional freedom in order to adopt appropriate conformation that closely matches the helical turns of DNA grooves. Minor groove binding drugs are usually narrow curve shaped, and are isohelical to the curve of the minor groove, facilitating the binding [8].

Eg: Antibiotic netropsin is a groove-binder.

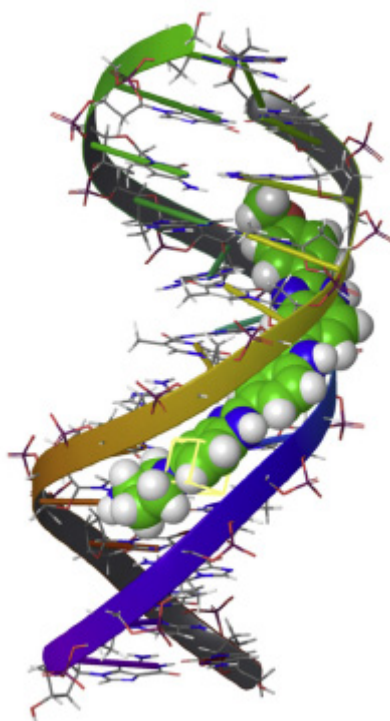


Fig. 7.2. Minor groove binding mode.

Various techniques available for studying the drug-DNA interaction are UV-visible, circular dichroism, electrophoresis, viscosity measurements etc. Of the lot, electronic spectroscopic method is the simplest and the most commonly employed technique for studying the stability of DNA and its interaction with molecules. The change in the spectral signature of the complex in the presence of DNA is used to deduce the binding mode.

7.2.1.1.1. Experimental: Spectrophotometric DNA titration

The binding studies were carried out using commercially available calf thymus DNA (CT-DNA) (Sigma Aldrich). DNA concentration per nucleotide was determined with the absorbance at 260 nm using the molar extinction coefficient ($6,600 \text{ M}^{-1}\text{cm}^{-1}$). Concentrated stock solutions of metal complexes were prepared with acetonitrile solvent and then diluted them suitably with 10 mM Tris-HCl/NaCl buffer at biological pH to required concentrations for all the experiments. The solution of CT-DNA gave a ratio of UV absorbance at 260 and 280 nm, A_{260}/A_{280} , of 1.8–1.9, indicating that the DNA was sufficiently free of protein. Absorption spectral titration experiments were performed by maintaining a constant concentration of the complex and varying the DNA concentration. This was achieved by dissolving an appropriate amount of the metal complex (5 μL) and DNA stock solutions (10, 15, 20, 25, 30 μL) while maintaining the total volume constant (1 mL). The spectra of the complex alone was recorded initially and then with incremental addition of DNA. The ratio of $[\text{DNA}]/[\text{complex}]$ was calculated to be 0.4, 0.6, 0.8, 1 and 1.2 with increase in DNA concentration, for all the test samples. This results in a series of solutions with varying concentrations of DNA but with a constant complex concentration. The absorption (A) was recorded after successive additions of CT-DNA on a Systronics double-beam UV-vis spectrophotometer using cuvettes of 1 cm path length. Prior to the experiment, DNA solutions were pre-treated with metal salt solutions to make sure that no change occurs in the absorbance value of DNA due to metal ions. Also, the possibility of increase in absorbance value with rise in concentration was ruled out. The Tris buffer was used as blank to make preliminary adjustments. The mixtures were incubated for 10 min at room temperature after each addition, before the spectra were recorded.

The intense ligand based ($\pi-\pi^*$) absorption band of the complexes was used to monitor the interaction of the complexes with CT-DNA. Any interaction of the complex with DNA is found to perturb the ligand centered transitions of the complex and the nature of spectra can be used to deduce the nature of non-covalent binding mode exhibited by our samples. The change in

the double helical structure of DNA that occurs due to this interaction is reflected as either “hyperchromic” or “hypsochromic” effect in the spectra. Hyperchromism occurs as a result of the destabilization of secondary structure of DNA while hypochromism is mainly due to the stabilization of the DNA structure by electrostatic effects or intercalation of small molecules [12,13].

The binding constants (K_b) were determined from the spectroscopic titration data using the following Wolfe–Shimer equation (1):

$$[\text{DNA}]/(\varepsilon_a - \varepsilon_f) = [\text{DNA}]/(\varepsilon_b - \varepsilon_f) + 1/K_b (\varepsilon_b - \varepsilon_f) \quad (1)$$

The ‘apparent’ extinction coefficient (ε_a) was obtained by calculating $A_{\text{obs}}/[\text{Cu}]$. The terms ε_f and ε_b correspond to the extinction coefficients of free (unbound) and the fully bound complexes. The binding constant (K_b) was calculated using a plot of $[\text{DNA}]/(\varepsilon_a - \varepsilon_f)$ versus $[\text{DNA}]$ from the ratio of slope to intercept [14].

7.2.1.1.2. Results and discussions

Binding studies

Complexes derived from *N,N*-dimethylethylenediamine and 3,5-dichloro-2-hydroxyacetophenone and *N*-methyl-1,3-propanediamine and 3,5-dichloro-2-hydroxyacetophenone were selected for our study. The absorption spectra of the complexes in the absence and presence of DNA was recorded and the spectral profiles are as shown in the Fig. 7.3. As the concentration of DNA is increased, the spectrum shows a hike in its absorbance value leading to hyperchromicity without any significant shift. The observed spectral features preclude the possibility of intercalative binding as it is associated with hypochromism. The ‘hyperchromic effect’ can be attributed to contraction and overall damage caused to the secondary structure of DNA double helix. Hyperchromism with less or no shift in absorbance is consistent with groove binding, and it may be due to external contact (surface binding) with the DNA duplex [15] or it may be due to the presence of unfused aromatic ring systems connected by bonds with torsional freedom to adopt appropriate conformation that closely matches the helical turns of DNA grooves.

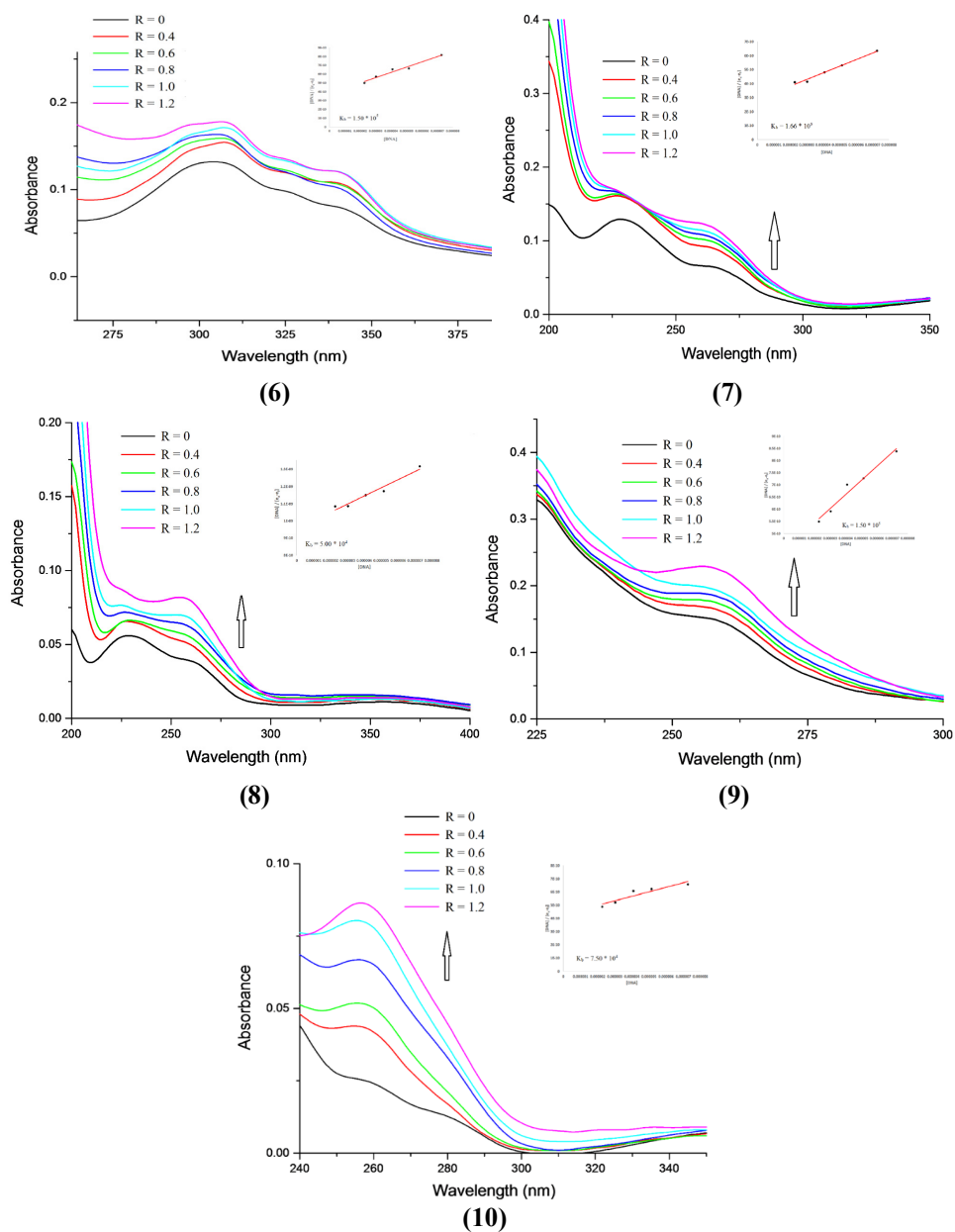


Fig. 7.3. Absorption spectra of $[\text{Cu}(\text{L}^3)(\text{N}_3)]_n$ (6), $[\text{Cu}(\text{L}^3)(\text{NCS})]$ (7), $[\text{Cu}(\text{L}^3)(\text{NCO})]$ (8), $[\text{Cu}(\text{L}^3)[\text{N}(\text{CN})_2]]_n$ (9) and $[\text{Cu}(\text{L}^4)(\text{N}_3)]_2$ (10) in the absence and with increasing amounts of CT-DNA. The arrow shows the changes in absorbance with increase in concentration of CT-DNA. (Inset: Plot of $[\text{DNA}]/(\epsilon_a - \epsilon_f)$ versus $[\text{DNA}]$).

All the five complexes exhibited an analogous electronic response on interaction with DNA. The set of absorbance values obtained from each spectra are then substituted into Wolfe-Shimer equation which gave linear plots. From the plots, the value of slope and intercept are calculated and then the ratio of slope to intercept is used to deduce the intrinsic binding constant values, K_b . The binding constant values of the complexes with DNA are tabulated [Table 7.1] and compared with that of the standard intercalator, ethidium bromide. The values fall in the range 10^4 - 10^5 for all the complexes and they are comparable with but [16] still lower than that of the standard compound ($1 * 10^7 M^{-1}$). It can be attributed to the steric hindrance of the Schiff-base coligand, which hampers the noncovalent interaction with DNA [17].

Table 7.1. The binding constant values of the complexes

| Complexes | Binding constants, $K_b (M^{-1})$ |
|----------------------------|-----------------------------------|
| $[Cu(L_3)(N_3)]_n$ (6) | $1.50 * 10^5$ |
| $[Cu(L_3)(NCS)]$ (7) | $1.66 * 10^5$ |
| $[Cu(L_3)(NCO)]$ (8) | $5.00 * 10^4$ |
| $[Cu(L_3)[N(CN)_2]]_n$ (9) | $1.50 * 10^5$ |
| $[Cu(L_4)(N_3)]_n$ (10) | $7.50 * 10^4$ |

The complex-DNA interaction follows groove binding mode symptomatic of the flexible ligand backbone that can fit into the grooves of DNA. The difference in the strength of binding (K_b values) of complexes with DNA, bearing almost the same coordinating ligands is a matter of debate and computational chemistry can play a definite role in rationalizing the observed affinity trends in terms of the electronic and structural properties. Also, the observed spectral features needs monitoring by other available techniques for assessing the drug-DNA interaction.

7.2.1.2. DNA cleavage

Binding of complexes to DNA followed by strand scission is also an area of topical importance, in view of the continuous demand for new anti-cancer

drugs. Among the host of DNA cleaving agents, transition metal complexes by virtue of its intrinsic chemical, electrochemical and photochemical reactivities are relevant. In addition to the redox properties of the metals present in these complexes, its ability to produce reactive oxygen species that mediate the cleavage by direct strand scission or base modification is exploited for the chemical nuclease activity. Cleavage of DNA can be achieved by targeting its basic constituents like base and/or sugar by an oxidative pathway or by hydrolysis of phosphoester linkages. Many complexes that cleave DNA under physiological conditions have been developed as artificial nucleases [18]. This cleavage of DNA strands are important with respect to the inhibition of uncontrolled growth of cancerous cells.

DNA cleavage follows two mechanisms: oxidative cleavage and hydrolytic cleavage. The oxidative cleavage involves the oxidation of deoxyribose by abstraction of sugar hydrogen or oxidation of nucleobases. Here, the cleavage is initiated by some external agents like light, oxidative/reductive species [19]

In hydrolytic cleavage, it is the phosphate ester bond that gets attacked and unlike the oxidative cleavage, the fragments of DNA can be enzymatically relegated [20].

7.2.1.2.1. Experimental set-up : DNA cleavage activity

The supercoiled pUC19 DNA cleavage with added reductant hydrogen peroxide was monitored using agarose gel electrophoresis. The tests were performed under aerobic conditions with H₂O₂ as co-oxidant. Five copper complexes were tested for their nucleolytic activity. Stock solutions of the complexes having a concentration of 1 mM were made up in acetonitrile medium.

Test samples were then prepared by mixing 1 μL of pUC19 DNA, 4 μL of the compound (or metal salt) in acetonitrile, and 2 μL of H₂O₂ followed by dilution with the Tris-HCl buffer to a total volume of 10 μL. The samples were incubated for 1 h at 37 °C. The prepared sample mixture along with 2 μL of

the loading buffer (containing 25% bromophenol blue, 0.25% xylene cyanol, and 30% glycerol) was then loaded into the wells and electrophoresis was performed at 80 V for 1 h in Tris-acetate–EDTA (TAE) running buffer. The gel was stained with 1% ethidium bromide and documented using a SYNGENE-GBOX imaging system.

Gel electrophoresis *via* nicking assay is a simple, rapid and highly sensitive analytical tool for the separation and analysis of macromolecules (DNA, RNA and proteins) and their fragments, based on their size and charge. Nucleic acids have a consistent negative charge imparted by their phosphate backbone, and hence migrate towards the anode. The analytes will migrate in a gel in response to the electrical field and the rate of migration depends on the strength of the field, net charge, size and shape of the molecules.

The DNA cleavage ability of complexes have been studied under physiological pH and temperature by the electrophoretic mobility shift assay using supercoiled plasmid DNA as the substrate and hydrogen peroxide as an activator. The cleavage activity of the complexes was assessed by the conversion of supercoiled DNA (Form I) to its nicked (Form II) and linear (Form III) forms. When plasmid DNA is subjected to electrophoresis, relatively fast migration is generally observed for the intact supercoiled form I. When scission occurs on one strand (nicking), the supercoil relaxes to generate a slower-moving, open-circular form II [21]. When both strands are cleaved, a linear form III is generated, which migrates between SC (supercoiled) form and OC (open circular) form of DNA.

The cleavage efficiency was measured by determining the ability of the complex to convert supercoiled DNA (SC) to nicked circular form (NC) and linear form (LC). The mechanistic aspects of the chemical nuclease activities were investigated with various quenchers like azide (singlet oxygen radical scavenger) and DMSO (hydroxyl radical scavengers).

7.2.1.2.2. Results and discussion

Cleavage studies

To assess the additional pharmacological performance of the complexes, chemical nuclease activity assay was done by gel-electrophoresis method in Tris-HCl/NaCl buffer (pH = 7.2) at 37 °C. All complexes show efficient DNA cleavage activity. Fig.7.4 shows the result of the gel-electrophoresis experiment carried out on our complexes and it shows moderate to good cleavage efficiency of the complexes.

Lanes 1, 2, 4, 5 & 11 carry the complexes along with DNA and H₂O₂. Electrophoretic separation of the DNA forms are quite evident in all cases, with complex **9** exhibiting almost complete conversion of supercoiled form to nicked form. Lanes 3 & 6 carry the metal salts along with pUC DNA and H₂O₂. It doesn't show any cleavage activity and lane 8 carries the DNA control. The control experiments reveal that only a proper combination of metal complexes along with the oxidizing agent can induce effectual cleavage of DNA.

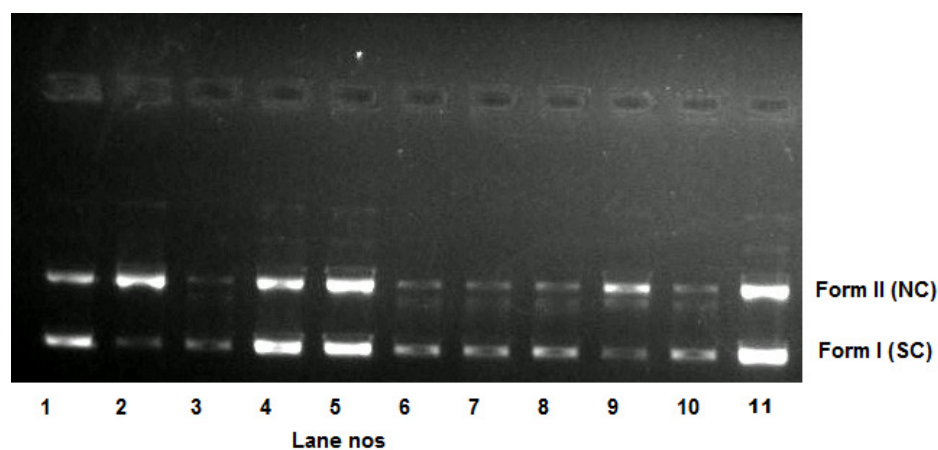
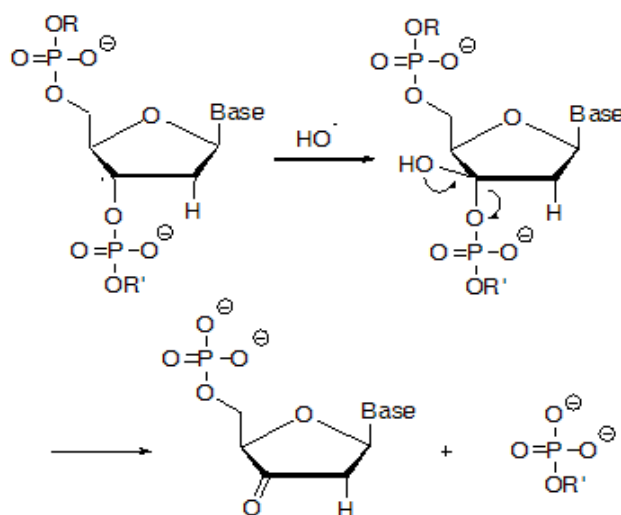


Fig. 7.4. Lane 1: Complex **6** + H₂O₂ + pUC, Lane 2: Complex **9** + H₂O₂ + pUC, Lane 3: Cu₂(OAc)₄. H₂O + H₂O₂ + pUC, Lane 4: Complex **7** + H₂O₂ + pUC, Lane 5: Complex **8** + H₂O₂ + pUC, Lane 6: CuCl. 2H₂O + H₂O₂ + pUC, Lane 7: Cu(NO₃)₂. 3H₂O + H₂O₂ + pUC, Lane 8: H₂O₂ + pUC, Lane 9: Complex **9** + H₂O₂ + pUC + NaN₃, Lane 10: Complex **9** + H₂O₂ + pUC + DMSO, Lane 11: Complex **10** + H₂O₂ + pUC.

The underlying mechanistic pathway responsible for the nucleolytic cleavage was investigated by using radical scavengers like azide and DMSO. We selected complex **9** for probing the cleavage mechanism as it is found to show significant nuclease activity. A combination of complex **9**, oxidizing agent, pUC DNA and singlet oxygen quencher, azide was loaded in lane 9. Lane 10 carries the same mixture except for the hydroxyl radical quencher, DMSO. If the cleavage occurs *via*. an oxidative pathway, then the addition of azide should have retarded the cleavage process which is not seen in lane 9. Whereas significant inhibition of DNA cleavage was observed upon the addition of DMSO (lane 10), suggesting a hydroxyl radical mediated cleavage process.

The cleavage ability of the complexes may be due to the reaction of the metal ions with H_2O_2 which produces diffusible hydroxyl radicals or molecular oxygen at ease which in turn damages DNA through Fenton type chemistry [22]. Nucleolytic activity of the copper(II) complexes in presence of hydrogen peroxide can be attributed to the participation of hydroxyl radicals in DNA cleavage. The mechanism involves oxidation of deoxyribose moiety by hydroxyl free radicals followed by the hydrolytic cleavage of the sugar phosphate backbone [Scheme. 7.1] [23].



Scheme 7.1. Hydroxyl radical mediated cleavage mechanism of sugar-phosphate backbone of DNA.

7.3. Non-linear Optical Studies

Design of non-linear optical materials is an active field of research in modern chemistry, physics and material sciences because of its potential applicability in optical fibers, data storage, optical computing, image processing, optical switching, and optical limiting [24]. The origin of NLO properties can be attributed to the delocalization of electron cloud [25]. A promising approach to developing materials with improved third-order NLO properties is to incorporate transition metal centers into organic materials [26,27]. Delocalization in inorganic compounds is mainly brought about by metal ions constructing the skeleton and organic ligands fixing the skeleton. Hence the electronic properties as such can be fine tuned either by

- modulating the central metal atom or
- by tailoring the conjugation in the organic counter part.

The introduction of metal atoms have two advantages over the pure organic entity.

- Metal incorporation introduces more sublevels into the energy hierarchy, which permits more allowed electronic transitions to take place and hence a larger NLO effect to be produced [28].
- It brings in metal–ligand and ligand–metal charge-transfer states [29].
- The valence shell structures of central metal ions can influence the NLO properties of one dimensional coordination polymers. Eg: Coordination polymers with $d < 10$ valence shell structures exhibit self-defocussing behavior [30].
- In case of copper atom as the metal centre, the electron delocalization is enhanced due to the unfilled d electron shell of Cu^{2+} which allows the possibility of low-energy charge–transfer transitions [31].

There are thus umpteen ways of tweaking the NLO properties of a metal-organic compound by altering the

- a) constructing units
- b) peripheral ligands
- c) central and skeletal metal atoms [32].

7.3.1. Fundamentals of non-linear optics

Light is a transverse electromagnetic (EM) wave. Therefore on interaction with matter, the effect of the electric (E) and magnetic fields (B) as well as their directional nature must be considered. The light-matter interaction in non-magnetic materials is described in terms of E only. In non-magnetic material, the value of B is less than E and therefore neglected [33].

Conventional light sources give a polarization, P, which is linearly dependent on electric field strength, E.

$$P = \epsilon_0 \chi^{(1)} E$$

where ϵ_0 is the susceptibility of vacuum.

With the advent of lasers, having coherence and directionality, it is possible to irradiate atoms and molecules with E that is comparable to inter-atomic field. This in turn is because the lasers can be focused to a small spot size resulting in high intensity and consequently high electric field strength, at the focal region. As a result, the vibration of electrons become highly anharmonic. In effect, the induced polarization becomes a function of higher powers of electric field, i.e. non-linear dependence on electric field strength as expressed by the equation,

$$P_{\text{NL}} = \epsilon_0 [\chi^{(1)} E + \chi^{(2)} E^2 + \chi^{(3)} E^3 + \dots]$$

Where $\chi^{(2)}$ and $\chi^{(3)}$ correspond to second and third order susceptibilities respectively.

The non-linear response of a material when the material interacts with the electric field of light is termed as NLO effect.

NLO research is mainly focussed on second order and third order properties. An ideal NLO material should have fast optical response, wide phase matchable angle, large non-linear figure of merit, flexibility for molecular design and morphology, processability into crystals or thin films, ease of fabrication, non-toxicity, optical transparency, good environmental stability and high mechanical and thermal stability [34].

7.3.1.1. Symmetry requirement for NLO materials

Anisotropic crystals which lack inversion symmetry display non-linearities of both even and odd order whereas those with inversion symmetry can display only odd order non-linearity.

7.3.1.2. Non-linear Optical effects

7.3.1.2.1. Non-linear absorption

Non-linear absorption involves the change in absorption of a material with input fluence [35]. The probability of absorption of more than a single photon before relaxing to the ground state can be increased with increase in intensity. It is determined by open aperture z-scan method. Non-linear absorption can be of two types – Reverse saturable absorption (RSA) which leads to increase in absorption of the material with increase in laser intensity and saturable absorption (SA) leads to decrease in absorption of a material with laser intensity [36,37]. In SA, the excited state absorption is lower than the ground state absorption resulting in an increase in transmission through the material with increase in intensity. On the other hand, when the excited state absorption is greater than the ground state absorption, there will be a decrease in transmission through the material as the input intensity is increased, resulting in RSA [38]. RSA generally represents positive absorption triggered either by excited state absorption (ESA) or by a two photon absorption process. In SA, open aperture z scan curve result in a peak at the focus ($z = 0$) and in RSA, a valley results at the focus.

7.3.1.2.2. Non-linear refraction

Non-linear refraction (NLR) is the change in refractive index of a medium when a material is exposed to electromagnetic radiation of suitable frequency. Optical switching, logic gates, optical limiting devices, data processing etc. are some of the fields where this property is exploited. The NLR depends on the intensity of illumination (I) according to the equation,

$$n = n_o + n_2I \text{ [35]},$$

where ' n_o ' is the linear refractive index and ' n_2 ' is non-linear refraction coefficient.

Non-linear refraction is determined by closed aperture z-scan method. Here, due to the change in refractive index at each position, the sample behaves like a thin lens of variable focal length and depending on the material, either a self-focusing effect or self-defocusing effect arises.

Self-focusing occurs as a result of a combination of a positive value of n_2 and an incident beam that is more intense in the center than at the edge. Here, the refractive index at the center of the beam is greater than that at its edge. The condition is similar to that of using a focusing lens [39].

Self-defocusing results from a combination of a negative value of n_2 and a beam profile that is more intense at the center than at the edge. In this situation the refractive index is smaller at the center of the beam than at the edge. This mimics a negative focal length lens and the beam gets defocused [39].

A peak followed by valley in the transmittance curve reveals the negative non-linearity of a material. Whereas, positive non-linear refraction gives valley-peak configuration [40].

Advantages and disadvantages of z-scan method

The technique has the following advantages like

- a). Simplicity and ease of interpretation
- b). The absorptive and refractive parts of non-linearity can be isolated
- c). Sign and magnitude of non-linearity can be measured simultaneously

The major drawback of the technique is that

Contributions to absorption and refraction at high light intensities can arise from a number of disparate processes. For example, the linear and non-linear absorption may contribute to local heating of the solution, causing thermo-optic phenomena (changes in the refractive index and absorption coefficient due to a change of the temperature). It is advisable to use low repetition rate, short laser pulses for z-scan measurements [41].

7.3.1.3. Methods for determining third order NLO property

Currently, the cubic NLO properties can be determined by third harmonic generation (THG), z-scan method and Degenerate Four Wave Mixing (DFWM). In all cases, solutions in liquid solvents or solid matrices can be examined. The THG experiments are performed with a pulsed laser and the intensity of the beam generated at the third harmonic is monitored as a function of the angle of inclination of the sample with respect to that of the fundamental beam [41]. DFWM is a relative method of measurement carried out using CS₂ as the standard reference while the z-scan technique is absolute and is used to measure two technologically relevant NLO parameters of a sample: the nonlinear refractive index and the nonlinear absorption coefficient.

7.3.2. Experimental: Z-scan method

In 1989, M. S. Bahae *et al.* [40,42] introduced z-scan method to determine the third-order non-linear optical coefficients of materials.

A laser beam (Nd-YAG laser) is focused by a lens, and the sample travels on a stage from a point before the beam focus (-z) through the focus ($z = 0$) to a point beyond the focus (+z). As the sample travels, it starts from a location where the light intensity is moderate, crosses the point of the highest intensity at $z = 0$ (because of the smallest beam diameter at that point) to a location where the intensity becomes much smaller again at +z [41] [Fig. 7.5].

The change in intensity causes two effects – a) the nonlinear absorption – measured by monitoring the total power in the transmitted beam as a function

of z (so-called open-aperture z-scan, imaginary part) b) the nonlinear refraction – determined by monitoring the power transmitted through a small pinhole located at the center of the beam in the far field (closed-aperture z-scan, real part). The nonlinear refraction and nonlinear absorption coefficients obtained from the z-scan data can then be used to compute the real and imaginary parts [41]. The main advantage of the method is that both the sign as well as the magnitude of the non-linear coefficients can be deduced from the transmittance curve [40].

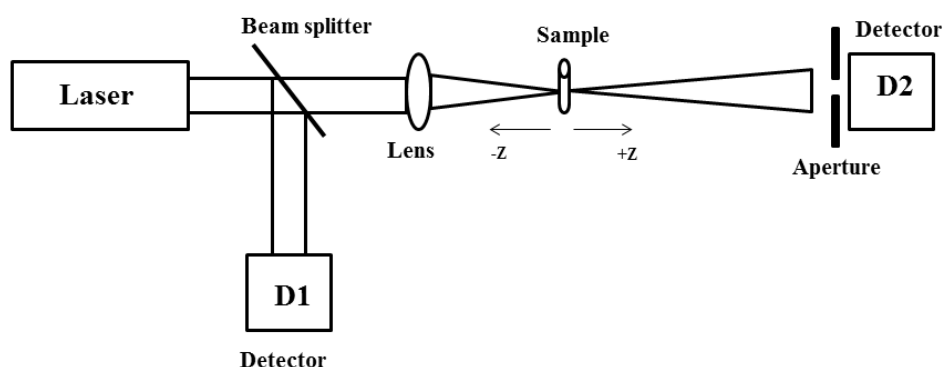


Fig. 7.5. Schematic representation of the experimental set-up of the z-scan technique.

7.3.3. Results and discussion

The non-linear transmission of the complexes were investigated at 532 nm (7 ns pulse) using z-scan method.

The NLO absorption coefficients were evaluated by z-scan technique using an open-aperture configuration. The scans were done in acetonitrile solution of the samples having a concentration of $2 * 10^{-3}$ M for **6**, **8** and **10** and a concentration of $1 * 10^{-3}$ M for the samples **7** and **9**. The open-aperture z-scan traces of the samples are given in Fig. 7.6. The red solid curves in the figure are the theoretical fit to the experimental data (black dots).

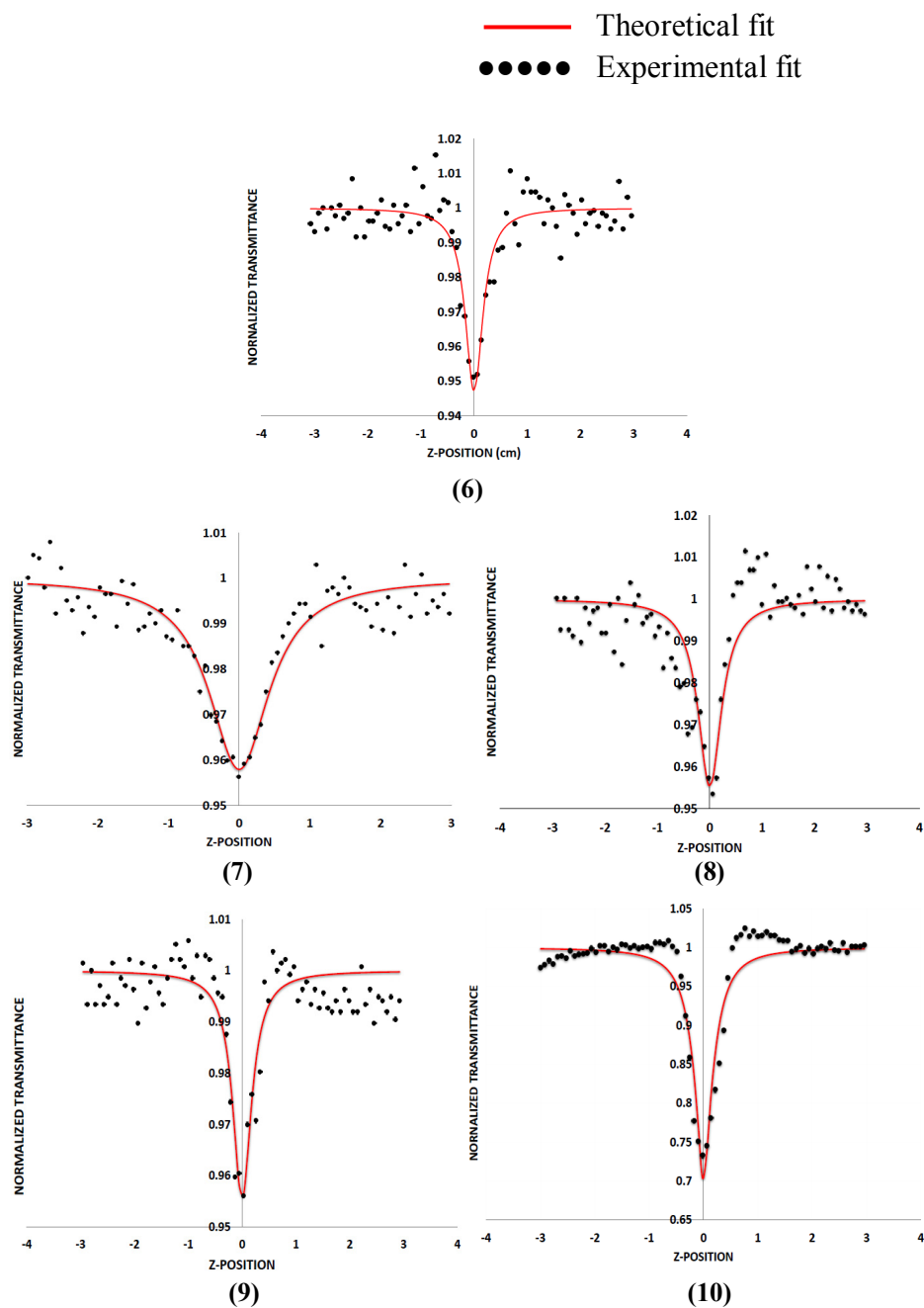


Fig. 7.6. Open aperture z-scan traces of the complexes (z-position in cm).

The open aperture scan for all the complexes show a normalized valley indicating the presence of reverse saturable absorption (RSA) with a positive NLO absorption coefficient.

The imaginary part of the third-order susceptibility is given by the equation (1) [40],

$$I_m \chi^3 = n_o^2 c^2 \beta / (240 \pi^2 \omega) \dots\dots\dots(1)$$

Where $n_o = 1.34$ is the linear refractive index of the complex in solution, c is the velocity of light in vacuum, ' ω ' is the angular frequency of radiation used.

The closed aperture scans of the same samples were also done and the traces obtained are given in Fig. 7.7. The pure z-scan curves after excluding non-linear absorption effects are obtained by dividing the CA z-scan data by the open aperture data.

The non-linear refractive index (n_2), the real parts of χ^3 ($\text{Re } \chi^3$) and third-order non-linear susceptibility (χ^3) are calculated by the following equations (2)-(4): [40]

$$n_2 \text{ (esu)} = (cn_o / 40\pi) \gamma \dots\dots\dots(2)$$

$$\text{Re } \chi^3 = n_o n_2 / 3\pi \text{ (esu)} \dots\dots\dots(3)$$

$$\chi^3 = \text{Re } \chi^3 + i \text{Im } \chi^3 \dots\dots\dots(4)$$

The spectra of all the complexes display a peak-valley pattern, indicating a negative NLR effect symptomatic of a self-defocusing effect.

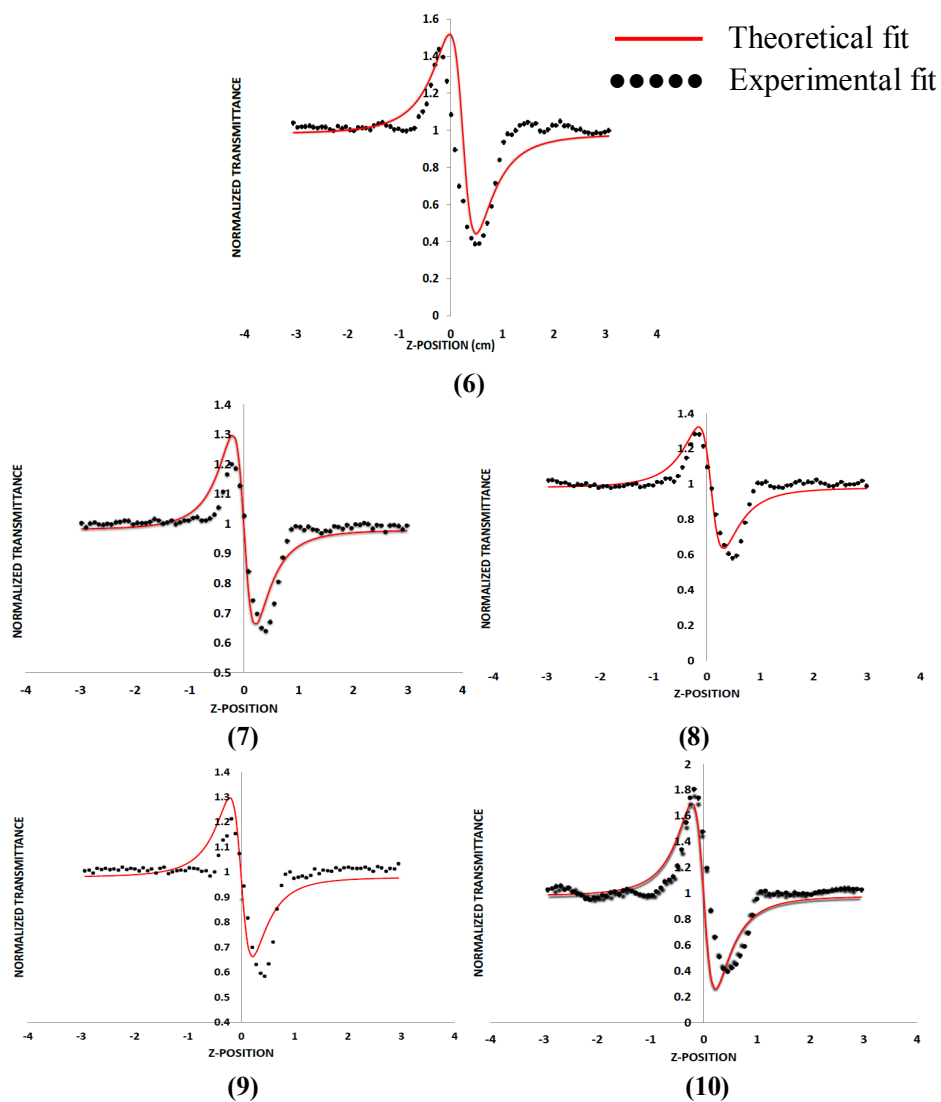


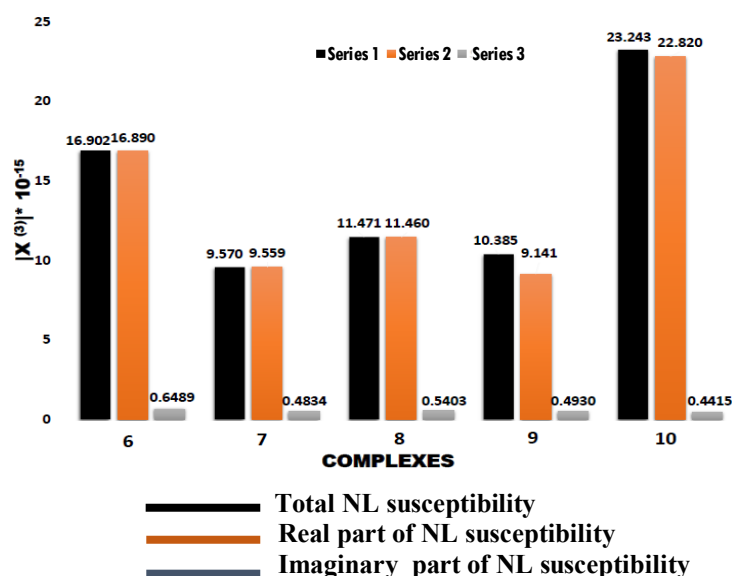
Fig. 7.7. Closed aperture z-scan traces of the complexes (z-position in cm).

The non-linear absorption coefficient (β , m/W), non-linear refraction coefficient (n_2 esu), the real and imaginary parts of non-linear susceptibility ($\text{Re } \chi^{(3)}$ & $\text{Im } \chi^{(3)}$, esu) and the total non-linear susceptibility, χ^3 (esu) for all the complexes are calculated and collated in Table 7.2. The non-linear absorption coefficients are of the order of 10^{-14} m/W and the non-linear refractive indices are of the order of 10^{-14} esu. The total non-linear susceptibility is of the order of 10^{-15} esu units.

Table 7.2. Various non-optical parameters of the complexes

| Complexes | Non-linear absorption coefficient ($\beta * 10^{-14}$, m/W) | Imaginary part of non-linear susceptibility ($\text{Im } \chi^{(3)} * 10^{-15}$, esu) | Non-linear refractive index ($n_2 * 10^{-14}$, esu) | Real part of non-linear susceptibility ($\text{Re } \chi^{(3)} * 10^{-15}$, esu) | Non-linear susceptibility ($\chi^{(3)} * 10^{-15}$, esu) |
|-----------|---|---|---|--|--|
| 6 | 3.370 | 0.6489 | -11.888 | -16.890 | 16.902 |
| 7 | 2.509 | 0.4834 | -6.723 | -9.559 | 9.570 |
| 8 | 2.804 | 0.5403 | -8.060 | -11.460 | 11.471 |
| 9 | 2.561 | 0.4930 | -6.431 | -9.141 | 10.385 |
| 10 | 22.930 | 0.4415 | -16.060 | -22.820 | 23.243 |

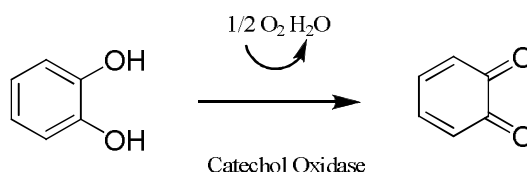
The contribution of the real and imaginary parts of the non-linear susceptibility to the total non-linear susceptibility is compared and a graph is plotted displaying the same [Fig. 7.8]. From the graph, we conclude that the NLO responses of the complexes are controlled by non-linear refractive processes and a predominant NLR effect is an attractive feature for optical switching applications [31].

**Fig. 7.8.** Graph depicting the contribution of real and imaginary parts to the total NL susceptibility.

7.4. Catecholase activity of copper complex

7.4.1. Bioinorganic catalysis

The synthesis of molecules that mimic the activity of enzymes have always posed a challenge to chemists [43]. The field remains challenging and stimulating especially because the artificial enzymes thus synthesized have the same catalytic function but are more stable and structurally less complex than the enzymes themselves. One such biochemically important process is the catecholase activity – involving the catalytic oxidation of 3,5-di-*tert*-butylcatechol to quinone through the four-electron reduction of molecular oxygen to water [44] undertaken by catechol oxidase [Scheme 7.2]. The quinones thus produced undergo polymerization to form the pigment, melanin. Catechol oxidase is a type-III copper(II) protein, the active site of which contains a dicopper core having both the copper ions surrounded by three nitrogen donor atoms of the histidine residues [45]. These reversibly bind dioxygen at ambient conditions.



Scheme 7.2. The conversion of catechol to quinone.

7.4.1.1. Structure of catechol oxidase

As proposed by Krebs and co-authors, the crystal structure of catechol oxidase as isolated from *ipomea batatas* (sweet potato) exists as [Fig. 7.9]:

Native *met* (Cu^{II} Cu^{II}) state : This state is characterized by the following structural features,

- Two cupric ions (blue) at a distance of 2.9 Å, each of them being coordinated by three histidine residues.
- They are bridged by hydroxide ion (red) at a distance of 1.8 Å units from each copper centre.

- Each copper centre has a coordination number of four and enjoys a trigonal pyramidal arrangement
- The apical positions of CuA and CuB centres being occupied by His 109 and His 240 residues

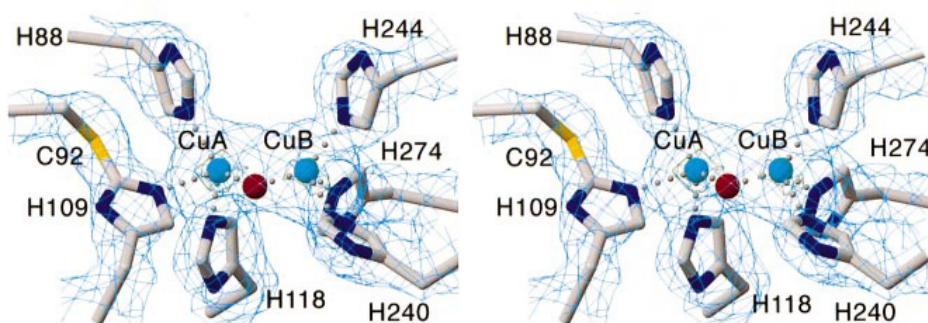


Fig. 7.9. Structure of catechol oxidase as proposed by Krebs.

Reduced deoxy ($\text{Cu}^{\text{I}} \text{Cu}^{\text{I}}$) state :

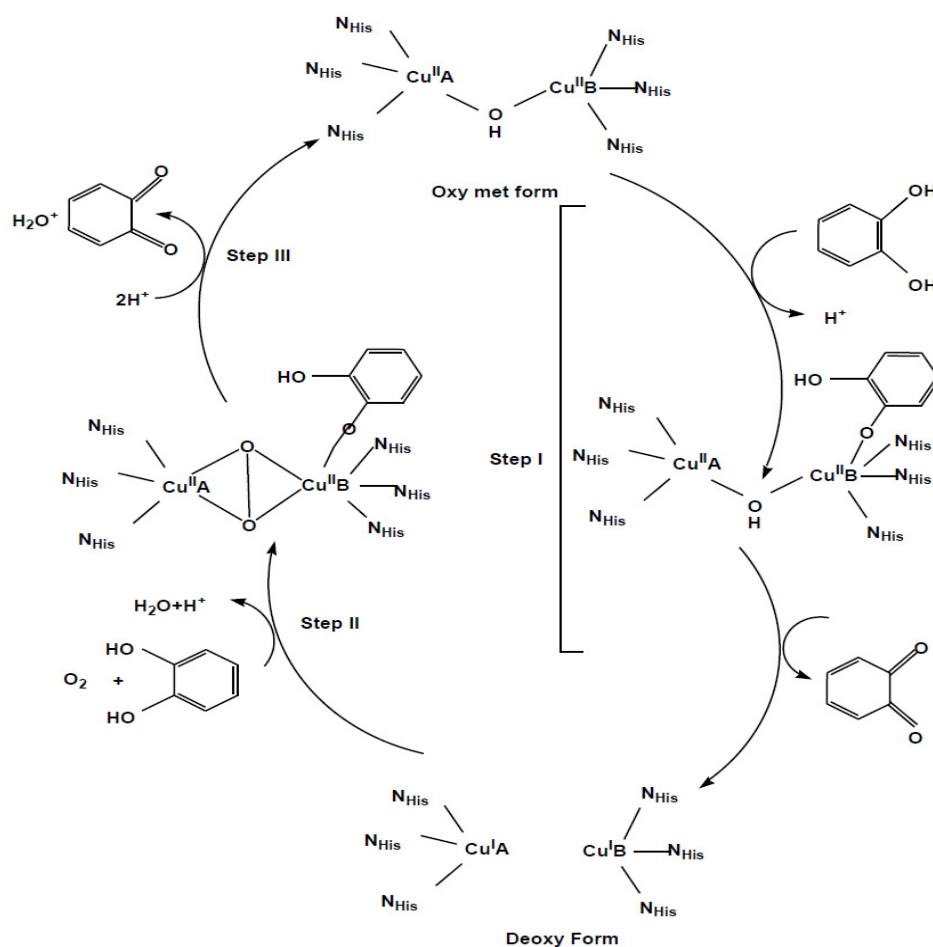
In reduced or deoxy state,

- The copper centres are in +1 oxidation state so that the distance between the centres increase from 2.9 Å (oxy) to 4.4 Å with slight change in the position of the His residues but the position of another residues remain the same [46].

7.4.1.2. General mechanism of catechol oxidation

The catalytic cycle starts with the *met* form of catecholase enzyme [Scheme 7.3]. The *met* form of the dinuclear complex reacts with catechol through the monodentate binding of catechol to CuB centre resulting in the formation of quinone and *deoxy* form in which copper is in Cu(I) state. Afterwards in the presence of oxygen, dioxygen and substrate bind simultaneously to the solvent bonded CuA center (by replacing the solvent molecule) and to the CuB center of *deoxy* form respectively. In this model, CuB is six-coordinated with a tetragonal planar coordination and the CuA site retains the tetragonal pyramidal geometry with a vacant sixth coordination site

followed by the cleavage of the O–O bond. This results in the formation of quinone with loss of a water molecule and restores the *met* form, completing the catalytic cycle [47].



Scheme 7.3. Catalytic cycle of catechol oxidase from *Ipomoea batatas*.

Of the various approaches used for the mechanistic study of catecholase activity, the structure-activity relationship is more frequently employed by the groups. This approach finds a correlation between the various structural criteria with that of the catecholase activity of the complexes.

7.4.1.3. Factors affecting catecholase activity

Some of the factors that affect the catecholase activity of the complexes are: Metal-metal distance, exogenous bridging ligand, nature of solvent *etc.*

a) Metal-metal distance

The metal-metal distance in the complex is a primary requirement as the steric match between the dicopper(II) centre and the catechol substrate largely depends on it [48]. The appropriate Cu···Cu distance for the catecholase activity falls in the range of 2.9-3.2 Å. The Cu···Cu distance should be within the optimum range as it is essential for the compatible coordination of the substrate (3,5-di-*tert*-butylcatechol) with the catalyst complex.

b) Exogenous bridging ligand

The bridging ligands like hydroxide [49a], alkoxide or phenoxide [49b,50a] and carboxylate [50b] which are readily displaced by the incoming catecholate accelerate the catecholase activity whereas strongly coordinated exogenous ligands like chloride and bromide doesn't show catecholase activity [51]. The binding ability of the complex to the substrate increases with decrease in the binding strength of exogenous bridge resulting in the efficient oxidation of the substrate.

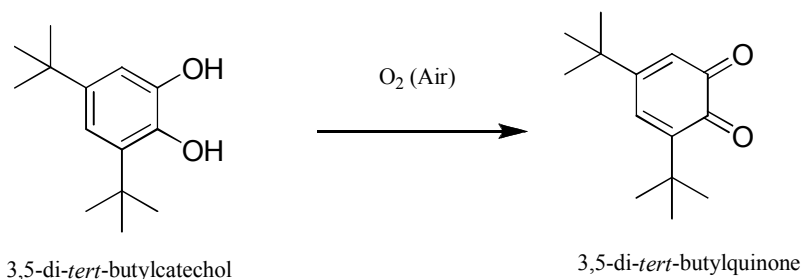
c) Nature of solvent

The choice of a solvent largely depends on the affinity of the media towards Cu(I) species, which is formed during the catalytic process. The catalytic activity is found to be enhanced in methanol-water media when compared to acetonitrile-water. The acetonitrile-water solvent mixture has got a greater affinity towards the Cu(I) species and

therefore interferes with the reoxidation of the catalyst thus disturbing the catalytic cycle. On the other hand, solvent like methanol has no comparable affinity for Cu(I) species, resulting in increased reversibility (for the conversion of reduced Cu(I) to oxidized Cu(II) species) and hence better activity.

7.4.1.4. Reaction mimicking the bioinorganic enzyme catalysis

Scheme 7.4. shows the substrate that we use to carry out the catalytic reaction and the product formed.



Scheme 7.4. Conversion of 3,5-DTBC to 3,5-DTBQ.

7.4.1.5. Why 3,5-DTBC as the substrate ?

- Low redox potential of 3,5-DTBC allowing it to be easily oxidised
- Presence of bulky substituent that prevent side reactions such as ring-opening
- Formation of very stable oxidation product, 3,5-DTBQ which can be easily detected by electronic spectroscopy, showing a maximum at 390 nm.

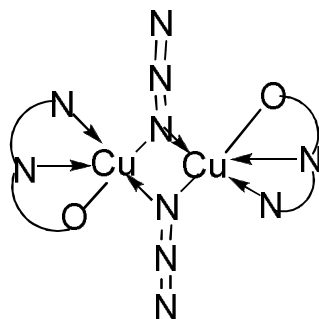
7.4.2. Experimental set-up

Prior to the detailed kinetic study of catalytic mechanism, the sample was checked for its activity. 100 equivalents of 3,5-di-*tert*-butylcatechol (3,5-DTBC) in methanol was added to 10^{-4} M of $[\text{Cu}(\text{L}^4)(\text{N}_3)]_2$ (catalyst) in methanol at room temperature under aerobic conditions. The reaction course was then monitored by electronic spectroscopy in the range 300-500 nm. The spectra

immediately after the addition and after a regular time interval of 15 min up to a total time of 120 min was recorded.

7.4.3. Results and discussion

The spectral profiles indicate that the original charge-transfer bands of the complex (373 nm) become red-shifted with gradual upsurge in intensity indicating more and more formation of 3,5-DTBQ and it is a clear cut evidence for the significant catalytic activity. The experiment was repeated by treating 10^{-4} M of the complex [Fig. 7.10] with varying concentrations of the substrate (10, 30, 50 and 70 equivalents) and the increase in the absorbance value at 390 nm as a function of time was observed in all cases [Fig. 7.11]. The dependence of rate on various substrate concentrations and the different kinetic parameters were obtained from the collected data. Therefore, our complex can be considered as biomimetic model of catechol oxidase.



Cu...Cu non bonded distance = 3.198(5) Å.

Fig. 7.10. The skeletal structure of the dicopper complex, $[\text{Cu}(\text{L}^4)(\text{N}_3)]_2$ showing catecholase activity.

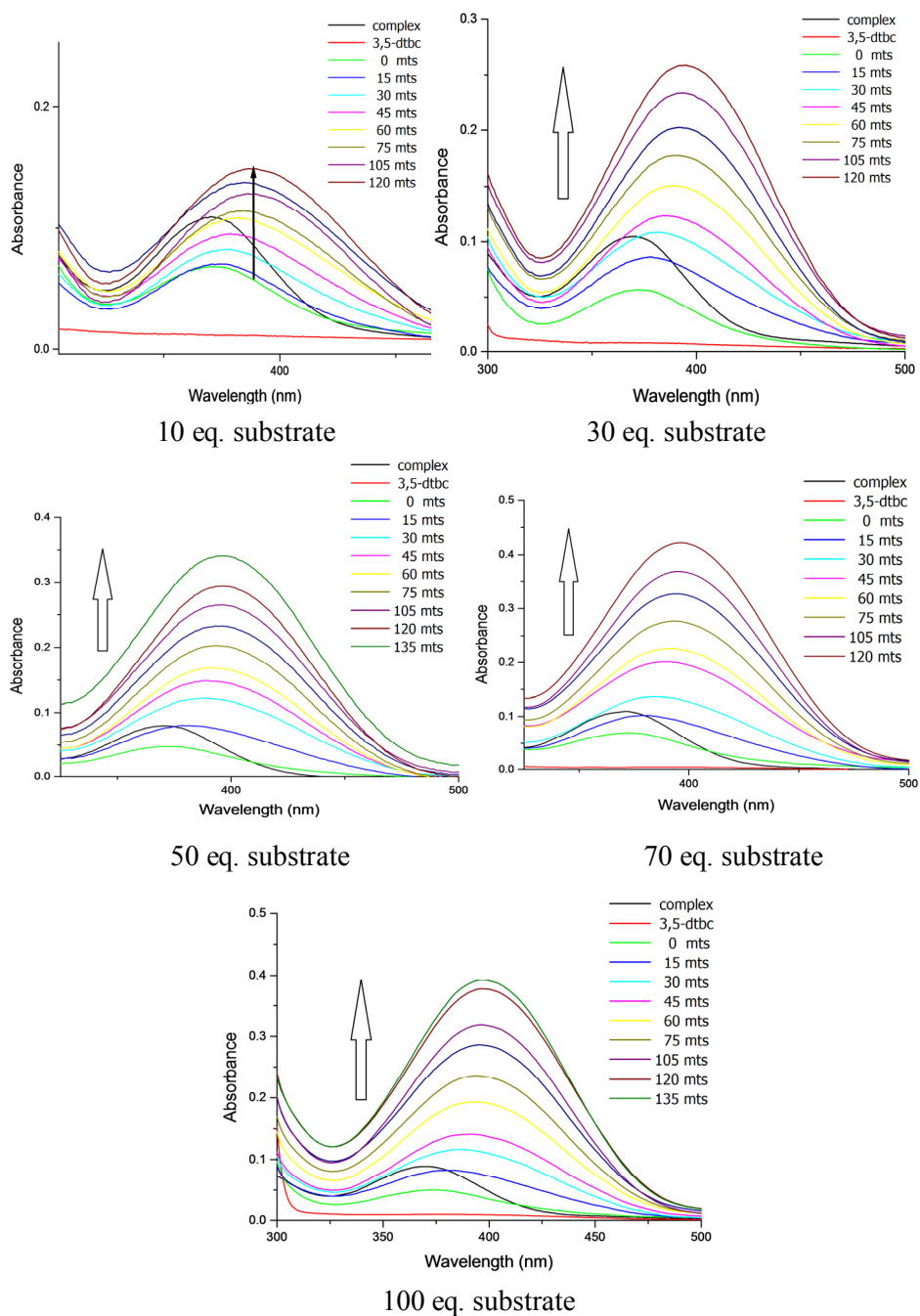


Fig. 7.11. Time dependant spectral profiles of mixture of various substrate concentrations with a constant complex concentration (10^{-4} M).

The next part of the experiment involves the determination of the kinetics of the oxidation of 3.5-DTBC through the method of initial rates by monitoring the growth of quinone band as a function of time. The observed rate versus the substrate concentration was then analyzed on the basis of Michaelis-Menten approach of enzyme kinetics to get the Lineweaver-Burk plot (double-reciprocal) plot and the values of kinetic parameters like V_{\max} and K_M were determined [Fig. 7.12]. The plot shows a first-order kinetic dependence at low concentrations of substrate whereas at higher concentrations, saturation kinetics was observed.

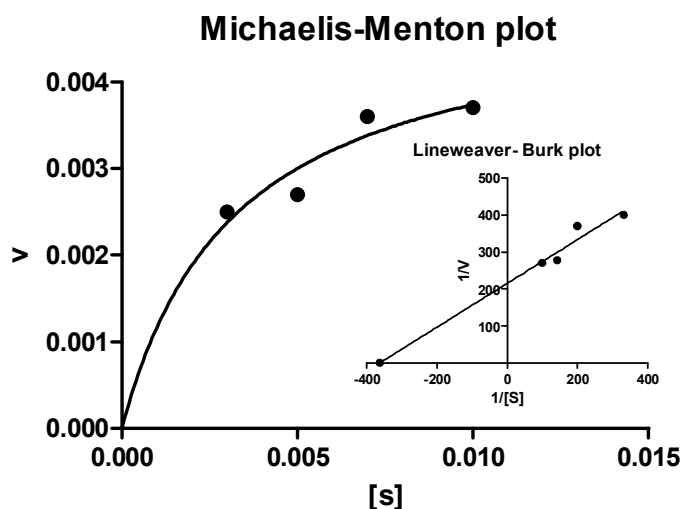


Fig. 7.12. The plot of rate versus substrate concentration (Inset shows Lineweaver-Burk plot).

The values of the rate as well as Michaelis constant as computed from the above plot are $V_{\max} = 4.95 \cdot 10^{-3} \text{ Mmin}^{-1}$ & $K_M = 3.24 \cdot 10^{-3} \text{ M}$. The calculated values of rate maxima and Michael Menton constants are compared with the other azido complexes exhibiting similar activity. The K_M values are almost similar to the reported ones whereas the rate maxima value of our complex is found to be higher than others [52,53].

References

- [1] Z. Wu, Q. Liu, X. Liang, X. Yang, N. Wang, X. Wang, H. Sun, Y. Lu, Z. Guo, *J. Biol. Inorg. Chem.* **2009**, *14*, 1313.
- [2] Y. Jung, S.J. Lippard, *Chem. Rev.* **2007**, *107*, 1387.
- [3] P.P. Netalkar, S.P. Netalkar, S. Budagumpi, V.K. Revankar, *Eur. J. Med. Chem.* **2014**, *79*, 47.
- [4] A-N.M.A. Alaghaz, M.E. Zayed, S.A. Alharbi, R.A.A. Ammar, A. Elhenawy, *J. Mol. Struct.* **2015**, *1084*, 352.
- [5] R. Anbazhagan, K.R. Sankaran, *Spectrochim. Acta Part A* **2015**, *135*, 984.
- [6] J. Tan, B. Wang, L. Zhu, *Bioorg. Med. Chem.* **2009**, *17*, 614.
- [7] M. Sirajuddin, S. Ali, A. Badshah, *J. Photochem. Photobiol. B* **2013**, *124*, 1.
- [8] C. Silvestri, J.S. Brodbelt, *Mass Spectrom Rev.* **2012**, *2*, 1.
- [9] W. Bauer, J. Vinograd, *J. Mol. Biol.* **1970**, *54*, 281.
- [10] A.M. Pizarro, N.P.E. Barry, P.J. Sadler, *Comprehensive Inorganic Chemistry II* **2013**, *3*, 752.
- [11] J.A. Smith, F.R. Keene, F. Li, J.G. Collins, *Comprehensive Inorganic Chemistry II* **2013**, *3*, 710.
- [12] Y. Song, D. Zhong, J. Luo, H. Tan, S. Chen, P. Li, L. Wang, T. Wang, *Luminescence* **2014**, *29*, 1141.
- [13] F. Arjmand, S. Parveen, M. Afzal, L. Toupet, T. Ben Hadda, *Eur. J. Med. Chem.* **2012**, *49*, 141.
- [14] A.M. Pyle, J.P. Rehmman, R. Meshoyrer, C.V. Kumar, N.J. Turro, J.K. Barton, *J. Am. Chem. Soc.* **1989**, *111*, 3051.
- [15] S. Kathiresan, T. Anand, S. Mugesh, J. Annaraj, *J. Photochem. Photobiol. B* **2015**, *148*, 290.

- [16] V. Rajendiran, R. Karthik, M. Palaniandavar, H. Stoeckli-Evans, V.S. Periasamy, M.A. Akbarsha, B.S. Srinag, H. Krishnamurthy, *Inorg. Chem.* **2007**, *46*, 8208.
- [17] G. Baronea, A. Terenzi, A. Lauriaa, A.M. Almericoa, J.M. Leal, N. Bustoc, B. Garcíac, *Coord. Chem. Rev.* **2013**, *257*, 2848.
- [18] a) S.A. Patil, S.N. Unkia, A.D. Kulkarni, V.H. Naika, P.S. Badami, *Spectrochim. Acta Part A* **2011**, *79*, 1128.
b) N. Raman, S. Sobha, *Spectrochim. Acta Part A* **2012**, *93*, 250.
- [19] a) M. Pitié, C. Boldron, G. Pratviel, *Adv. Inorg. Chem.* **2006**, *58*, 77.
b) Q. Li, W.R. Browne, G. Roelfes, *Inorg. Chem.* **2011**, *50*, 8318.
c) D-D. Li, J-L. Tian, W. Gu, X. Liu, H-H. Zen, S-P. Yan, *J. Inorg. Biochem.* **2011**, *105*, 894.
- [20] J-T Wang, Q. Xia, X-H, Zheng, H-Y Chen, H. Chao, Z-W Mao, L-N Jia, *Dalton Trans.* **2010**, *39*, 2128.
- [21] H. Keypour, M. Shayesteh, M. Rezaeivala, F. Chalabian, Y. Elerman, O. Buyukgungor, *J. Mol. Struct.* **2013**, *1032*, 62.
- [22] a) P. Krishnamoorthy, P. Sathyadevi, R.R. Butorac, A.H. Cowley, N.S.P. Bhuvanesh, N. Dharmaraj, *Dalton Trans.* **2012**, *41*, 4423.
b) V. Muniyandi, N. Pravin, P. Subbaraj, N. Raman, *J. Photochem. Photobiol. B* **2016**, *156*, 11.
- [23] K.R.S. Gowda, B. B. Mathew, C.N. Sudhamani, H.S.B. Naik, *Biomedicine and Biotechnology*, **2014**, *2*, 1.
- [24] a) T. S. Wang, Z. L. Ahmadi, T. C. Green, A. Henglein, M. A. Elsayed, *Science* **1996**, *272*, 1924.
b) M. Spassova, V. Enchev, *Chem. Phys.* **2004**, *298*, 29.
c) J. G. Qin, D. Y. Liu, C. Y. Dai, *Coord. Chem. Rev.* **1999**, *188*, 23.

- [25] a) T. Wada, L. Wang, H. Okawa, T. Masuda, M. Tabata, M. Wan, M. Kakimoto, Y. Lmai, H. Sasabe, *Mol. Cryst. Liq. Cryst. Sci. Technol. Sect. A* **1997**, 294, 245.
- b) S. Morina, T. Yamashita, K. Horie, T. Wada, H. Sadabe, *Rec. Func. Polymer* **2000**, 44, 183.
- c) H. S. Nalwa, *Adv. Mater.* **1993**, 5, 341.
- [26] N.J. Long, *Angew. Chem., Int. Ed. Engl.* **1995**, 34, 21.
- [27] G.M. Gray, C.M. Lawson, in: D.M. Roundhill, J.P. Fackler Jr. (Eds.), *Optoelectronic Properties of Inorganic Compounds*, Plenum Press, New York, **1998**, 1.
- [28] a) W.B. Lin, Z.Y. Wang, L. Ma, *J. Am. Chem. Soc.* **1999**, 121, 11249.
- b) H.W. Hou, X.R. Meng, Y.L. Song, Y.T. Fan, Y. Zhu, H.J. Lu, C.X. Du, W.H. Shao, *Inorg. Chem.* **2002**, 41, 4068.
- c) H. Chao, R.H. Li, B.H. Ye, H. Li, X.L. Feng, J.W. Cai, J.Y. Zhou, L.N. Ji, *J. Chem. Soc. Dalton Trans.* **1999**, 3711.
- [29] a) C.E. Powell, J.P. Morrall, S.A. Ward, M.P. Cifuentes, E.G. Notaras, A.M. Samoc, M.G. Humphrey, *J. Am. Chem. Soc.* **2004**, 126, 12234.
- b) N. J. Long, *Angew. Chem.* **1995**, 107, 37.
- [30] H. Hou, Y. Song, H. Xu, Y. Wei, Y. Fan, Y. Zhu, L. Li, C. Du, *Macromolecules* **2003**, 36.
- [31] X.B. Sun, X.Q. Wang, Q. Ren, G.H. Zhang, H.L. Yang, L. Feng, *Materials Research Bulletin* **2006**, 41, 177.
- [32] C. Zhang, Y. Song, X. Wang, *Coord. Chem. Rev.* **2007**, 251, 111.
- [33] N. Bloembergen, *Nonlinear Optics*, World Scientific, Singapore, **1996**.
- [34] Y. Zhang, J. Etxebarria, *Ferroelectric Liquid Crystals for Nonlinear Optical Applications, in Liquid Crystals Beyond Displays: Chemistry, Physics, and Applications (ed Q. Li)*, John Wiley & Sons, Inc., Hoboken, NJ, USA, **2012**.

- [35] R.L. Sutherland, *Hand book of nonlinear optics*, 2nd ed., Eastern Hemisphere Distribution, Marcel Dekker. Inc., USA, **2003**.
- [36] N.K.M.N. Srinivas, S.V. Rao, D.N. Rao, *J. Opt. Soc. Am. B: Opt. Phys.* **2003**, *20*, 2470.
- [37] U. Kurum, M. Yuksek, H.G. Yagliolu, A. Elmali, A. Ates, M. Karabutlut, G.M. Mamedov, *J. Appl. Phys.*, **2010**, *108*, 063102.
- [38] M.D. Zidan, Z. Ajji, *Opt. Laser Technol.* **2011**, *43*, 934.
- [39] K.J. Arun, *Investigations on the growth and characterisation of some technologically important single crystals for possible nonlinear optical applications- Thesis submitted to Cochin University of Science and Technology*, **2009**.
- [40] M.S. Bahae, A.A. Said, T.-H. Wei, D.J. Hagan, E.W. Van Stryland, *IEEE Journal of Quantum Electronics*, **1990**, *26*, 760.
- [41] M.G. Humphrey, T. Schwich, P.J. West, M.P. Cifuentes, M. Samoc, *Comprehensive Inorganic Chemistry II*, **2013**, *8*, 782.
- [42] M.S. Bahae, A.A. Said, E.W. Van Stryland, *Opt. Lett.* **1989**, *14*, 955.
- [43] a) P. Molenveld, J. F. J. Engbersen, , D.N. Reinhoudt, *Chem. Soc. Rev.* **2000**, *29*, 75.
- b) L. Zhu, O. Santos, C.W. Koo, M. Rybstein, L. Pape, J.W. Canary, *Inorg. Chem.* **2003**, *42*, 7912.
- c) K.M. Deck, T.A. Tseng, J.N. Burstyn, *Inorg. Chem.* **2002**, *41*, 669.
- [44] a) I.A. Koval, P. Gamez, C. Belle, K. Selmechib, J. Reedijk, *Chem. Soc. Rev.* **2006**, *35*, 814.
- b) A. Rompel, H. Fischer, D. Meiwes, K. Büldt-Karenzopoulos, R. Dillinger, F. Tuzcek, H. Witzel, B. Krebs, *J. Biol. Inorg. Chem.* **1999**, *4*, 56.
- [45] a) E.I. Solomon, U.M. Sundaram, T.E. Mackonkin, *Chem. Rev.* **1996**, *96*, 2563.
- b) E.I. Solomon, M.J. Baldwin, M.D. Lowery, *Chem. Rev.* **1992**, *92*, 521.

- [46] T. Klabunde, C. Eicken, J.C. Sacchetti, B. Krebs, *Nat. Struct. Biol.* **1998**, *5*, 1084.
- [47] I.A. Koval, P. Gamez, C. Belle, K. Selmeçzib, J. Reedijk, *Chem. Soc. Rev.* **2006**, *35*, 814.
- [48] N. Oishi, Y. Nishida, K. Ida, S. Kida, *Bull. Chem. Soc. Jpn.* **1980**, *53*, 2847.
- [49] a) J. Ackermann, F. Meyer, E. Kaifer, H. Pritzkow, *Chem.–Eur. J.* **2002**, *8*, 247.
b) C.-H. Kao, H.-H. Wei, Y.-H. Liu, G.-H. Lee, Y. Wang, C.-J. Lee, *J. Inorg. Biochem.* **2001**, *84*, 171.
- [50] a) F. Zippel, F. Ahlers, R. Werner, W. Haase, H.-F. Nolting, B. Krebs, *Inorg. Chem.* **1996**, *35*, 3409.
b) M. Merkel, N. Möller, M. Piacenza, S. Grimme, A. Rompel, B. Krebs, *Chem.–Eur. J.* **2005**, *11*, 1201.
- [51] P. Gentschev, A.A. Feldmann, M. Lüken, N. Müller, H. Sirgesand, B. Krebs, *Inorg. Chem. Commun.* **2002**, *5*, 64.
- [52] K.S. Banu, T. Chattopadhyay, A. Banerjee, S. Bhattacharya, E. Zangrando, D. Das, *J. Mol. Catal. A: Chem.* **2009**, *310*, 34.
- [53] K.S. Banu, T. Chattopadhyay, A. Banerjee, S. Bhattacharya, E. Suresh, M. Nethaji, E. Zangrando, D. Das, *Inorg. Chem.* **2008**, *47*, 7083.

.....✂.....

Summary, conclusions and outlook

Contents

- 8.1. *Summary of the work done*
 - 8.2. *Concluding remarks based on structure-spectroscopic correlation studies*
 - 8.3. *Outlook*
-

8.1. Summary of the work done

Building blocks in a toddler's hand results in a whole new creative world. Inorganic chemistry world is also witnessing such a boom with a variety of novel compounds which are appealing both by its structure and function. The field encompasses everything from the simple coordination complexes to the latest developments like MOFs and the upcoming COFs. Surprisingly, the toolbox of an inorganic chemist has only two components – the metal ions and the organic ligands. The investigative quest of the pioneers unveiled the role of both covalent and non-covalent forces in constructing umpteen structures with the available tools. Copious publications substantiate the significance of supramolecular forces in building aesthetic structures. Even the subtle difference in the structures created by these forces can modulate their applicability.

The thesis entitled “**Crystalline Architectures of Copper(II) Complexes Derived from Halogen Substituted Carbonyl Compounds: Interplay of Covalent and Non-Covalent Forces**” commences with an introduction to N₂O tridentate Schiff base systems as blocking ligands and the pseudohalides as the bridging ligands, its applicability in various disciplines like biological, optical,

catalytic and magnetic fields. The details of the various analytical methods used for the characterization of the synthesized systems are also outlined in Chapter 1.

Second chapter throws light upon the polymeric polymorphs and the monomers isolated from *N,N*-dimethylethylenediamine and 3,5-dichlorosalicylaldehyde. The polymers have helical *end-on* azido bridging and the monomers have cyanato and thiocyanato group incorporated. The various packing forces along with the halogen interactions are discussed herewith. Characterization techniques include elemental analyses, FTIR, UV-vis, emission studies, single crystal XRD analysis, TG-DTG-DSC and EPR studies. An attempt to discuss the variation in the geometry of the solid state structures in solvents of varying donor numbers were done by solvatochromic studies.

Azido and dicyanamido linked polymeric complexes from *N,N*-dimethyl-1,3-propanediamine and 3,5-dichlorosalicylaldehyde is the subject matter of third chapter. The ambidenticity of both the azide and dicyanamide is evidently seen from the *end-to-end* bridging mode adopted by them. Due to the involvement of various non-covalent forces, the azido complex develops into a supramolecular 3-D network whilst the dicyanamido species exists as a one dimensional polymer only. As in the previous chapter, we have carried out a similar set of characterization studies for these complexes.

A potpourri of single crystals obtained from the system which is prepared by the condensation of *N,N*-dimethylethylenediamine/*N*-methyl 1,3-propanediamine and 3,5-dichloro-2-hydroxyacetophenone is sketched in Chapter 4 and this includes two polymers, two monomers and a single azido dimer. While the azido polymer develops into a supramolecular 2D array along '*bc*' plane, the C-H $\cdots\pi$ interactions develop the dicyanamido species into a supramolecular structure. Although monomeric in its asymmetric unit, both cyanato and thiocyanato species is sewn together as a chain by C-H $\cdots\pi$ as well as $\pi\cdots\pi$ interactions. The azido complex forms a helix while the dicyanamido species forms a meso-helix. The complex from *N*-methyl-1,3-propanediamine and 3,5-dichloro-2-hydroxyacetophenone is a centrosymmetric

dimer with azide in *end-on* bridging fashion. It forms a box-type structure. Apart from the aforementioned characterization studies, quantum yield of the complexes were also calculated.

Seven single crystals were isolated from monohalogenated carbonyl compounds and *N,N*-dimethylethylenediamine. A cyanato, thiocyanato and an azido complex were derived from 5-chlorosalicylaldehyde. Unlike the cyanato complex where there is a possibility of both hydrogen bonds and weak non-covalent forces stretching them along '*ab*' plane, the thiocyanato complex has only stacking interactions steering them along a single dimension. The thiocyanato complex from 5-bromosalicylaldehyde also stretches down along a unique direction. The *end-to-end* azido complex and *end-to-end* thiocyanato complex from the fluoro substituted carbonyl compound are coordination polymers along '*c*' axis. We also obtained an unusual stair-like polymer from fluoropyridine carbonyl compound which self-assembled to a polymeric sheet. Thus, Chapter 5 discourses on the interplay of various interactions and the conclusions based on various spectroscopic studies.

A new Schiff base system is introduced in Chapter 6. We isolated single crystals of both the proligands as well as the complexes. Here 1-aminopyrrolidin-2-one hydrochloride was condensed with 5-chloro/5-bromosalicylaldehyde and two chlorido complexes - one from each of the ligand system was isolated. Various packing forces involved in both the proligand and the complex were compared. The structural variations due to complexation were analysed. All the characterization studies were done for these complexes too.

Any work becomes significant when we identify it with some applications and our work is also buttressed by such application level studies. The final chapter gives an idea about the pharmacological relevance, non-linear optical applications and catecholase like biomimetic activity of our complexes. It includes an excerpt highlighting the various studies like DNA binding/cleavage, NLO and catecholase like activity. Any chemotherapeutic drug to be used at the clinical level requires a preliminary investigation (DNA interaction

studies) i.e. its binding with DNA which we have assessed using UV-vis spectrophotometric method. The chemical-nuclease activity of our complexes was checked by gel-electrophoresis method. The third order non-linear optical activity – including the calculation of both non-linear absorption coefficients and non-linear refraction coefficients were carried out using z-scan technique and the refraction effects of our complexes were predominant over their absorption effects. Of all the complexes, only the single azido dimer with an optimum metal-metal separation of 3.198(5) Å units is found to show excellent catecholase like biomimetic activity and the kinetics follow Michaelis-Menton mechanism.

A total of twenty-two compounds including two ligands were synthesized – 10 monomers, 9 polymers and a single dimer. Of them, chosen compounds were tested for their pharmacological activity (DNA binding/cleavage), non-linear optical activity and the single dimeric compound showed catecholase like biomimetic activity.

8.2. Concluding remarks based on structure-spectroscopic correlation studies

8.2.1. Structure-spectroscopic correlation studies of Chapters 2 and 3

We have used two different ligand systems in Chapters 2 and 3 which differ by a single 'CH₂' group [Fig. 8.1]. Based on the spectroscopic data obtained, we have arrived at certain conclusions with respect to the number of 'CH₂' groups in the ligand skeleton system.

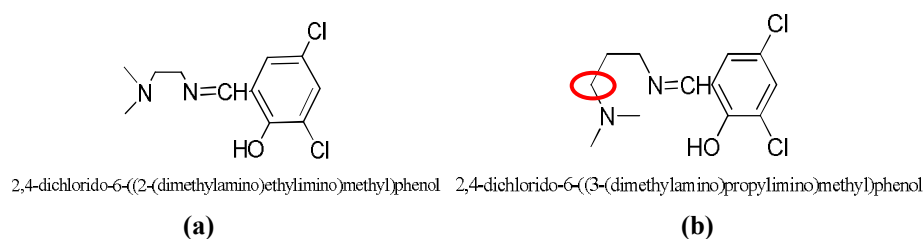


Fig. 8.1. Structure of ligands employed in synthesizing the complexes.

- For the comparative analysis, we have chosen the complexes **1a/1b** $\{[\text{Cu}(\text{L}^1)(\text{N}_3)]_n\}$ and **2** $\{[\text{Cu}(\text{L}^2)(\text{N}_3)]_n\}$ derived from the ligand systems **a** and **b** respectively. These complexes are structurally very similar except for the presence of an additional 'CH₂' group in **2**.
- The correlation is deduced by considering that the solvent molecules will occupy the axial sites.

For the same solvent, we observe a red shift of *d-d* bands as we move from system **a** to **b** [Table 8.1]. With increase in one 'CH₂' group, the ligand cavity opens up and there is a decrease in equatorial ligand field strength.

As the equatorial field strength decreases, the repulsion between the equatorially placed ligands and the electrons in $d_{x^2-y^2}$ orbital decreases and therefore not much energy is needed to excite electrons to this orbital which is reflected as red shift [1].

Table 8.1. Table consolidating the $\lambda_{\text{max}}(\text{nm})$ values of complexes **1a/1b** with **4** in different solvents

| Solvents | Donor number of solvents (DN) | Complex 1a $[\text{Cu}(\text{L}^1)(\text{N}_3)]_n$ | | Complex 1b $[\text{Cu}(\text{L}^2)(\text{N}_3)]_n$ | | Complex 4 $[\text{Cu}(\text{L}^3)(\text{N}_3)]_n$ | |
|----------|-------------------------------|--|--|--|--|---|--|
| | | $\lambda_{\text{max}}(\text{nm})$ | $\epsilon (\text{M}^{-1}\text{cm}^{-1})$ | $\lambda_{\text{max}}(\text{nm})$ | $\epsilon (\text{M}^{-1}\text{cm}^{-1})$ | $\lambda_{\text{max}}(\text{nm})$ | $\epsilon (\text{M}^{-1}\text{cm}^{-1})$ |
| DMSO | 29.8 | 639 | 164 | 639 | 128 | 675 | 49 |
| MeOH | 19.0 | 613 | 142 | 619 | 151 | 662 | 104 |
| AcN | 14.1 | 593 | 213 | 591 | 195 | 603 | 236 |
| DCM | 0.0 | 583 | 250 | 583 | 214 | 579 | 291 |
| | | 535 | 259 | 535 | 223 | | |
| | | 509 | 262 | 509 | 225 | | |

8.2.2. Structure-spectroscopic correlation studies of Chapters 2 and 4

8.2.2.1. Structural correlation of $[\text{Cu}(\text{L}^3)(\text{NCS})]$ (**7**) and $[\text{Cu}(\text{L}^3)(\text{NCO})]$ (**8**) with the electronic response

The *d-d* band energy can be correlated with the shift of the metal centre from the square basal plane. More *d-d* transition energy implies greater crystal field splitting. The greater shifting of copper centre towards the basal plane

indicates a more square planar environment, which in turn reflects a high crystal field splitting. Among the complexes **7** and **8**, the deviation of the copper centre follows the order **7** (0.0088 Å) < **8** (0.0449 Å) and the more square planar structure of thiocyanato complex **7** shows a blue shift as expected [Table 8.2].

Table 8.2. The deviation values (d), wavelength (λ) and the τ_4 values of the complexes under comparison

| | Complex 7 [Cu(L ³)(NCS)] | Complex 8 [Cu(L ³)(NCO)] |
|--|--|--|
| Deviation of metal centre from least-squares plane | $d = 0.0088$ | $d = 0.0449$ |
| λ (nm) (CH ₃ CN) | 598 | 601 |

Therefore we conclude that [Cu(L³)(NCS)] is more square planar than [Cu(L³)(NCO)] [2].

Although the same proposition didn't hold good for the square pyramidal environment, the value of Addison parameter, τ / deviation of metal centre from the least squares plane, d are taken as indicators of the relative extent of distortion of a square-pyramidal environment. Accordingly, the dicyanamido complex [0.2576/0.2035] deviates more than the azido complex [0.0868/0.0084].

8.2.2.2. Comparison of the complexes of Chapters 2 and 4

The ligand structures of the two chapters differ by the presence of an additional methyl group [shown in red circles in Fig. 8.2]. Structurally similar complexes derived from these two ligand systems are compared and conclusions are drawn based on the influence of the methyl group on the spectroscopic properties. In the $d-d$ bands of all the complexes obtained from system **b**, we observe a blue shift when compared to that of the complexes from system **a** [Table 8.3].

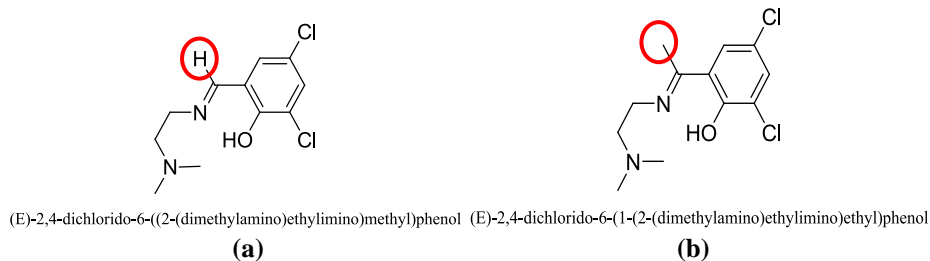


Fig. 8.2. Structure of ligands employed in synthesizing the complexes.

Table 8.3. The comparative analysis of the λ_{\max} (nm) values of complexes derived from system **a** and system **b**

| | Complex 6 / Complex 1a/1b (azido) | Complex 7 / Complex 3 (thiocyanato) | Complex 8 / Complex 2 (cyanato) |
|---|--|--|--|
| λ_{\max} (nm) (CH ₃ CN) | 573 / 583 / 583 | 598 / 621 | 601 / 633 |

Complexes **1a/1b**, **2** and **3** belong to Chapter 2 and complexes **6**, **7**, **8** to Chapter 4. We have employed system **a** for preparing complexes **1a**, **1b**, **2** and **3** and system **b** for complexes **6**, **7** and **8**.

The difference in the electronic response can be attributed to the electronic effect of the methyl group present. The methyl group, with its electron-releasing effect will make the chelate more electronegative thereby making the approach of solvents difficult. More energy needs to be expended which is mirrored as blue shift [3].

8.2.3. Structure-spectroscopic correlation studies of Chapters 2 and 5

8.2.3.1. Comparison of the complexes [Cu(L¹)(NCS)] (**3**) and [Cu(L⁵)(NCS)] (**12**)

The complexes [Cu(L¹)(NCS)] (**3**) and [Cu(L⁵)(NCS)] (**12**) (thiocyanato complexes) were compared and the two systems differ in the number of chloro substituents present [Fig. 8.3]. The λ_{\max} values indicate an increase (red shift) in the band value for the complexes prepared out of system **a** [Table 8.4]. This can be ascribed to the difference in the number of electron-

withdrawing groups present. Electron deficiency in chelate **a** will be higher due to the presence of two electron-withdrawing chloro groups over the other which has only one. Hence the axial solvation becomes quite easy making it red-shifted.

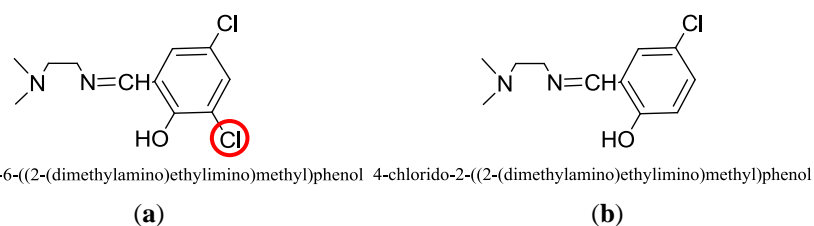


Fig. 8.3. Structure of ligands employed in synthesizing the complexes.

Table 8.4. The λ_{max} (nm) values of the complexes **3** and **12** in various solvents

| Wavelength, λ_{max} (nm) | Complex 3 / Complex 12 |
|---|------------------------|
| DMSO | 640 / 623 |
| MeOH | 636 / 616 |
| AcN | 621 / 614 |
| DCM | 619 / 584 |

The number of halogen substituents (only 5- or both 3- and 5-) is more effective than the kind of halogen (Cl or Br) substituents [4].

8.2.3.2. Structural correlation of $[\text{Cu}(\text{L}^8)(\text{N}_3)]_n$ (**15**) and $[\text{Cu}(\text{L}^8)(\text{NCS})]$ (**16**) with the electronic response

As seen for the complexes **7** and **8**, here also the *d-d* band energy can be correlated with the shift of the metal centre from the square basal plane [2] [Table 8.5].

Table 8.5. The deviation values (d) and the wavelength (λ) values of the complexes under comparison

| | Complex 15 [Cu(L⁸)(N₃)_n] | Complex 16 [Cu(L⁸)(NCS)] |
|--|--|--|
| Deviation of metal centre from least-squares plane | $d = 0.0077/0.0062$ (Cu1/Cu2) | $d = 0.1238$ |
| λ (nm) (CH ₃ CN) | 593 | 622 |

The greater shifting of copper centre towards the basal plane (less deviation) of the square pyramidal environment, results in a high crystal field splitting and hence a blue shift for complex **15** over the thiocyanato complex **16**. The $d-d$ bands clearly show that the azido complex fits better in to a square basal plane compared to the thiocyanato complex.

8.3. Outlook

8.3.1. Challenges before us.....

a. Nature of the final product

Although a number of factors like nature of metal ion, choice of solvent, blocking ligand, metal: pseudohalide ratio etc. can be stipulated as those that control the composition of final product, we still find it unmanageable to design and predict the product nature and structure and hence called ‘Serendipitous’. Work in the same field is underway in our group.

b. Structure-property correlation studies as applied to low-temperature magnetic properties of the systems

Prediction of low temperature magnetic studies on the basis of metrical parameters like metal–N–metal bridge angle, metal–N–N–metal torsion angle, metal–N–N angle and metal–N distance is difficult particularly for equatorial-axial $\mu_{1,1}$ -azido systems. More work needs to be done to arrive at a generalization based on structural factors.

8.3.2. Possibilities....

a. Computational sketch of the structures

A theoretical study of the synthesized compounds will give us a precise picture about the molecular orbitals – HOMO & LUMO, on the basis of which further fine tuning of the structures by varying the substituents is possible. The effect of anions on the various applications of these complexes can be found out.

b. Design of interesting and intriguing systems

The work can be extended by

- incorporating metals like iron, nickel, manganese which are magnetically active
- employing variety of halogen substituted carbonyl compounds and thereby to explore the halogen bonding interactions.

References

- [1] J. Tedim, S. Patrício, R. Bessada, R. Morais, C. Sousa, M.B. Marques, C. Freire, *Eur. J. Inorg. Chem.* **2006**, 3425.
- [2] L. Mandal, S. Bhattacharya, S. Mohanta, *Inorg. Chim. Acta* **2013**, 406, 87.
- [3] E. Movahedi, H. Golchoubian, *J. Mol. Struct.* **2006**, 787, 167.
- [4] T. Akitsu, Y. Einaga, *Polyhedron* **2005**, 24, 2933.

....✂....

Abbreviations

| | |
|------------------|-----------------------------------|
| Con. | Concentration |
| Calc. | Calculated |
| mmol | millimolar |
| M | molar |
| λ_{\max} | Maximum wavelength |
| ϵ | Molar absorptivity |
| DMSO | Dimethylsulphoxide |
| MeOH | Methanol |
| AcN | Acetonitrile |
| DCM | Dichloromethane |
| DMF | Dimethylformamide |
| 1D | One dimensional |
| <i>ca.</i> | Circa |
| UV-vis | Ultra violet-visible |
| FTIR | Fourier transform infrared |
| DNA | Deoxyribonucleic acid |
| TG | Thermogravimetry |
| DTG | Differential thermogravimetry |
| DSC | Differential Scanning Calorimetry |
| NLO | Nonlinear optic |

Appreviations

- HL¹ = 2,4-dichlorido-6-((2-(dimethylamino)ethylimino)methyl)phenol
HL² = 2,4-dichlorido-6-((3-(dimethylamino)propylimino)methyl)phenol
HL³ = 2,4-dichlorido-6-(1-(2-(dimethylamino)ethylimino)ethyl)phenol
HL⁴ = 2,4-dichlorido-6-((3-(dimethylamino)propylimino)methyl)phenol]
HL⁵ = 4-chloro-2-((2-(dimethylamino)ethylimino)methyl)phenol
HL⁶ = 4-chloro-2-(1-(2-(dimethylamino)ethylimino)ethyl)phenol
HL⁷ = 4-bromo-2-((2-(dimethylamino)ethylimino)methyl)phenol
HL⁸ = 2-((2-(dimethylamino)ethylimino)methyl)-6-fluorophenol
HL⁹ = N'-((3-fluoropyridin-2-yl)methylene)carbamohydrazonic acid
HL¹⁰ = (5-bromo-2-hydroxybenzylideneamino)pyrrolidin-2-one
HL¹¹ = (5-chloro-2-hydroxybenzylideneamino)pyrrolidin-2-one

.....SCB.....

Papers published

- [1] Polymeric polymorphs and a monomer of pseudohalide incorporated Cu(II) complexes of 2,4-dichlorido-6-((2-(dimethylamino)ethylimino)methyl)phenol]: Crystal structures and spectroscopic behavior, **N. Aiswarya**, M. Sithambaresan, S.S. Sreejith, S.W. Ng, M.R.P. Kurup, *Inorganica Chimica Acta* **2016**, *443*, 251.
- [2] Inclusion, pseudo-inclusion compounds and coordination polymer of Pd(II), Zn(II) and Cd(II) from salen-type Schiff base ligand with a 1,3-diimino spacer group: Crystal structures, spectroscopic and thermal studies, S.S. Sreejith, Nithya Mohan, **N. Aiswarya**, M.R.P. Kurup, *Polyhedron* **2016**, *115*, 180.
- [3] The ligating versatility of pseudohalides like thiocyanate and cyanate in copper(II) complexes of 2-benzoylpyridine semicarbazone: Monomer, dimer and polymer, R.J. Kunnath, M. Sithambaresan, A.A. Aravindakshan, **A. Natarajan**, M.R.P. Kurup, *Polyhedron* **2016**, *113*, 73.
- [4] Synthesis and spectral characterization of mono- and binuclear copper(II) complexes derived from 2-benzoylpyridine-N⁴-methyl-3-thiosemicarbazone: Crystal structure of a novel sulfur bridged copper(II) box-dimer, K. Jayakumar, M. Sithambaresan, **N. Aiswarya**, M.R.P. Kurup, *Spectrochimica Acta Part A: Molecular and Biomolecular Spectroscopy* **2015**, *139*, 28.
- [5] Crystal structure of (*E*)-N⁷-(5-bromo-2-hydroxybenzylidene)nicotinohydrazide monohydrate, S. Sravya, S. Sruthy, **N. Aiswarya**, M. Sithambaresan and M.R.P. Kurup, *Acta Cryst.* **2015**, *E71*, 734.
- [6] N⁷-[(*E*)-1-(2-Fluorophenyl)ethylidene]pyridine-4-carbohydrazide, P.B. Sreeja, M. Sithambaresan, **N. Aiswarya**, M.R.P. Kurup, *Acta Cryst.* **2014**, *E70*, o532.

- [7] *N*-[(1*E*)-1-(2-Fluorophenyl)ethylidene]pyridine-3-carbohydrazide, P.B. Sreeja, M. Sithambaresan, **N. Aiswarya**, M.R.P. Kurup, *Acta Cryst.* **2014**, *E70*, o115.
- [8] *N*-[(*E*)-2-Fluorobenzylidene]benzohydrazide, P.B. Sreeja, M. Sithambaresan, **N. Aiswarya**, M.R.P. Kurup, *Acta Cryst.* **2013**, *E69*, o1828.
- [9] Dichlorido{2-[(*E*)-phenyl(pyridin-2-yl- κ N)methylidene]-N phenylhydrazinecarboxamide- $K^2 N^2, O$ }copper(II), **N. Aiswarya**, M. Sithambaresan, M.R.P. Kurup, S.W. Ng, *Acta Cryst.* **2013**, *E69*, m588.
- [10] Bis(1-phenyl-3-{(Z)-[phenyl(pyridin-2-yl)methylidene]amino- $\kappa^2 N, N'$ } urea- κO)nickel(II) dinitrate, **N. Aiswarya**, J.M. Jacob, M.R.P. Kurup, S.W. Ng, *Acta Cryst.*, **2012**, *E68*, m918.
- [11] Bis{ μ^2 -[bis(pyridin-2-yl)methylidene]hydrazinecarbothioamido $K^4 S, N, N': N''; K^4 N'': N', N, S$ }bis[bromidocopper(II)] methanol disolvate, R.J. Kunnath, M. Sithambaresan, M.R.P. Kurup, **A. Natarajan**, A.A. Aravindakshan, *Acta Cryst.* **2012**, *E68*, m346.

Posters and Papers presented

- [1] 'Crystal structure of Molybdenum(VI) complex of nicotinoyl hydrazone: Coordination of two different solvent molecules to the hydrazine moiety' – Paper presentation in the Dept. of Chemistry, Sree Kerala Varma College, Thrissur, **2015**, National seminar jointly organized by Sree Kerala Varma College and CMET, Thrissur.
- [2] 'Synthesis and crystal structure of a Schiff base system derived from 1-aminopyrrolidin-2-one' – Paper presentation in Swadeshi Science Congress **2015**.
- [3] Poster presentation in CiTRIC **2012**, Dept. of Applied Chemistry, CUSAT.
- [4] Poster presentation in CiTRIC **2014**, Dept. of Applied Chemistry, CUSAT.
- [5] Poster presentation in International seminar, MatCon **2016**, Dept. of Applied Chemistry, CUSAT.

.....SCS.....